



TECHNISCHE
UNIVERSITÄT
WIEN

PhD Thesis

Dissertation

New Concepts for Two-Photon Micropatterning of Biocompatible Hydrogels

ausgeführt zum Zwecke der Erlangung des akademischen Grades eines
Doktors der technischen Wissenschaften

unter der Leitung von

Univ.Prof. Dipl.-Ing. Dr.techn. Robert Liska

Institut für Angewandte Synthesechemie

und Co-Betreuung von

Univ.Prof. Dr.rer.nat. Aleksandr Ovsianikov

Institut für Werkstoffwissenschaften und Werkstofftechnologie

eingereicht an der Technischen Universität Wien

Fakultät für Technische Chemie

von

Dipl.-Ing. Markus Lunzer, BSc

00709583

Haidgasse 12/14, 1020 Wien

Wien, 01.12.2019

Dipl.-Ing. Markus Lunzer



Die approbierte gedruckte Originalversion dieser Dissertation ist an der TU Wien Bibliothek verfügbar.
The approved original version of this doctoral thesis is available in print at TU Wien Bibliothek.

Danksagung

An dieser Stelle möchte ich Prof. Robert Liska und Prof. Aleksandr Ovsianikov meinen herzlichen Dank aussprechen, mir diese spannende und interessante Arbeit in ihren Forschungsgruppen ermöglicht zu haben. Zum einen möchte ich mich für die hervorragende fachliche Betreuung bedanken, aber auch für das mir entgegengebrachte Vertrauen. Vielen Dank auch für die vielen Konferenzteilnahmen und vor allem dafür, dass ich auch meine eigenen Ideen verwirklichen konnte.

Mein besonderer Dank gilt auch Dr. Marica Markovic, die mich immer mit größter Mühe bei den Zellversuchen unterstützt hat und im Allgemeinen immer einen großen Beitrag zum Funktionieren des *Biofabrication*-Labors leistet.

Weiters möchte ich Prof. Dmitri Ossipov und Dr. Liyang Shi für die gute Zusammenarbeit und Unterstützung beim Zweiphotonen-Sensitizer Projekt bedanken. In diesem Zusammenhang sei auch Dr. Orestis Andriotis gedankt, der die mikromechanischen Charakterisierungen in diesem Projekt sehr engagiert durchführte.

Einen wichtigen und nicht zu vernachlässigenden Beitrag zu dieser Arbeit haben die Bachelorstudenten Anna Schmidbauer und Simon Liedl sowie die Wahlpraktikanten Lukas Leutgeb, Sophia Thiele, Simon Scherrer und Daniel Glöcklhofer geleistet, bei denen ich mich für die Unterstützung bei den Synthesen und Experimenten sowie die gute Zeit bedanken möchte.

Vielen Dank auch meine direkten Laborkollegen Elise Zerobin, Yazgan Mete und Moritz Mitterbauer sowie allen anderen Studenten der *Macromolecular Chemistry* Gruppe (OTECH), die einzeln zu nennen das hier verfügbare Seitenmaß sprengen würde. Es hat viel Spaß gemacht; alle waren hochprofessionell und dabei maximal unseriös.

In gleicher Weise möchte ich mich auch bei all meinen Kollegen aus der *Biofabrication*-Gruppe bedanken. Insbesondere seien hier Peter Gruber, Wolfgang Steiger, Agnes Dobos, Franziska Gantner, Denise Mandt, Katja Hölzl und ein gewisser Jasper Van Hoorick erwähnt. Vielen Dank für die gute Zeit, die Unterstützung und die hilfreichen und konstruktiven Diskussionen.

Des Weiteren möchte ich auch Prof. Simone Knaus, Walter Dazinger, Patrick Knaack, Christian Gorsche und Stefan Baudis für ihre Unterstützung und Beratung danken; vor allem Stefan auch für das Korrekturlesen der vorliegenden Arbeit.

Ebenso möchte ich auch Prof. Jürgen Stampfl und allen Kollegen der Forschungsgruppe *Werkstoffe und Additive Fertigung* für die gute Zeit (u.a. Schiausflüge) und die hervorragende Zusammenarbeit danken.

Mein spezieller Dank gilt meiner Familie, meinen Freunden und allen außerordentlich besonderen Menschen, die mich durch meine Studienzeit begleitet haben.

Abstract

Multiphoton lithography is a powerful technology that permits the processing of light-sensitive materials by the use of pulsed NIR laser light. Owing to its unique features, including free-form 3D-patterning and the non-invasiveness to areas outside the focal volume, this method is particularly suited for micropatterning of hydrogels in the presence of cells. Besides two-photon polymerization where scaffolds-like constructs are built in a bottom-up approach from a macromer formulation, two-photon degradation of pre-formed photoactive hydrogels allows for localized microchannel formation or in situ modification of cell surroundings in 4D cell culture approaches. Due to the high resolution multiphoton lithography offers and the resulting small feature sizes of created constructs, maximizing the achievable writing speed, with the aim to push the feasible spatial dimensions in the cubic centimetre regime, is a current key interest. Along with advances in machine design and engineering, much improvement can be achieved in material development and the implementation of new chemistries to extend the range of processable materials and accessible materials properties. Within this thesis, two problems were addressed.

On the one hand, to expand the portfolio of highly efficient two-photon active compounds, two triazine-based chromophores were synthesized and evaluated as initiators for two-photon polymerization at two different technically relevant fs-laser wavelengths.

On the other hand, for photodegradable hydrogels photolabile bonds are integrated into a hydrogel network. However, as the reactivity of most respective groups towards two-photon excitation is rather low, high laser powers need to be applied and technically achievable writing speeds cannot be fully exploited. To advance this material class, existing methods should be improved and new photochemistries should be evaluated.

In concept studies, novel cleavable molecules, which could be fragmented upon radical attacks, were designed and tested, and a water-soluble thiol-releasing AFCT-reagent was synthesized and evaluated concerning its applicability for the cleavage of disulfide-bonds.

Moreover, a concept for sensitized two-photon cleavage of o-nitrobenzyl (oNB), the currently most used photolabile group, was developed and extensively tested. The biocompatibility of the process was demonstrated in the presence of stem cells. This approach was then translated onto much simpler disulfide linkages, in order to permit the two-photon cleavage of this functionality and avoid the use of oNB. In addition, to facilitate the formation of disulfide-based networks from thiol-terminated macromers, a disulfide containing photo-linker for the light-induced formation of such networks by thiol-ene “click” chemistry was developed. The applicability of this new hydrogel platform as well as the sensitized two-photon cleavage was finally confirmed by cell culture studies.



Die approbierte gedruckte Originalversion dieser Dissertation ist an der TU Wien Bibliothek verfügbar.
The approved original version of this doctoral thesis is available in print at TU Wien Bibliothek.

Kurzfassung

Multiphotonen-Lithographie ist eine Hochleistungstechnologie, welche die Bearbeitungen lichtsensitiver Materialien unter Verwendung von gepulstem NIR-Laser Licht ermöglicht. Aufgrund ihrer einzigartigen Merkmale, einschließlich Freiform-3D-Strukturierung und Nichtinvasivität in Bereichen außerhalb des Fokusvolumens, ist diese Methode besonders für die Mikrostrukturierung von Hydrogelen in Gegenwart von Zellen geeignet. Neben Zweiphotonen-Polymerisation, bei der Strukturen aus einer Makromer-Formulierung aufgebaut werden, ermöglicht die Zweiphotonen-Degradierung vorgeformter photoaktiver Hydrogele die lokalisierte Bildung von Mikrokanälen und in situ Modifizierung der Zellumgebung in der 4D-Zellkultur. Aufgrund der hohen Auflösung der Multiphotonen-Lithographie und der daraus resultierenden geringen Detailgrößen, ist die Maximierung der erreichbaren Schreibgeschwindigkeit mit dem Ziel die realisierbaren Objektmaße in den Zentimeter-Bereich zu bringen zurzeit von höchstem Interesse. Gemeinsam mit Fortschritten in der Maschinenkonstruktion können viele Verbesserungen durch Materialentwicklung und der Implementierung neuer Chemie erzielt werden, unter anderem um den Umfang der verarbeitbaren Materialien und erreichbaren Materialeigenschaften zu erhöhen. In dieser Arbeit sollen hierzu zweierlei Probleme angesprochen werden.

Einerseits wurden zwei Triazin-basierte Chromophore synthetisiert und als Initiatoren für die Zweiphotonen-Polymerisation evaluiert, um das Portfolio an hocheffizienten Zweiphotonen-aktiven Substanzen zu erweitern.

Zum anderen werden für die Bildung photospaltbarer Hydrogelen photolabile Bindungen in ein Netzwerk integriert. Allerdings ist die Reaktivität der meisten dieser Gruppen in Bezug auf Zweiphotonen Anregung eher gering, weshalb hohe Laserleistungen benötigt werden und die technisch erreichbaren Schreibgeschwindigkeiten nicht voll ausgeschöpft werden können. Um diese Materialklasse voranzutreiben, sollten existierende Methoden verbessert und neue Photochemie evaluiert werden. In Konzeptstudien wurden neuartige Moleküle erarbeitet, die im Zuge eines Radikal-Angriffs gespalten werden könnten, sowie ein wasserlösliches AFCT-Reagenz synthetisiert und im Hinblick auf seine Eignung zur Spaltung von Disulfidbindungen getestet.

Weiters wurde ein Konzept für die sensibilisierte Zweiphotonen-Spaltung von o-Nitrobenzyl (oNB), der am häufigst verwendeten photospaltbaren Gruppe, entwickelt und umfangreich getestet. Die Bioverträglichkeit dieses Prozesses wurde dabei in Gegenwart von Stammzellen demonstriert. Dieser Ansatz wurde dann auf wesentlich einfachere Disulfidbindungen übertragen, um die Zweiphotonenspaltung dieser Gruppe zu ermöglichen und die Verwendung von oNB zu umgehen. Zur Erleichterung der Bildung Disulfid-basierter Netzwerke ausgehend von Thiol-terminierten Makromeren wurde ein Disulfid-Linker für die lichtinduzierte Bildung solcher

Netzwerke unter Verwendung von Thiol-En-„Click“ Chemie entwickelt. Die Anwendbarkeit dieser neuen Hydrogel-Plattform sowie der sensibilisierten Zweiphotonenspaltung wurde dann durch Zellkulturstudien bestätigt.

TABLE OF CONTENTS

INTRODUCTION	1
OBJECTIVE	14
GENERAL PART	16
SUMMARY	173
MATERIALS, METHODS AND INSTRUMENTATION	183
ABBREVIATIONS	185
BIBLIOGRAPHY	186
CURRICULUM VITAE	192

	Gen. Exp.
1. SYNTHESIS AND EVALUATION OF YNE-MODIFIED TRIAZINES AS TWO-PHOTON ACTIVE INITIATORS	16
1.1 State of the Art	16
1.2 Synthesis of 1,3,5-triazine based chromophores	17 127
1.2.1 Synthesis of the alkyne-substituent 4-(ethynyl)- <i>N,N</i> -dibutylbenzeneamine, 3	17 127
1.2.2 Synthesis of octupolar triazine 3arm-Tri	19 128
1.2.3 Synthesis of dipolar triazine 1arm-Tri	19 130
1.3 Testing of 1,3,5-triazine-based dyes as two-photon initiators	21 131
1.3.1 Two-photon polymerization in presence of 1armTri	21
1.3.2 Two-photon polymerization in presence of 3armTri	22
1.4 Conclusion	24
2. RADICAL FRAGMENTATION INDUCED BY HYDROGEN ATOM ABSTRACTION	25
2.1 State of the Art and Basic Considerations	25
2.2 Molecular Design and Synthesis – Symmetric Approach	26 132
2.2.1 Synthesis of meso- <i>O,O'</i> -diBoc-hydrobenzoin, HBDB	26 132
2.2.2 Synthesis of meso-hydrobenzoin dipivalinate, HBDP	27 133
2.2.3 Reactivity testing of target compounds via ¹ H-NMR-experiments	28 134
2.2.4 ¹ H-NMR-experiments of symmetric test molecules HBDB and HBDP	29 134
2.3 Molecular design and synthesis – asymmetric approach	30 135

2.3.1	Synthesis of meso- <i>O</i> -mono-Boc-hydrobenzoin, HBMB	31	135
2.3.2	Synthesis of meso-hydrobenzoin monopivalinate, HBMP	31	136
2.3.3	¹ H-NMR test-experiments of asymmetric test molecule HBMB	31	137
2.3.4	¹ H-NMR-experiments of meso-hydrobenzoin monopivalinate, HBMP	34	137
2.4	EWG-conjugation Approach	37	137
2.4.1	Synthesis of 2-Phenyl-1-(phenylsulfonyl)propan-2-ol, PPSP	37	137
2.4.2	Synthesis of <i>O</i> -Boc-2-Phenyl-1-(phenylsulfonyl)propan-2-ol, BPPSP	38	139
2.4.3	¹ H-NMR-test-experiments of BPPSP	38	140
2.5	Conclusion	39	
3.	WATER-SOLUBLE AFCT REAGENTS FOR CLEAVAGE OF DISULFIDE NETWORKS	40	
3.1	State of the Art	40	
3.1.1	Chemical-induced disulfide cleavage	40	
3.1.2	Photochemical-induced disulfide cleavage	41	
3.1.3	Other methods to induce disulfide metathesis	42	
3.2	General Considerations	42	
3.3	Preliminary reactivity testing	43	140
3.4	Synthesis of water-soluble AFCT reagent 3-MPAMA	44	140
3.5	Reactivity testing of water-soluble AFCT reagent 3-MPAMA	45	141
3.6	Conclusion	46	
4.	A MODULAR APPROACH TO SENSITIZED TWO-PHOTON PATTERNING OF PHOTODEGRADABLE HYDROGELS	48	
4.1	State of the Art	48	
4.2	Design and synthesis of the photocleavable hydrogel platform	49	141
4.3	Sensitized two-photon micropatterning of photocleavable hydrogels	53	147
4.4	Micro-mechanical analysis of microptatterned regions by AFM	58	148
4.5	Biocompatibility & Cell Culture Application	60	148
4.6	Mechanistic considerations	65	150
4.7	Conclusion	68	

5.	SIMPLIFYING THE SYSTEM – TWO-PHOTON CLEAVAGE OF DISULFIDE BONDS	69	
5.1	State of the Art	69	
5.2	Two-photon degradation of 4arm-PEG5k-SH hydrogel in presence of two-photon sensitizers	71	151
5.3	One-photon irradiation of 4armPEG5k-SH hydrogel in presence of P2CK	74	151
5.4	Two-photon microchannel fabrication in organogels	75	151
5.5	Two-photon induced cleavage of a disulfide-based hyaluron network	76	152
5.6	Conclusion	78	
6.	INTRODUCING DISULFIDE LINKAGES BY THE USE OF LIGHT	79	
6.1	State of the art	79	
6.2	Development of disulfide-based crosslinkers	80	153
6.2.1	A Nor-SS-Nor crosslinker from cheap starting materials	80	153
6.2.2	Formal translocation of the carboxylic acid	84	156
6.2.2.1	Synthesis of Nor-L-Cys	84	156
6.2.3	Reactivity estimation on the molecular level by ¹ H-NMR	86	159
6.2.4	Optimization strategies of the linker on the molecular level	89	159
6.2.4.1	General Considerations	89	
6.2.4.2	Synthesis of modified linkers	92	159
6.2.4.2.1	Synthesis of exo-Nor-L-Cys and its Na salt	92	160
6.2.4.2.2	Synthesis of Nor-D,L-Cys and its Na salt	93	162
6.2.4.2.3	Synthesis of Nor-L-HCys and Nor-D,L-HCys and corresponding Na salts	93	163
6.2.4.2.4	Synthesis of Nor-L-CysMe	94	166
6.2.5	List of synthesized Nor-SS Linkers	95	
6.3	Development of the Disulfide-based Hydrogel Platform	96	167
6.3.1	Extended reactivity estimation on the molecular level by ¹ H-NMR	96	167
6.3.2	Hydrogel optimization	98	167
6.3.2.1	Optimization of the photoinitiator concentration	99	167
6.3.2.2	Thermostability of disulfide-crosslinked PEG hydrogel	101	168
6.3.2.3	Mechanostability of disulfide-crosslinked PEG hydrogel	102	168

6.3.3	Stabilization of 8arm-D,L-HCys (1:1) hydrogel	104	168
6.3.3.1	Stabilization by a non-cleavable background network	106	168
6.3.3.2	Capping of free thiols by maleimide	109	169
6.3.4	Stabilization of 8armPEG-based hydrogels by the use of Nor-L-HCys	114	169
6.3.5	Crosslinking 4armPEG-based hydrogels	116	169
6.4	Two-photon micropatterning of disulfide-crosslinked hydrogels in presence of DAS	118	170
6.5	Cell encapsulation and micro-channel formation	124	170
6.6	Conclusion	126	

INTRODUCTION

Tissue engineering

Tissue engineering is a multidisciplinary field that combines the principles of engineering and biology with the aim to provide solutions for tissue repair and maintenance and to develop functional substitutes for damaged tissue.^[1] In contrast to drug based therapies, tissue engineering has particular advantages as it can provide a permanent solution to the problem of organ failure.^[2]

In general, certain factors are crucial for tissue engineering including (i) *cells*, (ii) *(bio)materials* and (iii) *techniques to form particular tissue architectures*. Historically, three main approaches to tissue engineering have emerged: the use of isolated cells or cell substitutes as cellular replacement parts (scaffold-free approach), using acellular biomaterials capable of inducing tissue regeneration, and to apply a combination of cells and materials (typically in the form of scaffolds).^[2-3] Moreover, *signaling molecules* as for example growth factors play another key role in tissue engineering by providing biochemical cues for stem cell proliferation, migration, and differentiation.^[4] Nevertheless, an elaborate delivery system for growth factors is critical for tissue regeneration.^[5]

Tissue engineering is a highly innovative field and hence new technologies and emerging trends from different research disciplines are rapidly adapted and utilized (Figure 1).^[6] For example, (i) cells can be reprogrammed into induced pluripotent stem cells (iPSCs) or edited by the use of genetic tools such as CRISPR-Cas9. (ii) New biomaterials designed from natural or semi-synthetic sources can be combined with advanced chemistries to influence biomechanics or the local distribution and delivery of growth factors. (iii) To generate complex functional tissues, engineering strategies are applied, which allow to create constructs that provide a particular physiological environment. These strategies include programmed self-assembly, 3D-bioprinting or the use of decellularized organs.

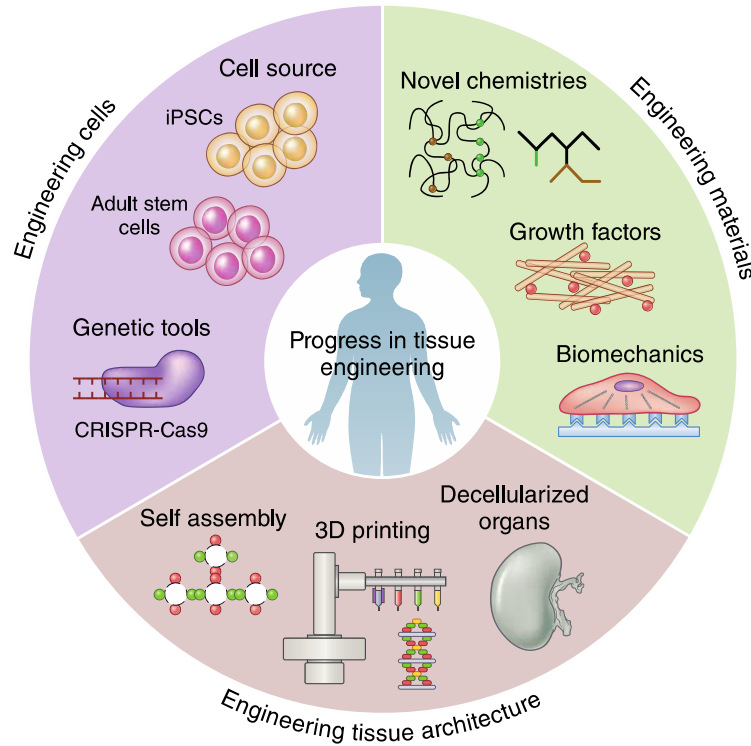


Figure 1: Recent progresses in the field of tissue engineering have been achieved based on advances and improvements of methodologies in different areas of research.^[6]

Hydrogels for Tissue Regeneration and 3D Cell Culture

Hydrogels are crosslinked and highly hydrated polymer networks with engineerable properties, which are utilized for various strategies for tissue engineering, regenerative medicine and cell or drug delivery. Due to their tunable physiochemical properties, hydrogels permit to mimic the native extracellular matrix (ECM) of soft biological tissues.^[7]

Generally, hydrogels can be classified according to their derivation and composition as either synthetic, biological or hybrid (Figure 2).^[8] Synthetic hydrogels are fabricated using synthetic chemistry strategies, typically involving the crosslinking of bioinert chemical monomers or macromers. Common traditional synthetic polymers used as hydrogel backbones include poly(hydroxyethyl methacrylate) (PHEMA), poly(ethylene glycol) (PEG), and poly(vinyl alcohol) (PVA). Besides, also hydrogels based on ionic materials as for example poly((meth)acrylic acid) (P(M)AA) and polyacrylamide (PAAm) are applied.^[9] While the properties of synthetic polymers can be easily and reproducibly tuned due to a wide variety of available molecular sizes and modifications with various functionalities, they are considered as biological inert and hence require modifications with biological tethers to permit cell compatibility.

Besides, supramolecular hydrogels mostly based on peptides or recombinant proteins are also considered as synthetic. However, these supramolecular hydrogels have the limitation of relatively weak mechanical strength and stiffness when compared to naturally derived and traditional synthetic hydrogels.^[8]

In contrast to traditional synthetic hydrogels, biological hydrogels originate from natural sources and are either protein or carbohydrate based materials.^[8] Examples include collagen, fibrin, hyaluronic acid (HA), alginate, agarose or chitosan. Since these materials are often key components of the native ECM, they are usually highly biocompatible.^[9] Moreover, complex biological hydrogels can also be directly derived from decellularized tissues.^[10]

The third group of hybrid hydrogels combines different material types to benefit from the advantages of the individual material classes. Hybrid approaches often involve blending, copolymerization, or interpenetration of different polymer types.^[8] Alternatively, hybrid hydrogels can also be generated by incorporating nanoparticles into hydrogels leading to so-called nanocomposite hydrogels, which were originally inspired by the compositions and structures of nanoreinforced native bone tissues.^[11]

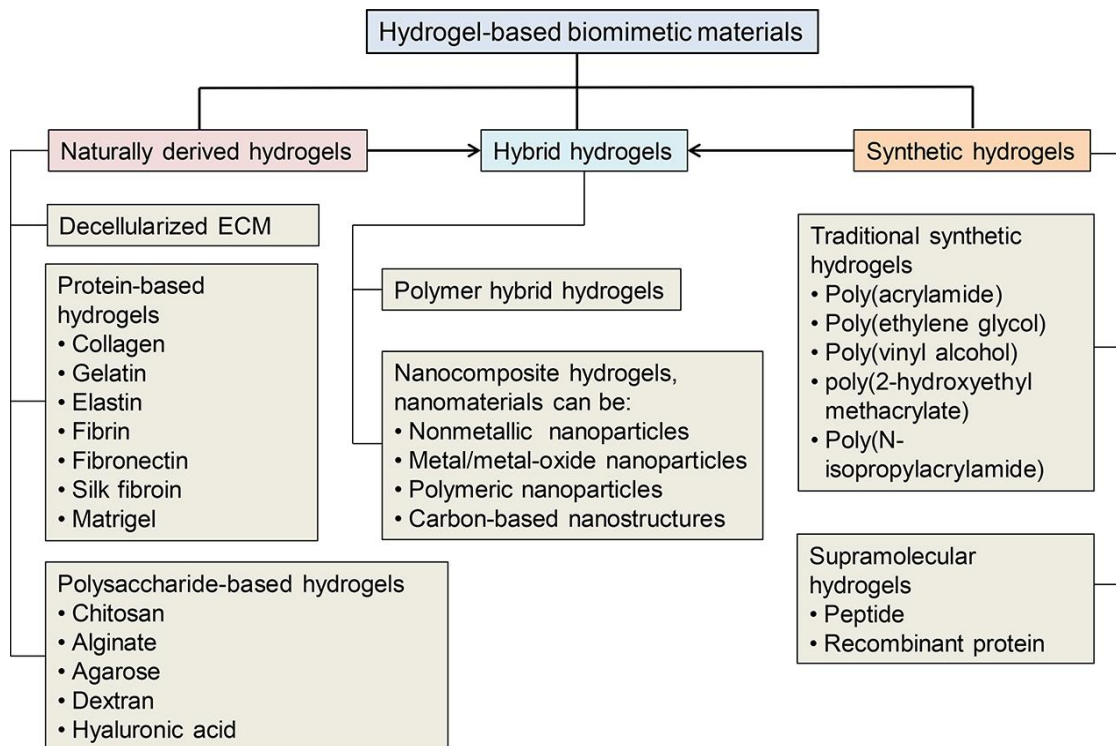


Figure 2: Hydrogel-based biomimetic materials can be classified into naturally derived, synthetic, and hybrid hydrogels, according to their origins and compositions.^[8]

Furthermore, often synthetic and biological materials are combined to form biohybrid hydrogels. For instance, PEG based hydrogels are often modified with certain amino acid sequences (e.g. RGD), which are derived from natural proteins such as fibronectin, laminin, or collagen, to increase cellular attachment.^[12] Beyond that, also protein-patterning approaches exist with the aim to guide the fate of encapsulated stem cells.^[13] Moreover, for example degradable hydrogels have been created by incorporating enzymatically degradable links into synthetic hydrogel matrices. Such hydrogels can be slowly degraded while cells produce their own ECM.^[9]

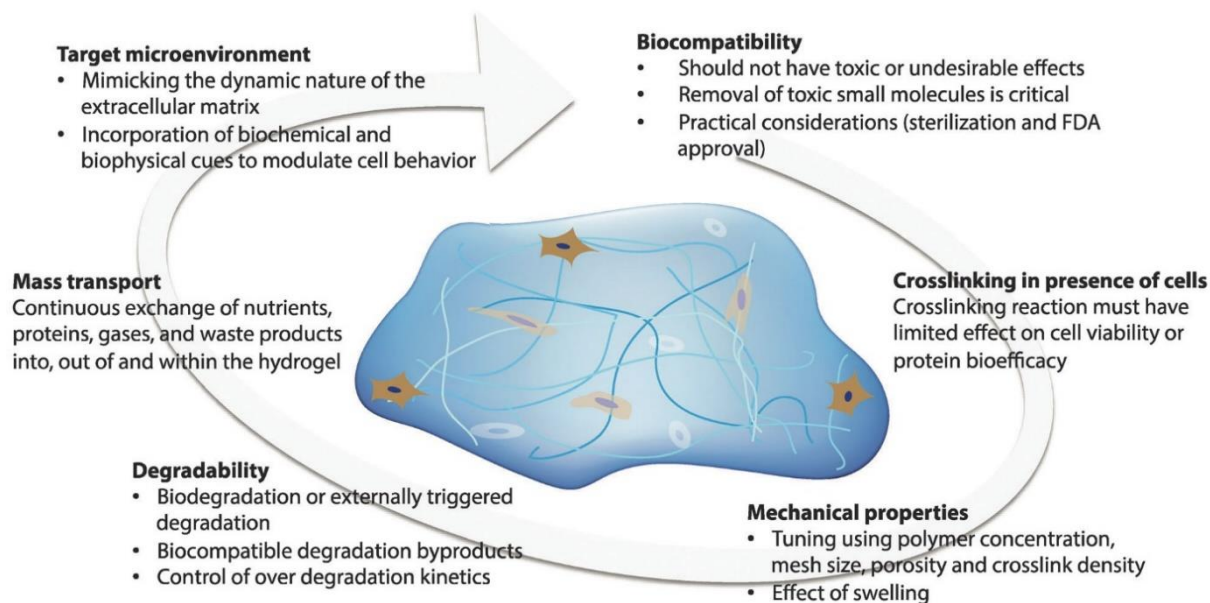


Figure 3: General requirements for hydrogels used as ECM-mimetic materials for cell encapsulation and 3D culture.^[14]

Hydrogels are appealing for biological applications because of their high water content and biocompatibility. While networks of hydrophilic polymers have a high affinity for water, they are prevented from dissolving due to physical or chemical crosslinks. Hence, water can penetrate in between the polymer chains of the network, subsequently causing swelling and the formation of a hydrogel. The ability to tailor the molecular structure of hydrogels enables the adjustment of their mechanical, responsive, and diffusive properties. As these networks are open, a constant exchange with the swelling medium takes place and nutrients and other soluble factors can diffuse in, supplying encapsulated cells, while waste materials are washed away.^[9] For many biological applications, cells are directly encapsulated into a 3D hydrogel matrix serving as cell-culture scaffold. Hence, basic requirements for ECM-mimetic materials are cytocompatibility of both the gel precursors as well as the gel crosslinking reaction, a proper hydrogel formation rate for cell encapsulation without sedimentation, and appropriate mass transport to support exchange of

nutrients and waste products (Figure 3).^[15] Moreover, the mechanical properties of the hydrogel have to be adjusted to match those of the ECM of the encapsulated cell type. Likewise, biochemical and biophysical cues need to resemble those found in the native microenvironment.^[14]

Cells *in vivo* are constantly interacting with and remodeling their surrounding ECM to enable various cell behaviors, including spreading, migration, proliferation, and differentiation. Hence, hydrogels need to be adapted to the changing cell requirements in order to mimic the dynamic nature of the ECM. Strategies for this purpose include (i) degradation of permanent crosslinks or (ii) breaking and reformation of reversible linkages to mimic the remodeling ECM (Figure 4).^[15-16]

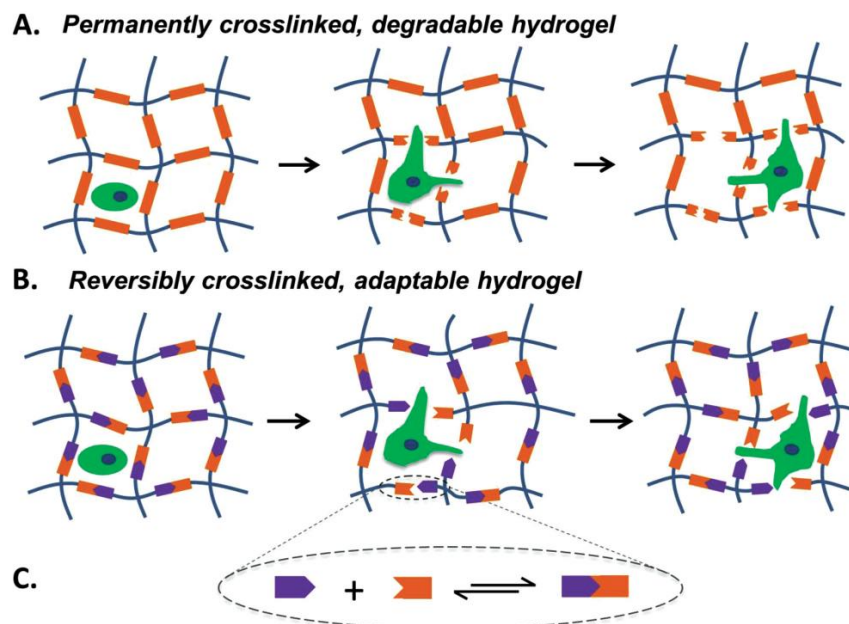


Figure 4: (A) In a permanently crosslinked hydrogel irreversible degradation can occur, leading to bulk degradation, whilst (B) an adaptable hydrogel is built from reversible crosslinks. (C) Such reversible linkages can be formed either by physical associations or reversible chemical reactions.^[15]

Dynamically tunable hydrogels

Classical 2D monolayer cell culture models oversimplify the 3D *in vivo* cell microenvironment. For instance, whereas cells cultured in 2D can only have cell-ECM adhesions on the substrate side and cell-cell adhesions in the horizontal plane, in 3D cells can generate adhesions on all sides.^[8] Nevertheless, the complex 3D environment that is surrounding mammalian cells *in vivo* is dynamically changing. Hence, dynamically tunable cell culture platforms permitting to modify the cell surrounding matrix at a user-defined location and time point are highly relevant for research

on cell and tissue physiology as well as for mechanobiology (Figure 5).^[7a] Such stimuli responsive hydrogels are also referred to as 4D-hydrogels (three spatial dimensions with changes over time) or spatiotemporal hydrogels in literature.^[17]

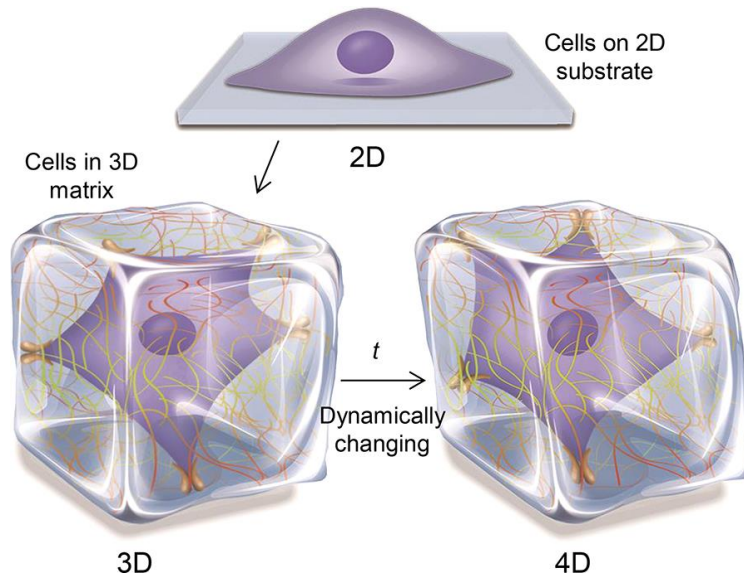


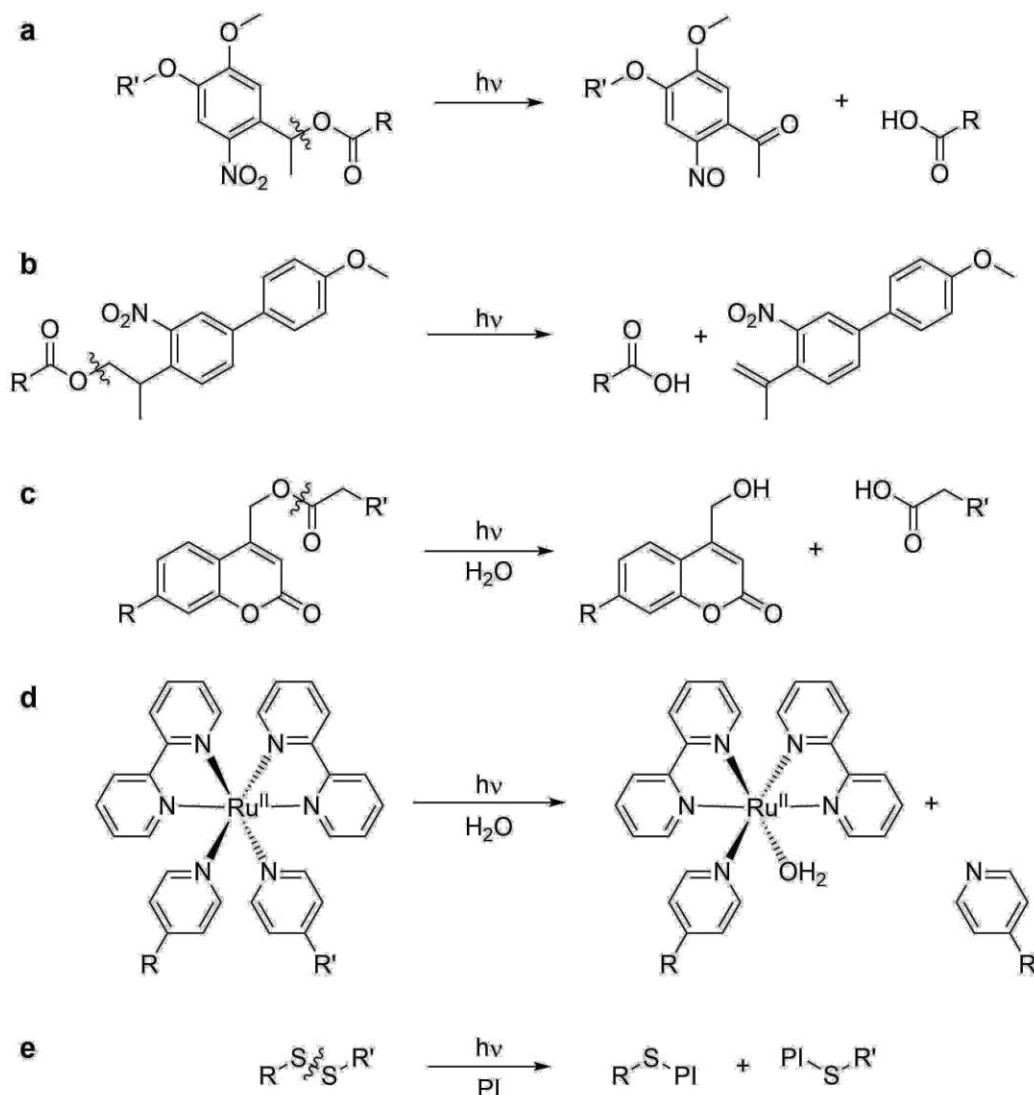
Figure 5: Cell culture platforms have been developed from 2D to 3D and 4D to model the dynamical changes of the native cell microenvironment.^[8]

Several strategies are used to engineer 4D hydrogel platforms including reversible linkages which facilitate cells to remodel their environment^[15] and bioorthogonal chemistries allowing dynamic modification of preformed hydrogels.^[18] Moreover, photoresponsive hydrogels which can be stimulated by the use of light become increasingly important.^[19]

Photodegradable hydrogels

A lately emerging, highly elaborated class of photoresponsive dynamically tunable hydrogels contains photolabile functional groups, which allow for user-directed real-time control of the biomaterial's (bio)chemical and mechanical properties at positions of interest by irradiation with cytocompatible doses of light.^[19b, 20] Such photoresponsive hydrogels have undergone a tremendous evolution in recent years from hydrogels containing photolabile groups on a photostable backbone for guided three-dimensional cell growth and migration,^[21] over hydrogels with a photodegradable backbone allowing for postgelation control of the physiochemical polymer properties,^[22] to a hydrogel matrix that permits photoreversible spatiotemporal immobilization of proteins,^[13] to mention only a few milestones of this rapid development. The photodegradability of such biomaterials is often enabled by the integration of *o*-nitrobenzyl (*o*NB) ester derivatives (especially the nitroveratryloxycarbonyl (NVOC) group),^[23] which beyond that have been utilized

in several other dynamically light triggered materials.^[24] Alternatively, photocleavable hydrogels based on coumarin-derivatives, disulfides, *o*-nitrobiphenylpropyl-derivatives or ruthenium-complexes have been reported (Scheme 1).^[25]



Scheme 1: Schematic photocissions of photolabile groups commonly utilized in photodegradable hydrogels. *o*-Nitro-based compounds such as (a) *o*-nitrobenzyl esters^[26] and (b) *o*-nitrobiphenylpropyl-derivatives^[25f] cleave via an intramolecular process, while (c) coumarins^[27] and (d) ruthenium-complexes^[25g] interact with solvent molecules. (e) Disulfides can be cleaved homolytically and are deactivated by a termination reaction with a radical species such as a photoinitiator fragment.^[25d]

In general, photo-degradable hydrogels can be photoeroded either by the use of UV-VIS light or upon two-photon excitation (Figure 6).^[23b, 28] While the former method allows for the generation of

2D patterns by applying traditional photolithographic techniques involving masked light,^[22] the later permits the generation of complex 3D patterns by the use of pulsed NIR laser light.^[29]

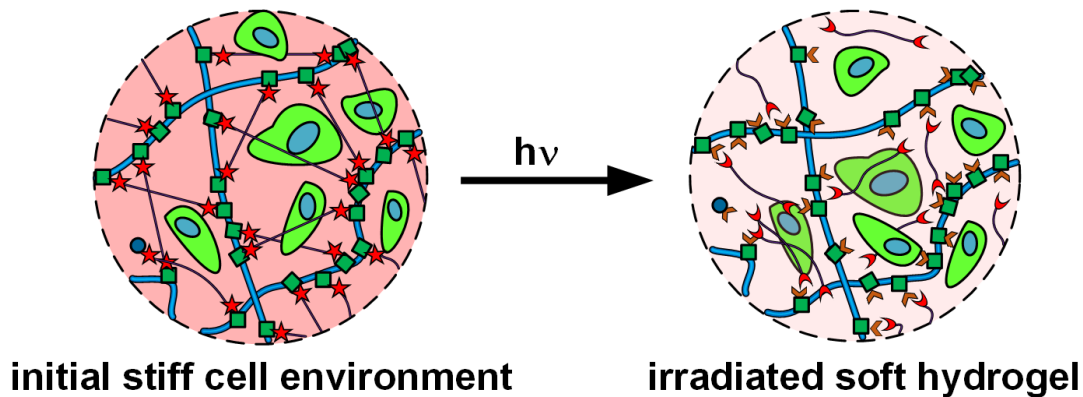


Figure 6: The crosslinking density of a photodegradable hydrogel can be reduced by irradiation at respective wavelengths. Depending on the dose applied the mechanical properties can be either reduced and the material softens or it can be fully degraded leading to reverse gelation.

Multiphoton Lithography

Multiphoton Lithography is a technology based on the non-linear absorption of light.^[30] While already theoretically predicted in 1931 by Maria Goeppert-Mayer,^[31] it was only 30 years later, after the invention of the laser, when Kaiser and Garrett could verify the effect by demonstrating two-photon absorption (2PA) in $\text{CaF}_2:\text{Eu}^{2+}$ crystals.^[32] However, after the invention of subpicosecond pulsed lasers the technical and scientific exploitation of multiphoton processes started. Webb *et al.* laid the foundation with the development of *two-photon laser scanning fluorescence microscopy*,^[33] a high resolution imaging technique that gained widespread use in bioscience.^[34] Multiphoton Lithography was demonstrated later by scanning a focused laser beam in a 3D pattern through a photoresist causing polymerization of arbitrary three dimensionally defined regions.^[35]

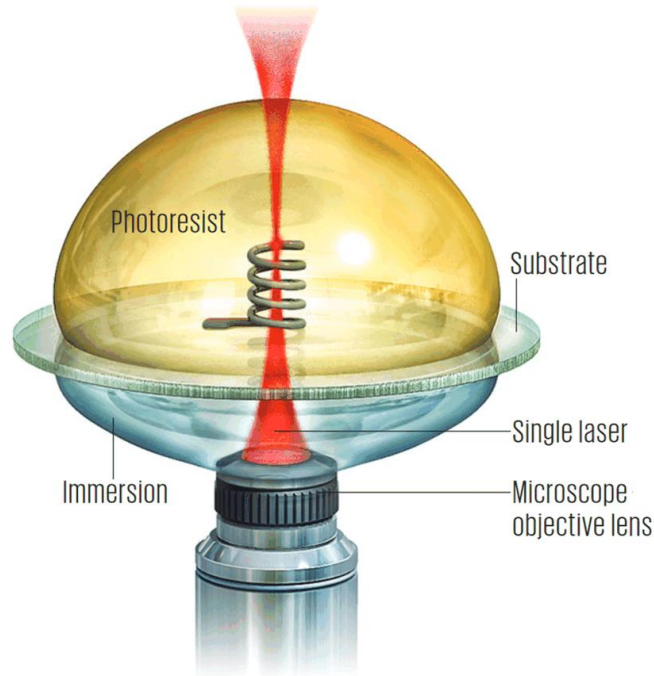


Figure 7: Multiphoton Lithography. A subpicosecond laser beam is focused into a two-photon active resin through an immersion medium and a substrate. Only in the focal point of the laser the photon flux is sufficiently high enough to induce the excitation of a two-photon active compound which in turn initiates locally confined polymerization.^[36]

The specific characteristic of two-photon absorption based processes is the fact that only within the focal volume of the laser beam the photon flux is high enough for a two-photon process to occur.^[37] Any subsequent process, such as fluorescence or a photo-induced chemical reaction, is localized within this small volume as well.^[38] Consequently, (i) the active volume (voxel) can be highly confined allowing the fabrication of very precise objects. Moreover, as the voxel has a limited longitudinal dimension, (ii) real 3D structuring of objects is possible, since layers above and below the active volume remain unexcited (Figure 8b).

Photoresists for Multiphoton Lithography usually consist of a prepolymer resin containing a two-photon active photoinitiator. Most common resins act as *negative-tone photoresists*, meaning that polymerization occurs in the regions that are exposed.^[39] On the contrary, *positive-tone photoresists* in which exposed regions are removed in the development step have been demonstrated as well.^[38, 40] Photolabile polymer networks in which the exposed areas are cleaved are also a type of positive-tone photoresists.^[21, 41]

In any case, after exposure, a development process generally involving washing with one or more solvents is required to remove any unhardened material. Further post-processing steps such as baking or bulk irradiation may be applied as well.^[39]

Two-Photon Absorption

In contrast to linear one-photon absorption (1PA) which follows Beer-Lambert law,^[42] two-photon absorption is a non-linear process by which a molecule or material absorbs a pair of photons simultaneously, the sum of whose energy equals the transition energy (Figure 8a).^[37] The transition property for this process to occur is inherently weak at standard light intensities,^[37] which is why the application of intense laser pulses is necessary to provoke the simultaneous absorption of two or more photons. The transition probability for the absorption of two photons is proportional to the square of the intensity I of the laser pulse I^2 .^[43] Upon excitation of a molecule from the ground state (S_0) to the excited state (S_1), several relaxation pathways are possible. Their respective probability depends on the nature of the molecule. While high fluorescence yield is important for dyes used in two-photon laser scanning fluorescence microscopy, the efficient initiation of a radical polymerization process is a key feature of an initiator applied in multiphoton lithography.^[44] Although not fully understood yet, the typical radical-generation pathway of common photoinitiator molecules most likely involves intersystem-crossing from S_1 to the lowest triplet state (T_1) from where the generation of polymerization-initiating radicals occurs.^[45] This is due to the fact that T_1 usually exhibits a much longer lifetime than S_1 .^[46]

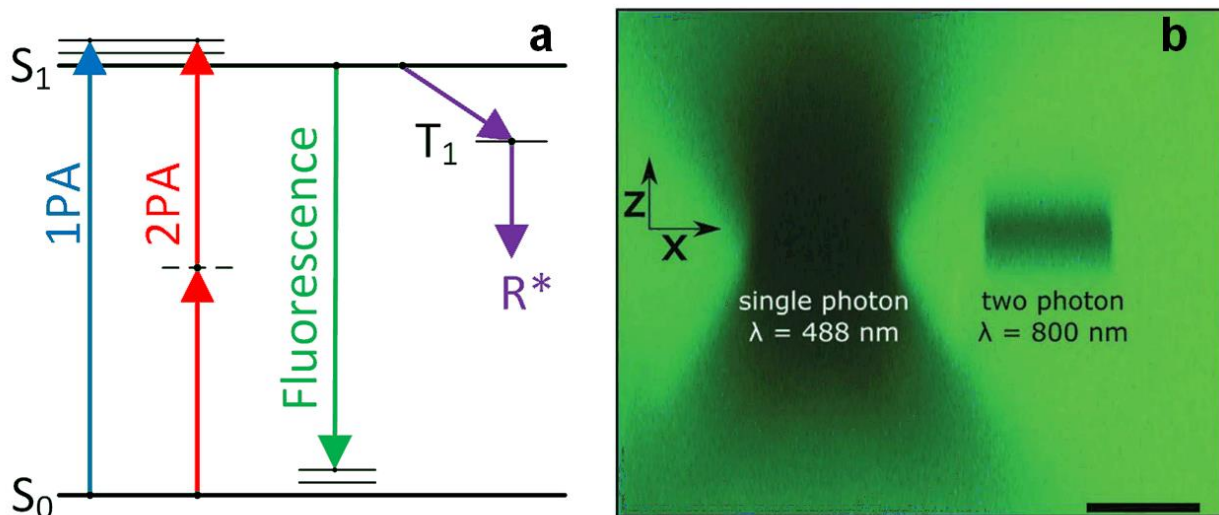


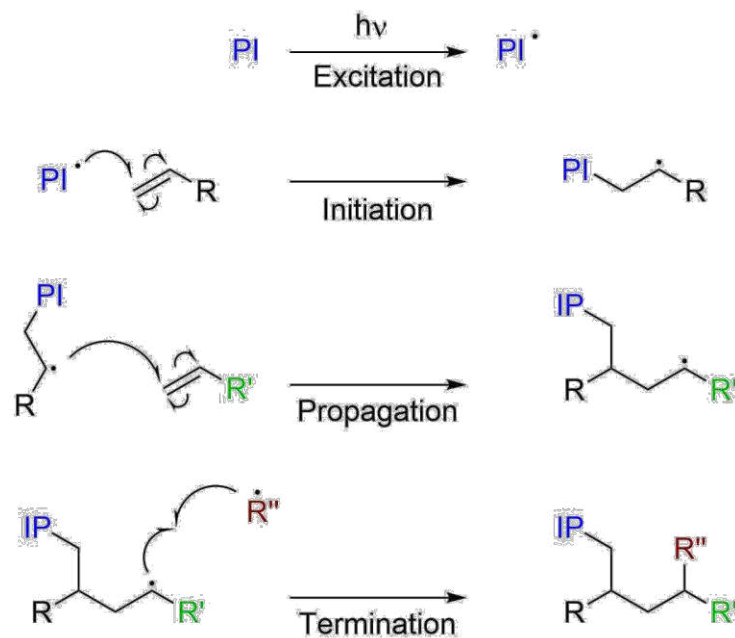
Figure 8: a) A molecule can be excited either by single photon absorption (1PA) or upon quasi-simultaneous absorption of two photons, whose sum of energy equals the transition energy (2PA). Relaxation can occur via various photophysical pathways, as for example fluorescence or intersystem crossing to a triplet state. b) Focused laser light can be used to illuminate regions with 3D resolution. The irradiation is illustrated by photobleaching uniformly bound fluorescein within a hydrogel at a single plane with light of 488 nm (1PA) and 800 nm (2PA). Only 2PA events are localized to the imaging plane. Photobleaching and confocal imaging have been performed with a 1.0 NA objective. Scale bar = 25 μ m.^[17c]

Two-Photon Absorption Cross-section

The 2PA cross-section δ_{2PA} is a crucial parameter for the quantification of 2PA-efficiency.^[46] It is a wavelength-dependent parameter characterizing the average two-photon absorption per photon and molecule. Its informal unit is named Göppert-Mayer (GM) with 1 GM being equal to $10^{50} \text{ cm}^4 \text{ s photon}^{-1} \text{ molecule}^{-1}$. In order to maximize 2PA, two-photon active chromophores usually consist of an extended delocalized π -systems (π) with high coplanarity and usually involve donor (D) and acceptor (A) groups at the center and ends of the molecule. Common molecular design motifs involve linear asymmetric dipolar A- π -D or centrosymmetric quadrupole D- π -D or A- π -A arrangements. Besides, also branched octupolar molecules and such of higher complexity have been investigated extensively. In practice, two-photon active chromophores commonly have $\delta_{2PA, \text{max}}$ values in the range of 10^{-1} - 10^4 GM.^[44] However, molecules with increased π -systems or branched molecules often work well as initiators but such chromophores usually require complex synthesis and are in many cases sparingly soluble without respective modifications.^[44-45] In contrast, conventional UV-photoinitiators are optimized for one-photon excitation, hence often exhibit relatively low $\delta_{2PA, \text{max}}$ values and are inefficient initiators in the two-photon excitation regime.^[47] Consequently, resins containing initiators not optimized for two-photon application can be only polymerized by means of long exposure times and high excitation intensities, resulting in slow writing speeds and frequently structural damage.^[48] While many organo-soluble two-photon dyes do exist,^[44] water-soluble two-photon initiators required for biological applications are still rare.^[49]

Radical Photopolymerization

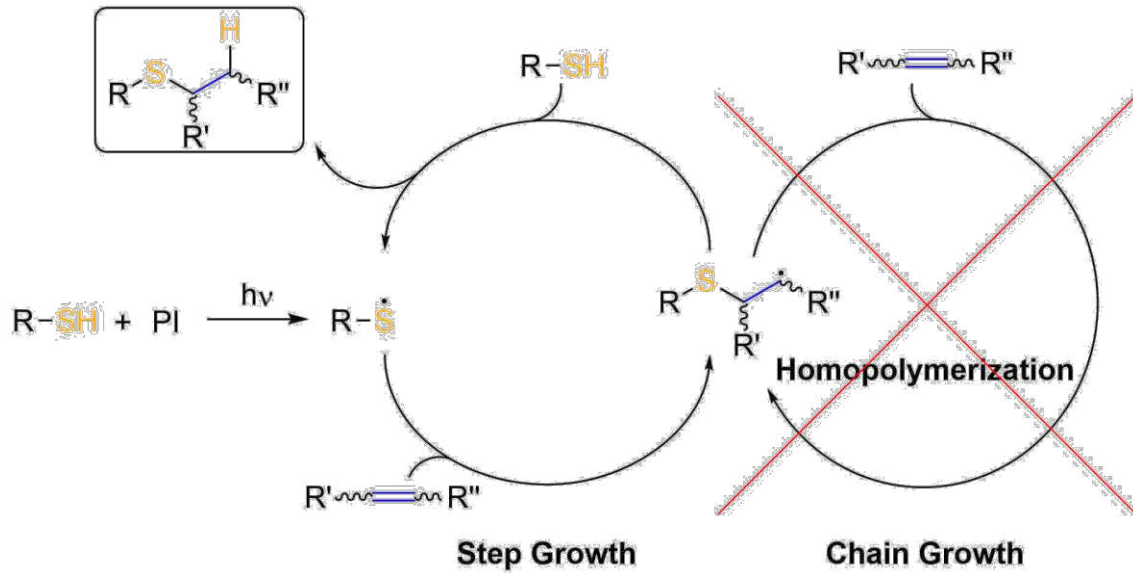
The process of radical photopolymerization allows the synthesis of polymers or crosslinked networks from a usually liquid prepolymer or macromer solution by the use of the external stimulus of light. Radical photopolymerization can proceed either as a (i) *chain-growth* or a (ii) *step-growth* process. To start a radical photopolymerisation reaction, a photosensitive molecule, the PI, is excited by irradiation with light of a suitable wavelength (Scheme 2). Upon excitation the PI either cleaves homolytically giving two radicals (type I) or abstracts a hydrogen atom from a co-initiator (type II).^[50] The thus generated radical species attacks a polymerizable group (e.g. a double bond) causing the *initiation* of the polymerization process. In a (i) chain-growth process, the newly generated radical attacks a further polymerizable group and so on, leading to the *propagation* of the growing chain.^[51] This growth process proceeds until *termination* of the polymerization occurs by e.g. recombination of two radicals.



Scheme 2: The process of radical photopolymerization. Upon excitation of the photoinitiator a radical species is formed that initiates the polymerization by attacking a monomer. The polymer grows by propagation of the radical until a termination process occurs.

Chain growth processes are usually based on the polymerization of (meth)acrylates or vinyl groups and result in stiff kinetic chains. Hence, chain polymerization leads to inhomogeneities in the material, which compromise the material properties as stress is focused on weak portions of the network. Moreover, networks formed by chain polymerization degrade with heterogeneous byproducts. On the contrary, step-growth polymerization leads to highly homogeneous networks with ideal microstructures improving mechanical integrity. For step-growth polymerization, complementary, end-terminated comonomers are reacted.^[52]

The ideal radical-mediated thiol–ene reaction represents an archetype of a step-growth photopolymerization and is considered a “click” reaction (Scheme 3).^[53] Ideal thiol-ene reactions occur when e.g. norbornenes or vinyl ethers are being used as ene-component. Here, no homopolymerization or chain growth is observed, thus implying that the overall rates of chain transfer and are essentially identical.^[54] Thiol-ene reactions are often used as a tool for gelation or post-gelation modification of hydrogels.^[19a] Besides, also the thiol–Michael addition reaction, which is based on an anionic chain process, resembles an ideal thiol-ene reaction (Scheme 3).^[53a]



Scheme 3: The idealized free-radical thiol–ene reaction proceeds with alternating chain transfer and propagation while no homopolymerization of the ene-compound is occurring. An analogous mechanism also applies to the thiol–Michael addition reaction when undergoing an anionic chain process, if the radicals are replaced by their anionic counterparts.^[53a]

Near-UV light is commonly used to induce both radical photopolymerization and photocleavage of linkages in 3D cell culture applications. Recently, the downstream effects of such light on cell function have been investigated by examining the global effects of common light treatments on NIH3T3 fibroblasts and human mesenchymal stem cells (hMSCs).^[55] In this study, unchanged proliferation rates, an absence of apoptotic induction, and an unaltered proteome were observed following low-dose 365 nm light exposure, implying that near-UV-based radical-free photochemistries can be exploited in tissue engineering without deleteriously affecting cell fate.

OBJECTIVE

4D cell culture is a current key topic in the field of tissue engineering, as it allows to create artificial cell environments that are needed to study basic biological processes and develop advanced methods for drug screening and diagnostics.^[17b, 19b] Two-photon 3D-printing is a powerful emerging technology with great potential for the precise fabrication of 3D cell scaffolds or the spatiotemporal modification of cell surrounding matrices. Although tremendous progress has been made to demonstrate two-photon microfabrication and material modification in presence of cells, there are still many obstacles and challenges to be met in order to advance this technology to a standard procedure for the manipulation of 4D cell matrices that can be operated by end users beyond the expert level. Aside from advances in machine design and engineering, much improvement can be achieved in material development and the implementation of new chemistries to extend the range of processable materials and accessible materials properties. Anyhow, for practical purposes simple approaches should be investigated.

In this thesis, two problems should be addressed. On the one hand, to initiate two-photon-based processes highly active two-photon absorbing compounds are needed. Such molecules are often not commercially available and thus need to be synthesized. While some structure-activity relationships are known that help to design molecules with increased two-photon absorption, the distribution of the two-photon absorption spectrum of a compound is difficult to predict. Nevertheless, for economic and engineering reasons compact non-tunable lasers with fixed wavelengths are often applied in devices. Consequently, active compounds must be designed and synthesized to match these specific emission lines. Hence, two triazine-based two-photon active compounds should be prepared and their applicability as initiators for two-photon polymerization should be evaluate at technically relevant fs-laser emission wavelengths.

On the other hand, photo-uncaging is a key technology for designing photodegradable hydrogels for 4D cell culture or the fabrication of micro-fluidic devices. To produce such materials, photolabile bonds are integrated into a hydrogel network. Whereas several functional groups have been applied for this purpose, their reactivity towards two-photon excitation is still rather low. Consequently, high laser powers need to be applied and technically achievable writing speeds cannot be fully exploited. In order to advance this material class, existing technologies should be improved and new photochemistries should be evaluated. In any case, to facilitate biomedical applications, biocompatibility of the approaches is required.

In a concept study model compounds, which could be fragmented upon radical attacks, should be designed and tested, since such linkages could be spatiotemporally cleaved upon addition and excitation of a photoinitiator. In a second concept, water-soluble thiol-releasing AFCT-reagents should be synthesized and evaluated concerning their applicability for the cleavage of disulfide-bonds. These small molecules could be modularly added to pre-existing disulfide-based hydrogels in order to cleave the linkages upon excitation. Information about the reactivity of these test molecules can be acquired by simple $^1\text{H-NMR}$ studies.

Currently, the most commonly used photolabile group is the oNB group, which has been extensively studied. Nevertheless, its two-photon absorption and hence reactivity is rather low. In order to enhance the two-photon response of oNB-based networks, two-photon active chromophores could be added to such materials as sensitizers. To avoid laborious synthetic modifications and for the ease of handling, a photolabile hydrogel should be formed from easily accessible precursors and the sensitizer added modularly to the hydrogel. The effect of the sensitizer should be evaluated by both optical as well as mechanical methods.

In addition, the same approach should also be tested on disulfides, which are much simpler cleavable linkages as oNB but do not react to two-photon excitation. Albeit disulfide-based networks do exist, their formation usually involves oxidation of free thiols, a procedure only slightly controllable. In order to ease the handling, such networks could be created by using the external stimulus of light. For this purpose, a disulfide-containing linker should be designed. By integrating highly reactive norbornene groups such a linker could be used for crosslinking of readily available thiol-terminated macromers utilizing thiol-ene chemistry. Finally, this approach would lead to photoorthogonality, as network formation could be accomplished by the use of UV-VIS light, whereas cleavage could be performed in the two-photon excitation regime. The applicability of this new photocleavable hydrogel platform should be evaluated by cell culture studies.

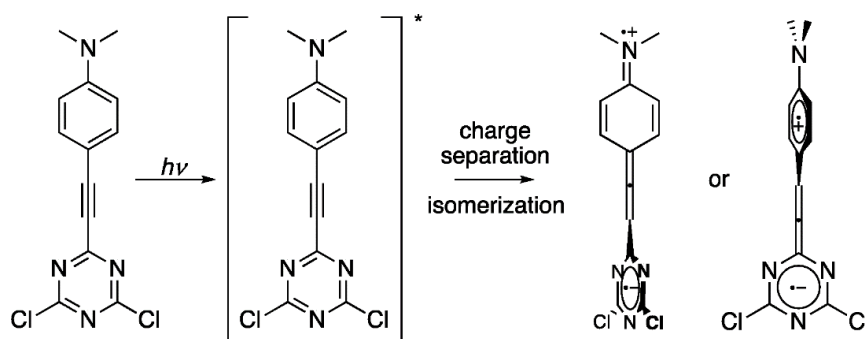
GENERAL PART

1. SYNTHESIS AND EVALUATION OF YNE-MODIFIED TRIAZINES AS TWO-PHOTON ACTIVE INITIATORS

1.1 State of the Art

Multiphoton active chromophores are the key components needed for several applications based on the non-linear absorption of light.^[56] There is an ongoing quest for new efficient multiphoton active chromophores to (i) improve the technological applications of these materials and (ii) further increase the understanding of the excitation process and structure-property correlations. Although clear principles for the design of 2PA dyes have been developed, yet all the best 2PA chromophores still come from serendipitous discoveries (which can often be rationalized retrospectively in terms of transition dipole moments and energy gaps), rather than from rational design.^[44]

Information about the excitation process and further photochemistries can be obtained by ultrafast transient absorption spectroscopies. For example, in an earlier cooperation with the Vauthy research group at the University of Geneva, an unforeseen photochemical alkyne–allene transformation accompanying an intramolecular charge-transfer process upon excitation has been discovered (Scheme 4 **Fehler! Verweisquelle konnte nicht gefunden werden.**)^[57]



Scheme 4: Alkyne to allene phototransformation of a 1,3,5-triazine coupled to a benzenamine via an alkyne.^[57]

In another earlier study by our group, a series of structurally related 1,3,5-triazine-derivatives bearing 1-3 aminostyryl-donor arms have been synthesized and characterized. These molecules proved to be suitable initiators for two-photon polymerization.^[58]

For an in-depth investigation of the discovered alkyne to allene phototransformation,^[57] two yne-modified 1,3,5-triazines were required, namely the respective mono- (dipolar, **1-armTri**) and

trisubstituted (octupolar, **3-armTri**) derivatives (Figure 9). To facilitate solubility in a various organic solvents the target molecules should contain alkane chains (butyl). Nevertheless, also polar or organic functionalities could potentially be introduced to permit water-solubility.

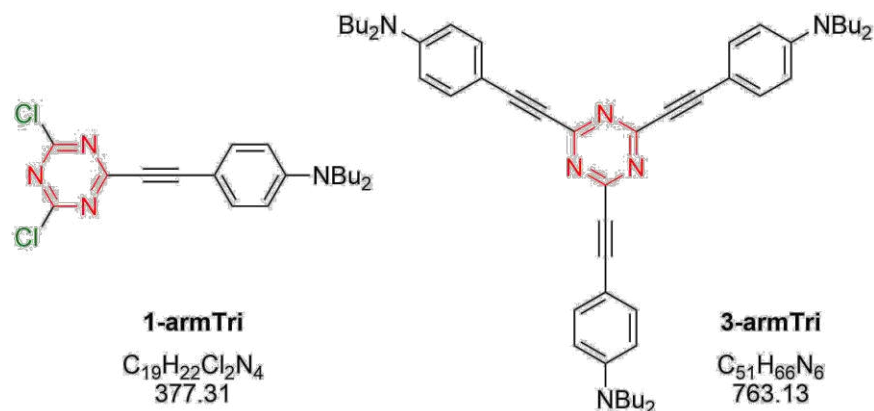


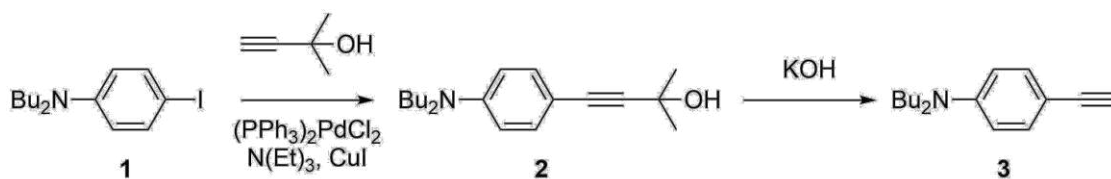
Figure 9: 1,3,5-triazine-based target molecules **1-armTri** (linear) and **3-armTri** (quadrupolar).

1.2 Synthesis of 1,3,5-triazine based chromophores

Both molecules could be synthesized starting from alkyne **3** and cyanur chloride **4** by Pd-catalyzed cross-coupling reactions. Both a Negishi or Sonogashira reaction could potentially be utilized. As the cross-coupling reaction proceeds gradually, depending on the equivalents applied of alkyne **3** either target molecule **1-armTri** or **3-armTri** is the final product.

1.2.1 Synthesis of the alkyne-substituent 4-(ethynyl)-*N,N*-dibutylbenzeneamine, **3**

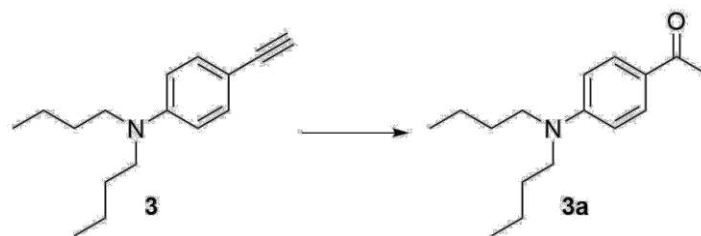
The synthetic route towards the alkyne substituent 4-(ethynyl)-*N,N*-dibutylbenzeneamine **3** was known from a previous study (Scheme 5).^[48a] 4-(4-(*N,N*-Dibutylamino)phenyl)-2-methylbut-3-yn-2-ol **2** was synthesized from *N,N*-dibutyl-4-iodobenzeneamine **1** by Sonogashira cross-coupling with 2-methylbut-3-yn-2-ol using (PPh₃)₂PdCl₂ as catalyst. Compound **2** was further converted to the terminal alkyne 4-(ethynyl)-*N,N*-dibutylbenzeneamine **3** by deprotection with KOH.



Scheme 5: Synthetic route towards alkyne substituent **3**.

Although this route was already established in our lab an unexpected result occurred, as the majority of alkyne **3** oxidized to acyl **3a** (53%) in the course of column chromatography (determined by ¹H-NMR, GCMS) (Scheme 6, Figure 10). This unwanted Markovnikov-type

hydratization most properly occurred due to the presence of metal catalyst residues (Pd, Cu) from the previous synthetic step. Generally, this reaction is known to be catalyzed by strong acids or transition metal catalysts.^[59] Hence, trace metal impurities should be removed thoroughly before deprotection of the alkyne to avoid hydratization of the alkyne. Furthermore, the reaction mixture should be degassed carefully, as also Glaser-coupling reaction can as well occur as side reaction in presence of oxygen.^[60]



Scheme 6: The unexpected hydratization product 3a formed from alkyne 3 during column chromatography.

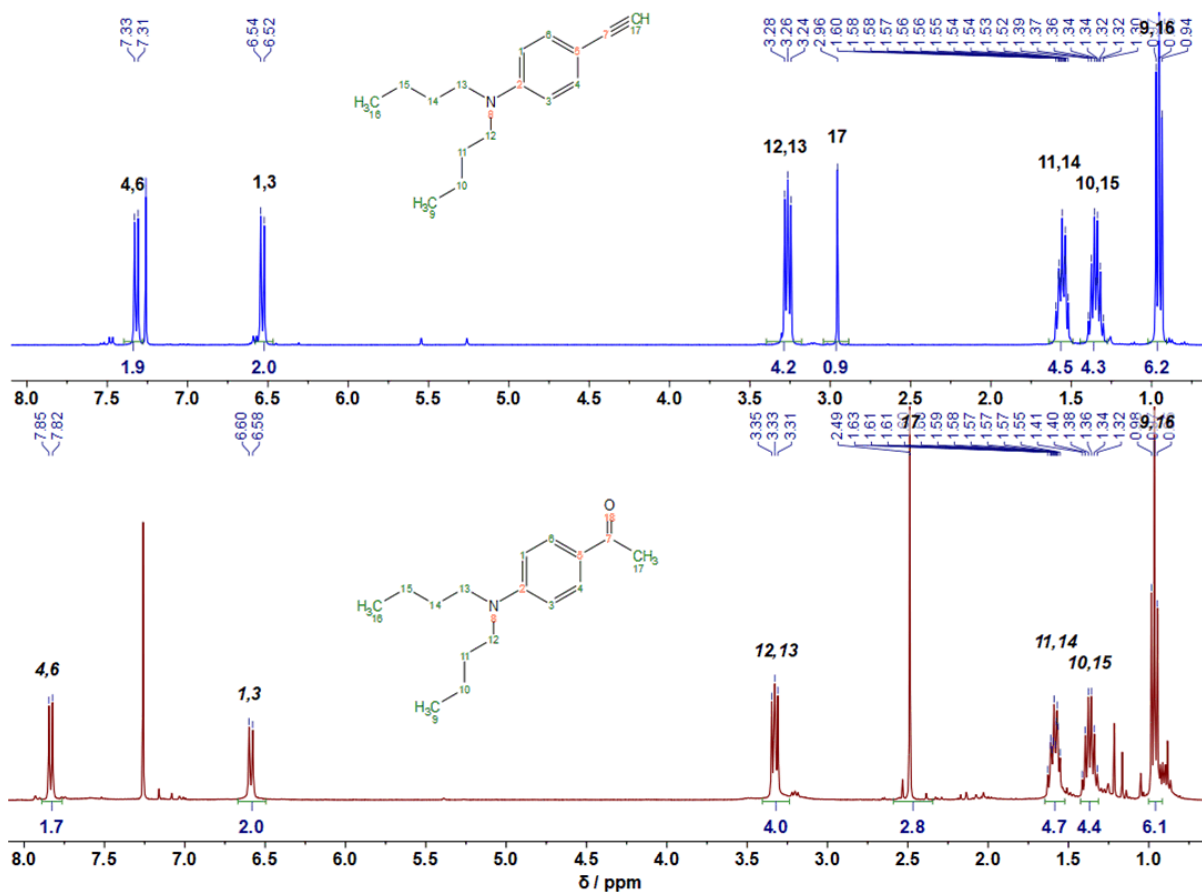
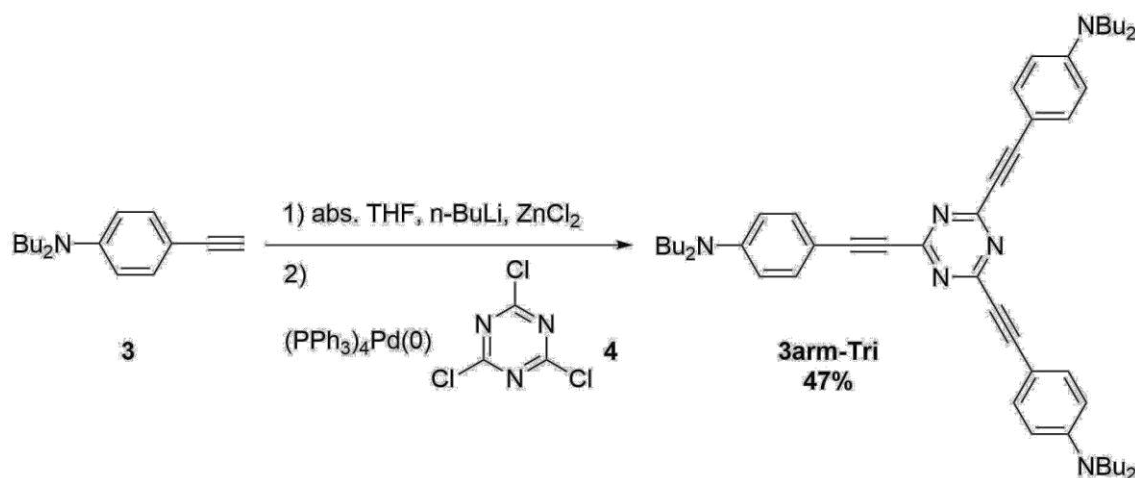


Figure 10: While the singlet at 2.96 ppm in the $^1\text{H-NMR}$ of 3 (blue) can be assigned to the terminal alkyne proton, the spectra of 3a (maroon) shows a singlet at 2.49 ppm with integral 3, which derives from the acetyl substituent.

1.2.2 Synthesis of octupolar triazine 3arm-Tri

First, the octupolar target molecule **3arm-Tri** was successfully synthesized in a one-pot reaction from cyanuric chloride by Negishi cross-coupling reaction following the modified protocol for the mono-substituted alkyne reported in the earlier study (Scheme 7).^[57] **3arm-Tri** was purified by column chromatography and received as an orange solid in good yield (47%) considering the three-fold coupling. Here, reflux in THF was essential to fully convert the 2-arm analogue into the octupolar compound (reaction monitoring by TLC). Comparable routes were described by Sonoda *et al.*^[61], however stating the reaction occurred at room temperature, and Braml *et al.* stating reflux conditions.^[62] The alternative route via Sonogahira cross-coupling using CuI, Pd(OAc)₂ and PPH₃ as catalyst in triethylamine according to Raut *et al.* proved not to be successful.^[63]

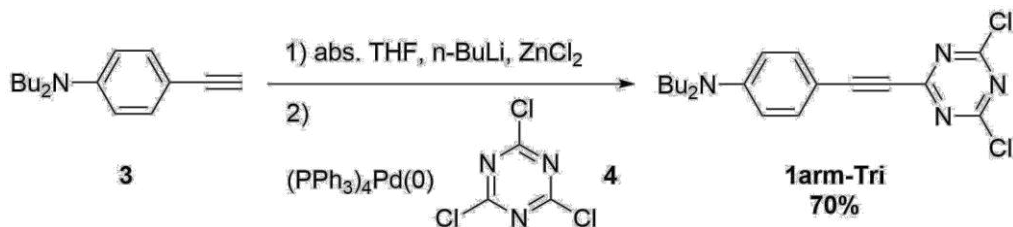


Scheme 7: „One-pot“-synthesis of octupolar 3armTri from cyanuric chloride 4 by Negishi cross-coupling.

Although the quadripolar disubstituted analogue **2-arm-Tri** was not required for the spectroscopic study, this molecule could be easily synthesized via Negishi cross-coupling at room temperature, since the conversion of **2arm-Tri** to **3arm-Tri** was traced during the synthesis of the latter by TLC and requires elevated temperature (reflux in THF).

1.2.3 Synthesis of dipolar triazine 1arm-Tri

Next, the dyad **1-armTri** was synthesized as described in the earlier study by Negishi cross-coupling reaction and was received as a red solid in 70% yield after column chromatography (Scheme 8).^[57]



Scheme 8: Synthesis of 1arm-TriCl₂ by Negishi cross-coupling.

In an initial synthesis attempt, a decomposition product of **1armTri** was discovered which readily formed over prolonged time in CDCl_3 solution (Figure 11, Figure 12). Chloroform can decompose to HCl and usually contains traces thereof. Svechkarev suggests purification by column chromatography using CHCl_3 as eluent.^[57] Following this procedure a HCl adduct to the alkyne of **1arm-Tri** (deep red solid) can form in increased yield, which was identified by $^1\text{H-NMR}$ and GCMS. Hence, elution using PE:DEE is highly advised.

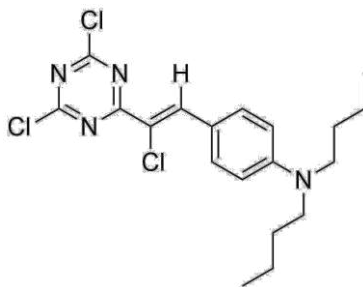


Figure 11: Most probable decomposition product of 1arm-TriCl₂ as identified by NMR and GCMS.

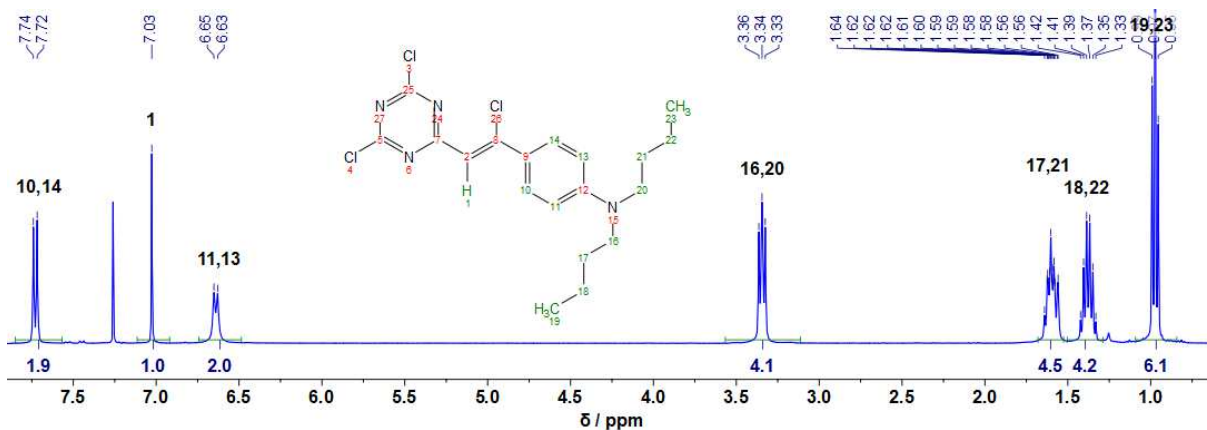


Figure 12: $^1\text{H-NMR}$ spectra of the HCl adduct of 1arm-TriCl₂.

1.3 Testing of 1,3,5-triazine-based dyes as two-photon initiators

Since the structurally related alkene-modified 1,3,5-triazines proved to be suitable initiators for two-photon polymerization,^[58] the newly synthesized alkyne analogues were tested as two-photon initiators as well. For that reason, sample solutions of the target molecules in a 1:1 (w/w) mixture of acrylate monomers trimethylolpropanetriacrylate (TTA, Genomer 1330) and ethoxylated-(20/3)-trimethylolpropane triacrylate (ETA, Sartomer 415) at the low concentration of 1 $\mu\text{mol g}^{-1}$ were prepared. Samples were drop casted onto methacrylate functionalized glass-bottom ibidi μ -dishes and then two-photon polymerized using a tunable fs-pulsed NIR-laser.

Arrays of μ -cubes ($100 \times 100 \times 100 \mu\text{m}^3$) at different writing speeds and laser powers were fabricated at 720 nm and 780 nm using a 10x / 0.4 NA microscope objective (Olympus). While 720 nm marks the lower end of the emission spectrum of tunable fs-pulsed Ti:Sapphire lasers, 780 nm represents the emission wavelength of compact high power fiber-based fs-lasers. The laser power was increased from 10-100 mW ($\Delta 10 \text{ mW}$) while the writing speed was varied from 100-900 mm s^{-1} ($\Delta 200 \text{ mm s}^{-1}$). The hatch and dz were maintained constant at 0.4 μm and 0.5 μm respectively.

After two-photon polymerization the arrays were examined by light microscopy first, and via laser scanning microscopy (LSM) after development with 2-propanol. In the latter case, the fluorescence emission signal of the two-photon chromophores embedded in the polymer network was exploited. As expected from the earlier study, the octupolar **3armTri** exhibited a much broader processing window at the low laser powers (<100 mW) investigated compared to the dipolar **1armTri**.^[58]

1.3.1 Two-photon polymerization in presence of 1armTri

The dipolar dye **1armTri** exhibited a small processing window at 720 nm with solid cubes preferably forming at high laser powers and low writing speeds (Figure 13). For instance, at 900 mm s^{-1} and 100 mW no stable cube formed. At 780 nm cubes exclusively formed at low writing speeds and high laser powers, but unfortunately detached from the glass support. Due to ongoing reconstructions of the z-Scan setup at the Institute of Materials Science and Technology the two-photon spectrum of compound **1armTri** could not be measured yet. Nevertheless, these results indicate a significantly higher two-photon absorption cross-section at 720 nm than at 780 nm.

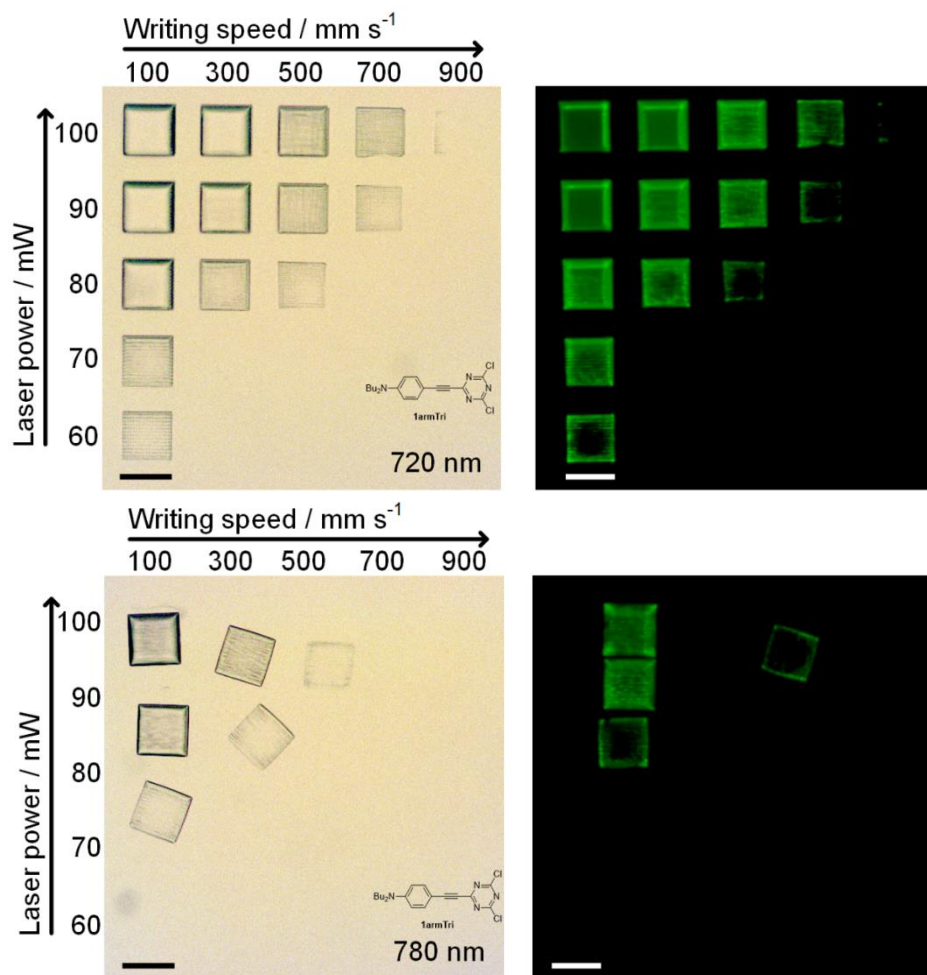


Figure 13: Arrays of cubes were two-photon polymerized from ETA:TTA in presence of 1armTri ($1 \mu\text{mol g}^{-1}$). The writing speed was increased from 100-900 mm s^{-1} along the x-axis, whereas the laser power was increased from 10-100 mW along the y-axis. Light microscopy images (left) were taken from the undeveloped resin. After development the cubes were examined by LSM (right).

1.3.2 Two-photon polymerization in presence of 3armTri

In contrast to the dipolar analogue, the octupolar **3armTri** showed a much broader processing window at both wavelengths using the same parameters. Polymerization occurred at all writing speeds, with the lower threshold of polymerization at 780 nm. Here, optimal shaped cubes could be created with a laser power of 40 mW at all writing speeds and even with 20 mW still a cube formed at 100 mm s^{-1} . At 720 nm overexposure leading to explosions occurred at laser powers above 60 mW and a low writing speed of 100 mm s^{-1} . These preliminary results demonstrate good two-photon initiation properties and indicate high two-photon absorption at both 720 nm and 780 nm. As overexposure occurs at lower writing speeds, this high performance two-photon initiator is especially applicable for high writing speeds, which poses a current key challenge in the development of multiphoton lithography.^[45]

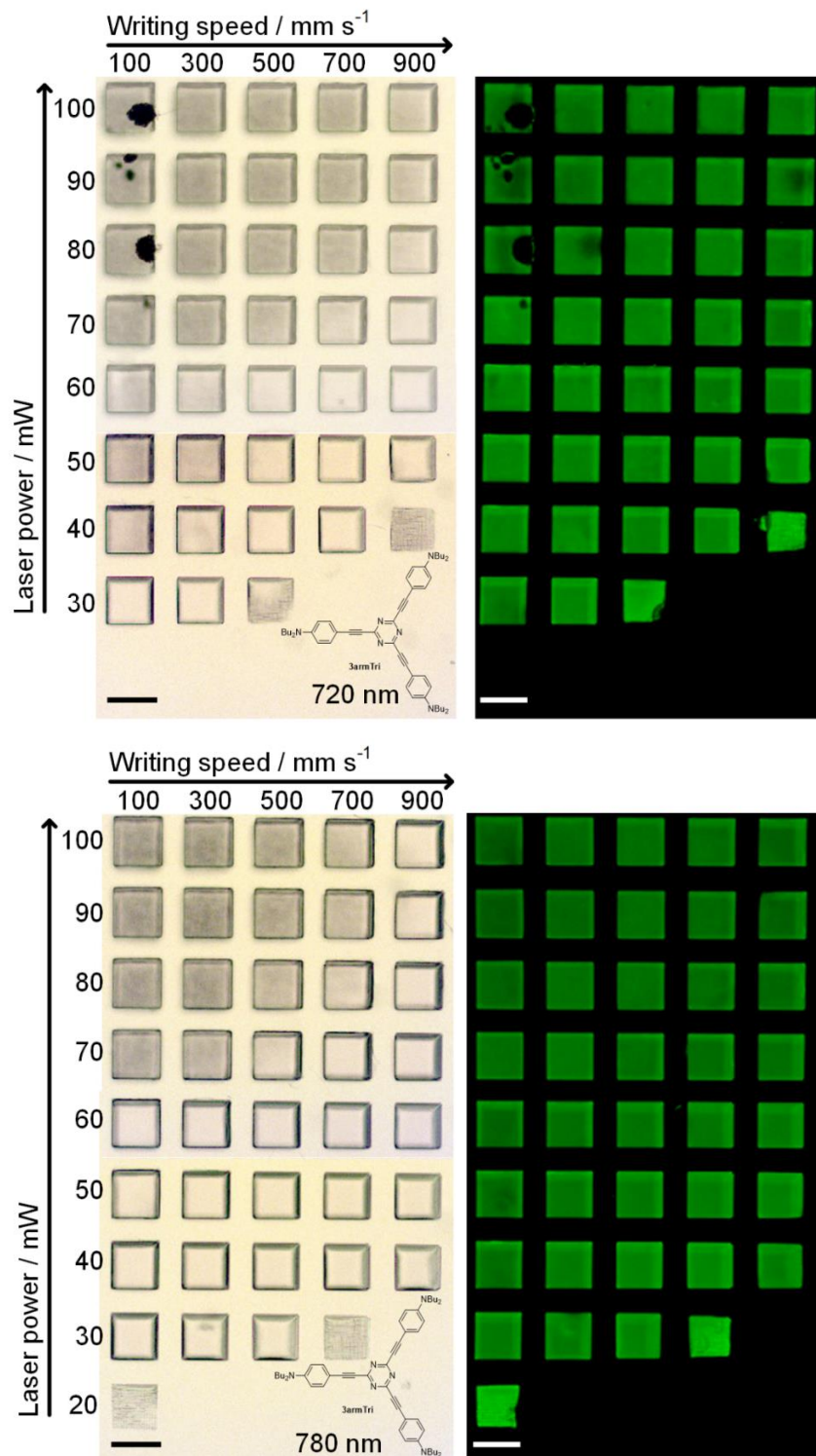


Figure 14: Arrays of cubes were two-photon polymerized from ETA:TTA in presence of 3armTri (1 $\mu\text{mol g}^{-1}$). The writing speed was increased from 100-900 mm s^{-1} along the x-axis, whereas the laser power was increased from 10-100 mW along the y-axis. Light microscopy images (left) were taken from the undeveloped resin. After development in 2-propanol the structures were examined by LSM (right).

1.4 Conclusion

Both target molecules have been synthesized successfully with substantial optimizations of the reaction procedure and work-up being done. Both compounds can be used as initiators for two-photon polymerization. However, the octupolar **3armTri** performs much better than the dipolar derivative, especially at high writing speeds. Moreover, it is also more versatile, as good polymerization results could be achieved at both 720 nm and 780 nm. These findings are in accordance with observations discussed in literature demonstrating that the two-photon absorption and performance is increasing with the number of branches when comparing a dipolar to an octupolar molecule.^[44, 58] For application in aqueous environment the target molecules can be modified with water-soluble functionalities instead of butyl groups in the future.^[49b]

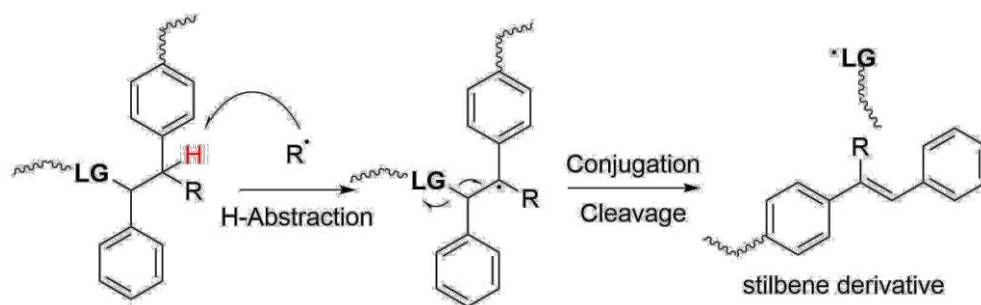
Samples of both compounds have been committed to the Vauthey research group at University of Geneva. A photophysical in-depth investigation of the compounds was performed and a manuscript is currently in preparation.

2. RADICAL FRAGMENTATION INDUCED BY HYDROGEN ATOM ABSTRACTION

2.1 State of the Art and Basic Considerations

While the inherent light-sensitivity of photocleavable functionalities, for example oNB- and coumarin-derivatives, allows for quick and simple irradiation-experiments, it can as well be considered a drawback, since it necessitates sample handling under light protection for the total course of the experiment and in particular light-based examination methods (e.g. microscopy) can be complicated.

Hence, a photocleavable molecular system, in which the light sensitivity is decoupled from the cleavable functionality would be an interesting approach. Such a system could be activated by addition of a small molecule photoinitiator modularly added to the system when needed. A option would be to create a molecular core unit that can be integrated into a polymer backbone, and which upon hydrogen atom transfer (HAT)^[64] responds with an intramolecular single electron transfer (SET) cascade,^[65] finally leading to fragmentation and therefore disintegration of the backbone. In order to design such a system, several driving factors should be included to provoke the occurrence of a SET cascade resulting in fragmentation. A reasonable driving factor might be the **(I) formation of a conjugated delocalized π -system** upon HAT. This event could be combined with an **(II) irreversible fragmentation of a covalent linkage** within the polymer backbone, for instance the decarboxylation of a carbonyl-based functional group. This way, a **(III) radical leaving group** should be formed, which tends to undergo subsequent hydrogen abstraction elsewhere on the polymer backbone initiating an iterative HAT-SET cycle. The key steps of such a cycle except decarboxylation are illustrated in Scheme 9.



Scheme 9: Expected hydrogen atom transfer-single electron transfer (HAT-SET)-fragmentation cascade.

Initiating radicals capable of hydrogen abstraction can either be generated thermally or photochemically by addition of an appropriate initiator or hydrogen abstractor and if necessary monomer. Within the scope of this work only photochemical initiation should be considered.

2.2 Molecular Design and Synthesis – Symmetric Approach

As the radical fragmentation unit would be integrated into a polymer backbone on multiple sites, simple and convenient synthetic strategies from inexpensive starting materials should be utilized here. Based on this consideration, two symmetric small molecule test compounds were synthesized from *meso*-hydrobenzoin **1** with either two ester or two carbonate functionalities (Scheme 10). Due to the symmetry, this strategy allows for modification with polymerizable side chains in order to integrate this core group into a polymer backbone by substituting the *tert*-butyl group **R** with an appropriate polymerizable or conjugatable moiety (e.g. azides, (meth)acrylates, thiols, etc.). Decarboxylation of the test compounds should result in the formation of a stilbene derivative as indicated in Scheme 9.

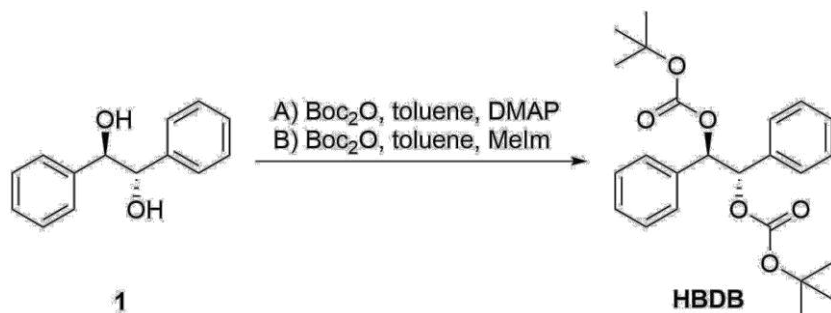


Scheme 10: Modification of *meso*-hydrobenzoin **1 to the symmetric test molecules by esterification. The R-groups could be exchanged for a functionality allowing to form a linkage.**

The synthesis of the ester derivative **HBDP** was realized by esterification with pivaloyl chlorid **2**, since after decarboxylation of the ester a stabilized tertiary radical (*tert*-butyl radical) is formed and due to its commercial availability (Scheme 10). The carbonate analogue **HBDB** was introduced by reaction with di-*tert*-butyl dicarbonate Boc₂O, since this reagent is readily available and, what is more, because of its common use as protecting agent various very convenient protocols for its application do exist.^[66] Decarboxylation of **HBDB** would give a *tert*-butyloxy radical.

2.2.1 Synthesis of *meso*-O,O'-diBoc-hydrobenzoin **HBDB**

The test molecule **HBDB** was synthesized following two protocols by Basel and Hassner using either 4-dimethylaminopyridine DMAP or 1-methylimidazole Melm as base and toluene as solvent (Scheme 11).^[66] The reaction mixtures were stirred at room temperature and the progress of the reaction was controlled by GCMS.

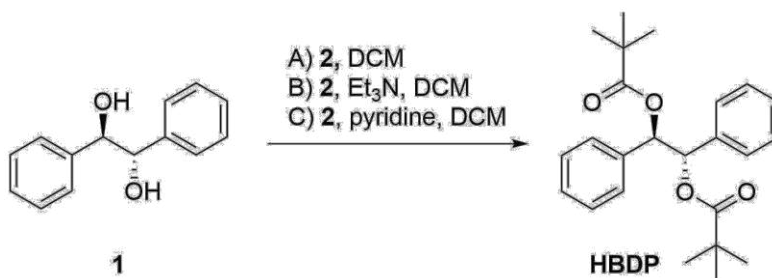


Scheme 11: Synthetic approaches towards HBDB.

As it turned out, **HBDB** decomposes in the course of the GCMS run giving a deceiving chromatogram. For that reason, the reactions were unnecessarily maintained for 9 days, although a reaction time of below 18 h would have been sufficient. Nevertheless, both syntheses yielded a clean white solid product only after liquid-liquid extraction in excellent yields (>95%).

2.2.2 Synthesis of meso-hydrobenzoin dipivalinate HBDP

For the synthesis of **HBDP** three different procedures were tested including neat and base catalysed reaction conditions.



Scheme 12: Synthetic approaches towards HBDP.

A recent publication by Rao *et al.* entitled “An Efficient Protocol for Alcohol Protection Under Solvent- and Catalyst-Free Conditions” stated the synthesis of compound **HBDP** under neat and almost equimolar conditions (1.1 eq per functional group) at room temperature within 15 min.^[67] However, as the reaction batch size was rather small (1 mmol), it was considered beneficial to perform this reaction in concentrated solution (DCM) rather than in a slurry to avoid issues caused by stirring. Under this condition, the reaction did not proceed as quick as described and according to GC-MS analysis almost only conversion to the mono-functionalized product was achieved overnight. The reaction was therefore dismissed and a modified protocol by Marshall and Xie describing the conversion of (*R,R*)-hydrobenzoin with acryloyl chloride to the corresponding bisacrylate in the presence of triethylamine was performed.^[68] The reaction was maintained overnight according to the protocol. Since reaction control by GC-MS was unclear, crude $^1\text{H-NMR}$

was performed revealing only 40% conversion to the mono-substituted product. Finally **HBDP** was synthesised according to the Einhorn-Variante of the Schotten–Baumann reaction^[69] over the course of one week by using pyridine as base and 2.5 eq of pivaloyl chloride **2**.¹ The product was purified by recrystallization from EtOH yielding 51% of a fluffy white solid.

2.2.3 Reactivity testing of target compounds via ¹H-NMR-experiments

In order to test the reactivity of the target compounds towards the anticipated HAT-SET fragmentation cascade, the test molecules **HBDP** or **HBDB** were irradiated with UV/VIS–light in benzene-*d*₆ solution in presence of either monomer and PI or a hydrogen abstractor and then analysed by ¹H-NMR. Monomers with moderate reactivity, thus forming reactive radicals, as for e.g. methacrylates, vinyl esters and vinyl ethers were used in combination with the type I photoinitiator Ivocerin® to provide a sufficient radical concentration for HAT to occur, while hydrogen abstractors as camphorquinone, benzophenone and ITX were expected to directly abstract hydrogen from the test compounds. Moreover, the reactions containing monomers were also conducted in the presence of an equimolar amount of thiol.

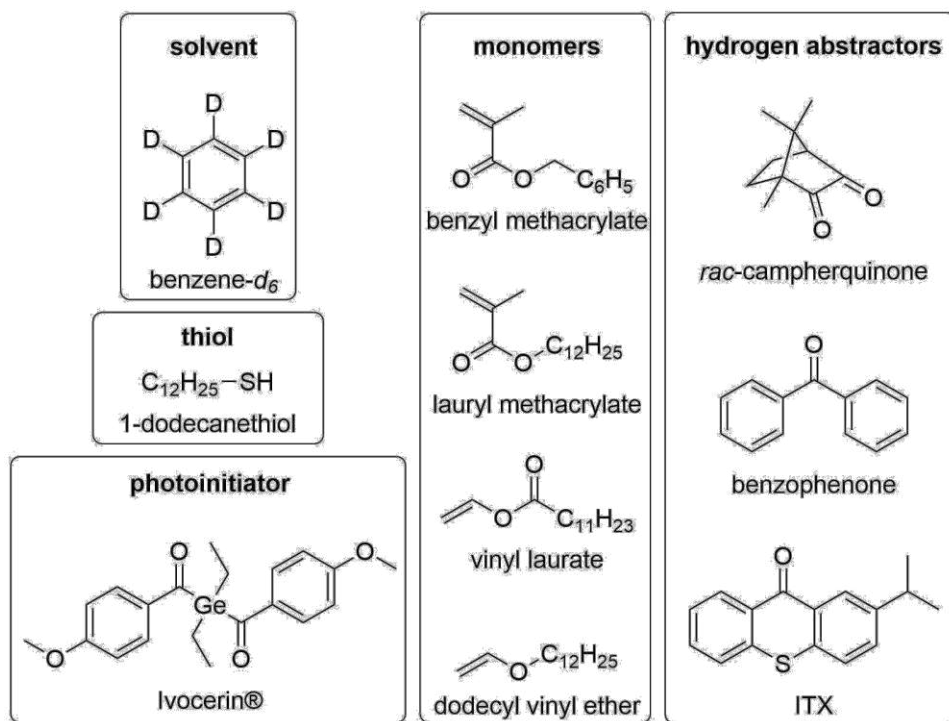


Figure 15: Reagents and reactants used in the ¹H-NMR model reactions.

¹Given this circumstances, in case the product shall be synthesized again the neat method should be reconsidered.

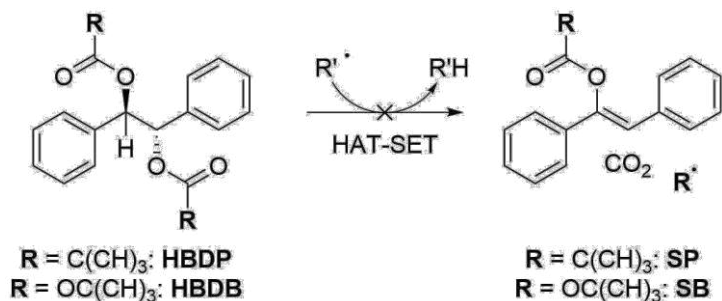
2.2.4 ¹H-NMR-experiments of symmetric test molecules HBDB and HBDP

To test the concept, the symmetric test compounds **HBDB** or **HBDP** were either reacted with photoinitiator Ivocerin® (4 mol%, Mixture A), monomers (4 eq, Mixtures B) or combinations of monomer (4 eq) and thiol (4 eq, Mixtures C) in presence of Ivocerin®. Moreover, the compounds were also irradiated in presence of hydrogen abstractor benzophenone (1 eq, Mixture D1). The compositions of the individual reaction mixtures are listed in Table 1. The symmetric test compounds and the corresponding reactants were dissolved in benzene-*d*₆ in GCMS vials and degassed for about 5 min with argon before they were either irradiated for 10 min in an Ivoclar Vivadent irradiation apparatus using program P2 for initiation of Ivocerin® or with a Lumen Dynamics OmniCure® S2000 UV-curing system with an intensity of 3 W cm⁻² (320-500 nm) in the case benzophenone was applied. During the degassing process, some solvent evaporated. As this were preliminary tests, only intended to proof the concept rather than a systematic study, such fluctuations of concentrations were ignored. After irradiation, the samples were diluted with benzene-*d*₆ to provide sufficient volume for ¹H-NMR measurements.

Table 1: Reactivity screening of symmetric test compounds HBDB and HBDP. All mixtures were initially dissolved in 0.8 mL benzene-*d*₆.

Mixture	Test compound	Monomer (4 eq)	Thiol (1 eq)	Photoinitiator / Hydrogen abstractor
A	HBDB / HBDP (1 eq)	–	–	Ivocerin (4 mol%)
B1		benzyl methacrylate	–	
B2		vinyl laurate	–	
B3		dodecyl vinyl ether	–	
C1		lauryl methacrylate	dodecylthiol	
C2		vinyl laurate		
C3		dodecyl vinyl ether		
D		–	–	benzophenone (1 eq)

In none of these experiments, the formation of the corresponding stilbene fragmentation product **SB** or **SP** nor the respective *tert*-butanol or *tert*-butane fragment of symmetric test compounds **HBDB** or **HBDP** could be observed (Scheme 13).



Scheme 13: Anticipated but not observed HAT-SET fragmentation of symmetric test compounds HBDB and HBDB.

A possible explanation for these results could be based on the steric hindrance of the two relevant H-atoms caused by the bulky adjacent phenyl and *tert*-butyl groups. A possibility to circumvent this limitation but conserve the molecular constellation of the core concept would be an asymmetric approach, in which only one of the two hydroxyl-groups is modified with a respective leaving group in order to reduce the steric hindrance.

2.3 Molecular design and synthesis – asymmetric approach

The asymmetric functionalisation of hydrobenzoin **1** is synthetically convenient, since the already established protocols with adapted equivalents of reactants from the symmetric approach can be used. An overall drawback of the asymmetric strategy is the synthetically more challenging further derivatisation of the core unit to permit integration into a polymer backbone due to the loss of symmetry. Therefore, one of the two macromers has to be connected to the core unit *via* the leaving group, whereas the other must be bound to one of the phenyl moieties or to the free hydroxy group (Figure 16). As the asymmetric core unit contains only one potentially cleavable bond, the efficiency of the network cleavage process is formally reduced.

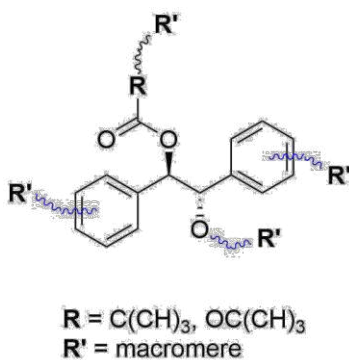
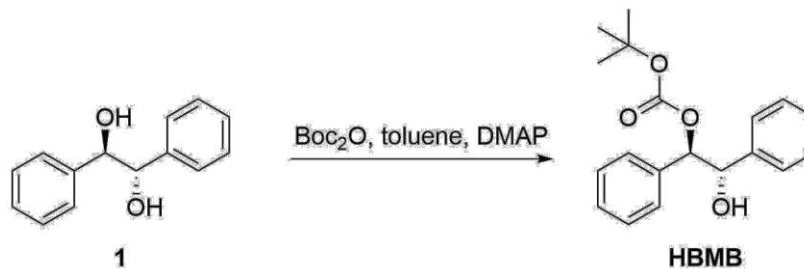


Figure 16: Possible attachment points for macromer moieties on an asymmetric core unit in blue. One branch (black) must certainly be connected *via* the leaving group R to permit degradation of the network.

2.3.1 Synthesis of *meso*-O-mono-Boc-hydrobenzoin **HBMB**

HBMB was synthesized according to a modified procedure from Basel and Hassner.^[66]



Scheme 14: Synthesis of HBMB.

Hydrobenzoin **1** was reacted with 1.01 eq Boc_2O and 0.13 eq DMAP in dry toluene at room temperature (Scheme 14). After 2 h TLC indicated full consumption of starting material and the reaction mixture was worked up. Crude $^1\text{H-NMR}$ revealed that the extracted solid consisted of starting material **1** (16%), desired product **HBMB** (66%) and difunctionalized product **HBDB** (16%, 1:4:1). Separation was performed by silica column chromatography yielding **HBMB** (56%) as a white solid.

2.3.2 Synthesis of *meso*-hydrobenzoin monopivalinate **HBMP**

HBMP was synthesised following a modified protocol of the synthesis of **HBDP**.



Scheme 15: Synthesis of HBMP.

Here, **1** was converted using 2 eq of pivaloyl chloride **2** in presence of pyridine (Scheme 15). After a reaction time of 24 h the formation of both mono- and diester (**HBMP** and **HBDP**) was confirmed by GCMS. Purification *via* silica column chromatography yielded **HBMP** (61%) as a white solid.

2.3.3 $^1\text{H-NMR}$ test-experiments of asymmetric test molecule **HBMB**

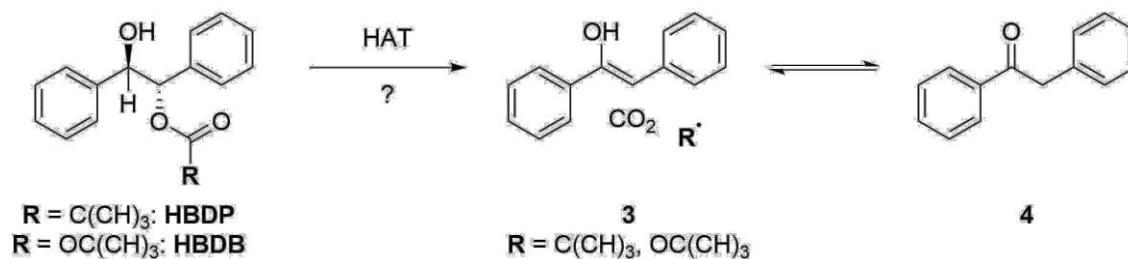
The $^1\text{H-NMR}$ test-experiments of **HBMB** were realized in a similar manner as those of the symmetric test molecules. The sample mixtures were irradiated for 10 min in an Ivoclar Vivadent irradiation apparatus using program P2 for initiation of Ivocerin®. The mixtures containing hydrogen abstractors were irradiated using a Lumen Dynamics OmniCure® S2000 UV-curing

system with an intensity of 1 W cm⁻² (320-500 nm). The experiment with benzophenone was also conducted at 3 W cm⁻². An overview of the individual reaction mixtures is given in Table 3.

Table 2: Reactivity screening of HBMB: All mixtures were dissolved in 0.8 mL benzene-*d*₆.

Mixture	Test compound	Monomer (4 eq)	Thiol (1 eq)	Photoinitiator / Hydrogen abstractor
A	HBMB (1 eq)	–	–	Ivocerin (4 mol%)
B1		lauryl methacrylate	–	
B2		vinyl laurate	–	
B3		dodecyl vinyl ether	–	
C1		lauryl methacrylate	dodecylthiol	
C2		vinyl laurate		
C3		dodecyl vinyl ether		
D1		–	–	benzophenone (1 eq)
D2		–	–	ITX (1 eq)
D3		–	–	campherquinone (1 eq)

Finally, only in the formulation containing benzophenone a significant effect of irradiation could be observed. Scheme 16 depicts the expected fragmentation sequence of the asymmetric test molecules. As no relevant literature entries concerning enol **3** could be found, it is anticipated that in case of fragmentation a signal of tautomeric ketone **4** should be observed in the ¹H-NMR-spectrum of the irradiated formulation.



Scheme 16: Expected fragmentation product of asymmetric test compounds. As, there are no significant literature entries concerning enol **3, it is anticipated that ketone **4** forms after tautomerisation.**

However, in the ¹H-NMR spectrum of the irradiated sample an intense signal possibly corresponding to the fragment *tert*-butanol in benzene-*d*₆ could be observed^[70] (Figure 17 and Figure 18) with the ratio between *tert*-butyl and *tert*-butanol being 11.8 : 13.8.

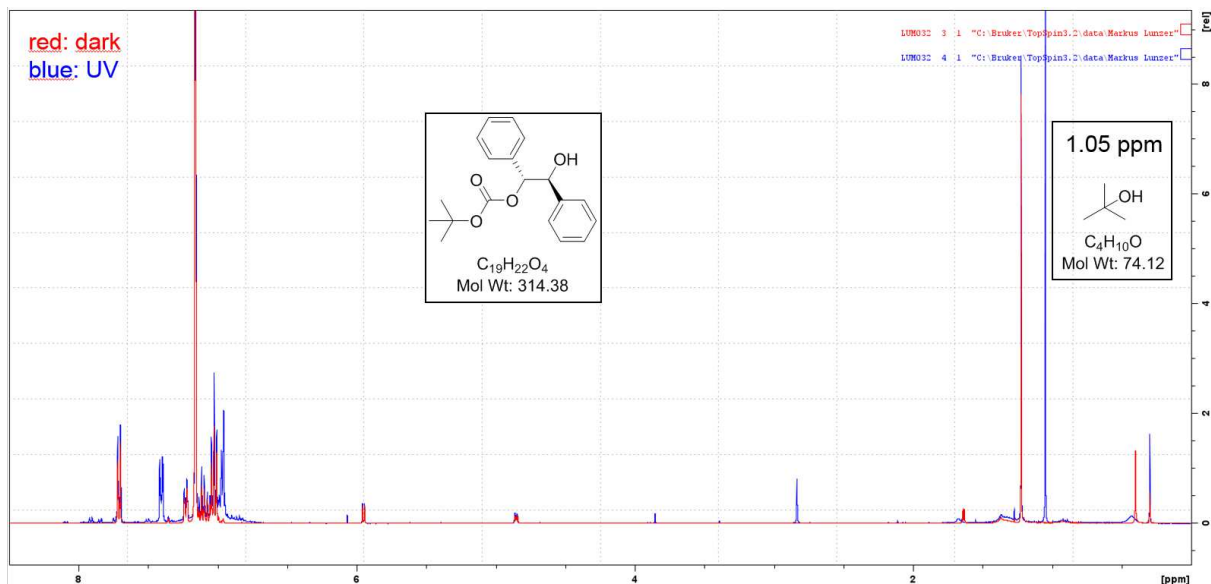


Figure 17: Overlay of $^1\text{H-NMR}$ spectra of non-irradiated sample (red) and irradiated sample (blue) of the formulation containing benzophenone and HBMB in benzene- d_6 . The sample was irradiated with an intensity of 1 W cm^{-2} .

A closer look at the spectrum of the irradiated sample reveals that the ratio of the two aliphatic protons of **HBMB** (4.85 ppm and 5.95 ppm) remained unaltered, whereas the integral of the *tert*-butyl group relatively increased to 11.8 (Figure 18). Also the OH-signal flattened out somewhat. However, no signal, which could be possibly correlated to ketone **4** was detected.

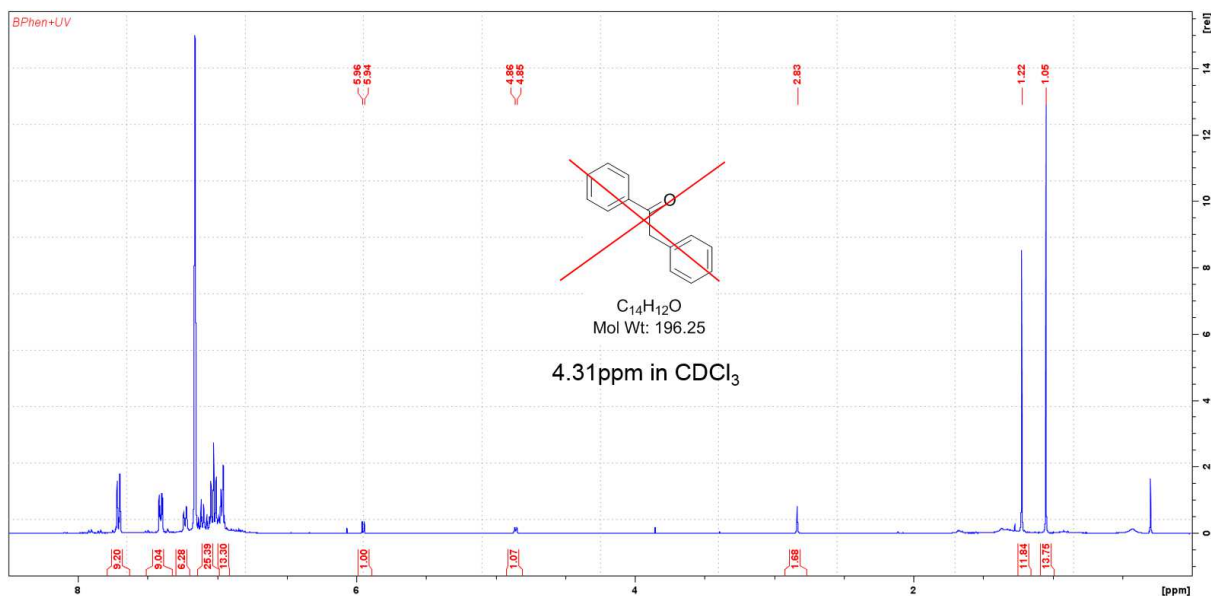


Figure 18: $^1\text{H-NMR}$ spectra of irradiated sample containing benzophenone and HBMB in benzene- d_6 . The intensity of irradiation was 1 W cm^{-2} . No signal which, could be related to ketone **4** is present. The reference value of 4.31 ppm of the α -carbonyl protons in CDCl_3 was taken from Dong *et al.*^[71]

The relatively intense singlet at 2.83 ppm was also present in the spectrum of an irradiated sample containing only benzophenone in benzene- d_6 (**Figure 19**) and is thus considered to originate from a fragmentation product thereof.²

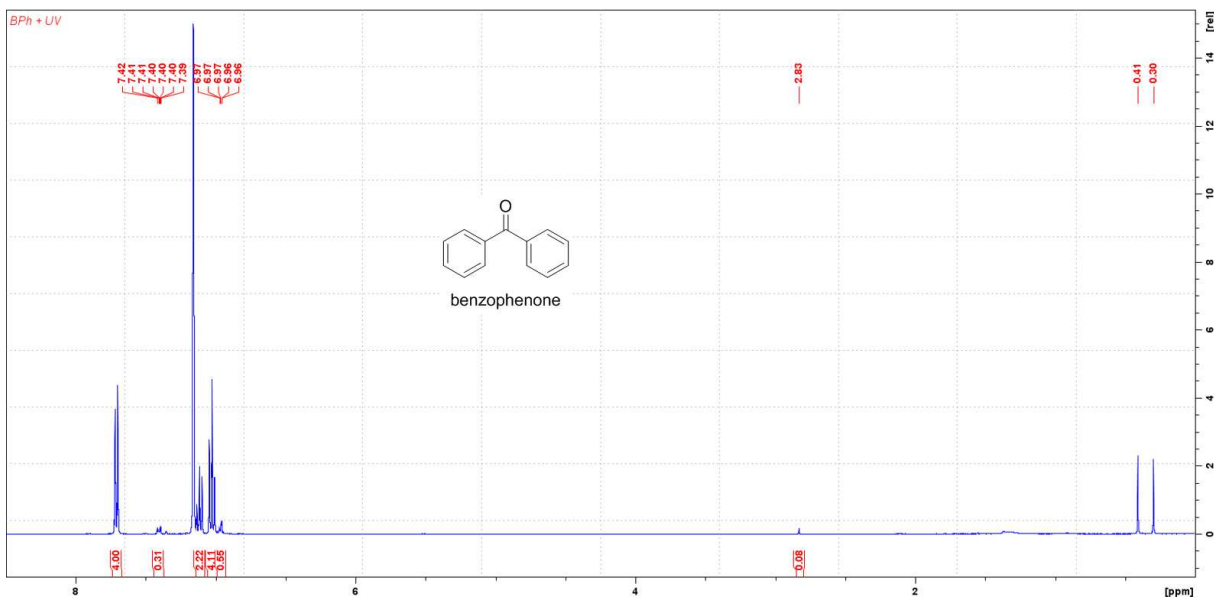


Figure 19: $^1\text{H-NMR}$ spectra of an irradiated solution of benzophenone in benzene- d_6 . The sample was irradiated with an intensity of 3 W cm^{-2} for 10 min.

2.3.4 $^1\text{H-NMR}$ -experiments of *meso*-hydrobenzoin monopivalinate **HBMP**

The $^1\text{H-NMR}$ -test-experiments of *meso*-hydrobenzoin monopivalinate **HBMP** were realized in a similar manner as those before. **HBMP** was irradiated in combination with equimolar amounts of hydrogen abstractors benzophenone, ITX or *rac*-champhorquinone in benzene- d_6 using a Lumen Dynamics OmniCure® S2000 UV-curing system with an intensity of 1 W cm^{-2} (320-500 nm). The experiment with benzophenone was also repeated at 5 W cm^{-2} . Since the reactions including Ivocerin® and monomer gave no positive result with **HBMB**, these were not repeated with **HBMP**. Table 4 gives an overview of the reaction mixtures.

Table 3: Reactivity screening of **HBMP**: All mixtures were initially dissolved in 0.8 mL benzene- d_6 .

Mixture	Test compound	Hydrogen abstractor
D1	HDMP	benzophenone
D2		ITX
D3		campherquinone

² Other singlets, which may appear to have a certain intensity in Figure 19 could not be reproduced as prominent in a second irradiation experiment using 3 W cm^{-2} (not depicted).

As in the previous experiments with **HBMB** significant alterations of the ^1H -NMR spectrum of the irradiated formulation containing **HBMP** and benzophenone compared to the dark sample could be observed (Figure 20).

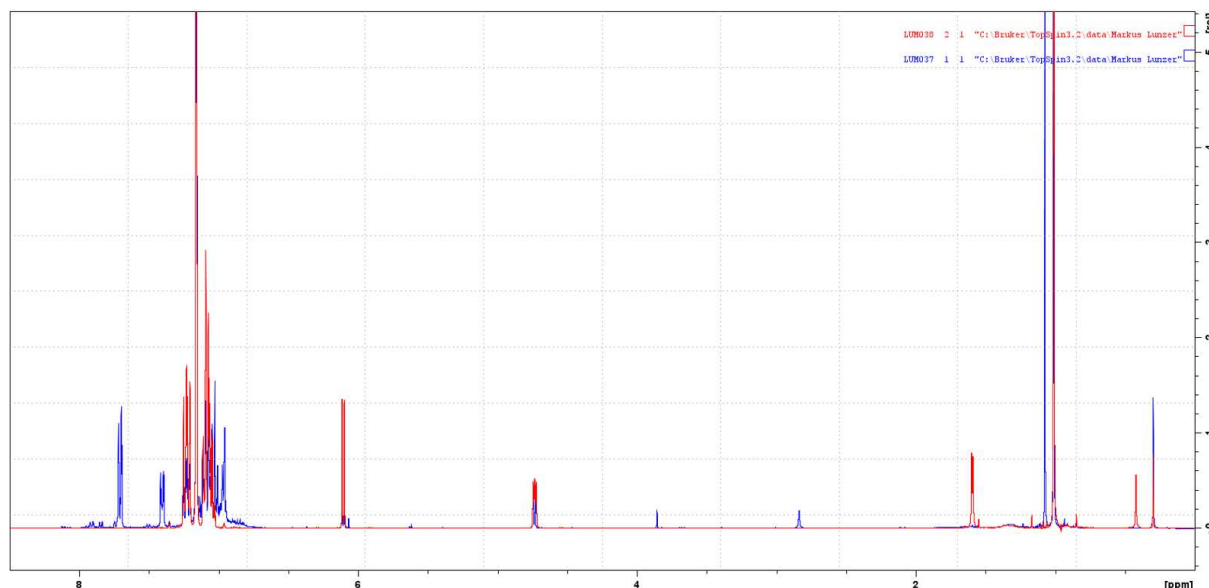


Figure 20: Overlay of ^1H -NMR spectra of non-irradiated sample (red) and irradiated sample (blue) of the formulation containing benzophenone and HBMP in benzene- d_6 . The sample was irradiated with an intensity of 1 W cm^{-2} .

The irradiated sample again shows an intense signal in the aliphatic region, in this case at 1.07 ppm (Figure 21). This signal does not correspond to the reference values of the volatile fragment isobutane [^1H -NMR (250 MHz, C_6D_6): $\delta = 1.637$ (dectet, $J = 6.6 \text{ Hz}$, 1H), 0.863 (d, $J = 6.6 \text{ Hz}$, 10H)].^[72] Furthermore, the singlet at 2.83 ppm is present as well. A noteworthy fact is the disappearance of the OH-signal at 1.60 ppm after irradiation. Besides, no other relevant signals are present, which could correspond to ketone **4**. Moreover, irradiation at 5 W cm^{-2} did not provoke any further changes in the spectrum (Figure 22).

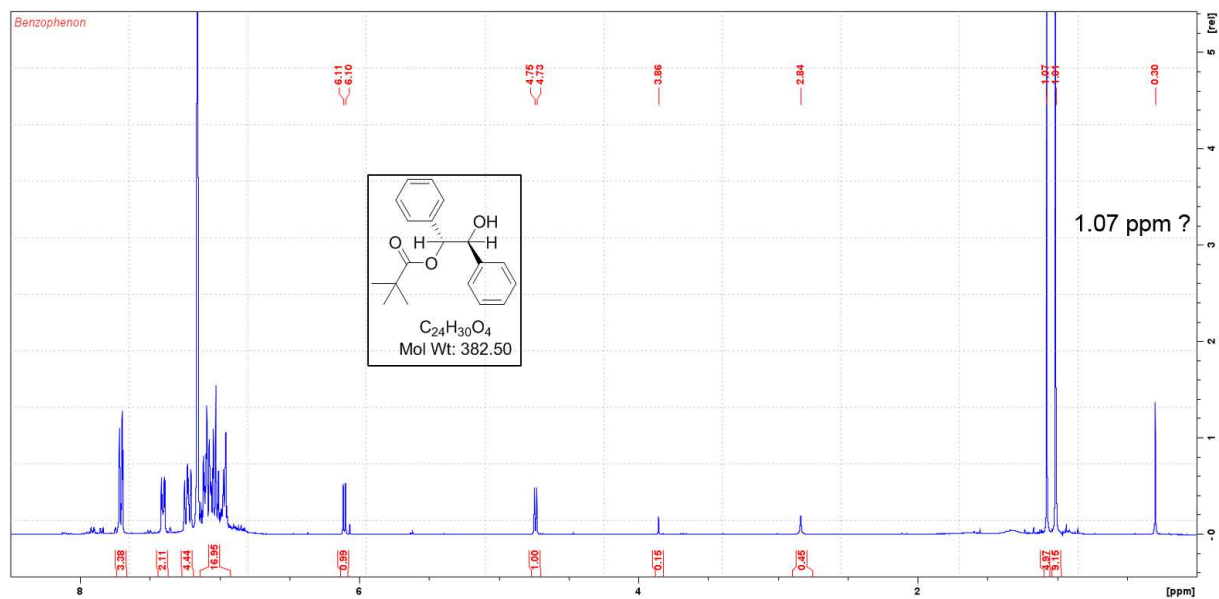


Figure 21: $^1\text{H-NMR}$ spectra of the irradiated sample containing benzophenone and HBMP in benzene- d_6 . The intensity of irradiation was 1 W cm^{-2} . No signal which can be related to ketone 4 is present.

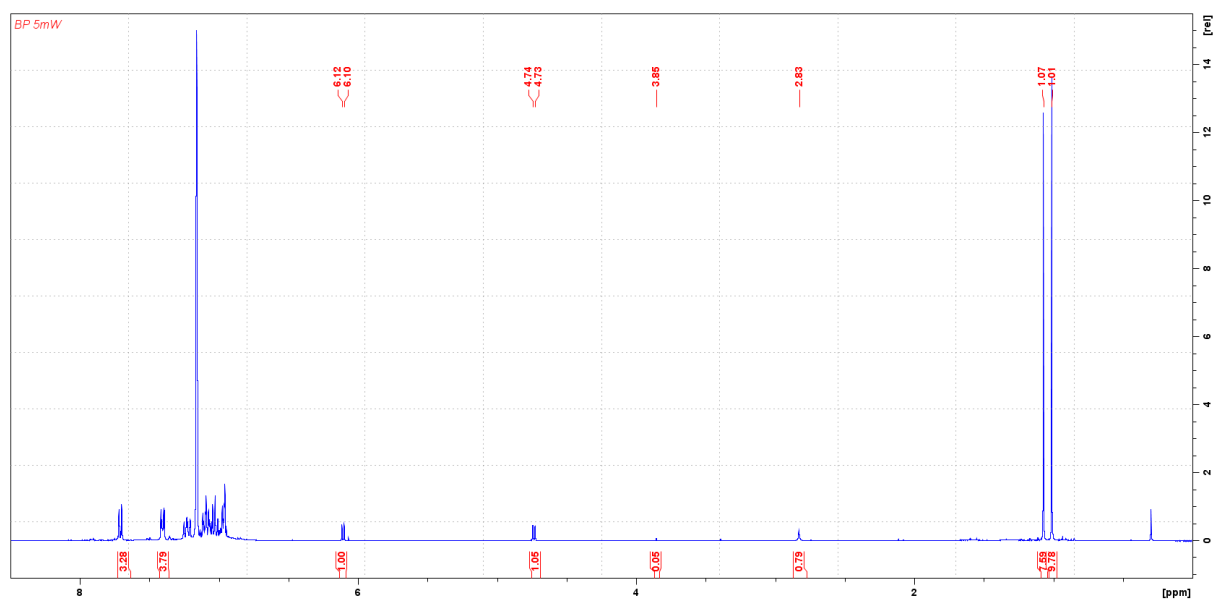


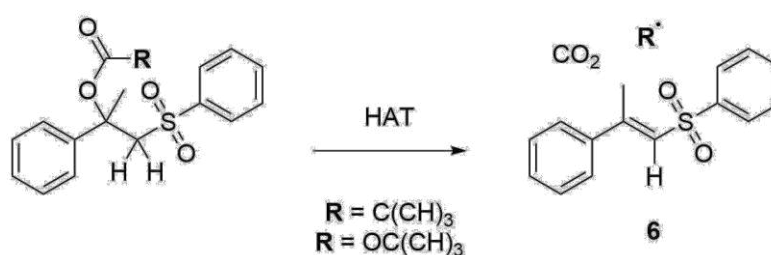
Figure 22: $^1\text{H-NMR}$ spectra of the irradiated sample containing benzophenone and HBMP in benzene- d_6 . The intensity of irradiation was 5 W cm^{-2} . No signal which can be related to ketone 4 is present.

Contrary to the symmetric test molecules, in the case of the asymmetric compounds some reaction did occur in the course of irradiation in the presence of benzophenone. Nevertheless, no relevant fragmentation product of the investigated compounds could be detected *via* $^1\text{H-NMR}$

measurement. GC-MS measurement of the NMR-samples did not give any useful information except the presence of benzophenone.

2.4 EWG-conjugation Approach

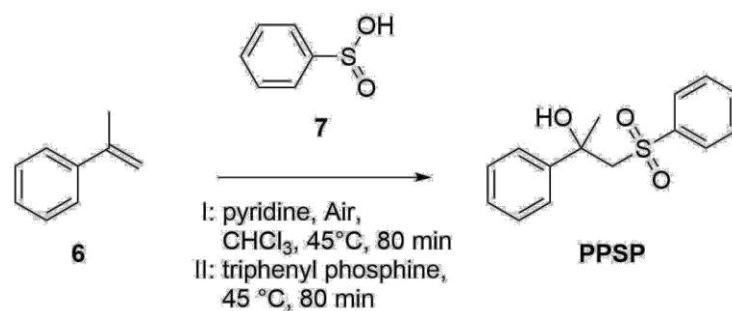
A further approach is based on derivatives of 2-phenyl-1-(phenylsulfonyl)propan-2-ol (**PPSP**), which is easily accessible *via* aerobic oxysulfonylation from α -methylstyrene and phenylsulfonic acid.^[73] At this asymmetric compound HAT can only occur in α -position to the electron withdrawing group (EWG) sulfone resulting in the formation of a delocalized π -system. Again, decarboxylation could be a second driving force in this concept. The resulting compound resembles stilbene, but contains an additional sulfonyl functionality in the conjugated system (Scheme 17).



Scheme 17: HAT from PPSP derivative would result in a delocalized π -system 5 in which the electron withdrawing group (EWG) phenyl sulfonyl is conjugated with phenyl *via* vinylene.

2.4.1 Synthesis of 2-Phenyl-1-(phenylsulfonyl)propan-2-ol (PPSP)

PPSP was synthesized according to Lu *et al.*^[73]



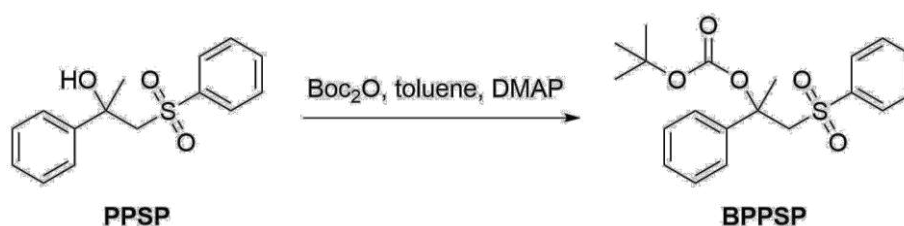
Scheme 18: Synthesis of **PPSP** by aerobic oxysulfonylation of styrene **6** with phenylsulfonic acid **7**.

PPSP was synthesized according to Lu *et al.*^[73] α -Methylstyrene **6** was reacted with 2.0 eq of phenylsulfonic acid **7** and 0.9 eq of pyridine in chloroform in the presence of air at 45°C for 2 days. Then 1.0 eq of triphenylphosphine was added for reduction of intermediately formed hydroxy peroxide (Scheme 18).^[73] Purification was performed by silica column chromatography giving **PPSP** (63%) as a white solid.

The reaction time of 2 days clearly exceeded the 80 min reported in literature. A possible explanation for this deviation could be that the applied α -methylstyrene contained 15 ppm *p*-tert-butylcatechol as inhibitor. In literature, the presence of this inhibitor is not stated and must therefore be considered as absent. For further experiments this inhibitor should be removed from α -methylstyrene prior to synthesis by washing with 1 N aqueous NaOH followed by vacuum distillation. Furthermore, the presence of crystal water in the solid sulfinic acid has not been investigated before the reaction. Afterwards a melting interval from 68-79°C instead of a melting point at 83-84°C has been observed indicating the presence of crystal water. An attempt to dry sulfinic acid $x n H_2O$ by dissolving in toluene and subsequently drying in vacuum to remove water resulted in a colour change of the colourless solution to dark yellow.

2.4.2 Synthesis of O-Boc-2-Phenyl-1-(phenylsulfonyl)propan-2-ol (BPPSP)

Compound **BPPSP** was synthesized according to an adopted protocol from Basel and Hassner.^[66]



Scheme 19: Synthesis of BPPSP.

Sulfone **PPSP** was reacted with 1.25 eq of Boc_2O and 0.1 eq DMAP in dry toluene at room temperature overnight (Scheme 19). Full conversion of starting material was confirmed by GCMS and the off-white solid product (97%) was isolated only by washing with 5% aqueous HCl and evaporation of the solvent.

2.4.3 $^1\text{H-NMR}$ -test-experiments of BPPSP

The $^1\text{H-NMR}$ -test-experiments of **BPPSP** were realized in a similar manner as before. The formulations were either irradiated for 10 min in an Ivoclar Vivadent irradiation apparatus using program P2 for initiation of Ivocerin®. When hydrogen abstractors were investigated, a Lumen Dynamics OmniCure® S2000 UV-curing system with an intensity of 3 W cm^{-2} (320-500 nm) was used. Experiments including thiols were not repeated. Table 4 gives an overview of the investigated reaction mixtures. None of these experiments gave a positive result.

Table 4: Reactivity screening of BPPSP: All mixtures were initially dissolved in 0.8 mL benzene-d₆.

Mixture	Test compound	Monomer (4 eq)	Thiol (1 eq)	Photoinitiator / Hydrogen abstractor
A	BPPSP (1 eq)	–	–	Ivocerin (4 mol%)
B1		lauryl methacrylate	–	
B2		vinyl laurate	–	
B3		dodecyl vinyl ether	–	
D1		–	–	benzophenone (1 eq)
D2		–	–	ITX (1 eq)
D3		–	–	campherquinone (1 eq)

2.5 Conclusion

Apparently, the hypothesized HAT-SET fragmentation mechanism does not work upon simple radical mediated hydrogen abstraction. This could be either due to sterical hindrance of H-abstraction or due to thermodynamic barriers. Quantum calculations could give further evidence here. However, as these molecular systems do not easily cleave under these simple experimental conditions in solution, this type of fragmentation is not considered robust enough for application in polymer networks, especially in hydrogels. Hence, this approach was not further investigated.

3. WATER-SOLUBLE AFCT REAGENTS FOR CLEAVAGE OF DISULFIDE NETWORKS

3.1 State of the Art

Disulfide linkages are of particular interest, as they can be reversibly formed and cleaved and have an essential function in the stabilization of biomaterials such as proteins. Generally, cleavage and remodelling of disulfide-based networks relies on the thiol-disulfide metathesis reaction,^[74] in which either a thiyl radical or a thiol anion reacts with a disulfide by forming a new disulfide and releasing a sulfur-species. This reaction can be induced chemically by the use of an excessive amount of a thiol-containing component via a nucleophilic attack or photochemically at high UV-light intensities. Due to their reversible character, disulfide networks are dynamic and therefore exhibit self-healing properties.^[25d, 75]

3.1.1 Chemical-induced disulfide cleavage

Prestwich and co-workers presented a synthetic mimic of the extracellular matrix (sECM) based on disulfide-containing polyethylene glycol diacrylate block copolymer cross-linkers, which were used to cross-link thiol-modified hyaluronan and gelatine macromers in the presence of cells. User-controllable decomposition permitting rapid recovery of viable cells under mild, non-enzymatic conditions was facilitated by thiol-disulfide exchange using an excess of *N*-acetyl-cysteine or glutathione to dissociate the reductively cleavable hydrogels.^[76]

In an earlier work, Tsarevsky and Matyjaszewski demonstrated the cleavage of internal disulfide bonds of a polymer by reduction with dithiothreitol (DTT) to the corresponding thiol. Re-oxidation to the corresponding disulfide-linkage was performed with FeCl_3 .^[77]

Singh and Whitesides developed several dithiol reagents for reduction of disulfides, which provide a higher reactivity than DTT including *N,N'*-dimethyl-*N,N'*-bis(mercaptoacetyl) hydrazine (DMH) and bis(2-mercaptoethyl)sulfone (BMS) (Figure 23). The design of these dithiol reagents is based on two requirements: (i) a low value of pK_a (~ 7 to 8) of their thiol groups and (ii) a high reduction potential.^[78] In another attempt disulfide linkages in polymers were directly reduced by reducing agents such as NaBH_4 .^[79]

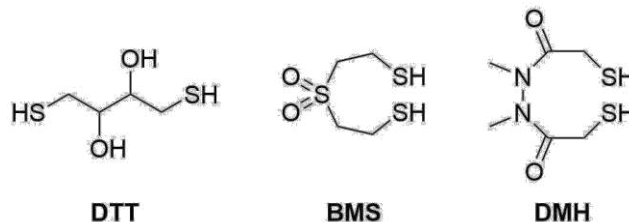


Figure 23: Molecular structures of dithiothreitol (DTT), N,N'-dimethyl-N,N'-bis(mercaptoacetyl)hydrazine (DMH) and bis(2-mercaptoethyl)sulfone (BMS).

3.1.2 Photochemical-induced disulfide cleavage

Direct photochemical scission of disulfides can be induced by high intensity UV-irradiation utilising the radical disulfide metathesis reaction. Otsuka *et al.* presented a dynamic covalent polymer driven by disulfide metathesis upon photoirradiation.^[80] For this purpose, two disulfide-containing polyesters containing no chromophores but different molecular weights were irradiated using a 400 W high-pressure mercury lamp with the maximum peak of the radiation intensity at 365 nm. In this study, also a model reaction was carried out, in which equimolar quantities of alkyl disulfides were photoirradiated for 1 h in deaerated THF (0.1 mol L⁻¹) at 30 °C, and the progress of the reaction was monitored by HPLC analysis. The authors observed a molar product equilibrium after 1 h near the statistical product ratio (1:2:3 = 24:27:49).

Based on the same concept, Anseth and co-workers have developed a photodegradable, photoadaptable hydrogel exploiting the radical-mediated disulfide fragmentation reaction induced by a photoinitiator.^[25d] Hydrogels were formed by the oxidation of thiol-terminated 4-armed PEG macromolecules using 1% H₂O₂ and 1 mM NaI. These disulfide cross-linked hydrogels were then swollen in a lithium acylphosphinate (LiTPO) photoinitiator (PI) solution. Upon exposure to light, radicals formed from the scission of the photoinitiator attacked and cleaved disulfide bonds liberating thiyl radicals, which then again underwent fragmentation and exchange reaction with other disulfides. Depending on the ratio of radicals to sulfur atoms in the gel either photodeformation, photowelding, or photodegradation was induced. When the concentration of radicals generated by the initiator was in the order of the concentration of sulfur atoms in the network, the network could be completely degraded into soluble PEG segments. Thus, degradation of hydrogels up to 2 mm thickness was possible within 120 s at low light intensities (10 mW cm⁻² at 365 nm). If, however, the number of radicals generated was much less than the number of sulfur atoms in the gel (accomplished by limiting the initial photoinitiator concentration), the network instead adapted to an applied strain to minimize the free energy of the system. Under such conditions, self-healing was possible by disulfide exchange reaction.

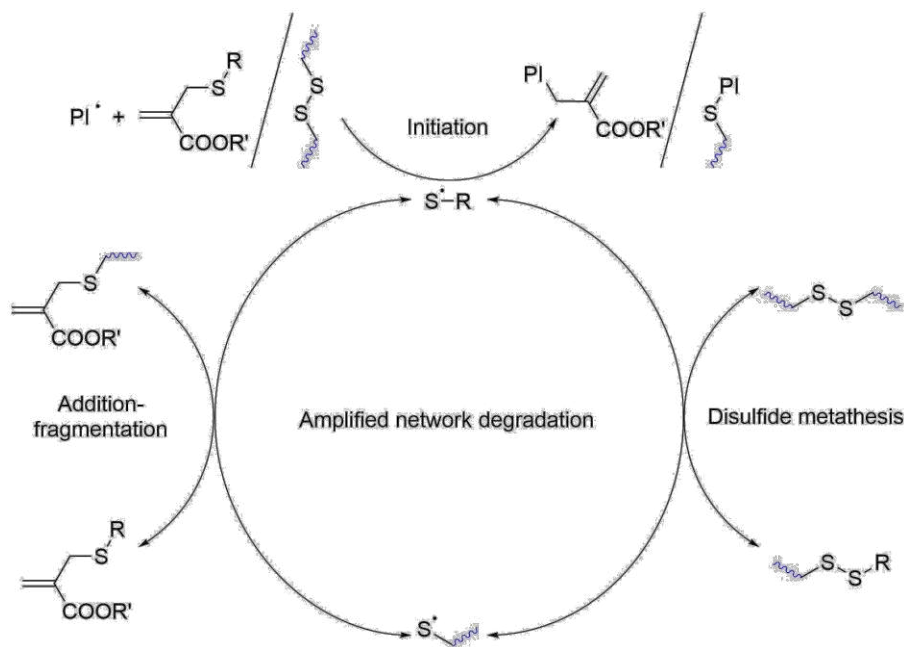
Moreover, an initiator-free self-healing covalently cross-linked polymer was developed by Matyjaszewski and co-workers by integrating thiuram disulfide moieties into a polyurethane backbone.^[81] Here, the radical reshuffling of thiuram disulfide units is exploited, which can be induced by irradiation with visible light in air, at room temperature and in the absence of a solvent. Due to the reactivity of thiuram disulfide units at ambient conditions, this functional group has potential for integration into dynamic hydrogel networks, albeit its inherent light sensitivity.

3.1.3 Other methods to induce disulfide metathesis

Fritze and Delius reported the generation of clean equilibrium mixtures of disulfides by ultrasound irradiation,^[82] while Ramström and co-workers described a Brønsted base-free, phosphine-catalyzed disulfide metathesis.^[83] Moreover, Wei *et al.* reported disulfide metathesis in an ion gel under heat and pressure catalyzed by an ionic liquid in the presence of copper salt.^[84] Sanders and co-workers presented a mechanochemical approach that requires a base, but no reducing agent.^[85]

3.2 General Considerations

Photocission of disulfide-linkages in polymers can be directly induced by irradiation with high intensity UV light leading to metathesis reaction resulting in rearrangement and self-healing of materials.^[80, 86] For the permanent cleavage of disulfides and prevention of reformation of linkages by the use of light, an equimolar amount of photoinitiator is required, which upon scission consumes free thiyl radicals.^[25d] Nevertheless, depending on the number of crosslinks the photoinitiator concentration required for complete degradation can surpass the concentration acceptable for cells by far,^[87] making this degradation mode irrelevant for biomedical applications. Alternatively, simple small molecule thiol-releasing water-soluble addition-fragmentation chain transfer (AFCT) reagents could as well be added to a disulfide-based network to promote degradation (Scheme 20).



Scheme 20: Upon addition of an initiator radical fragment to either an AFCT reagent or a disulfide, a thiyl radical is released. Addition of the thiyl radical to the double bond of the AFCT reagent releases another thiyl radical, which can then either attack a disulfide in the polymer backbone (disulfide metathesis) or add to another AFCT molecule (addition-fragmentation). A thiyl radical from the polymer backbone can likewise either attack an AFCT reagent or undergo disulfide metathesis with another disulfide linkage, leading to amplified network-degradation.

The advantage of this system would be the amplification of the photodegradation cycle by chain transfer. Addition of a photoinitiator-derived radical to the double bond of an AFCT reagent leads to the release of a thiyl radical,^[88] which can then either undergo metathesis with a disulfide in the polymer backbone or add to another AFCT molecule. A thiyl radical from the polymer backbone can likewise either attack an AFCT reagent or undergo metathesis with another disulfide linkage, leading to network degradation.

3.3 Preliminary reactivity testing

To proof the concept of amplified disulfide metathesis by AFCT a small molecule study was performed, in which previously investigated AFCT reagent ethyl 2-((n-dodecylthio)methyl)acrylate **ADTE**^[88] was reacted with 2,2'-dihydroxyethyl disulfide (Figure 24). Both compounds were combined with 1:1 stoichiometry (0.17 M) in acetone- d_6 in presence of photoinitiator Darocur 1173 (3 mol%). The sample was irradiated in an UV-oven (Intelli-Ray 600) for 5 min at 50% power. By comparing $^1\text{H-NMR}$ spectra of irradiated and non-irradiated reaction mixtures ~50% conversion was estimated. Both the ene-signals (a,b,e) as well as the signals of protons in α -positions to the sulphur atom (c,d,f,g) changed accordingly (Figure 24).

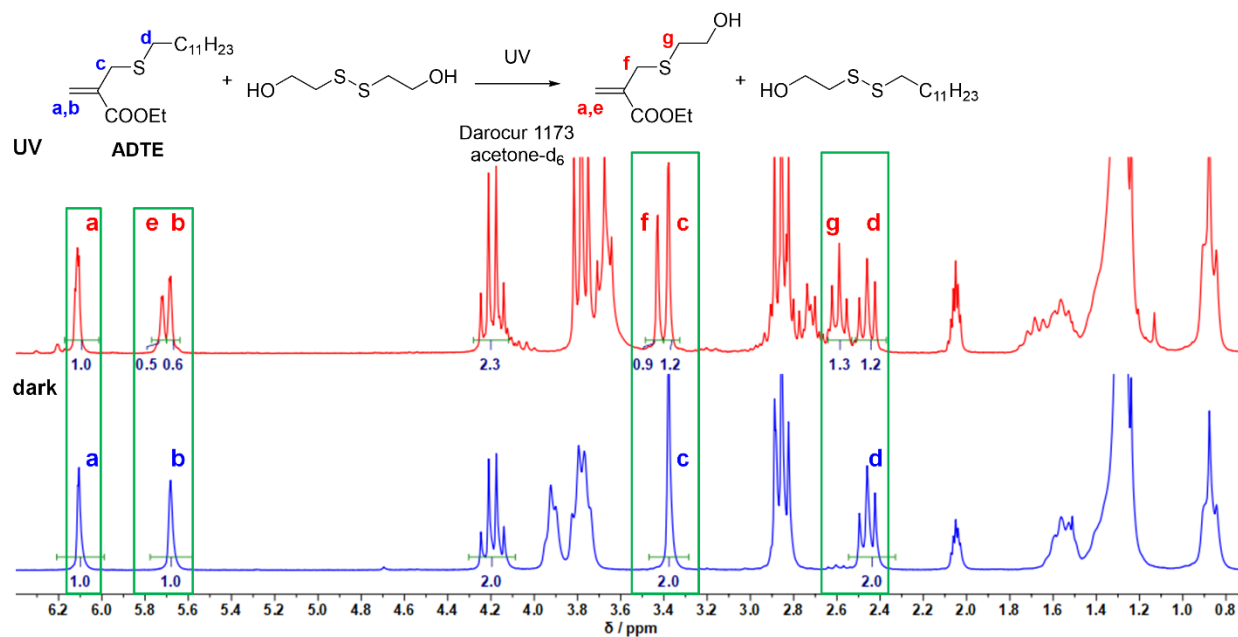


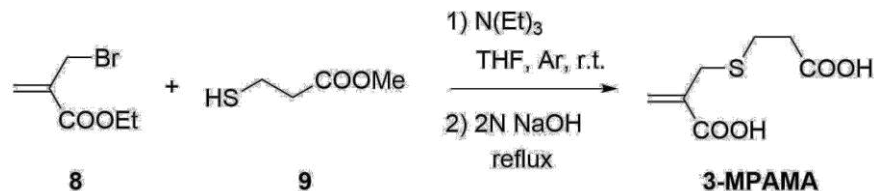
Figure 24: Reaction of ADTE with 2,2'-dihydroxyethyl disulfide in acetone- d_6 upon UV irradiation in presence of Darocure 1173. Conversion was confirmed by comparing $^1\text{H-NMR}$ spectra of irradiated (red) and non-irradiated (blue) reaction mixtures.

As the addition of the thiol species is reversible, a conversion of the AFCT reagent in the range of 50% implies equilibrium state, confirming the proposed reaction mechanism.

Due to the promising result of the experiment with **ADTE**, the amplified photo-triggered disulfide metathesis should be tested in aqueous environment as well.

3.4 Synthesis of water-soluble AFCT reagent 3-MPAMA

Hence, the water-soluble AFCT reagent **3-MPAMA** was synthesized by reacting methyl 3-mercaptopropionate **9** with ethyl α -bromomethacrylate **8** in a straightforward and quick (30 min) reaction following a modified protocol (Scheme 21).^[89] In a second step, 2N NaOH was added to the reaction mixture and it was refluxed to hydrolyse the ester. By recrystallization from water 74% of a white solid where obtained. The molecule is soluble in basified water.



Scheme 21: Water-soluble AFCT reagent **3-MPAMA** was synthesized from ethyl α -bromomethacrylate **8** and methyl 3-mercaptopropionic acid **9** in a two-step one-pot reaction.

Since the first synthetic step is very reactive, further modifications could also include the use of bioactive thiol compounds such as *N*-acetylcysteine or glutathione.

3.5 Reactivity testing of water-soluble AFCT reagent 3-MPAMA

As in the preliminary experiment, the efficacy of the newly synthesized water-soluble AFCT reagent was first tested with 2,2'-dihydroxyethyl disulfide in acetone- d_6 (Figure 25). Hence, the reaction mixture was irradiated for 5 min in an UV-oven at 50% power in presence of 5 mol% Darocur 1173. A comparison of $^1\text{H-NMR}$ spectra of irradiated and non-irradiated reaction mixture revealed approximately 50% conversion of **3-MPAMA** to the corresponding reaction product. While the signal of α -methylene protons **c** did not change, the singlet of ene-proton **b** splitted to form signal **d**. Furthermore, changes in other overlapping signals also indicated conversion, but could not be integrated satisfyingly.

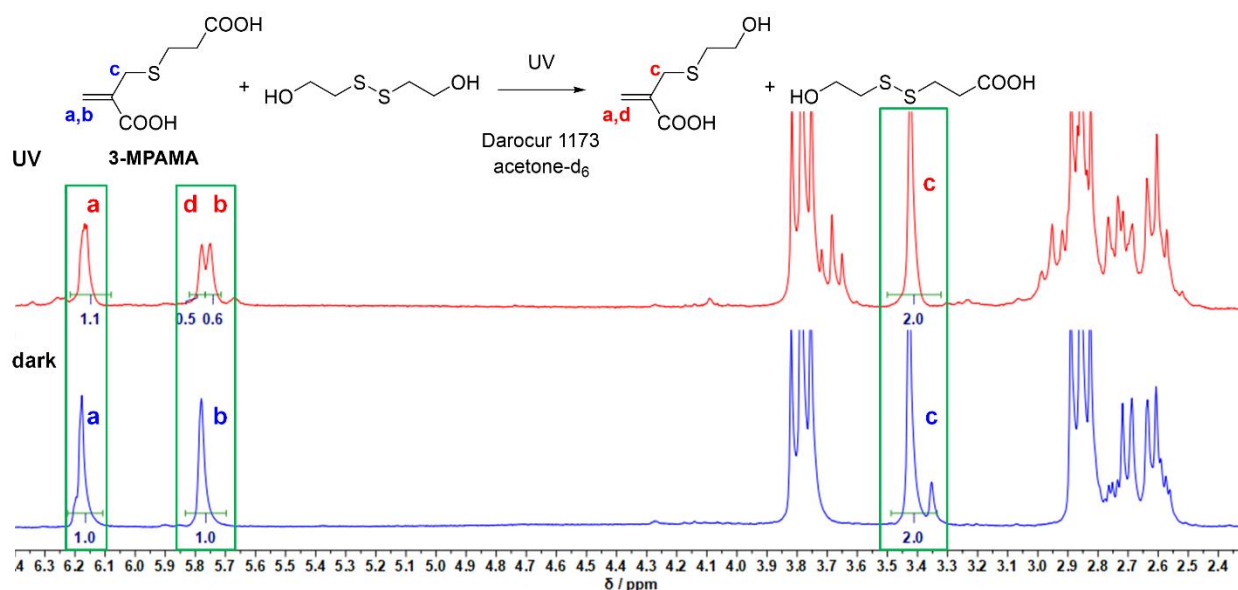


Figure 25: Reaction of 3-MPAMA with 2,2'-dihydroxyethyl disulfide in acetone- d_6 upon irradiation in presence of Darocur 1173. $^1\text{H-NMR}$ spectra before (blue) and after 5 min of UV irradiation (red). The conversion is clearly visible as double bond signal **b** turns into signal **d**. The singlet besides signal **c** derives from an impurity and disappears after UV treatment.

However, when the same reaction was conducted in D_2O in presence of 1 equivalent of NaOD and LiTPO (5 mol%) only marginal conversion was observed after 5 min of UV-irradiation at 50% of power (Figure 26). While the signals of ene-protons (**a,b**) and the α -methylene-singlet (**c**) did not change upon irradiation, only a marginal signal of the α -hydroxymethylene of the AFCT conversion product (**e**) indicates some reaction taking place. Hence, again 5 mol% of LiTPO were added and the reaction mixture was irradiated at 90% of power for 5 min. Nevertheless, signal **e**

only increased slightly by this repeated irradiation. The reason for the hindered reactivity in aqueous environment is not clear.

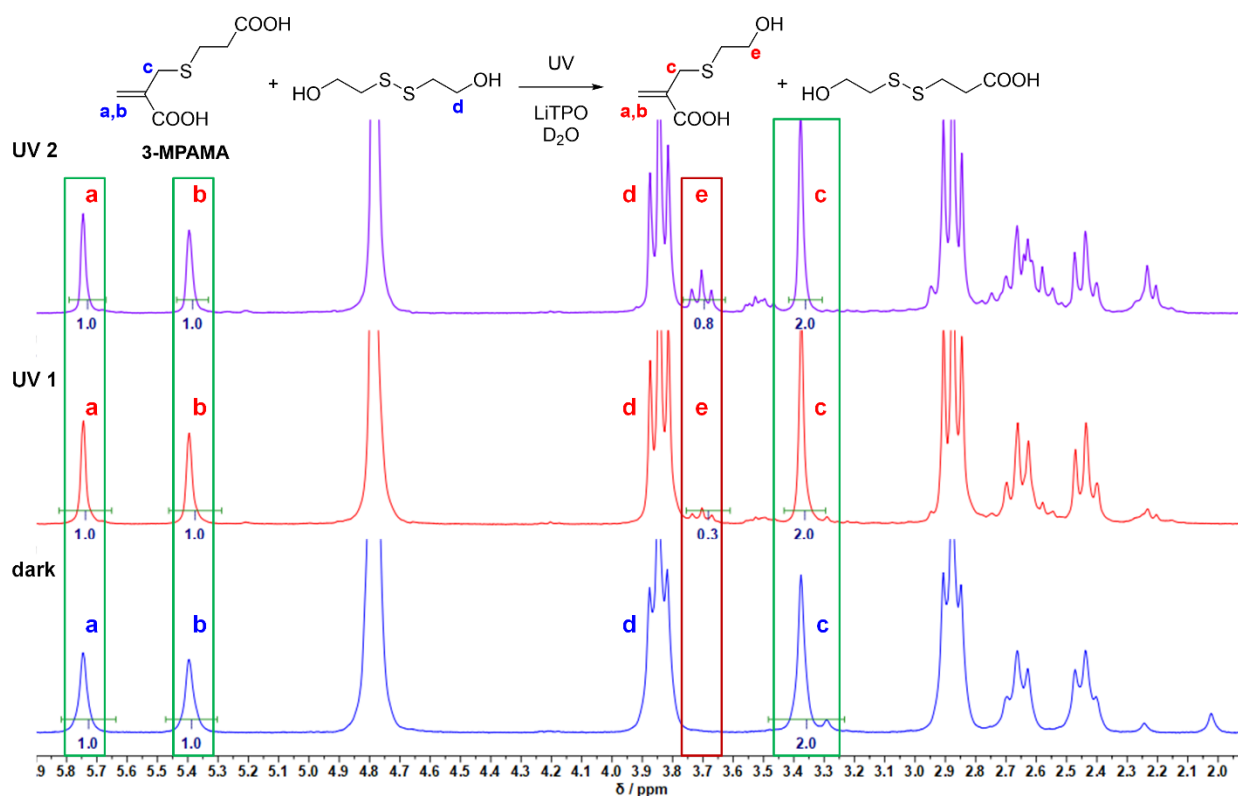
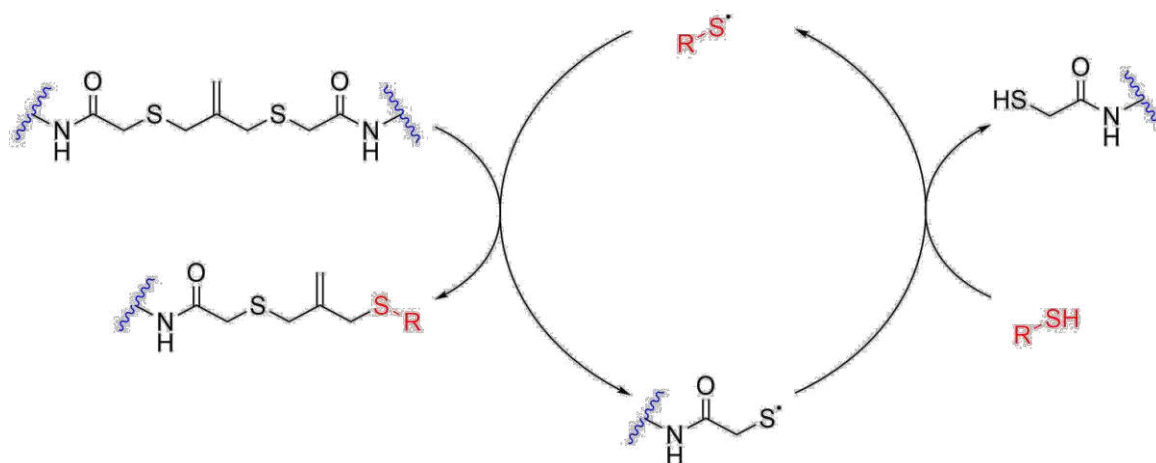


Figure 26: $^1\text{H-NMR}$ spectra of the untreated reaction mixture (blue), after 5 min of UV irradiation (red) in presence of 5 mol% LiTPO and after additional 5 min of UV irradiation with more LiTPO being added (violet). In comparison to acetone- d_6 the reaction seems to be hindered in D_2O .

3.6 Conclusion

Anyhow, in the course of this experimental investigation, a closely related concept was published by the Anseth group (Scheme 22).^[90] In their work, AFCT cross-links were integrated into a PEG network by strain-promoted azide-alkyne cycloaddition (SPAAC). By swelling this preformed hydrogel in a LiTPO solution, the hydrogel could be partially degraded upon irradiation. However, for complete reverse gelation the addition of free thiol was necessary. In contrast to conventional ortho-nitrobenzyl ester- or coumarin-based photolabile hydrogels the light attenuation was significantly decreased. Hence, the photodegradation of much thicker hydrogel samples became possible and due to the amplification of degradation the velocity of erosion was significantly increased. Moreover, cytocompatibility of the hydrogel platform was demonstrated by encapsulating and later releasing primary human mesenchymal stem cells (hMSCs).



Scheme 22: Amplification of photodegradation by chain transfer. Addition-fragmentation chain transfer (AFCT) crosslinks exposed to a photogenerated monothiol radical (red) transition from a crosslinked state to a non-crosslinked state and also regenerate a monothiol radical capable of additional crosslink fragmentation reactions.^[90]

This approach was also used for reversible and repeatable thiol-ene bioconjugation for dynamic patterning of biochemical ligand in hydrogels upon both one- and two-photon irradiation.^[91] The aim here was to exchange signaling proteins in hydrogels to overcome the limitation of these proteins poor stability under cell culture conditions making them lose their bioactivity over time. The integration of an allyl sulfide chain-transfer agent enabled a reversible, photomediated, thiol-ene bioconjugation of signaling proteins to hydrogels. Upon addition of a thiolated protein to the allyl sulfide moiety, a previously tethered protein was released, and the “ene” functionality was regenerated. As this thiol-ene reaction was reversible the patterned protein could then be released again through a subsequent thiol-ene reaction of a PEG thiol. The method was demonstrated to be fully repeatable through multiple iterations and proceed at physiologically relevant signaling protein concentrations in presence of encapsulated cells.^[91b]

Since the concept under investigation was already extensively researched and comprehensively demonstrated, the study was terminated at this point. As this thesis in particular focuses on two-photon degradation of photolabile hydrogels, other concepts had higher priority.

4. A MODULAR APPROACH TO SENSITIZED TWO-PHOTON PATTERNING OF PHOTODEGRADABLE HYDROGELS

4.1 State of the Art

oNB ester derivatives are photolabile molecular building blocks often integrated into linkers or the backbone of hydrogels to create elaborate dynamically tunable cell-culture platforms that can be triggered by the use of light.^[92] Applications, for instance, range from spatiotemporally defined changes of physio-chemical hydrogel properties,²⁴ over engineering of multicellular vascularized tissues,²⁷ to complex photoreversible protein-patterning for guidance of stem cell fate.²⁶ Beyond these applications, oNB derivatives have been utilized in several other dynamically light triggered materials.³¹

A particular drawback of the two-photon induced micropatterning of such materials is the fact that oNB derivatives typically exhibit relatively low two-photon absorption cross sections (δ_a) and uncaging action cross sections ($\delta_u = \delta_a Q_{u2}$, with Q_{u2} being the quantum efficiency for uncaging by two-photon excitation) both in the sub-GM range.^[44, 93] Hence, the reactivity of oNB derivatives towards two-photon excitation is rather low. For that reason, relatively high laser intensities and long irradiation times are required for photoscission, parameters at which living cells are prone to be damaged.^[94] Moreover, since the laser power required for two-photon absorption based processes increases with the square root of increasing scanning speed, designing more efficient two-photon active compounds and processes is a current key challenge in the advancement of high performance multiphoton lithography.^[45] There have been several optimization efforts to promote the efficiency of the oNB photocleavage reaction by varying the number and pattern of substituents on the benzyl group^[23b, 93a, 93b, 95] or by including oNB derivatives into π -conjugated molecular systems to particularly enhance δ_u .^[25f, 93a, 93b, 96] Alternatively, π -conjugated compounds have been covalently linked to photocleavable oNB or 7-nitroindoliny derivatives in order to sensitize the photoscission reaction by a FRET process.^[97] Nevertheless, chemical modifications of this kind are labor intensive and usually involve multistep synthesis, whereas certain photolabile oNB based macromer precursors which are known to be cytocompatible are commercially available.^[98] Moreover, the sensitivity of such permanently modified hydrogel systems towards two-photon excitation is an intrinsic property of the respective precursors that cannot be controlled nor adjusted independently. For these reasons, a modular system in which a small molecule sensitizer is added to the preformed hydrogel in order to promote the two-photon induced photocleavage reaction would be beneficial.

In this work, a modular system that permits the sensitization of the oNB photoscission under two-photon excitation regime on the example of a photocleavable PEG-crosslinked HA based hydrogel (PEG-HA-SH) is presented. It is shown that by addition of a small molecule exhibiting large two-photon absorption the efficiency of the oNB-photoscission can be effectively promoted in a concentration dependent manner. The efficacy of this process is demonstrated in the presence of cells.

4.2 Design and synthesis of the photocleavable hydrogel platform

To this date, the majority of photodegradable hydrogels is based on synthetic polymers as poly(ethylene) glycol (PEG), a material which is biocompatible but offers low cell adhesion and therefore requires the addition of cell-binding peptide sequences such as Arg-Gly-Asp (RGD) or others.^[9, 22, 99] Studies that describe the use of other biopolymers including gelatin^[100] or polysaccharides^[101] as backbone for photocleavable hydrogels are still rare. Among natural biopolymers, hyaluronic acid (HA) provides a versatile platform for the synthesis of hydrogel precursors owing to its biocompatibility, chemical modifiability and tunable properties as well as its native biofunctionality due to respective binding receptors such as CD44.^[102] Several studies about light-controlled postgelation modifications of HA based hydrogels by the use of thiol-ene chemistry exist, where either hydrogel mechanics have been altered,^[16, 103] or biomolecules have been photo-patterned into the hydrogels^[104] or both was performed independently.^[105] However, only few of these reports involve the use of photocleavable groups.^[16, 104a] The utilization of HA as biopolymeric backbone for photodegradable hydrogels is hence an attractive design approach and alternative to currently utilized biomaterials that should definitely be considered.

Such a photocleavable HA based material has been developed in cooperation with the group of Dr. Dmitri Ossipov at the University of Uppsala.

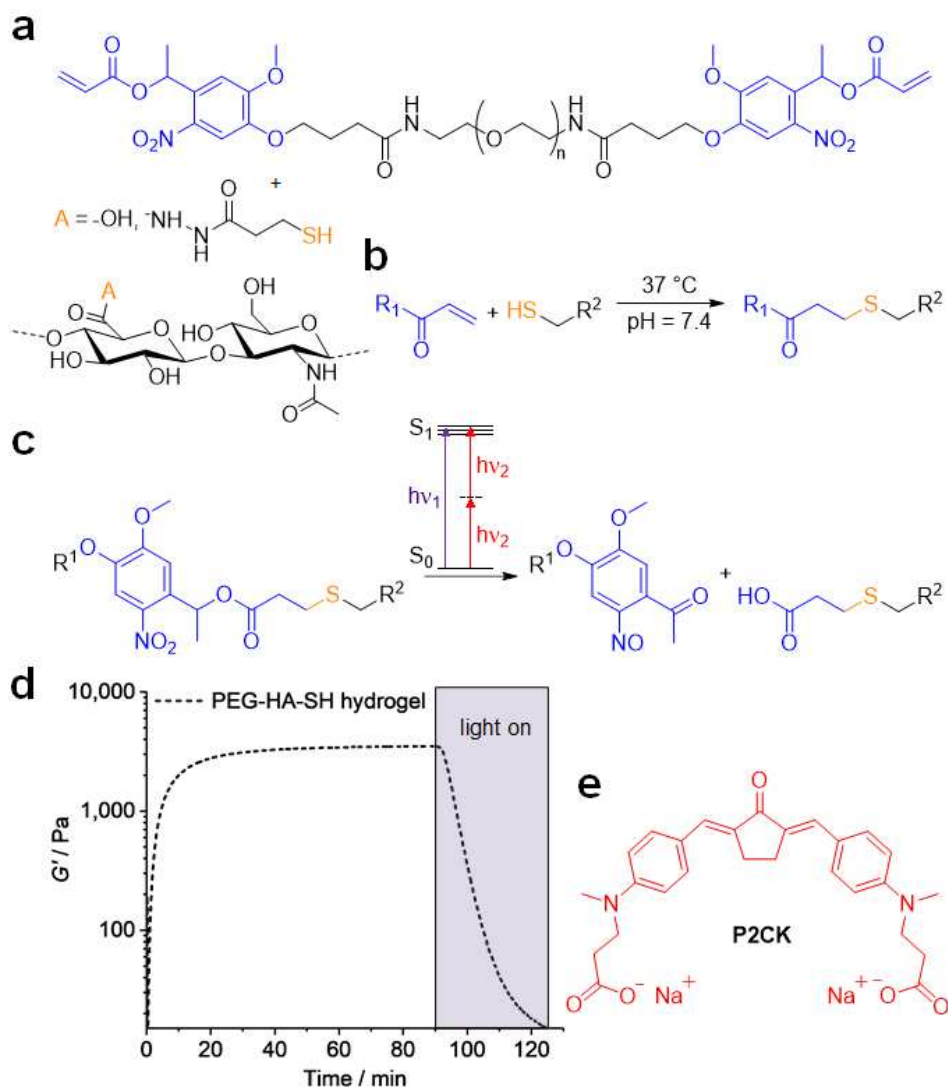


Figure 27: Hydrogel components and reactions used for formation and photo-degradation of PEG-HA-SH hydrogel. a) Molecular structure of photocleavable linker PEG-(oNB-A)₂ and thiol modified hyaluronic acid HA-SH, which undergo b) crosslinking by Michael-type thiol-ene addition at physiological conditions and c) photocleavage of o-nitrobenzyl ester functionalities induced by either UV light or upon two-photon excitation. d) Network formation and UV-VIS-induced degradation was monitored by oscillatory measurements of the shear storage modulus G' (320-500 nm, 20 mW cm⁻²). e) Molecular structure of water-soluble two-photon sensitizer P2CK.

First, a photo-degradable hydrogel system was designed to be covalently formed and later photo-patterned based on two orthogonal and biocompatible chemical reactions, namely Michael-type addition of thiols to acrylates and the photo-induced cleavage of oNB esters Figure 27b and c).^[106] Hyaluronic acid (HA), a major non-sulfated glycosaminoglycan component of the ECM,^[107] was chosen as backbone and functionalized with thiol groups to provide the possibility of 3D in situ cell encapsulation by thiol-ene “click” reaction.^[108] Thiol modified hyaluronic acid (HA-SH, Figure

27a) was synthesized as previously described with a degree of substitution (DS) estimated to be ~50% by the use of $^1\text{H-NMR}$ analysis (Figure 28).^[109]

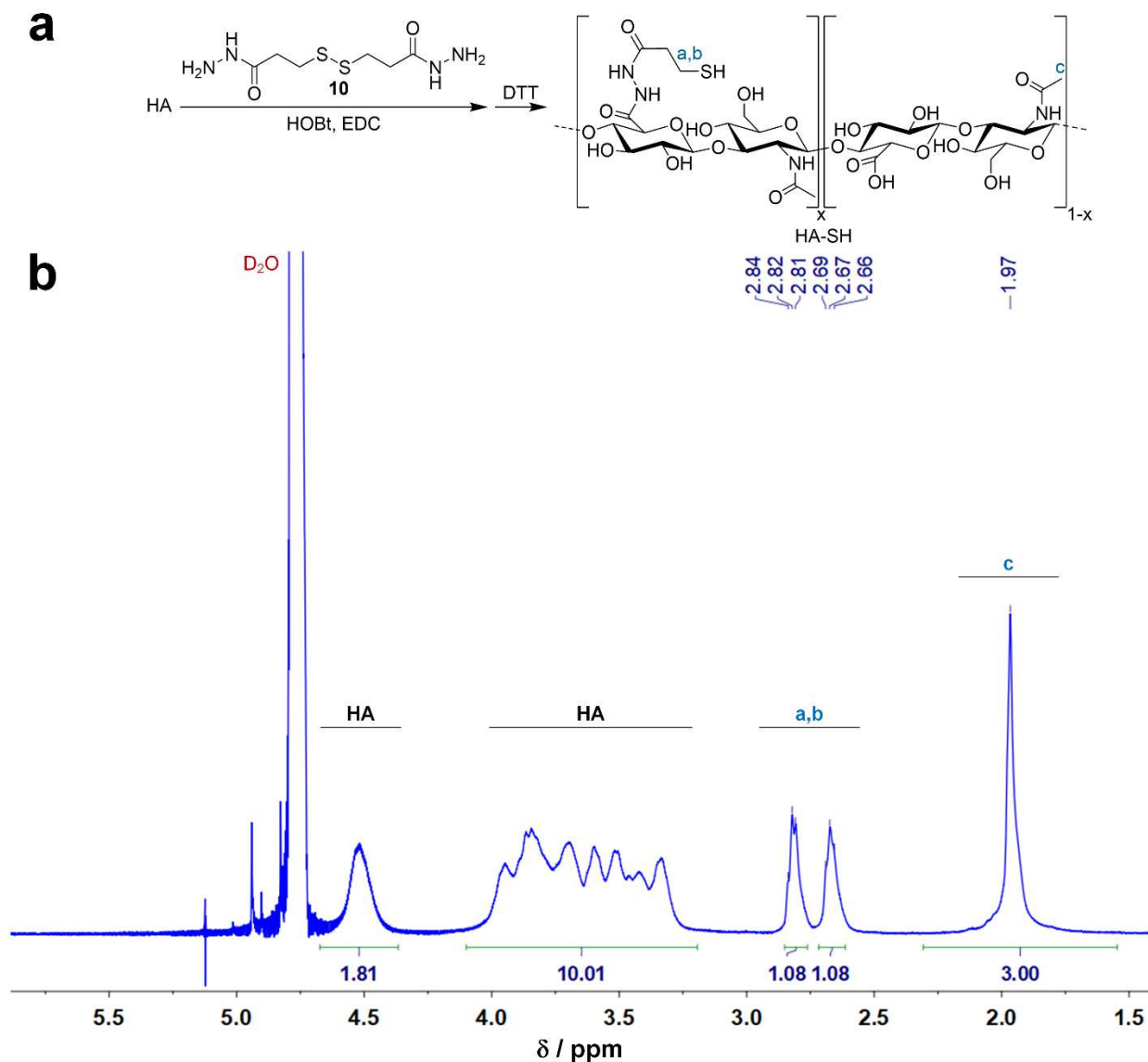
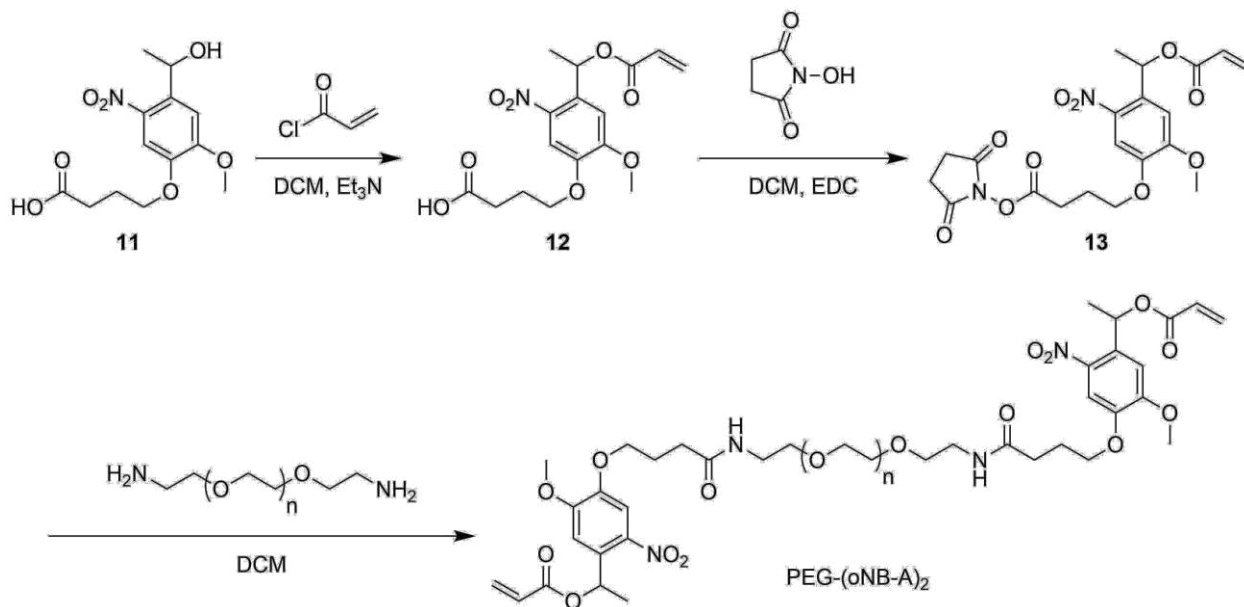


Figure 28: Synthesis route and characterization of HA-SH. a) Hyaluronic acid was reacted with 3,3'-dithiobis(propionic hydrazide) **10** in presence of *N*-hydroxybenzotriazole (HOBt) and 1-ethyl-3-(3-dimethylaminopropyl) carbodiimide (EDC) and subsequently reduced to HA-SH using *D,L*-dithiothreitol (DTT). b) $^1\text{H-NMR}$ spectra for HA-SH. The corresponding groups of each peak are shown in the plot. The degree of thiol functionalisation of HA-SH (DS) was estimated to be ~50% via $^1\text{H-NMR}$ analysis. The integral of the methyl peak of the acetyl group **c** was utilized as reference for the determination of the DS by calculating its relative ratio to that of the methylene groups in α,β -position to the thiol group **a,b**.

To form the hydrogel, a symmetrical linear poly(ethylene glycol) (PEG, $M_w \sim 6,000$ Da) based crosslinker containing photo-labile oNB ester moieties between the PEG chain and terminal acrylate groups was added (PEG-(oNB-A)₂, Figure 27a). The photocleavable linker was synthesized following a modified version of a previously described protocol (Scheme 23).^[98]



Scheme 23: Synthesis route towards photocleavable linker PEG-(oNB-A)₂. The photocleavable linker was synthesized following a modified version of a previously described protocol.^[98] 1-Nitrobenzyl alcohol 11 was reacted with acryloyl chloride in presence of trimethylamine to 1-nitrobenzyl ester 12. After activation of ester 12 by conversion into the corresponding *N*-hydroxysuccinimidyl ester 13 using EDC chemistry it was coupled to PEG diamine ($M_n = 6,000$ Da) to give the photocleavable linker PEG-(oNB-A)₂.

To generate a hydrogel formulation, stock solutions of both HA-SH (18 mg mL⁻¹) and PEG-(oNB-A)₂ (150 mg mL⁻¹) in cell culture medium were combined with 1:1 stoichiometry of functional groups at neutral pH. It is noteworthy that the Michael-type thiol-ene addition is a robust crosslinking reaction for hydrogel formation, which can be performed at cytocompatible conditions in complex formulations including cell culture medium at neutral pH.^[110] Gelation and UV light induced degradation of the networks was examined by irradiation of in situ formed hydrogel samples on a rheometer coupled to a mercury arc lamp. PEG-HA-SH hydrogel reached an equilibrium shear storage modulus G' of 3.7 ± 0.3 kPa within 90 min. Photo-induced disintegration of the photocleavable hydrogel network was verified by irradiation with UV-VIS light (320-500 nm, 20 mW cm⁻²) for 35 min leading to a decrease of G' in the course of illumination (Figure 27d). However, when the light was shuttered, consistency was observed during periods when irradiation was interrupted, confirming that the degradation is strictly related to photoirradiation (Figure 29).

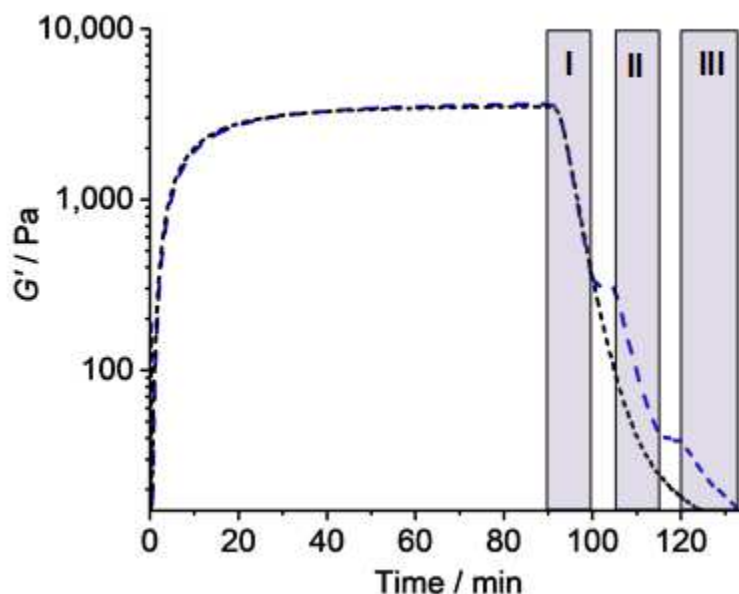


Figure 29: Rheology measurement of the shear storage modulus G' . Optically thin photocleavable hydrogel networks ($50\ \mu\text{m}$) have been formed in situ between a peltier glass plate and a measuring plate ($25\ \text{mm}$) on a phorheometer. After constant G' was observed (90 min) photo-induced degradation of hydrogel networks was demonstrated by irradiation with shuttered UV-VIS light (I, II, III, $320\text{--}500\ \text{nm}$, $20\ \text{mW cm}^{-2}$, blue dashed line) leading to a decrease of G' in the course of illumination but consistency during periods when irradiation was interrupted, confirming that the effect is strictly related to photoirradiation. In contrast, when the network was continuously irradiated a stepless decline of G' occurred (black dotted line).

4.3 Sensitized two-photon micropatterning of photocleavable hydrogels

Next, the degradation of the oNB based photocleavable hydrogel was investigated by means of multiphoton processing.^[111] In order to improve the efficiency of the oNB ester cleavage under two-photon excitation regime it was hypothesized that this process could be promoted by the addition of a two-photon active compound, which absorbs light at two-photon conditions more efficiently and then transfers the energy to the oNB functionalities acting as a two-photon photosensitizer. To investigate this hypothesis preformed photocleavable hydrogel samples were soaked in solutions of the previously studied water-soluble and biocompatible cyclic benzylidene ketone-based two-photon chromophore P2CK^[49b, 112] (Figure 27e, $\delta_a \sim 180\ \text{GM}$) at different concentrations ranging from 0.05 to 0.5 mM in cell culture medium for 5 h (Figure 30).

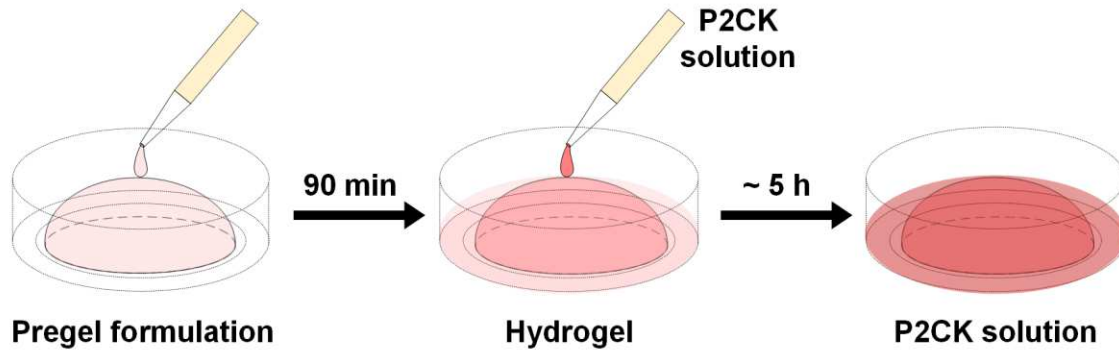


Figure 30: Workflow of hydrogel treatment with P2CK prior to two-photon micropatterning. Photocleavable PEG-HA-SH hydrogels were formed by Michael-type thiol-ene reaction within 90 min. Thereafter hydrogels were swollen in solutions of P2CK for approx. 5 hours.

The hydrogel samples were then two-photon micropatterned using a fs-pulsed NIR-laser (800 nm) at a constant writing speed of 200 mm s^{-1} focused through an water immersion objective (32x, 0.85 NA). Parallel channels with rectangular cross sections ($300 \mu\text{m} \times 20 \mu\text{m} \times 50 \mu\text{m}$) were eroded from the edge into the bulk of the hydrogel at different laser powers ranging from 10–100 mW (Figure 31a). For examination of the fabricated channels the samples were swollen in a solution of fluorescein modified dextran (FITC–dextran, 1 mg mL^{-1}) with an average molecular weight of $\sim 2,000 \text{ kDa}$ (Figure 31b). Due to its size the dextran stain only infiltrates the photocleaved areas of the network, but cannot penetrate the bulk hydrogel, permitting visualization of the photoeroded channels by LSM. By these means, a distinct relation of the threshold power for the fabrication of an open microchannel by two-photon degradation in dependence of the P2CK concentration was evaluated.

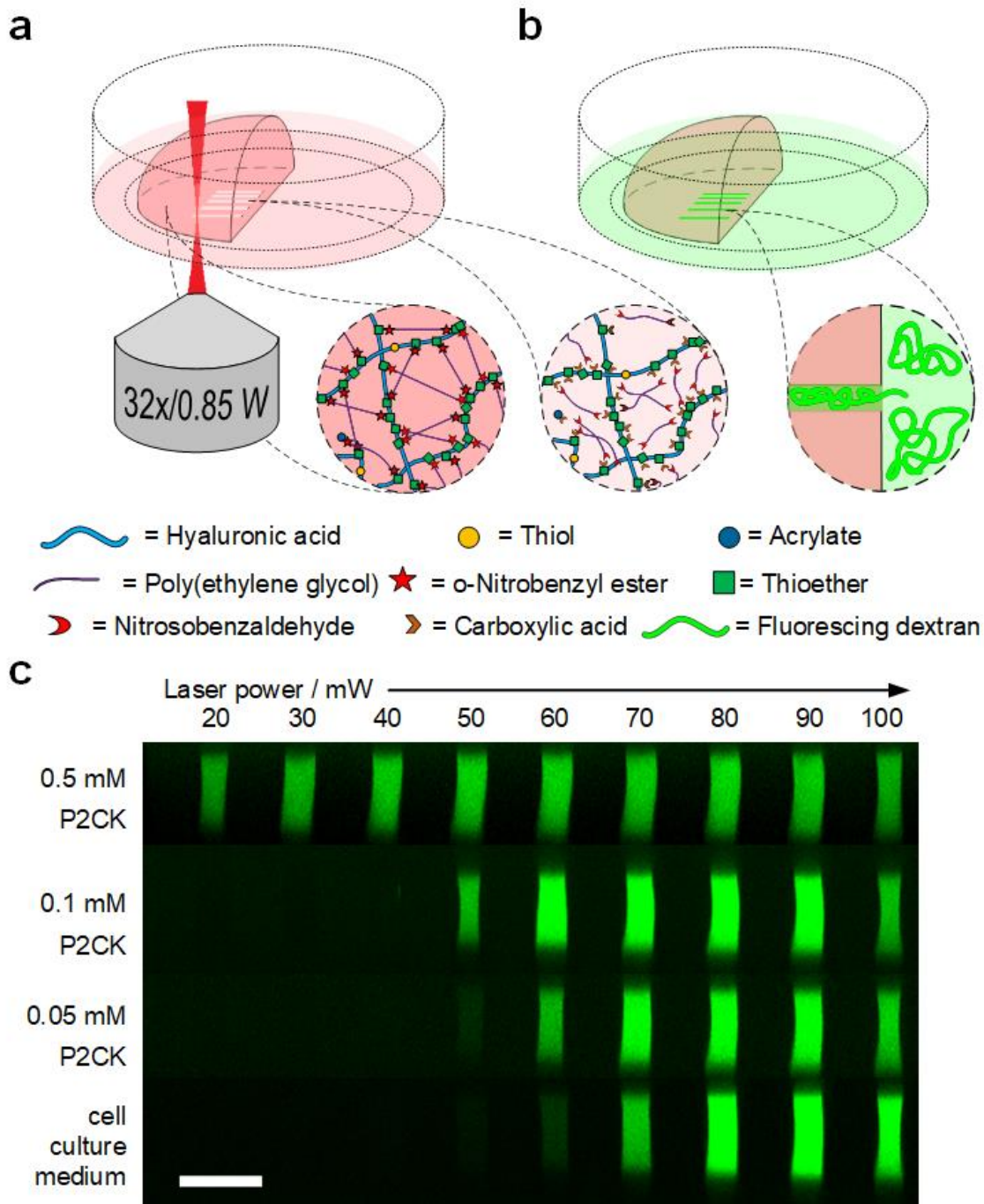


Figure 31: Micro-channel fabrication by two-photon degradation of PEG-HA-SH hydrogel in presence of two-photon sensitizer P2CK. a) Schematic illustration of the two-photon micropatterning of a preformed hydrogel network using a focused NIR-laser and (b) visualization of micro-channels by soaking in a solution of fluorescent dextran ($M_w \sim 2,000$ kDa), which due to its size only infiltrates the micro-channels. c) Confocal microscopy images displaying orthogonal cross sections (y,z-plane) of micro-channels fabricated with varying laser powers in PEG-HA-SH hydrogels after swelling in different solutions of P2CK ranging from 0.05–0.50 mM or pure cell culture medium DMEM. Scale bar 50 μm .

In untreated PEG-HA-SH hydrogel bright fluorescence could be observed in channels fabricated at laser powers of 70 mW and above. In contrast, with increasing concentration of two-photon sensitizer P2CK the threshold power decreased accordingly and hence in presence of 0.5 mM P2CK was reduced down to 20 mW (Figure 31c and Figure 32).

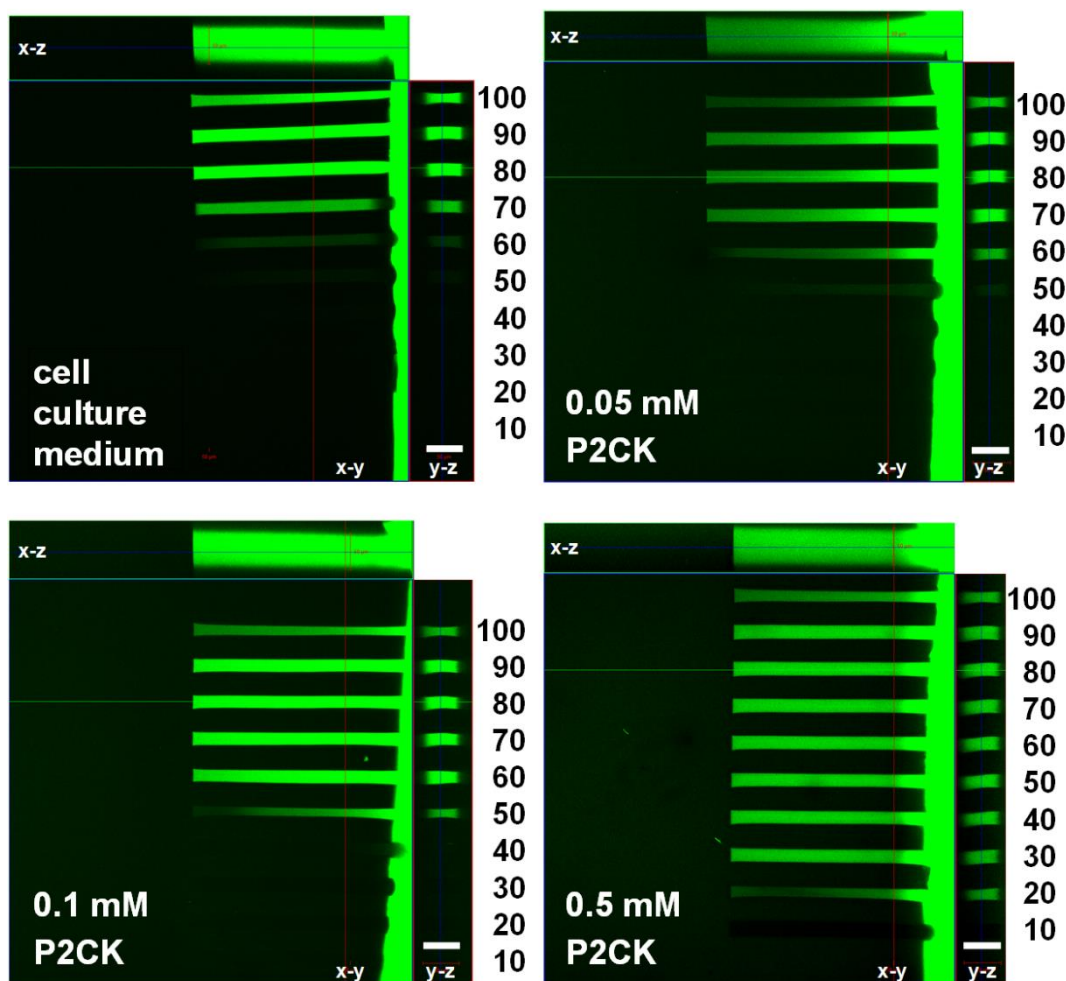


Figure 32: Top-down views of confocal z-stacks with corresponding orthogonal projections of channels ($300 \times 20 \times 50 \mu\text{m}^3$) fabricated at increasing laser powers (10–100 mW) in PEG-HA-SH hydrogel after swelling in different solutions of P2CK ranging from 0.05–0.5 mM or pure cell culture medium. Micro-channels were visualized by soaking in a solution of fluorescent dextran (FITC2000, Mw ~2,000 kDa). Scale bars = 50 μm .

To demonstrate the generality of the two-photon sensitization approach, another photodegradable hydrogel platform based on a thiol-terminated four-armed PEG^[52] (4armPEG-SH, Mw ~ 5 kDa) and PEG-(oNB-A)₂ with 12.5 wt% total macromere content was formed and then two-photon micropatterned in presence of different concentrations of P2CK as described above. Similar results were achieved in these experiments (Figure 33).

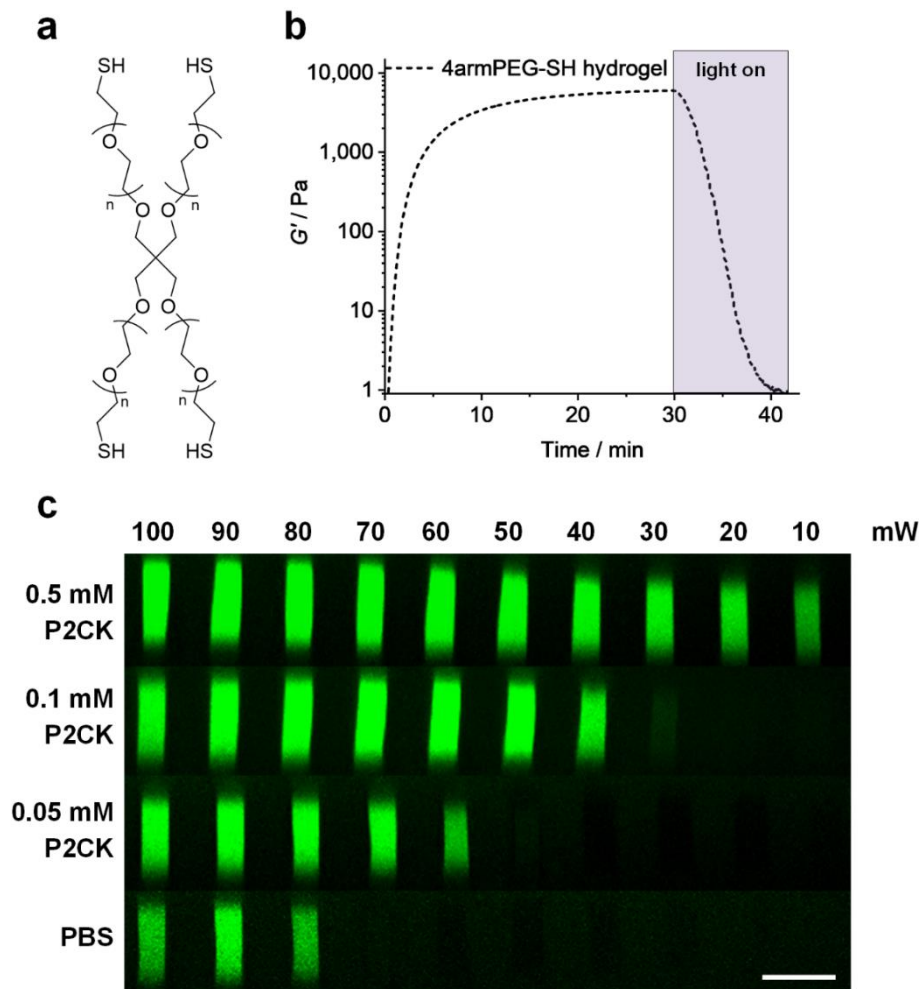


Figure 33: Formation and degradation of photodegradable 4armPEG-SH hydrogel. a) A photodegradable hydrogel based on 4armPEG-SH and PEG-(oNB-A)₂ with a total macromere content of 12.5 wt% was formed by Michael-type thiol-ene reaction in a 1:1 ratio of functional groups. b) Network formation and UV-VIS-induced degradation was monitored by oscillatory measurements of the shear storage modulus G' . The photodegradable 4armPEG-SH hydrogel reached an equilibrium G' of 6.5 ± 2.2 kPa (mean \pm s.d.) within 30 min. Upon irradiation with UV-VIS light (320–500 nm, 20 mW cm^{-2}) the hydrogel degraded within 12 min. c) Micro-channels were fabricated by two-photon micro-patterning at varying laser powers (10–100 mW) in 4armPEG-SH hydrogels after swelling in PBS or solutions of P2CK (0.05–0.50 mM). Micro-channels were visualized by confocal microscopy using FITC-dextran. Images display orthogonal cross sections (y,z-plane). As in the case of PEG-HA-SH hydrogel the threshold laser power for two-photon erosion decreases with increasing concentration of P2CK accordingly. While in untreated hydrogel channel erosion occurs at 80 mW and above, when 0.5 mM P2CK is used the threshold can be reduced to 10 mW. Scale bar 50 μm .

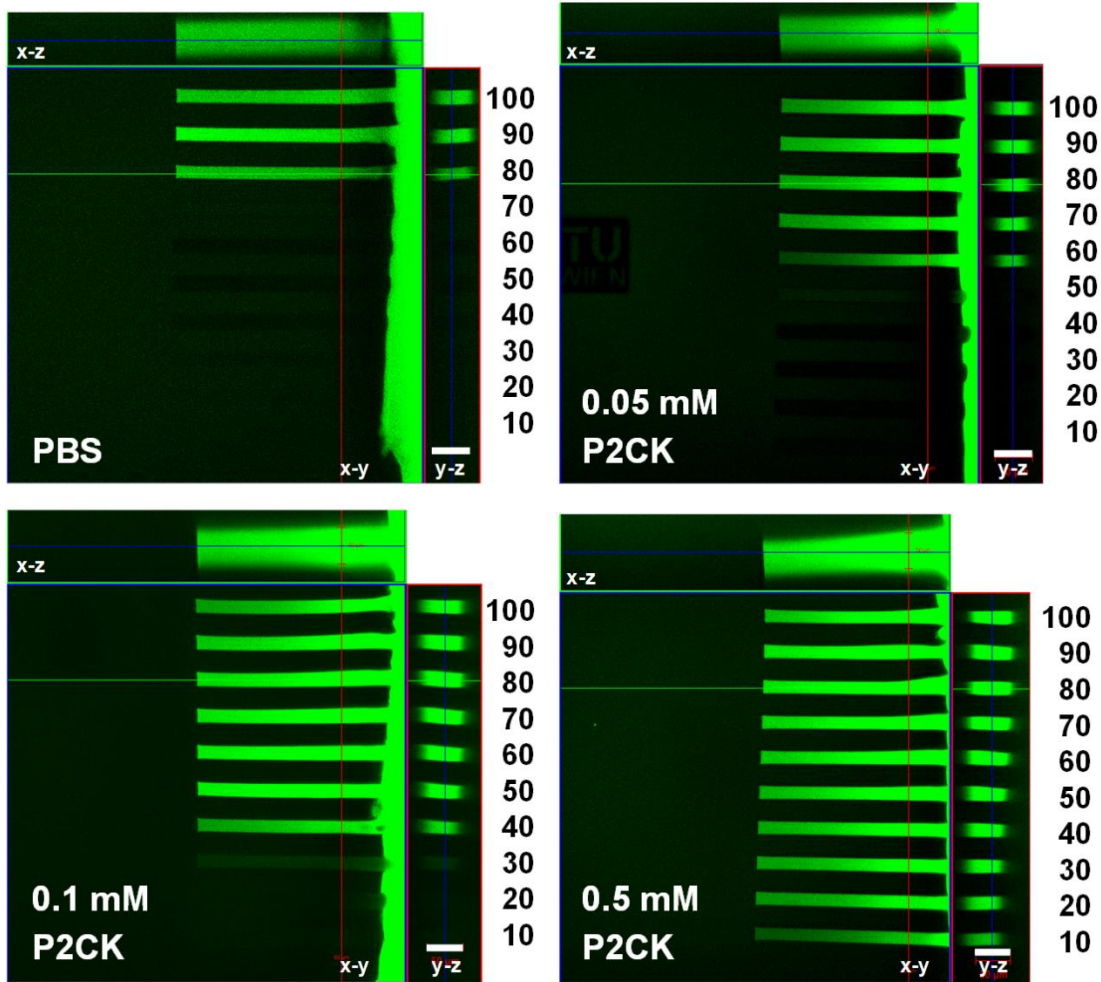


Figure 34: Micro-channel fabrication by two-photon degradation of 4armPEG-SH hydrogel in presence of two-photon sensitizer P2CK. Top-down views of confocal z-stacks with corresponding orthogonal projections of channels ($300 \times 20 \times 50 \mu\text{m}^3$) fabricated at different laser powers (10–100 mW) in 4armPEG-SH hydrogel after swelling in solutions of P2CK in PBS (0.05–0.5 mM) or PBS only. Micro-channels were visualized by soaking in a solution of FITC-dextran (Mw $\sim 2,000$ kDa). Scale bars = $50 \mu\text{m}$.

4.4 Micro-mechanical analysis of micropatterned regions by AFM

An in situ analysis of the microscale mechanical properties of irradiated sections on PEG-HA-SH hydrogel was performed via atomic force microscopy (AFM) cantilever-based microindentation.^[113] These experiments were conducted together with Dr. Orestis Andreotis at the Institute of Lightweight Design and Structural Biomechanics (E317).

For this purpose, cuboids ($A = 100 \times 100 \mu\text{m}^2$) with a depth of more than $100 \mu\text{m}$ were micropatterned into the surface of a hydrogel sample swollen either in PBS or a 0.1 mM solution of P2CK. Again, laser powers from 10–100 mW at a constant writing speed of 200 mm s^{-1} were used. Besides the indentation moduli, the relative heights of the irradiated regions were measured

using AFM by referencing to a non-irradiated position close to the respective region (0 mW). Above a certain laser power the material is eroded and a cavity is formed. The actual depth of the cavities could not be determined by AFM. The laser power thresholds for cavity formation (PBS: 70 mW; 0.1 mM P2CK: 50 mW; Figure 35a) equal those observed in the experiments in which channels were fabricated (Figure 31c and Figure 32). However, below the respective threshold the material is incompletely degraded. The decreased crosslinking density results in swelling of the material within the irradiated volume. The degree of swelling increases with the laser power. At 10 mW no swelling is observed in the PBS-treated PEG-HA-SH hydrogel whereas distinct swelling occurs in presence of P2CK.

The indentation modulus, E_{AFM} , of PEG-HA-SH hydrogel is 15.9 ± 0.2 kPa (Figure 35b; 0 mW; mean \pm s.e.m.). In presence of P2CK (0.1 mM) E_{AFM} decreases readily upon irradiation with increasing laser power until a cavity is formed at 50 mW. In absence of P2CK a significant decrease of E_{AFM} is observed at 30 mW while cavity formation occurs at 70 mW.

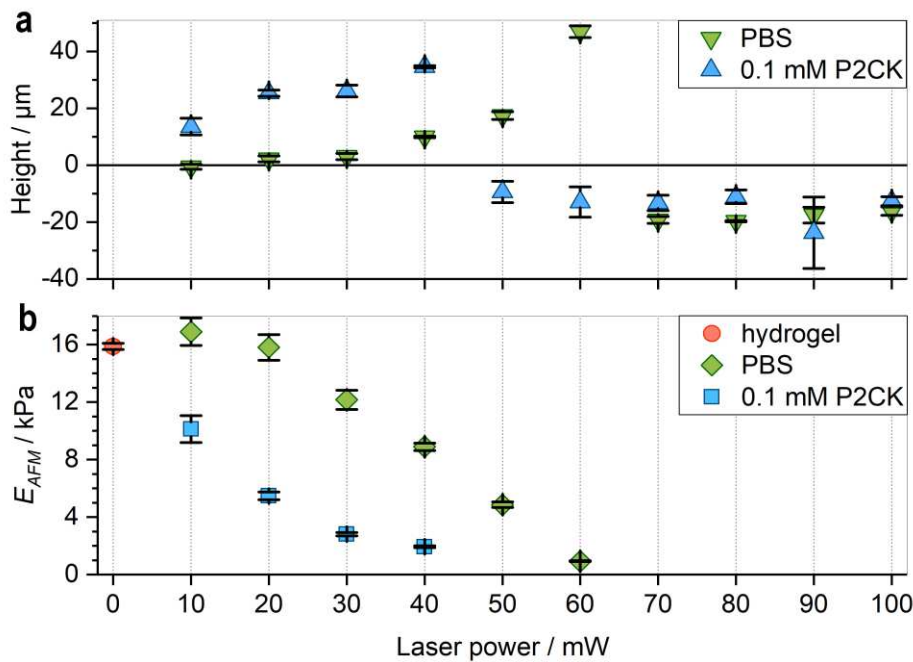


Figure 35: Micro-mechanical characterization of irradiated sections in PEG-HA-SH hydrogel by AFM. a) The relative heights (mean \pm s.d.) of two-photon micropatterned sections in relation to non-irradiated regions (0 mW) were analyzed by AFM. In PBS soaked hydrogel cavity formation sets in at 70 mW (\blacktriangledown), whereas after P2CK-treatment (0.1 mM) cavities already form at 50 mW (\blacktriangle). Exposure below the respective threshold laser power leads to incomplete degradation and results in swelling of the irradiated regions. **b)** The indentation modulus E_{AFM} (mean \pm s.e.m.) decreases upon irradiation with increasing laser power until the threshold is reached and a cavity is formed.

4.5 Biocompatibility & Cell Culture Application

As photolabile hydrogels are commonly micropatterned by two-photon irradiation the qualification for cell culture applications of both the novel PEG-HA-SH hydrogel as well as the P2CK promoted two-photon degradation process was examined. These experiments were conducted together with Dr. Marica Markovic who performed cell culture and encapsulation experiments as well as metabolic activity assays at the Institute of Materials Science and Technology (E308).

The biocompatibility of P2CK at concentrations below 0.50 mM with both GFP-labeled^[114] hTERT immortalized human adipose-derived mesenchymal stem cells (ASC/TERT1) and human osteosarcoma cells (MG-63) was verified by metabolic activity assay (Figure 36).

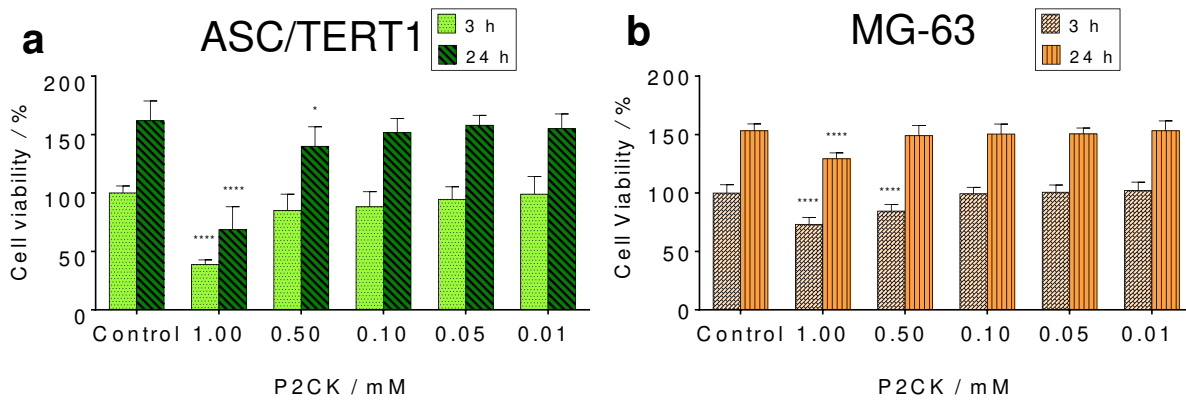


Figure 36: Effect of P2CK on human cell-lines a) ASC/TERT1 and b) MG-63. The cell viability of both cell-lines exposed to P2CK for 3 h and 24 h was examined by PrestoBlue® metabolic activity assay. Data are shown as mean + standard deviation (n = 8 replicates per group) and were analyzed by one-way ANOVA followed by Dunnett's multiple comparison test. The 3 h group was compared to the 3 h control and the 24 h group was compared to the 24 h control respectively (* P < 0.05, ** P < 0.0001). Incubation of both cell-lines in solutions of P2CK at concentrations below 0.50 mM revealed no significant difference to the untreated control. The cell viability decreases slightly after 24 h in contact with 0.50 mM P2CK and more significantly upon incubation in 1.00 mM P2CK solution.**

Spheroids of GFP-labeled^[114] hTERT immortalized human adipose-derived mesenchymal stem cells (ASC/TERT1) were encapsulated in PEG-HA-SH hydrogel. 24 h after encapsulation the hydrogel was first soaked in a 0.1 mM solution of P2CK for 5.5 h and then horseshoe-shaped channels were micropatterned around spheroids at different laser powers ranging from 30–100 mW (Figure 37 and Figure 38). Biocompatibility of both the hydrogel and the micropatterning process was verified by propidium iodide staining after 7 d and 14 d showing excellent cell viability (Figure 37 and Figure 38).

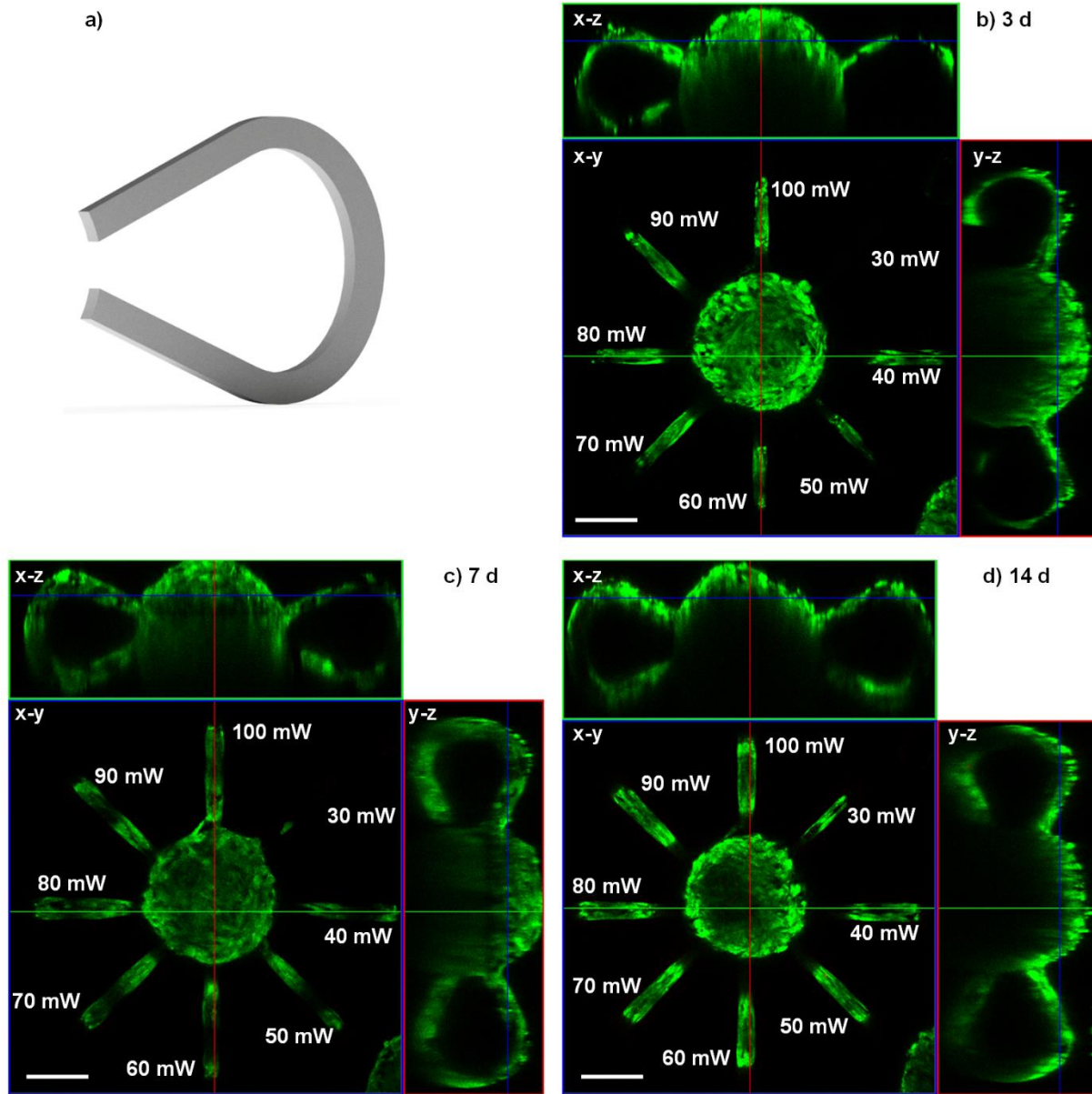


Figure 37: ASC/TERT1 spreading into loops micropatterned with P2CK. a) 3D model of a horseshoe-shaped channel ($\text{\O} = 20 \mu\text{m} \times 20 \mu\text{m}$) generated by CAD. 24 h after spheroid encapsulation the hydrogel was soaked in a solution of P2CK (0.1 mM) for 5.5 h and then horseshoe-shaped channels ($\text{\O} = 20 \mu\text{m} \times 20 \mu\text{m}$) were micropatterned from spheroids into the bulk hydrogel at different laser powers ranging from 30–100 mW. b) Within 3 days after micropatterning, cells had entered loops fabricated at laser powers down to 40 mW, indicating that at these conditions the network in the irradiated areas had been sufficiently disintegrated for cells to penetrate. c) While the area irradiated at 30 mW remained unoccupied for 7 days, d) cells filled up this loop after 14 days, most likely due to ester hydrolysis of remaining linkages. c,d) Excellent cell viability is indicated by high GFP- (green) and very low propidium iodide-signal (red). Scale bars 100 μm .

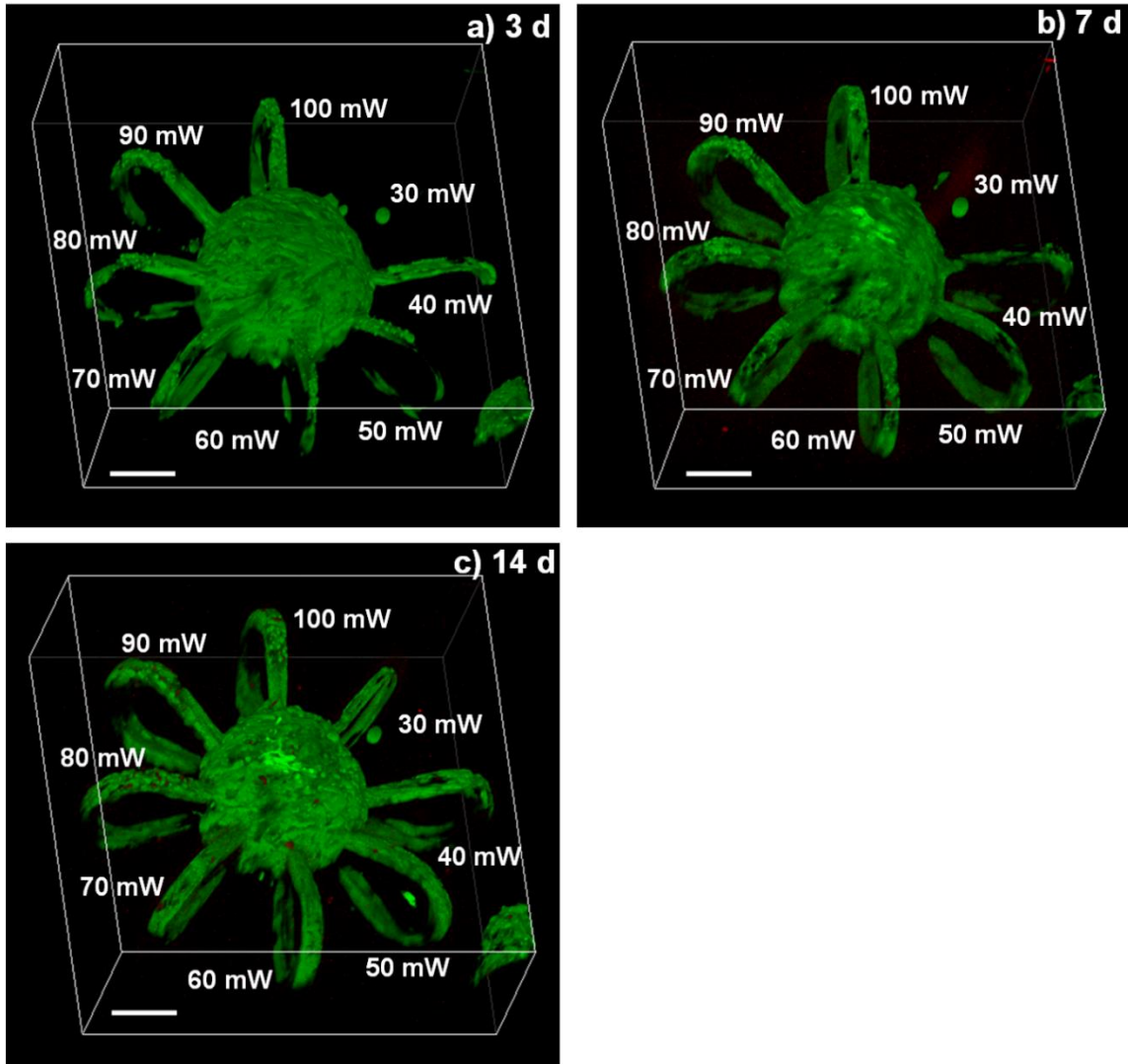


Figure 38: ASC/TERT1 spreading into loops micropatterned with P2CK. 3D renderings of confocal z-stacks (Figure 37) of GFP-labeled ASCs spreading into horseshoe-shaped channels ($\text{\O} = 20 \mu\text{m} \times 20 \mu\text{m}$). Loops were micropatterned in presence of P2CK (0.1 mM) at laser powers ranging from 30–100 mW at 200 mm s^{-1} . b,c) Excellent cell viability is indicated by high GFP- (green) and very low propidium iodide-signal (red). Scale bars 100 μm .

Within 3 d after micropatterning cell spreading was observed in loops fabricated at laser powers down to 40 mW, indicating that at these conditions the network in the irradiated areas had been sufficiently disintegrated for cells to penetrate. Moreover, after 14 d cells also entered the area irradiated at 30 mW, most likely due to ester hydrolysis of remaining linkages.^[100c] On the contrary, in a control sample two-photon micropatterned without P2CK, cells only entered channels fabricated at laser powers of 60 mW and above within 7 d (Figure 39).

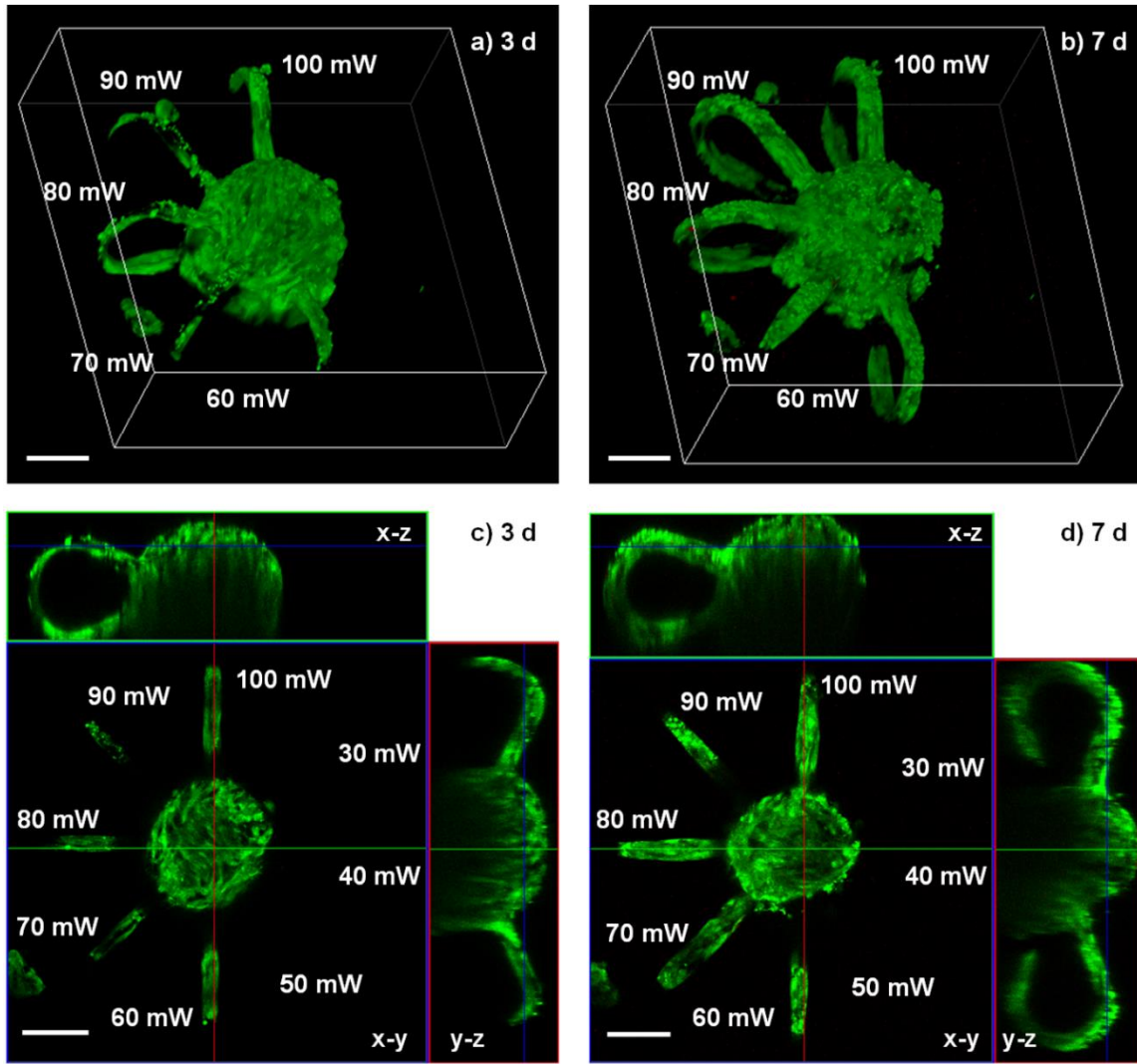


Figure 39: ASC/TERT1 spreading into loops micropatterned without P2CK. In a control experiment, horseshoe-shaped channels were micropatterned around a spheroid at different laser powers (30–100 mW) in the absence of P2CK. a,c) Within 3 days after two-photon micropatterning cells had only partially entered channels fabricated at laser powers of 60 mW and above. b,d) Cells did not spread into channels fabricated at lower laser power even after 7 days. Excellent cell viability is indicated by high GFP- (green) and very low propidium iodide-signal (red) after 7 days. Scale bars 100 μ m.

To further demonstrate the power of the two-photon micropatterning approach two complex spirals were produced and connected to a spheroid in presence of 0.1 mM P2CK at laser powers of 50 mW and 100 mW (Figure 40).

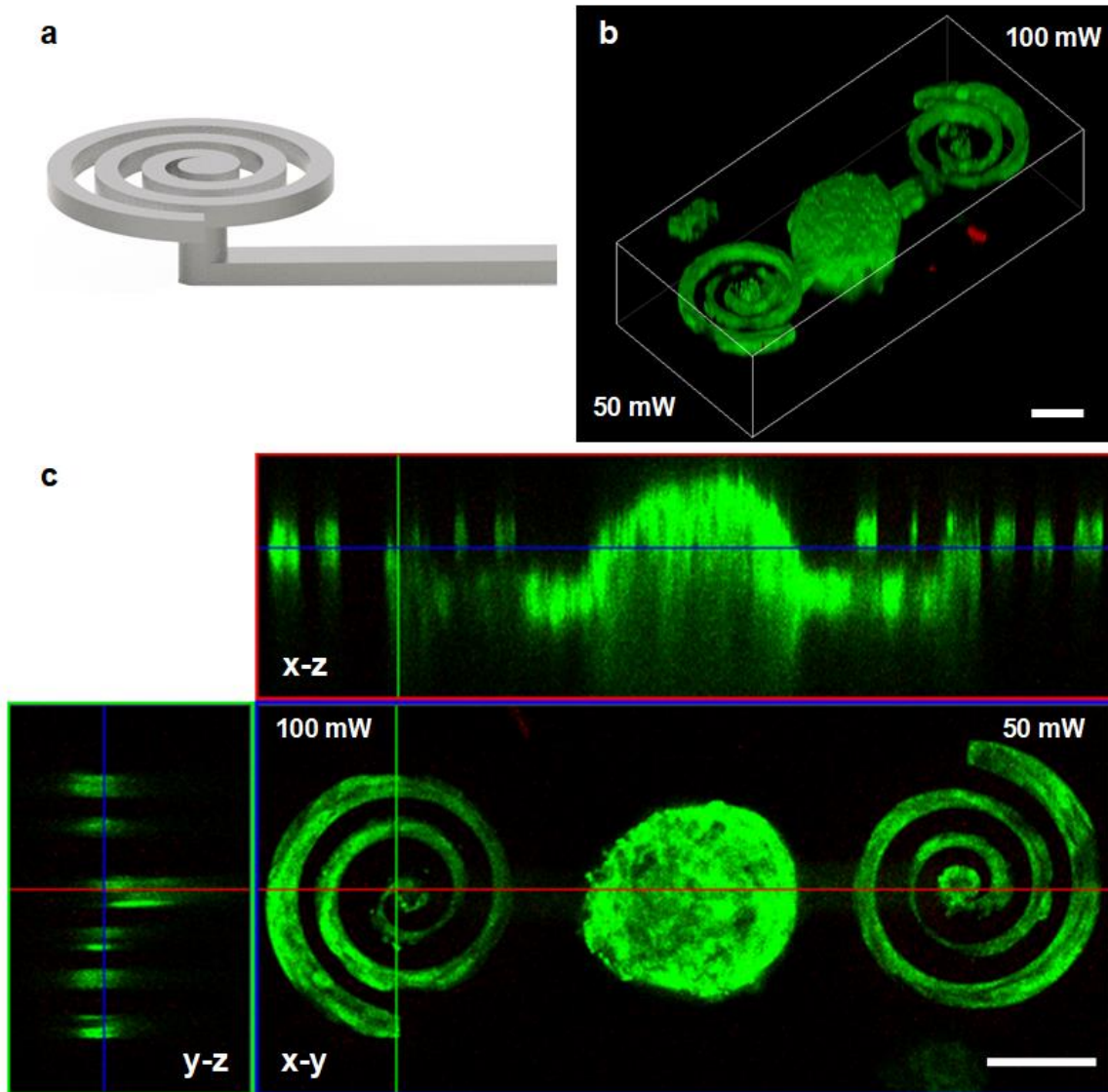


Figure 40: ASC/TERT1 spreading into two-photon micropatterned spirals. a) A complex 3D-object consisting of a spiral which is connected to a channel in another z-plane was generated by CAD. Spirals were produced at 50 mW and 100 mW in presence of P2CK (0.10 mM) in a way that they were connected to a spheroid via the channel. After 7 d cells filled up both spirals as visualized by b) 3D renderings and c) orthogonal projections of confocal z-stacks. High GFP- (green) and very low propidium iodide-signal (red) indicate excellent cell viability. Scale bars = 100 μm.

Additionally, human osteosarcoma cells (MG-63) exhibited similar spreading behavior as ASC/TERT1 in a preliminary experiment when linear channels had been patterned (Figure 41).

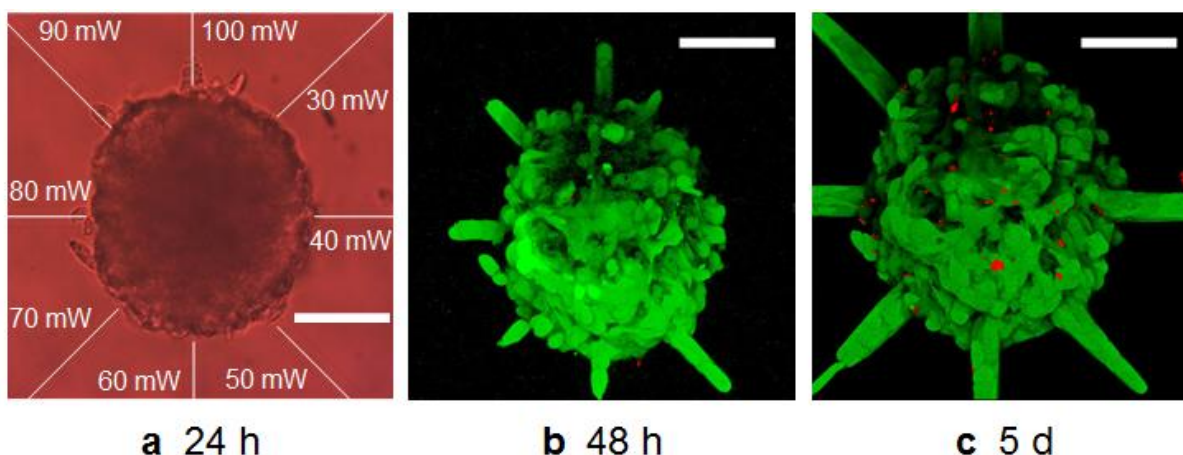


Figure 41: Spreading of human osteosarcoma cells (MG-63) into channels two-photon micropatterned in PEG-HA-SH hydrogel. a) Light microscopy image of a MG-63 spheroid encapsulated in PEG-HA-SH hydrogel (DS = 40%). Linear micro-channels ($300\ \mu\text{m} \times 20\ \mu\text{m} \times 20\ \mu\text{m}$) were eroded from the spheroid into the bulk hydrogel with increasing laser powers ranging from 30–100 mW in a clockwise manner, after swelling the hydrogel for 1 h in a 0.1 mM P2CK solution. The light microscopy image was taken 24 h after the channels were produced. Micro-channels are indicated by thin white lines. LIVE/DEAD staining was performed to investigate both the viability and spreading of MG-63 cells into the channels after b) 48 h and c) 5 days showing high cell viability. Green: calcein AM; Red: propidium iodide; Scale bars = $100\ \mu\text{m}$.

4.6 Mechanistic considerations

While it has been reported that the two-photon triggered decomposition of photolabile groups can be sensitized by covalently linking two-photon chromophores to such chemical entities and utilizing a FRET process, multiple synthetic transformations are required therefor.^[97] Moreover, the use of such tandem systems in photocleavable hydrogels would involve the covalent integration of chromophores with unknown bioactivity to the hydrogel backbone. However, by modularly adding a two-photon active small molecule to the respective hydrogel as solute at an user-defined point of time the interaction between encapsulated cells and hydrogel matrix is not interfered by chromophores permanently attached to the hydrogel backbone. Additionally, a modular sensitizer system permits the combination of different hydrogel precursors allowing for greater flexibility on achievable materials properties. The sensitized two-photon patterning was performed at 800 nm, which is a common wavelength of fs-pulsed Ti:sapphire lasers. Therefore, the developed approach can be used with commercially available multi-photon microscopes and

turn-key low-power fs-pulsed lasers, which became available at a reasonable price in the recent years.

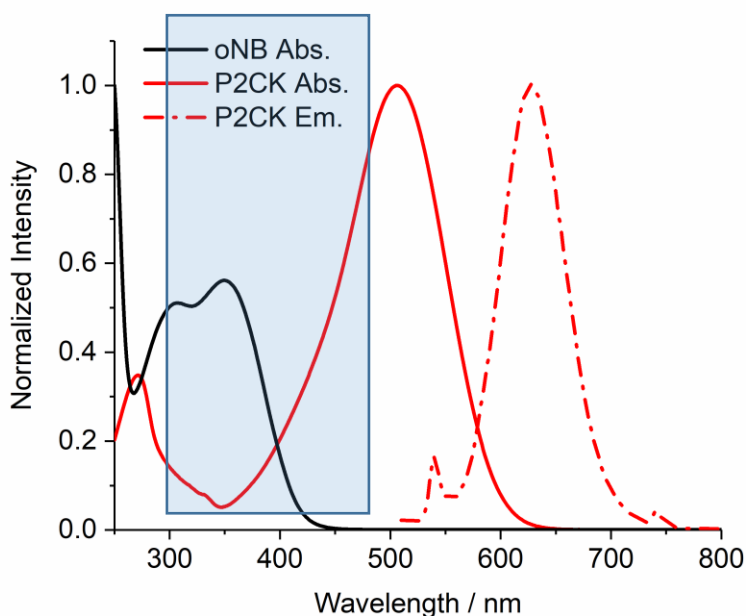


Figure 42: One-photon spectroscopy of P2CK and oNB moiety 11. The linear absorption spectrum of oNB moiety 11 (190 μM) as well as the absorption and emission spectra of P2CK (11 μM) were measured in PBS. The absorption spectra of P2CK (red line) and oNB moiety 11 (black line) overlap with the UV-light source used in the photorheology experiments (320–500 nm, blue area) whereas only P2CK is excited by the 460 nm LED. However, the emission spectrum of P2CK (red dotted line) does not overlap with the absorption spectrum of oNB 11. Hence, a FRET-based sensitization mechanism can be excluded.

Interestingly, as there is no overlap between the P2CK emission and the oNB absorption (Figure 42), a FRET-based mechanism can clearly be excluded. Besides, the photosensitizing effect of P2CK on the oNB ester cleavage reaction was not observed under UV-VIS light irradiation in respective rheological studies, neither when only P2CK (460 nm), nor when both oNB and P2CK (320-500 nm) were excited (Figure 43 and Figure 44). Hence, the interaction between P2CK and oNB is not trivial and advanced spectroscopic investigations are required to gain an in-depth understanding of the mechanism.

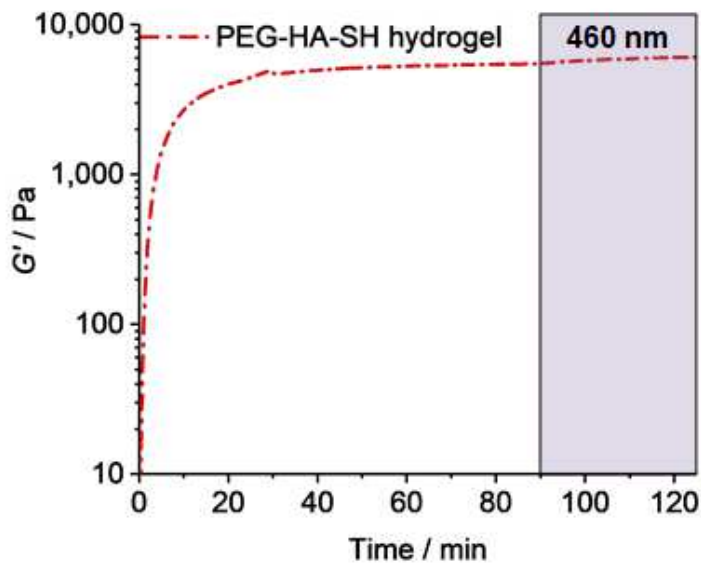


Figure 43: Irradiation of PEG-HA-SH hydrogel in presence of P2CK at 460 nm. Optically thin hydrogels (50 μm) were in situ formed on the measuring platform of a photorheometer in presence of P2CK (0.1 mM). The hydrogel was irradiated at 460 nm using an LED ($\sim 17 \text{ mW cm}^{-2}$, 35 min). While P2CK is specifically excited at 460 nm, this wavelength lies outside the absorption range of oNB. No decrease of G' could be observed. A slight increase of G' in the course of irradiation can be attributed to polymerization of unreacted pending groups due to weak initiation properties of typical two-photon initiators.^[115]

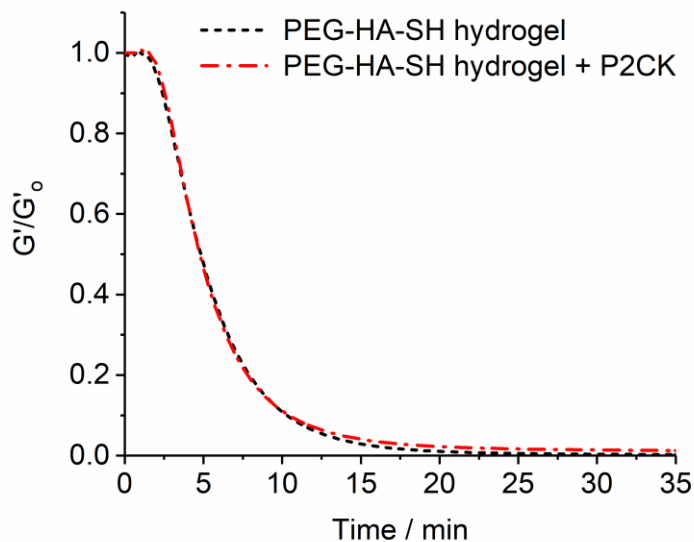


Figure 44: UV-VIS degradation of PEG-HA-SH hydrogel in presence of P2CK and without. Optically thin hydrogels (50 μm) were in situ formed on the measuring platform of a photorheometer either in presence of P2CK (0.1 mM) or without. No pronounced effect of P2CK on the one-photon induced degradation (320–500 nm, $\sim 20 \text{ mW cm}^{-2}$) of the photocleavable hydrogel networks could be observed.

4.7 Conclusion

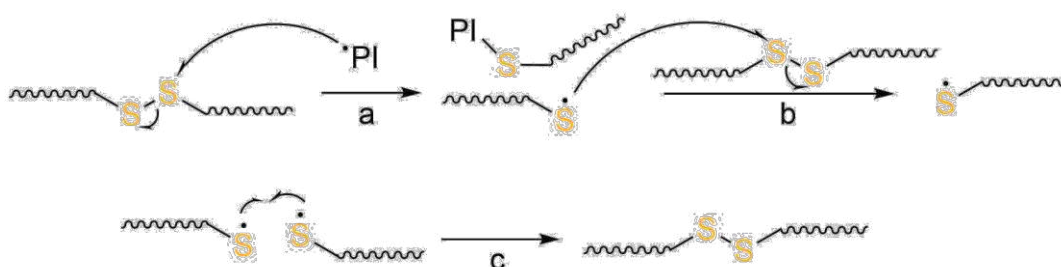
In summary, a modular photosensitizing approach for the two-photon induced degradation of a hydrogel based on the new combination of a thiol modified hyaluronic acid and an established PEG-linker containing photocleavable oNB ester groups was developed. By addition of the two-photon active molecule P2CK to the preformed hydrogel the threshold power for two-photon induced photoerosion could be successfully decreased. The presented modular system is biocompatible and can be operated in the presence of encapsulated cells. Due to its modularity, this platform is a useful tool for fundamental studies of cell matrix interactions in 3D culture where spatiotemporal control over the cell surrounding matrix by two-photon micropatterning of photocleavable hydrogels at moderate laser powers is needed. Moreover, this platform also has great potential in the field of microfluidics, as open channels can easily be produced at high writing speeds without the need of repeated scanning.^[29b]

This work has recently been published as Communication in the journal *Angewandte Chemie International Edition*.^[116]

5. SIMPLIFYING THE SYSTEM – TWO-PHOTON CLEAVAGE OF DISULFIDE BONDS

5.1 State of the Art

While the sensitized two-photon cleavage of oNB ester-based photodegradable hydrogels improves the micro-structuring process,^[116] it still relies on a photolabile chromophore (oNB), which requires multi-step synthesis.^[98] Another drawback of photolabile chromophores is their inherent UV-light sensitivity making handling under light-protection necessary. In contrast, Fairbanks *et al.* described the degradation of a disulfide-crosslinked network through the radical-mediated disulfide fragmentation as alternative photo-triggered bond-scission (Ch. 3.1 and Scheme 24).^[25d] Here, in the presence of a photoinitiator, light exposure generates chemical radicals that propagate and cause multiple crosslink degradation.^[19b] Hence, in the absence of a photoinitiator the disulfide network is stable. Moreover, while common photocleavable groups undergo irreversible scission, disulfide cleavage can be reversible. Thus, materials containing disulfide linkages also exhibit self-healing behavior.^[25d, 86]



Scheme 24: (a) Upon excitation a radical initiator fragment attacks a disulfide bond within the network, transferring an electron to one of the two sulfurs generating a thiyl radical and a terminated network-chain. (b) A thiyl radical transfers to another sulfur by fragmentation and degradative chain transfer. The radical disulfide exchange minimizes the free energy of the system, allowing it to accommodate an applied stress on the network. (c) Reversible termination occurs by thiyl radical recombination, re-forming the disulfide bond.^[25d]

Surprisingly, this radical-mediated cleavage reaction has only been examined in one-photon excitation regime so far. Reasonably, the two-photon induced cleavage of disulfide-based networks in presence of two-photon active compounds such as P2CK^[49b] or DAS^[49a] (Figure 45) should also be explored as missing link in the techniques for disulfide network degradation, especially for spatially targeted cleavage.

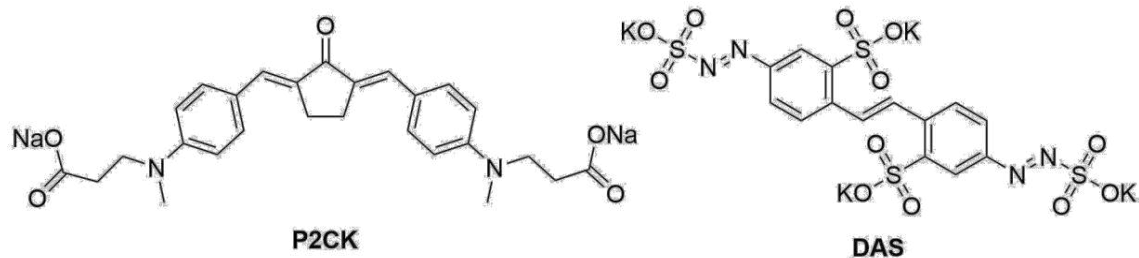


Figure 45: Molecular structures of water-soluble two-photon active chromophores P2CK^[49b] and DAS.^[49a]

On the contrary, Barner-Kowollik and co-workers developed a photoresist based on thiol-terminated macromers and a phenacyl sulfide linker for the direct formation of disulfide networks upon two-photon irradiation at 700 nm (Figure 46).^[117] Here, the phenacyl sulfide releases a photo-caged thioaldehyde species, which reacts with a thiol to form a disulfide bond.

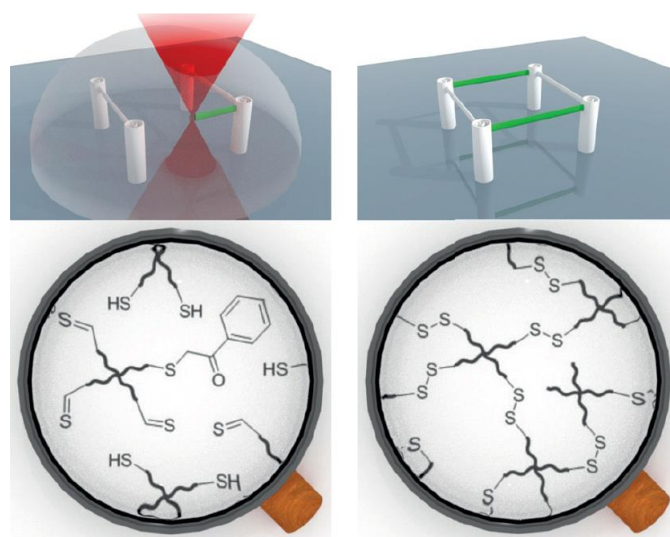


Figure 46: Direct writing of disulfide networks was demonstrated by irradiating a photoresist based on thiol-terminated macromers and a phenacyl sulfide linker at 700 nm. Upon two-photon excitation, the phenacyl sulfide releases a photo-caged thioaldehyde species, which reacts with thiol to a disulfide.^[117]

Hence, the two-photon induced cleavage of disulfide networks would bridge the gap towards photo-orthogonal formation and degradation of disulfide networks by means of two-photon irradiation.

5.2 Two-photon degradation of 4arm-PEG5k-SH hydrogel in presence of two-photon sensitizers

To examine the applicability of two-photon sensitizers for the cleavage of disulfide-crosslinked polymer networks, a hydrogel was prepared from thiol-terminated four-armed polyethylene glycol with a molecular weight of 5 kDa (4armPEG5k-SH) as described in literature.^[25d] Thus, to a 10% solution of 4arm-PEG5k-SH in deionized water was added 30% H₂O₂ to a final concentration of 1% and sodium iodide (10 mM) to a final concentration of 1 mM. Hydrogel samples were formed in molds on methacrylated glass-bottom μ -dishes (ibidi) and allowed to gel for 1 h, before the samples were swollen in deionized water in the fridge for two days.

One sample was cut and microchannels (300 μ m x 20 μ m x 50 μ m) were structured in the absence of a sensitizer at 800 nm (10-100 mW, 200 mm s⁻¹, 0.1 μ m hatch, 0.5 μ m dz). In order to visualize these channels, they were swollen in fluorescein modified dextran (FITC2000, M_w ~ 2000 kDa), which due to its size can only enter open pore channels. Indeed, diffuse channels scanned at laser powers >50 mW were visible via light microscopy but these channels were not filled with FITC2000 (1 mg mL⁻¹) indicating incomplete network degradation. However, the hydrogel sample was later treated with P2CK (0.1 mM) and hence channels formed in the absence of the chromophore could also be visualized indirectly as dark areas at high LSM settings utilizing the fluorescence signal of P2CK (Figure 47).

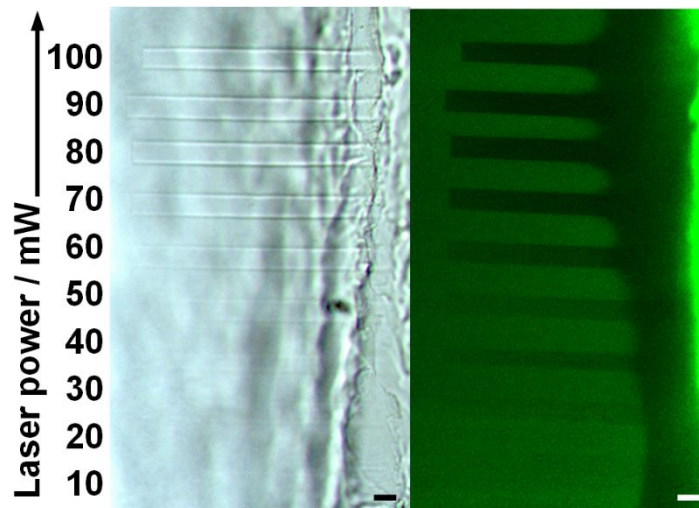


Figure 47: Untreated 4armPEG5k-SH hydrogel was micro-structured at laser powers from 10-100 mW and a writing speed of 200 mm s⁻¹. Channels could be visualized by light microscopy (left) or indirectly via LSM utilizing the fluorescence signal of P2CK (right). Scale bars 20 μ m.

In contrast, when the hydrogel sample was two-photon structured using the same scanning parameters after 90 min of swelling in a 0.1 mM P2CK solution,³ channels fabricated at all laser powers used were visible by light microscopy (Figure 48). Moreover, after staining with FITC2000, cavities scanned at laser powers >50 mW could be visualized by LSM. However, even after prolonged treatment with FITC2000 some channels were not fully filled, which may be caused by local irregularities in the gel.

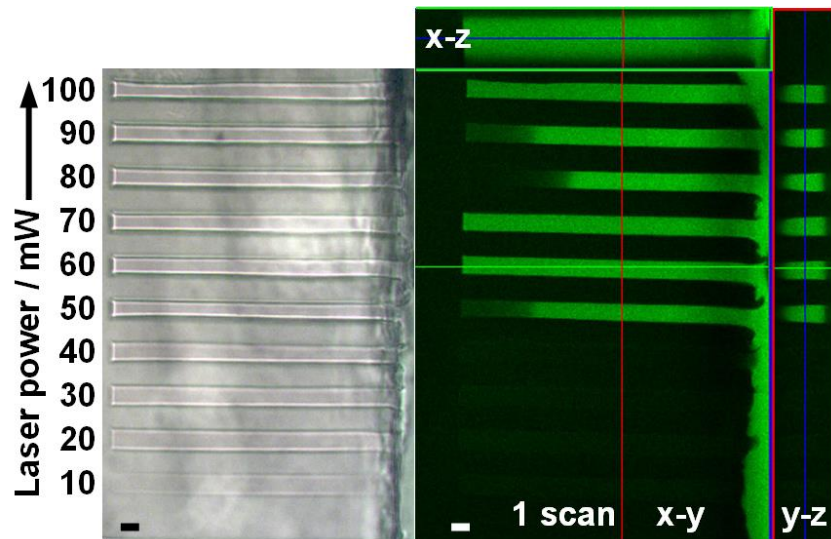


Figure 48: When the hydrogel sample was structured in presence of 0.1 mM P2CK, channels fabricated at all laser powers were visible by light microscopy (left). After staining with FITC2000, cavities scanned at laser powers >50 mW could be visualized by LSM. Some channels were not fully filled, which may be due to local irregularities in the gel (right). Scale bars 20 μm .

Nevertheless, to increase hydrogel degradation x,y-planes were irradiated in two consecutive scans. This way, cavities produced at laser powers of 20 mW and above became visible and channels fabricated at >20 mW were completely filled with FITC2000 (Figure 49). However, channels produced at 10 mW still appeared diffuse in light microscopy indicating insufficient degradation.

³ In contrast, when the swelling time in P2CK was significantly reduced (~15 min) only incomplete erosion of microchannels could be achieved and channels could not be examined by LSM.

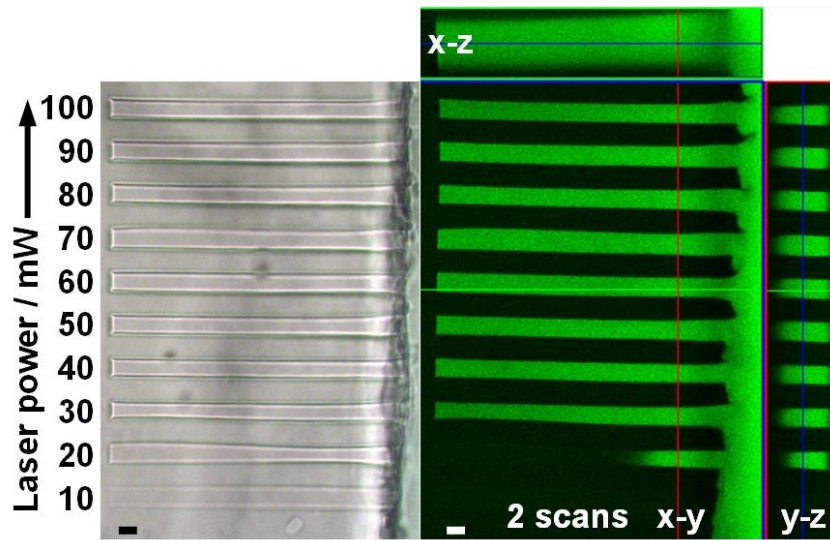


Figure 49: A set of channels was fabricated by scanning the hydrogel twice in presence of 0.1 mM P2CK. After washing with PBS and swelling in FITC2000, channels fabricated at 20 mW and above showed fluorescence. Scale bars 20 μm .

A further hydrogel sample was cut and swollen (>120 min) in a 1 mM solution of water-soluble cleavable two-photon initiator DAS.^[49a] In contrast to P2CK, the two-photon absorption spectrum of DAS is shifted to lower wavelengths and hence it was scanned at 720 nm. However, to compensate for the lower two-photon cross section compared to P2CK at 800 nm, DAS was used at a concentration of 1 mM. Interestingly, while channels were visible in light microscopy, they appeared to be deformed and were not properly filled with FITC2000 (Figure 50).

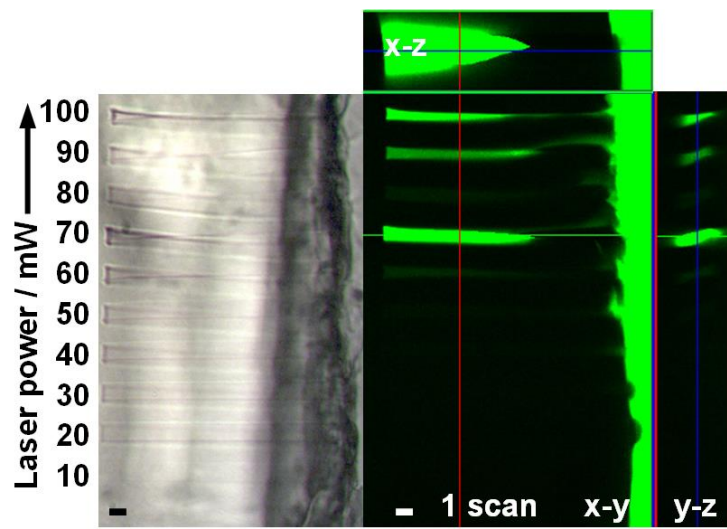


Figure 50: Channels fabricated in presence of 1 mM DAS were obviously deformed. Scale bars 20 μm .

To exclude improper degradation as cause for incompletely filled channels, the experiment was repeated by scanning x,y-planes in two consecutive scans (Figure 51). Consequently, channels fabricated at laser powers of 30 mW and above exhibited fluorescence, but all channels seemed to be collapsed. It is not clear if this is a result of the cleavage process or caused by irregularities in the hydrogel.

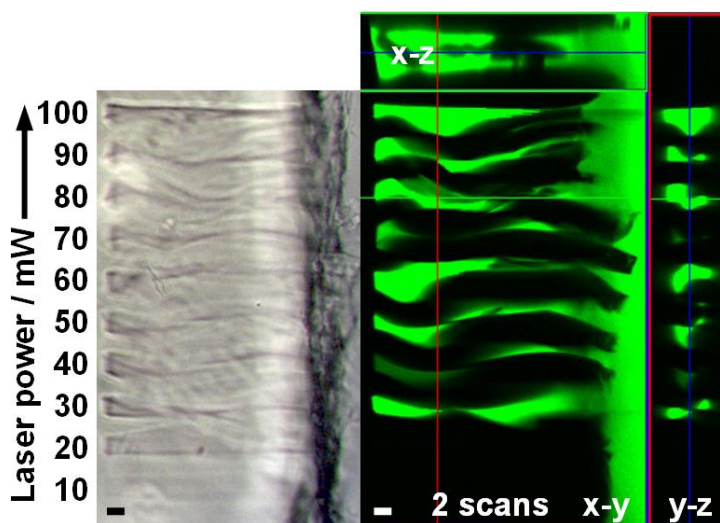


Figure 51: Microchannels produced in 4armPEG5k-SH hydrogel in presence of 1 mM DAS by double scanning collapsed. Scale bars 20 μ m.

With this experimental series it could be demonstrated that open micro-channels in disulfide-crosslinked 4armPEG5k-SH hydrogel can be produced by two-photon patterning in presence of P2CK (0.1 mM) or DAS (1 mM). In absence of these two-photon active chromophores, areas scanned at higher laser powers become visible but are not fully cleaved at the scanning conditions used. A reason for the appearance of these microstructures in absence of two-photon active compounds might be due to thermal effects. In general, the process of hydrogel formation by the use of hydrogen peroxide is not convenient, as the formulation quickly reaches it's gel point and is difficult to handle, which might be the cause for inhomogeneities in thus formed hydrogels.

5.3 One-photon irradiation of 4armPEG5k-SH hydrogel in presence of P2CK

To examine if P2CK also acts as a sensitizer for disulfide-cleavage upon one-photon irradiation, a 10% 4arm-PEG5k-SH hydrogel was irradiated in presence of 0.5 mM P2CK with 460 nm LED-light, which is close to the compound's absorption maximum (Figure 42). Hence, 4arm-PEG5k-SH hydrogel was prepared as described above and swollen in 0.5 mM P2CK solution at room temperature overnight. It was then shaded half ways with aluminum foil and placed under the focus of a 460 nm LED for 15 min. The distance from the LED was 5 cm corresponding to a light

intensity of 6 mW cm^{-2} . After irradiation, no alteration of the irradiated area could be observed, neither with blank eye, nor by light microscopy (2.5x). The irradiated hydrogel was also scanned by LSM at 20x magnification (488 nm, z-stack) revealing no alteration of the irradiated area.

5.4 Two-photon microchannel fabrication in organogels

Since water-soluble two-photon sensitizers are rare, further experiments were conducted in organogels to extend the scope of the study and test the feasibility with additional two-photon sensitizers known from literature, namely M2CMK^[48a] and R8^[118] (Figure 52).

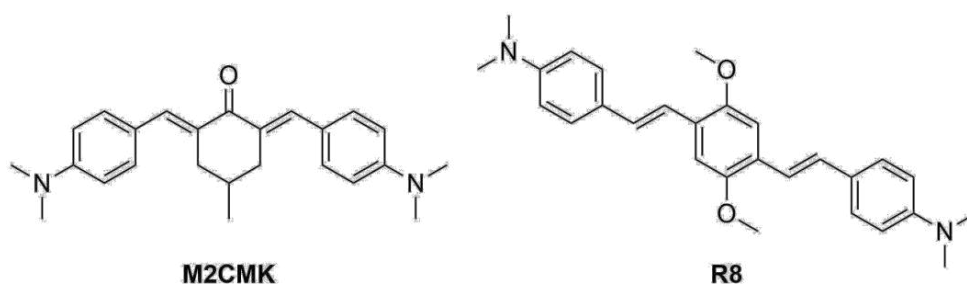


Figure 52: Molecular structures of two-photon sensitizers M2CMK^[119] and R8^[118].

Hence, an organogel from a 10% solution of 4arm-PEG5k-SH in acetonitrile (MeCN) was prepared by oxidation via $\text{H}_2\text{O}_2/\text{NaI}$ following the protocol used before.^[25d] After swelling in 2-propanol overnight, organogels were either submersed in solutions of M2CMK or R8 in MeCN (0.5 mM) for at least 3 h and then cut with a scalpel. Microchannels were fabricated at 800 nm and laser powers from 10-100 mW at a scanning speed of 200 mm s^{-1} using the parameters applied earlier. Additionally, also a sample swollen in pure MeCN was tested. After two-photon scanning, the organogels were analysed by light microscopy (Figure 53).

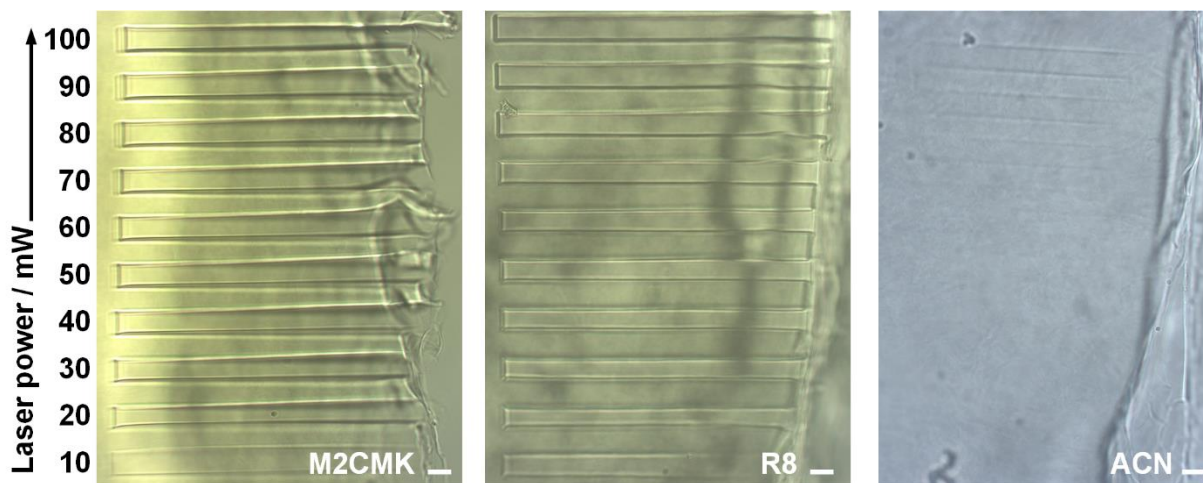


Figure 53: Channels were microstructured in 4armPEG5k-SH organogel using 800 nm irradiation at 10-100 mW. *left*: 0.5 mM M2CMK, *center*: 0.5 mM R8, *right*: MeCN only. Scale bars 20 μm .

Channels produced in the absence of two-photon sensitizers were hardly visible and only appeared at laser powers above 80 mW. In contrast, when organogels were scanned in presence of two-photon sensitizers distinct channels formed at all laser powers used, demonstrating the positive effect of utilizing two-photon sensitizers for two-photon micro-patterning of disulfide-based gels.

5.5 Two-photon induced cleavage of a disulfide-based hyaluron network

In a further experiment, a hydrogel was produced from thiol-modified hyaluronic acid with a DS of 8% (HA-SH 8%, Figure 54) by oxidative crosslinking to investigate the effect of two-photon sensitization on a different substrate. HA-SH 8% was synthesized by Dr. Davide Ret in the course of his dissertation at the Institute of Applied Synthetic Chemistry.^[120]

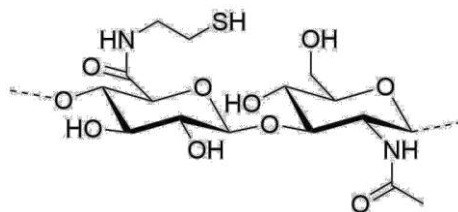


Figure 54: Molecular structure of the repetition unit of hyaluronic acid modified with cysteamine. The material used in the experiment had a degree of substitution of 8%.

From a precursor formulation containing 3% of HA-SH dissolved in DMEM a network was formed by drop casting. Gelation was induced oxidatively by adding a droplet (10 μ L) of a 3% solution of H_2O_2 atop of a drop (70 μ L) of the HA-SH precursor solution (Figure 55). The formulation was maintained at room temperature for 30 min, before formation of a solid gel was verified by tilting. Here, H_2O_2 diffuses into the precursor solution. In contrast, direct mixing of H_2O_2 into the precursor solution resulted in the instantaneous formation of a stable hydrogel foam. The hydrogel hemisphere was cut in half using a scalpel and soaked in a 0.1 mM solution of P2CK for 45 min.

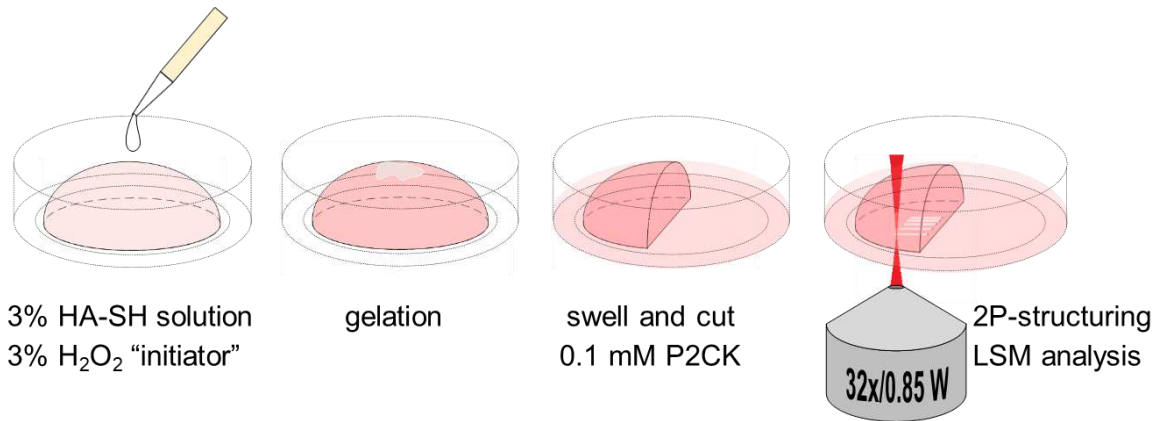


Figure 55: Schematic steps from hydrogel formation to two-photon erosion of the HA-SH based hydrogel in presence of 0.1 mM P2CK.

Then micro-channels ($300\ \mu\text{m} \times 20\ \mu\text{m} \times 20\ \mu\text{m}$) were eroded into the hydrogel at 800 nm using laser powers from 10-100 mW and a writing speed of 200 mm/s. For evaluation of the scanned channels, the hydrogels were swollen in a solution of FITC2000 in PBS ($5\ \text{mg mL}^{-1}$), permitting visualization of the microchannels by LSM. As depicted in Figure 56, microchannels fabricated at laser powers of 40 mW and above show bright fluorescence. Contrary, in an additional experiment in the absence of P2CK no open channels formed.

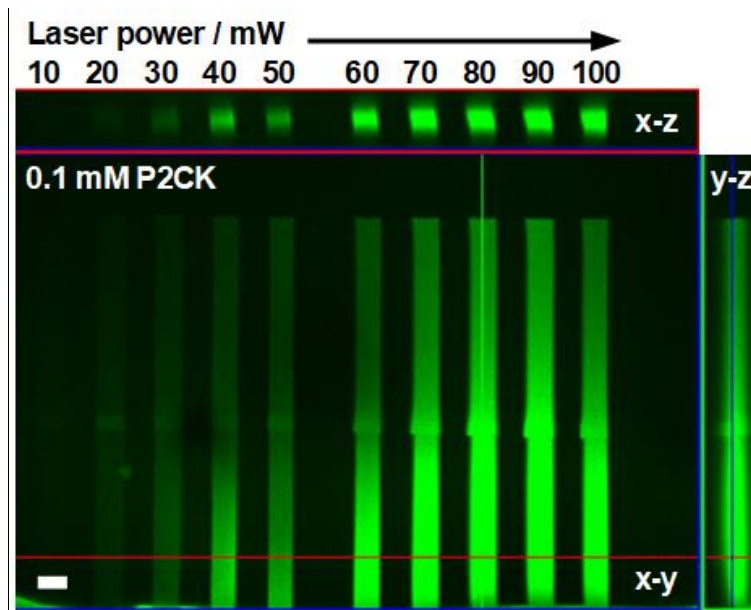


Figure 56: HA-SH 8% hydrogel was micro-patterned after swelling in 0.1 mM P2CK by irradiation at 800 nm. Microchannels were visualized with FITC2000 by LSM. Scale bar 20 μm .

5.6 Conclusion

This simple study successfully demonstrates the feasibility of two-photon sensitized disulfide-cleavage (Figure 57). Moreover, it shows that two-photon degradable hydrogels can be produced directly from a thiol-containing precursor without the use of any additional linkers containing photolabile chromophores as oNB, significantly simplifying precursor preparation. However, the formation of disulfide-crosslinked hydrogels by direct oxidation of thiols to disulfides is unpractical since it is hard to control and mediated by harmful compounds as hydrogen peroxide. Hence, it might be advantageous to introduce disulfide linkages via simple linkers into networks.

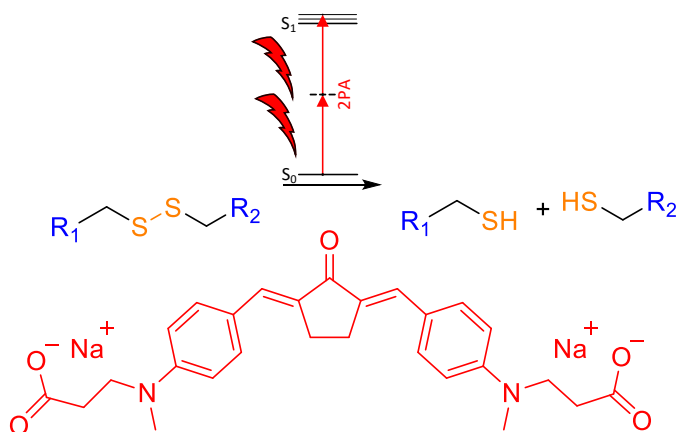


Figure 57: Schematic illustration of the sensitized two-photon cleavage of disulfide linkages.

6. INTRODUCING DISULFIDE LINKAGES BY THE USE OF LIGHT

6.1 State of the art

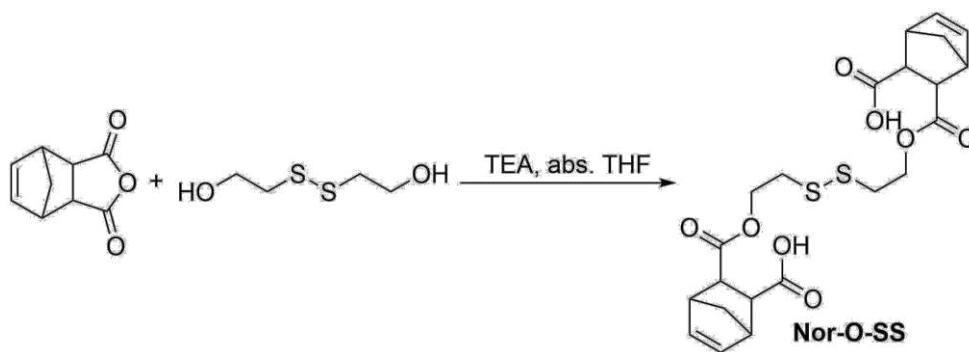
Photoresponsive hydrogel platforms have great potential for targeted drug delivery and 4D cell culture applications, as they permit spatiotemporal tunability of the materials properties.^[19b] Moreover, this material class is also highly useful and convenient for the fabrication of microfluidic devices by simply casting of the bulk material and degradation of microchannels by the use of multiphoton-irradiation techniques.^[29b] Common photodegradable hydrogels are based on photocleavable chromophores as oNB,^[22] coumarin^[121] or Ru-complexes,^[25g] which all require rather complex multistep syntheses. Besides, these photolabile chromophores are inherently photosensitive and hence require handling under light protection. A structurally simpler alternative to these chromophores are disulfides, which can be degraded through a radical-mediated disulfide fragmentation reaction.^[25d] However, this reaction requires the presence of a photoinitiator, which upon irradiation generates the required radicals and initiates degradation. Hence, in the absence of a photoinitiator disulfide-linked networks are light stable. Disulfide-based networks have been reported to be directly formed from thiol-terminated macromers by oxidative coupling of thiols to disulfides mediated by oxygen,^[109] in presence of hydrogen peroxide,^[25d, 122] or enzymatically using horseradish peroxidase (HRP).^[123] However, reactions mediated by oxygen are difficult to control. In the case of hydrogen peroxide the concentration used has to be adjusted accordingly for every different formulation to avoid polymerization occurring too quickly.^[25d] Besides, H₂O₂ is cell affecting and cytotoxic. In contrast, the HRP-mediated crosslinking proceeds rather slowly.^[123] Other approaches include the application of disulfide-containing linkers with acrylate terminals.^[76, 124] These linkers were either incorporated into networks by thiol-Michael addition with thiol-terminated macromers^[76] or free radical copolymerization with acrylates using thermal initiator systems^[124] or even a photoinitiator.^[125] Nevertheless, crosslinking formulations based on Michael-type thiol-ene additions have to be handled very skilled and quickly as the gelation reaction sets in fast upon combination of the reactive components,^[116] which can be challenging especially when it comes to cell encapsulation or molding of complex geometries. Besides, acrylates are considered cytotoxic.^[126] For the ease of handling, an externally triggered gelation-reaction would hence be highly advantageous, as for example photo-induced step growth polymerization. However, since disulfides can be cleaved by higher concentrations of radicals,^[25d] a highly reactive coupling reaction is required. Besides being an ideal step-growth polymerization, the thiol-norbornene addition is extremely reactive and well tolerated in cell encapsulation.^[127]

Hence, a water-soluble disulfide-containing linker with norbornene terminals **Nor-SS-Nor** from cheap and readily available starting materials should be developed, which allows fast and complete crosslinking of thiol-terminated precursors to form disulfide-based hydrogels.

6.2 Development of disulfide-based crosslinkers

6.2.1 A Nor-SS-Nor crosslinker from cheap starting materials

The most simple approach to such a disulfide-containing photo-crosslinker is based on the readily available chemicals 2-hydroxyethyl disulfide and carbic anhydride leading to the simple symmetric target molecule **Nor-O-SS**. The straightforward synthesis was conducted in dry THF in presence of TEA (Scheme 25). Purification from remaining starting materials was performed by means of column chromatography. A part of the resulting **Nor-O-SS** was further converted into the corresponding sodium salt by reaction with sodium bicarbonate (1 M, 2 eq) to provide water-solubility.



Scheme 25: Synthesis of the 2-hydroxyethyl disulfide based linker Nor-O-SS.

However, **Nor-O-SS** could not be completely purified from starting materials. In fact, the compound proved to be unstable in DMSO- d_6 solution. ^1H -NMR experiments revealed that >50% of the linker decomposed in the course of one week (Figure 58). Since DMSO- d_6 is an aprotic solvent, hydrolysis can be excluded. In contrast, as the signals of the starting materials reappeared again, a reaction appears to take place, in which carbic anhydride is eliminated.

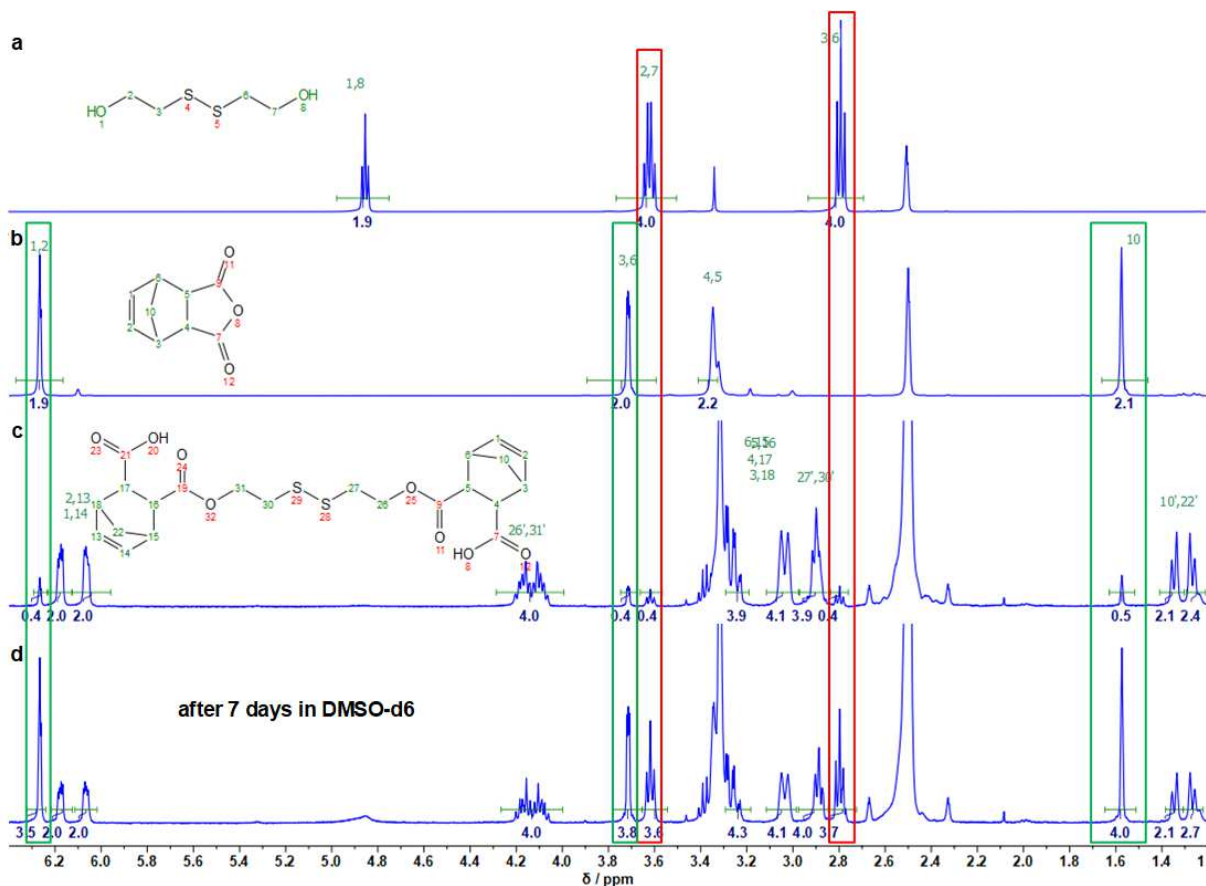
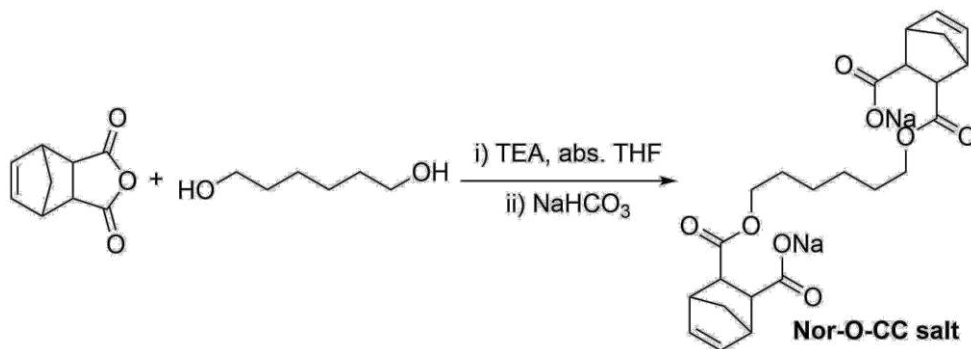


Figure 58: Comparison of ¹H-NMR spectra of starting materials (a) hydroxyethyl disulfide, (b) carbic anhydride and product Nor-O-SS (c) after column chromatography and (d) after 7 days in DMSO-d₆ solution. The linker obviously decomposes back into its starting materials, as signals of both compounds reappear over time.

Additionally for comparison reasons, the non-cleavable crosslinker analogue **Nor-O-CC** based on 1,6-hexanediol and carbic anhydride was synthesized following the same procedure (Scheme 26). It was subsequently converted into its sodium salt by addition of 2 eq of NaHCO₃.



Scheme 26: Synthesis of non-cleavable linker Nor-O-CC based on 1,6-hexanediol and subsequent conversion into its sodium salt.

Interestingly, no elimination of carbic anhydride was observed for the corresponding aliphatic linker **Nor-O-CC**, which remained stable in DMSO-d₆ for 7 days (Figure 59).

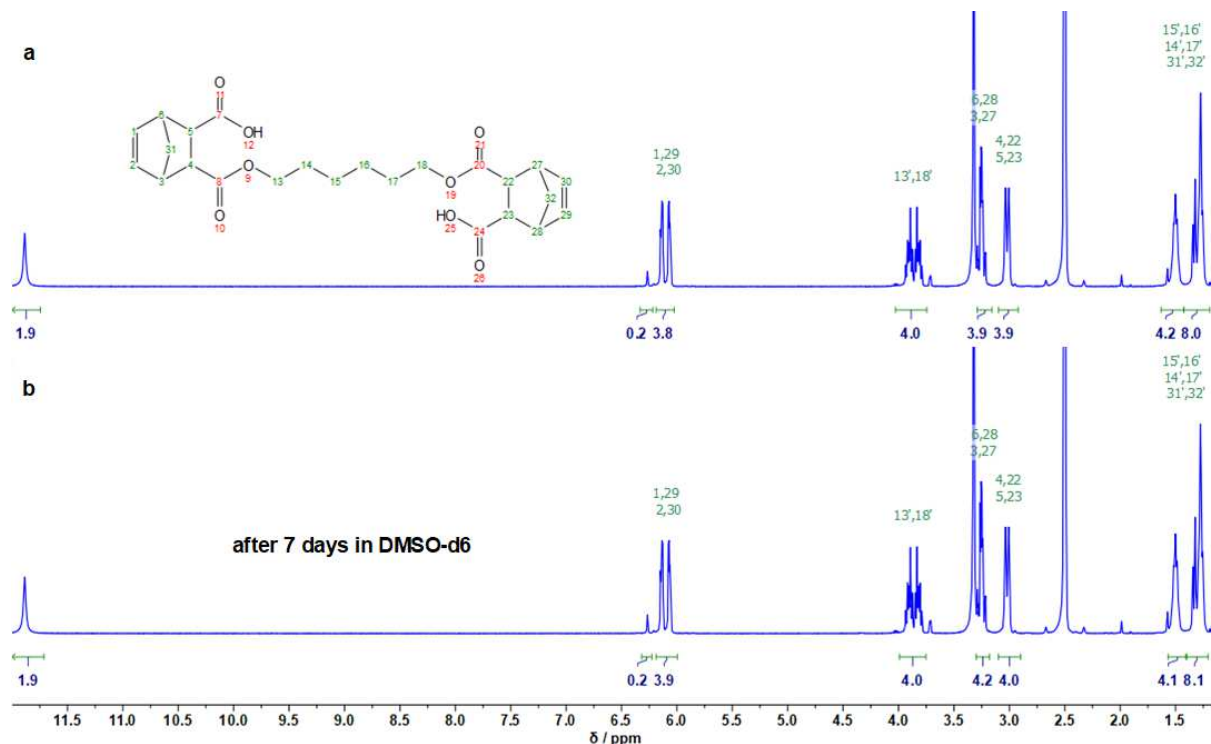
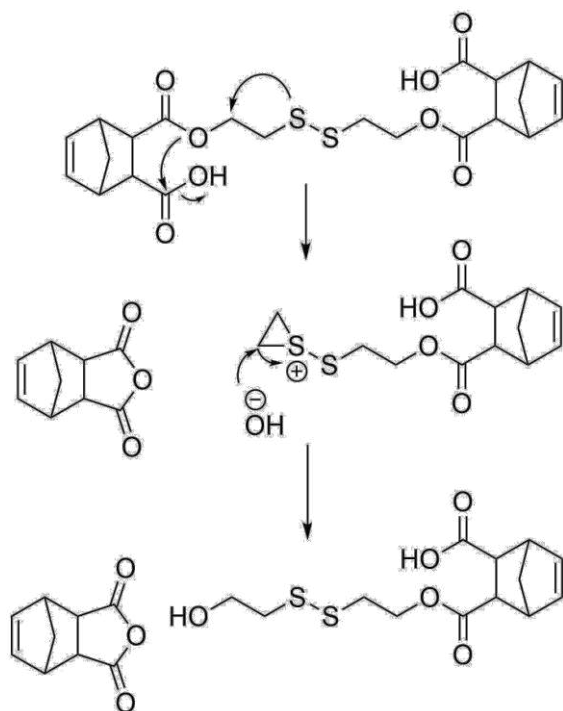


Figure 59: Comparison of ¹H-NMR spectra of non-cleavable linker **Nor-O-CC** (a) after column chromatography and (b) after 7 days in DMSO-d₆ solution. This linker proved to be stable against elimination in DMSO-d₆.

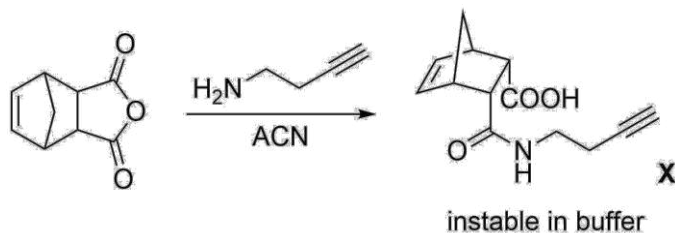
These results indicate that the presence of the disulfide is triggering the elimination reaction, which occurs most probably due to a neighboring group effect of the disulfide in combination with the free carboxylic acid in close proximity to the ester.^[128] Thioethers in β -position to reactive sites are known to participate in elimination reactions via the formation of an intermediate cyclic sulfonium ion.^[129] Most likely the elimination of carbic anhydride from linker **Nor-O-SS** (Figure 58) occurs via the formation of a cyclic sulfonium ion (Scheme 27).^[129]



Scheme 27: Assumed elimination mechanism of carbic anhydride from Nor-O-SS triggered by the neighbouring group effect of the β -positioned sulfur atom via formation of an intermediate cyclic sulfonium ion. This elimination does not occur in the analogue disulfide-free linker Nor-O-CC.

Hence, the simple disulfide-based linker **Nor-O-SS** is not expected to withstand prolonged incubations of a hydrogel made thereof. Moreover, the purity and hence the crosslinking properties could not be guaranteed.

Nevertheless, one might expect the corresponding amide based on cystamine **Nor-N-SS** to give a more stable cross-linker. However, recent literature demonstrates that amide **X** synthesized from carbic anhydride completely hydrolyzes in aqueous puffer solution within 24 h (Scheme 28).^[130]

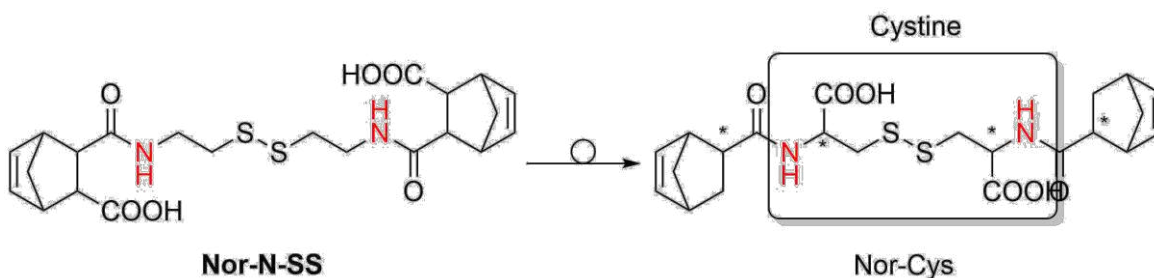


Scheme 28: Alcock and al. demonstrated that amide X readily hydrolyses in aqueous buffer solution by $^1\text{H-NMR}$ and LC-MS. Interestingly, a $^1\text{H-NMR}$ of the amide X in D_2O without hydrolysis product ($t = 0$ s) could not be obtained as the hydrolysis appears to occur rapidly under these conditions. However, a $^1\text{H-NMR}$ of amide X in DMSO-d_6 could be measured.^[130]

Besides stability issues, the synthesis of the corresponding amide from cystamine can be troublesome, due to solubility issues, the formation of mixed carboxylate-ammonium salts and intramolecular imide formation.

6.2.2 Formal translocation of the carboxylic acid

Consequently, it seemed reasonable to change the molecular design by moving the carboxylic acid away from the β -position to the amide. A formal translocation of the carboxylic acid groups leads to a cystine-based core, again a readily available starting material. However, due to the translocation the stereochemistry of the linker becomes more complex, as an asymmetric carbon is introduced at each branch of the core. *L*-Cystine is the cheaper option as it is the dimer of the essential amino acid *L*-cysteine. In contrast the *D,L*-derivative is much more expensive (factor 25 at Sigma-Aldrich). In this case, 5-norbornenecarboxylic acid chloride can be used as norbornyl-reactant, again introducing stereocenters.

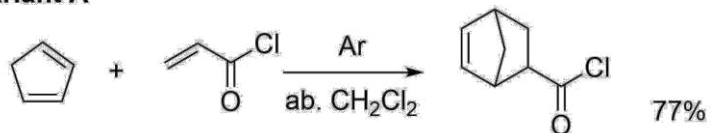


Scheme 29: A formal translocation of the carboxylic acid from the norbornyl moiety of Nor-N-SS to the α -position of the amino group leads to a cystine-based core structure. The resulting linker contains 4 stereocenters.

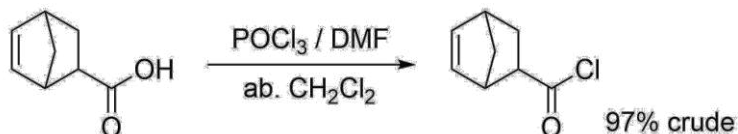
6.2.2.1 Synthesis of Nor-L-Cys

The *L*-cystine-based linker with norbornene terminals **Nor-L-Cys** was synthesized in a Schotten-Baumann-type reaction.^[124a] Norbornene carboxylic acid chloride NorCOCl was coupled to the amino-groups of *L*-cystine in methanol, due to the limited solubility of cystine in most solvents. NorCOCl can be obtained via two synthetic routes in good yield. In both cases, the product can be easily purified by distillation. Variant A is the Diels-Alder reaction between acryloyl chloride and cyclopentadiene (Scheme 30A).^[131] Due to the nature of the Diels-Alder reaction both the *exo*- and the *endo*-product are formed with the *endo*-product being predominant. Variant A requires a preliminary distillation step, as cyclopentadiene has to be obtained from its dimer dicyclopentadiene in a retro-Diels-Alder reaction.

Variant B is the synthesis from commercial available 5-norbornenecarboxylic acid NorCOOH by reaction with phosphoryl chloride in presence of a catalytic amount of DMF (Scheme 30 B).^[132]

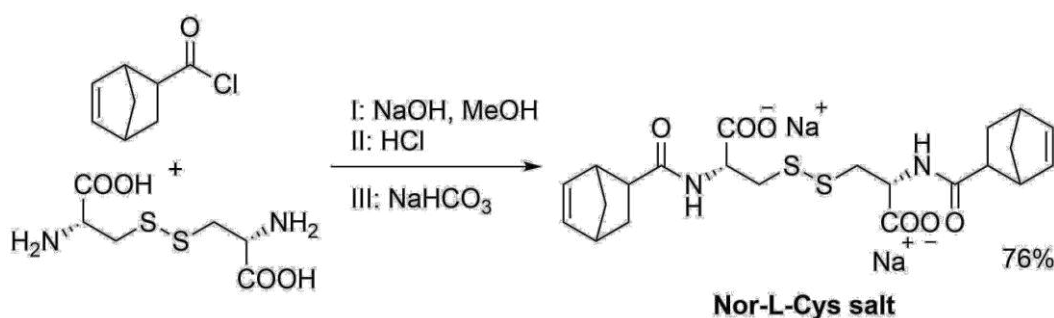
Variant A

mixture of exo and endo

Variant B

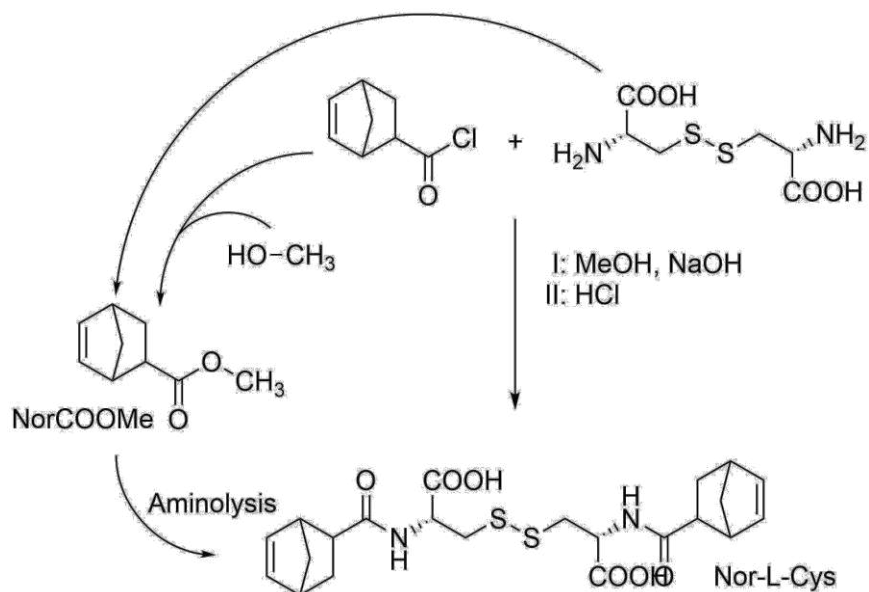
Scheme 30: Synthesis of 5-norbornenecarboxylic acid chloride NorCOCl via a Diels-Alder reaction between cyclopentadiene and acryloyl chloride (Variant A) or via conversion of 5-norbornenecarboxylic acid NorCOOH to the corresponding acid chloride by the use of phosphoryl chloride (Variant B).

NorCOCl (2 eq) was then linked to *L*-cystine in presence of finely ground NaOH (4 eq) in absolute MeOH (Scheme 31).



Scheme 31: Two-step synthesis of Nor-L-Cys from *L*-cystine and NorCOCl in a Schotten-Baumann reaction and subsequent conversion into the corresponding sodium salt.

Due to the weak solubility of NaOH and *L*-cystine in MeOH rather large volumes of solvent were required for complete dissolution, which impacts the reaction velocity. Methanol can also react with the acid chloride to form the corresponding ester NorCOOMe, which is further converted to the target product by aminolysis (Scheme 32). For these reasons, the reaction mixture was stirred at room temperature for several days for complete conversion of the starting material. Reaction control was performed by $^1\text{H-NMR}$.

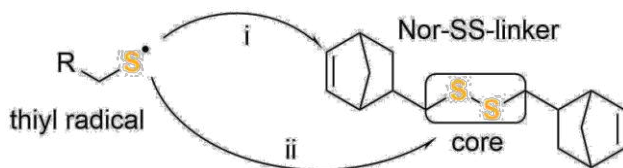


Scheme 32: Mechanism of the Schotten-Baumann reaction towards Nor-L-Cys. Intermediately, 5-norbornenecarboxylic acid methyl ester NorCOOMe is formed, which can react with the amine in an aminolysis reaction.

The product was precipitated by acidification of the reaction mixture with HCl. After extraction, the raw product contained the side product norbornyl carboxylic acid methyl ester NorCOOMe, which was removed by washing with organic solvents yielding 76% of the target molecule. **Nor-L-Cys** was then converted into the corresponding sodium salt by reaction with sodium bicarbonate (2 eq) to facilitate water-solubility (Scheme 31).

6.2.3 Reactivity estimation on the molecular level by $^1\text{H-NMR}$

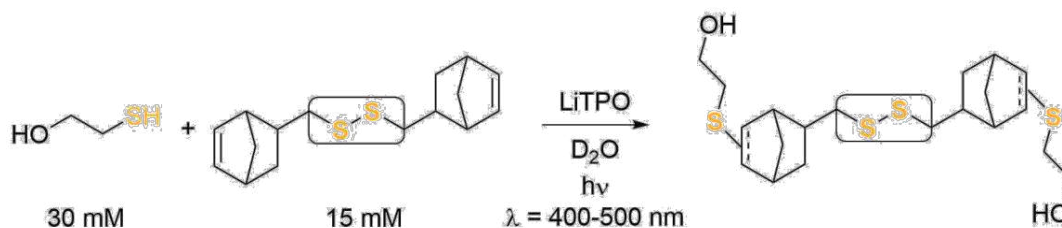
The disulfide-based linker is expected to efficiently react with thiols in an thiol-ene “click”-reaction.^[53a, 127a] However, thiyl-radicals could attack either the norbornene in a thiol-ene addition or the disulfide in a disulfide-metathesis reaction (Scheme 33).^[80]



Scheme 33: Thiyl radicals potentially can attack both (i) norbornenes in a thiol-ene coupling addition and (ii) disulfides in a thiol-disulfide metathesis.

To examine the reactivity of the linkers towards thiol-ene coupling, a $^1\text{H-NMR}$ study on the molecular level was performed (Scheme 34). Therefore, the respective linker (15 mM) was combined with 2-mercaptoethanol (30 mM) in an equimolar thiol-ene ratio and irradiated in presence of LiTPO in D_2O for different time periods. A low concentration of LiTPO (0.6 mM,

2 mol% of SH) was chosen to reduce interaction of initiator fragments with disulfide bonds, as described in literature.^[25d] Moreover, to avoid possible UV-mediated disulfide metathesis, samples were irradiated in the visible light region (400-500 nm, 20 mW cm⁻²).^[80] The consumption of the double bond signals (~6.0-6.4 ppm, HC=CH, 4H at t = 0 s) in dependence of the irradiation duration was analyzed. Irradiation periods of up to 10 min were investigated since longer irradiation is unpractically for cell encapsulation. The signal of the proton at the α -carbon (~4.2-4.5 ppm, CH-NH, 2H) served as internal reference. Both the instable **Nor-O-SS** as well as the **Nor-L-Cys** linker were tested.



Scheme 34: 2-Mercaptoethanol served as molecular probe to estimate the reactivity of the thiol-ene coupling reaction in a ¹H-NMR study. LiTPO (0.6 mM) was used as photoinitiator at $\lambda = 400-500$ nm (20 mW cm⁻²) in D₂O.

Unexpectedly, the ¹H-NMR study revealed that double bond conversion was incomplete for the **Nor-L-Cys** linker (~37%) upon photoirradiation for 10 min, whereas the double bond signals of **Nor-O-SS** fully disappeared within 5 min of irradiation (Figure 60). Here, ~50% consumption was already observed after 1 min of irradiation. The phenomenon of incomplete ene-consumption was even observed in an additional experiment when **Nor-L-Cys** (15 mM) was reacted with two equivalents of thiols (60 mM, SH:ene = 2:1). Again, ene-conversion remained incomplete (78%) after 10 min of irradiation.

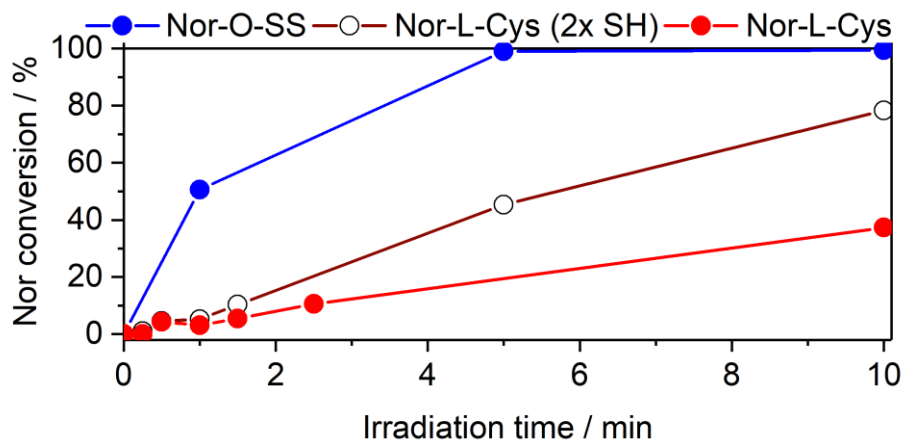


Figure 60: Evaluation of linker reactivity towards thiol-ene addition was performed in an $^1\text{H-NMR}$ study. Linkers (15 mM) were reacted with 2-mercaptoethanol (30 mM) in presence of LiTPO (0.6 mM) upon irradiation with VIS-light (400-500 nm, 20 mW cm^{-2}). While the double bonds of Nor-O-SS (blue dots) were readily consumed within 5 min of irradiation, full conversion of Nor-L-Cys (red dots) seemed to be retarded. Even with a SH:ene ration of 2:1 full conversion of Nor-L-Cys (white dots) could not be achieved within 10 min. Solid lines are only intended to guide the eye.

These results suggest that the instable linker **Nor-O-SS** is highly reactive, while the thiol-ene reaction of **Nor-L-Cys** appears to be hindered. Consequently, **Nor-L-Cys** might not react sufficiently efficient with thiols for proper hydrogel formation.

Although the radical-mediated thiol-ene reaction is often considered an archetype of “click”-reactions,^[53a] in recent literature also retarded or hindered thiol-ene coupling reactions have been reported.^[133] Nevertheless, the retardation of the highly reactive thiol-norbornene addition has not been discussed to this date.

Colak *et al.* investigated the molecular parameters controlling photoinitiated thiol-ene chemistry under biologically relevant conditions.^[133a] Hence, a series of alkenes and thiols, including peptides, were reacted in buffered conditions. $^1\text{H-NMR}$ and HPLC were used to quantify the efficiency of couplings and the impact of the pH of the buffer, as well as the molecular structure and local microenvironment close to alkenes and thiols to be coupled. An important finding was that the pKa of thiols (and its variation upon changes in molecular structure) have a striking impact on coupling efficiencies. Moreover, positively charged as well as aromatic amino acids were found to have some impact on thiol-ene couplings.

Bowman and coworkers presented the effect of amines on the kinetics and efficacy of radical-mediated thiol-ene coupling reactions of allyl ethers in organic medium.^[133b] It was shown that by varying the thiol reactant and amine additive, amines retard thiol radical-mediated reactions, when the amine is adequately basic enough to deprotonate the thiol affording the thiolate anion. For example, by adding the weakly basic amine tetramethylethylenediamine to the reaction between

butyl 2-mercaptoacetate and an allyl ether at 5 mol%, the final conversion was reduced from quantitative to <40%. Conversely, no effect was observed when the less acidic thiol butyl 3-mercaptopropionate was employed. The thiolate anion was established as the retarding species and the formation of a metastable two-sulfur three-electron bonded disulfide radical anion species by the reaction of a thiyl radical with a thiolate anion was determined as the cause for the reduction in catalytic radicals and the conversion rate. The degree of retardation increases with the ratio of thiyl to carbon radicals present, thiolate anion concentration, and the stability of the resulting disulfide radical anion.

Both studies demonstrate that the molecular design should be carefully optimized in order to achieve high conversion levels or promote the efficient formation of hydrogels by thiol-ene addition.

6.2.4 Optimization strategies of the linker on the molecular level

6.2.4.1 General Considerations

The final application of the Nor-SS linker includes complex reaction conditions involving the photo-induced crosslinking of thiol-terminated macromers in cell culture media at constant pH for hydrogel formation in presence of cells. Hence, the linkers must be optimized on the molecular level to avoid any retardation but achieve quantitative conversion of the thiol-ene coupling reaction. Therefore, finding a target molecule that gives quick and quantitative conversion in the molecular test system is essential, since reactivity can be lowered in the macromolecular case of hydrogel formation due to reduced mobility of pending functionalities upon progressing gelation. Nevertheless, for practical and economic reasons a racemic mixture of 5-norbornenecarboxylic acid is used in the synthesis of target molecules. As a result, the linkers are obtained as mixtures of diastereomers, which should be applicable as received without complex purification protocols. Reasonable molecular optimization strategies include both the (I) norbornene group as well as the (II) disulfide-based core unit, since the reduced reactivity could be based on either the configuration of the norbornene or the core subunit.

(I) Although the norbornene group is considered the most rapidly reacting ene in a radical-mediated thiol-ene process,^[53a] the ene might be sterically blocked in the spatially crowded **Nor-L-Cys**. As endo-norbornene is the favored product of the Diels-Alder reaction between acryl-derivatives and cyclopentadiene, commercial 5-norbornenecarboxylic acid usually consist of a mixture of exo- and predominantly endo-species. However, since the ene in exo-5-norbornenecarboxylic acid faces away from the carboxylic group, the exo-derivative might be sterically less hindered than the corresponding endo-based analogue (Figure 61).

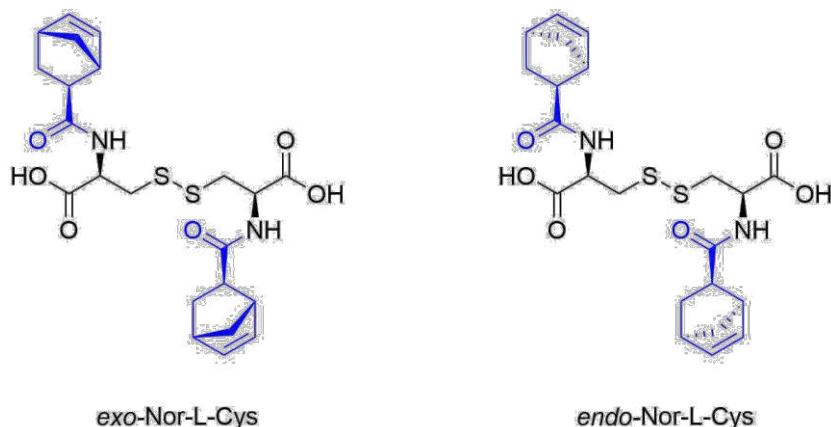


Figure 61: Strategy I: Variation of the norbornene configuration. Molecular structures of exo-Nor-L-Cys and endo-Nor-L-Cys, with the latter being the predominant component of Nor-L-Cys. Changing the stereochemistry of the norbornene might influence the reactivity of the linker towards thiol-ene addition.

Interestingly, no information about any different reactivity between exo- and endo-norbornene in thiol-ene additions could be found in literature. Nevertheless, it should be noted that a thiyl radical can add to the exo- or endo-face of the double bond of a norbornene. Thereby, the exo-attack of a thiyl radical to norbornene was estimated to be thermodynamically favored over the endo attack by computational methods.^[134]

Thus, to test the influence of the stereoisomerism of the norbornene functionality, the exo-only linker **exo-Nor-L-Cys** should be synthesized from L-cystine and commercially available exo-5-norbornene-carboxylic acid (CAS: 934-30-5).

(II) In contrast to 2-hydroxyethyl disulfide, cystine is a chiral compound possessing two stereocenters. Due to the close proximity of the functional groups, the relative orientation of the functionalities might affect the reactivity of the norbornenes by intramolecular non-covalent interactions. Additionally, disulfide dihedral angles are usually in the range of 90° ,^[135] adding up to the overall sterical interactions based on the configuration of functional groups.

Nevertheless, the core unit can be simply modified by changing the stereochemistry of cystine from the enantiopure L-cystine to the racemic D,L-cystine giving the linker **Nor-D,L-Cys** (Figure 62). DL-Cystine (CAS: 923-32-0) is a racemic mixture of the proteinogenic amino acids L-cystine and the non-proteinogenic D-cystine.

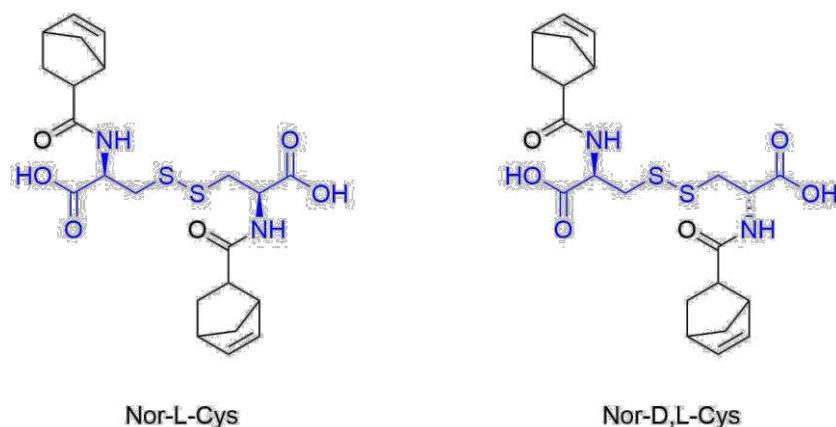
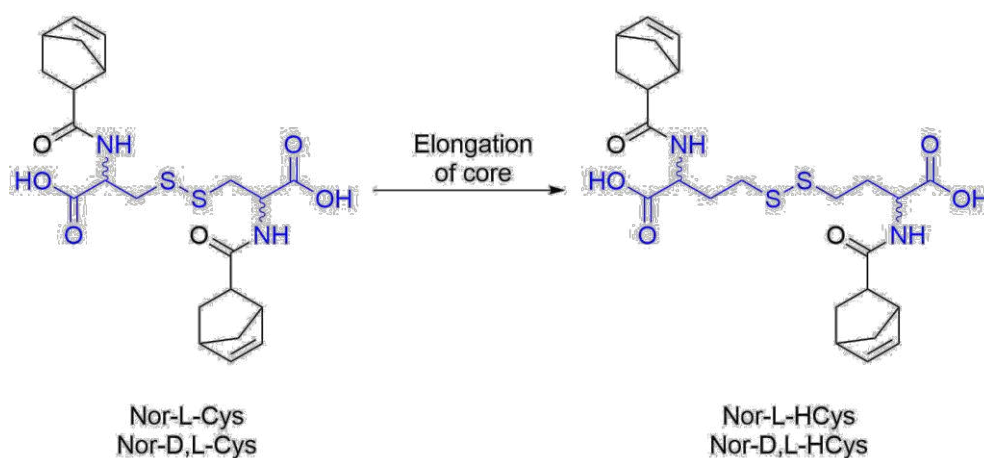


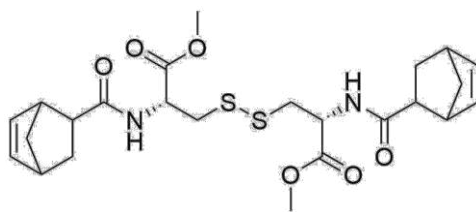
Figure 62: Variation of the core unit i. Molecular structures of Nor-L-Cys and Nor-D,L-Cys. The relative orientation of the norbornene side groups depends on the stereochemistry of the cystine core element.

Furthermore, an approach to reduce the steric hindrance between the two branches of the molecule is the elongation of the linker by exchanging cystine for homocysteine, an S-demethylation product of methionine containing an additional methylene group per subunit (Scheme 35).



Scheme 35: Variation of the core unit ii. Nor-Cys is a relatively crowded molecule. By exchanging the cystine core to homocysteine the linker is elongated, potentially reducing non-covalent intramolecular interactions between opposed side groups, which might impede norbornene conversion.

Finally, the reactivity of the linker in aprotic medium should be tested as well. As the water-solubility of the linker is facilitated by carboxylate anions, also hydration effects could impact the reactivity of the ene. Since L-cystine dimethyl ester dihydrochloride (CAS: 32854-09-4) is readily available, the dimethylated linker **Nor-L-CysMe** is easily accessible (Figure 63). A benefit of this linker is that it allows forming hydrogels without ionic groups.



Nor-L-CysMe

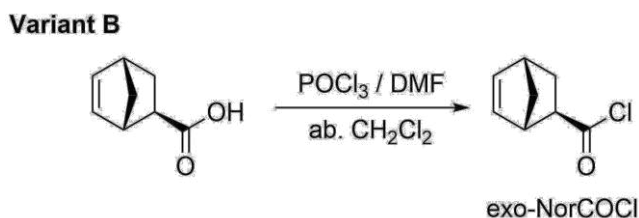
Figure 63: Molecular structure of non-ionic organosoluble dimethylated linker Nor-L-CysMe.

6.2.4.2 Synthesis of modified linkers

The modified linkers were synthesized following the preliminary established Schotten-Baumann protocol. However, due to experience the work-up and purification procedure was improved. Hence, syntheses have been optimized and even performed at multi-gram scale (**Nor-D,L-HCys**: yield: 6.7 g, 59%).

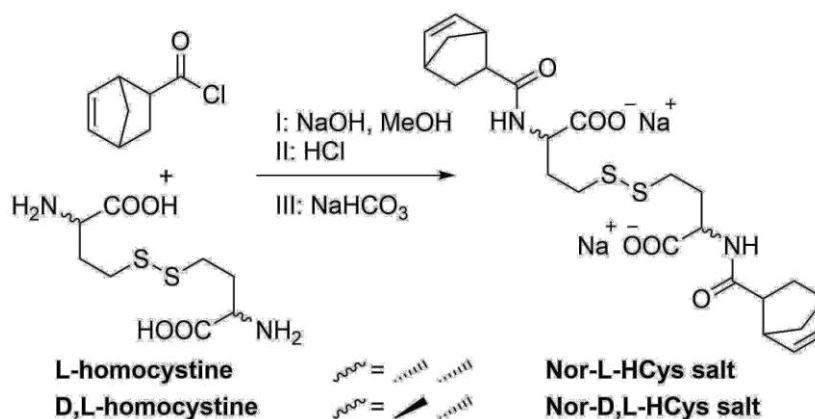
6.2.4.2.1 Synthesis of *exo*-Nor-L-Cys and its Na salt

exo-NorCOCl was synthesized from *exo*-5-norbornenecarboxylic acid (CAS: 934-30-5) as described above by variant B (Ch. 6.2.2.1) and obtained in 91% yield after distillation (Scheme 36).



Scheme 36: Synthesis of *exo*-5-norbornenecarboxylic acid chloride *exo*-NorCOCl via conversion of *exo*-5-norbornenecarboxylic acid using phosphoryl chloride (Variant B).

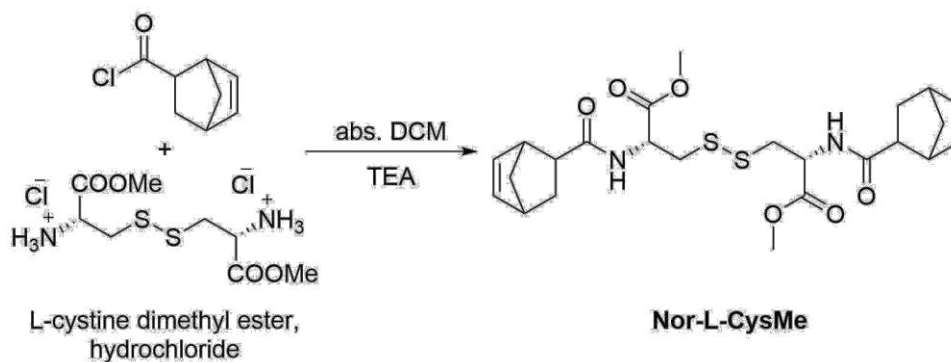
exo-Nor-L-Cys was synthesized analog to **Nor-L-Cys** (Scheme 37) by linking **exo-NorCOCl** (2 eq) to *L*-cystine in presence of finely ground NaOH (4 eq) in dry MeOH yielding 72% of **exo-Nor-L-Cys**. The product was subsequently converted to the corresponding sodium salt in quant. yield by reaction with NaHCO₃ (2 eq).



Scheme 39: Nor-D,L-HCys was synthesized from *D,L*-homocystine and NorCOCl according to the general procedure and subsequently converted into the sodium salt.

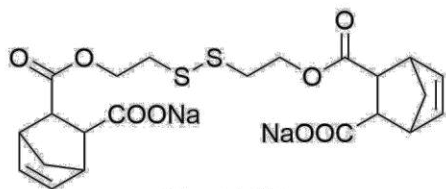
6.2.4.2.4 Synthesis of Nor-L-CysMe

Nor-L-CysMe, the dimethyl ester of **Nor-L-Cys**, was synthesized from L-cystine dimethylester, hydrochloride (CAS: 32854-09-4) and **NorCOCl** in presence of trimethylamine (4.2 eq) in DCM (Scheme 40). After purification by column chromatography two fractions were received (total yield: 85%) of which one exclusively contained the endo-norbornene based product (yield: 56%). Identification was possible via ¹H-NMR by comparison with the double bond signals of **exo-Nor-L-Cys**, which were absent in this fraction.



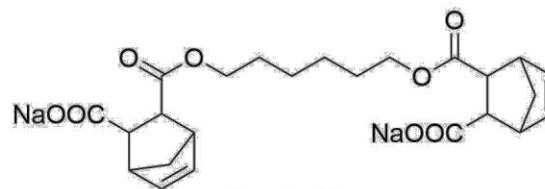
Scheme 40: Nor-L-CysMe was synthesized from L-cystine dimethyl ester, hydrochloride and NorCOCl in presence of TEA.

6.2.5 List of synthesized Nor-SS Linkers



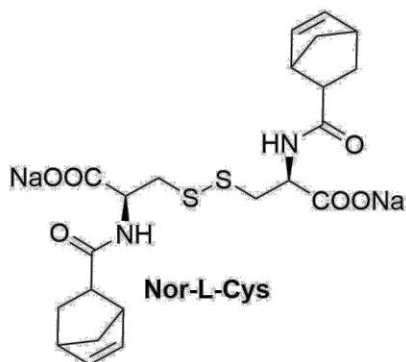
Nor-O-SS

$C_{22}H_{24}Na_2O_8S_2$
526.53



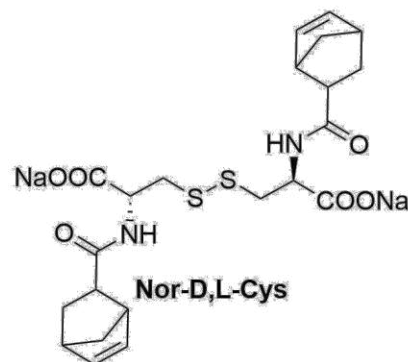
Nor-O-CC

$C_{24}H_{28}Na_2O_8$
490.46



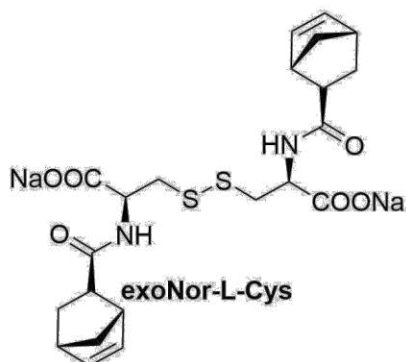
Nor-L-Cys

$C_{22}H_{26}N_2Na_2O_6S_2$
524.56



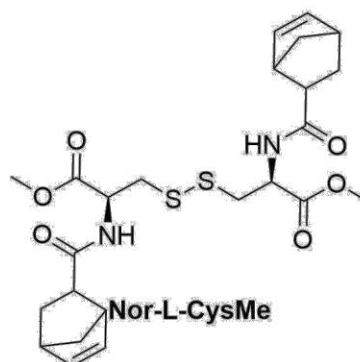
Nor-D,L-Cys

$C_{22}H_{26}N_2Na_2O_6S_2$
524.56



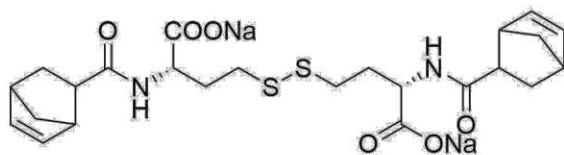
exoNor-L-Cys

$C_{22}H_{26}N_2Na_2O_6S_2$
524.56



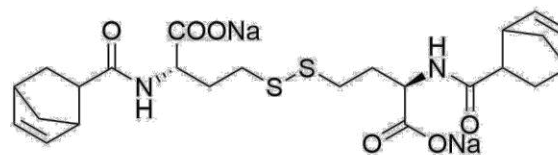
Nor-L-CysMe

$C_{24}H_{32}N_2O_6S_2$
508.65



Nor-L-HCys

$C_{24}H_{30}N_2Na_2O_6S_2$
552.61



Nor-D,L-HCys

$C_{24}H_{30}N_2Na_2O_6S_2$
552.61

6.3 Development of the Disulfide-based Hydrogel Platform

6.3.1 Extended reactivity estimation on the molecular level by $^1\text{H-NMR}$

To investigate the effect of the molecular design on the reactivity of thiol-norbornene coupling, the synthesized linkers were reacted with 2-mercaptoethanol as described above and the evolution of the ene-signal was monitored by $^1\text{H-NMR}$ (Figure 64).

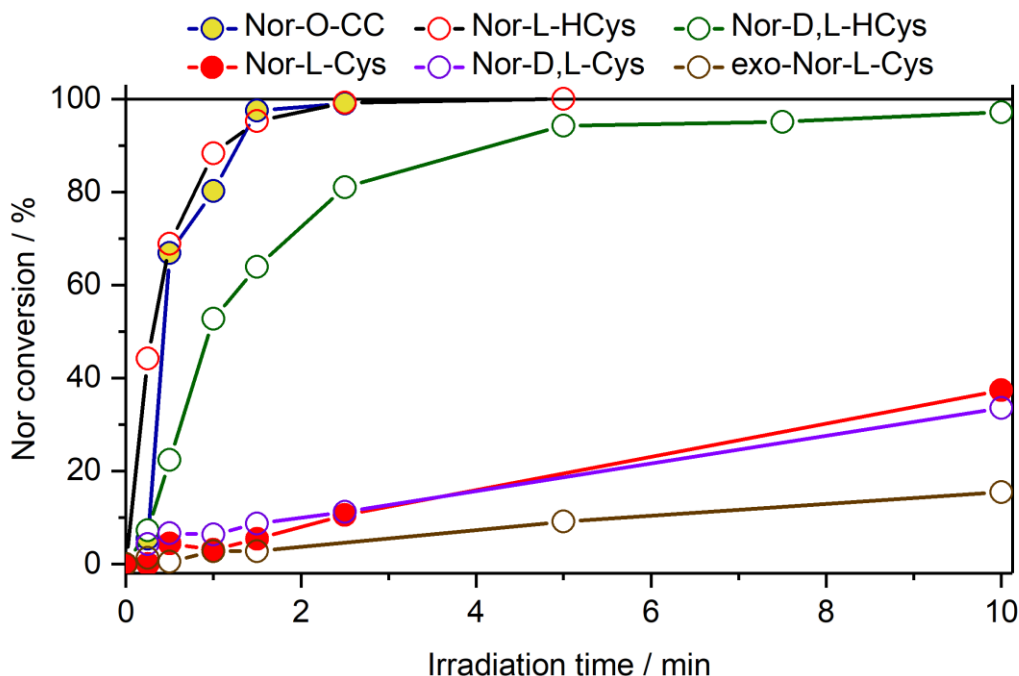


Figure 64: Evolution of the ene-signals of linkers upon reaction with 2-mercaptoethanol in D_2O . Linkers (15 mM) were reacted with 2-mercaptoethanol (30 mM) in presence of LiTPO (0.6 mM) by irradiation with VIS-light (400-500 nm, 20 mW cm^{-2}) and subsequently analyzed by $^1\text{H-NMR}$. Solid lines are only intended to guide the eye.

Interestingly, the exo-norbornene-based linker **exo-Nor-L-Cys** showed the lowest reactivity with only ~15% ene-conversion after 10 min of irradiation. Evidently, the combination of exo-norbornene and L-cystine has a negative effect on thiol-ene reactivity, as the overall molecular configuration seems to impede the reaction. On the other hand, changing the configuration of the cystine-core from enantiopure L-cystine to racemic D,L-cystine does not significantly impact the reactivity of the thiol-ene coupling reaction, since both **Nor-L-Cys** as well as **Nor-D,L-Cys** show relative equal reactivity with an ene-conversion of ~37% and ~34% respectively upon 10 min of irradiation.

On the contrary, elongating the linker by changing the core to homocysteine drastically improves the reactivity towards full consumption of ene. Here, the configuration of the homocysteine core does influence the reactivity of the norbornene, since the **Nor-L-HCys** linker is reacting much faster than the **Nor-D,L-HCys** derivative and shows full consumption of ene within 2.5 min of irradiation. In contrast, with **Nor-D,L-HCys** high (~94%) but not quantitative consumption of norbornene is achieved within 10 min of irradiation. Hence, the thiol-ene reaction of **Nor-D,L-HCys** seems to be retarded when compared to **Nor-L-HCys**.

To study the cause for the observed retardation, also the non-cleavable reference linker **Nor-O-CC** was reacted with 2-mercaptoethanol. As in the case of **Nor-L-HCys**, full consumption was achieved within 2.5 min of irradiation. Since this molecule contains a non-rigid hexamethylene-spacer without a distinct configuration of side groups, minimal intramolecular interactions can be assumed. Due to the fact, that **Nor-L-HCys** shows equal reactivity and thus no retardation, minimal intramolecular interactions and hence a non-retarded thiol-ene reaction are expected for this linker as well. Based on these results, the reactivity of the linkers regarding thiol-ene addition can be graded in the following order:

Nor-O-CC ~ Nor-L-HCys > Nor-D,L-HCys >> Nor-L-Cys ~ Nor-D,L-Cys > exo-Nor-L-Cys

Furthermore, also organosoluble linkers (15 mM) were reacted with 2-mercaptoethanol (30 mM, SH:ene = 1:1) in DMSO- d_6 using TPO-L (0.6 mM) as photoinitiator. While the free acid of **Nor-L-Cys** showed low norbornene conversion (~44%) within 10 min of irradiation, as already observed in D_2O , its methylated derivative **Nor-L-CysMe** was much more reactive with a final conversion of ~88% being reached after 10 min (Figure 65). Nevertheless, both compounds do not reach quantitative ene-conversion. However, the significant higher reactivity of **Nor-L-CysMe** indicates that the free carboxylate of **Nor-L-Cys** might be involved in intramolecular interaction causing retardation. On the other hand, as **Nor-L-Cys** shows comparable reactivity in both solvents, hydratization effects become unlikely as cause of retardation.

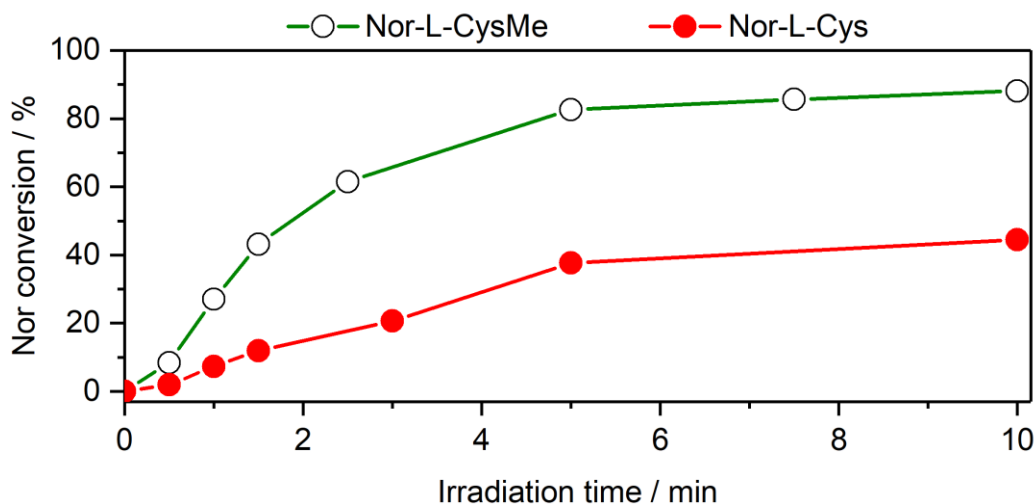


Figure 65: Evolution of the ene-signals of linkers upon reaction with 2-mercaptoethanol in DMSO-d₆. Linkers (15 mM) were reacted with 2-mercaptoethanol (30 mM) in presence of TPO-L (0.6 mM) by irradiation with VIS-light (400-500 nm, 20 mW cm⁻²) and subsequently analyzed by ¹H-NMR. The methylated derivative Nor-L-CysMe shows much higher reactivity than Nor-L-Cys free acid. Solid lines are only intended to guide the eye.

This simple ¹H-NMR study strikingly demonstrates the significant differences in reactivity depending on the molecular design of the respective linkers, as already suggested by Colak et al.^[133a] Obviously, both the length of the spacer as well as the configuration of the side groups affect ene-conversion. Hence, intramolecular interactions are expected to influence the reactivity. As the length of the spacer is critical, these interactions probably occur between functionalities of opposing linker-subunits. Nevertheless, as the linkers were synthesized from racemic starting materials (especially NorCOCl), for reasons of economy and convenience, they are mixtures of different diastereomers. Since the synthesized linkers are relatively complex molecules and molecular rotations might be hindered due to steric reasons, computational calculations of the preferred conformations in solution is required to gain further insight into the cause of the observed thiol-ene retardation and further evaluate a structure-property relationship.

6.3.2 Hydrogel optimization

This chapter describes the characterization and optimization of hydrogel formulations by means of photorheology. This iterative process was conducted simultaneously to swelling tests of hydrogel samples produced in the course of rheological experiments.

Hydrogel formation was investigated with selected linkers of the series by means of photorheology. Hence, linkers were reacted with 10 wt% of a thiol-terminated 8-armed PEG (8armPEG20k-SH, M_w ~20 kDa, tripentaerythritol core, Figure 66) using Li-TPO as photoinitiator

by irradiation with an LED (385 nm, $\sim 6 \text{ mW cm}^{-2}$). The rheological analysis was performed with a plate-plate geometry using a tool diameter of 8 mm and a gap size of 0.8 mm.⁴ Thus, the formed hydrogel disks could be utilized for subsequent swelling tests. All measurements were performed at least in triplicates, except for experiments in which a high amount of photoinitiator was used or the thermal or mechanical stability of the hydrogel was investigated. Error bars are illustrating the standard deviation in graphs.

In order to investigate their swelling behavior and long-term stability, hydrogel samples were weighted and then swollen in PBS in tared petri dishes. To determine the weight, the solution was frequently removed from the petri dishes and the dishes and hydrogels were carefully patted dry using paper towels before weighting. If not otherwise stated, samples were measured until progressed degradation became apparent and a reliable measurement was not possible anymore.

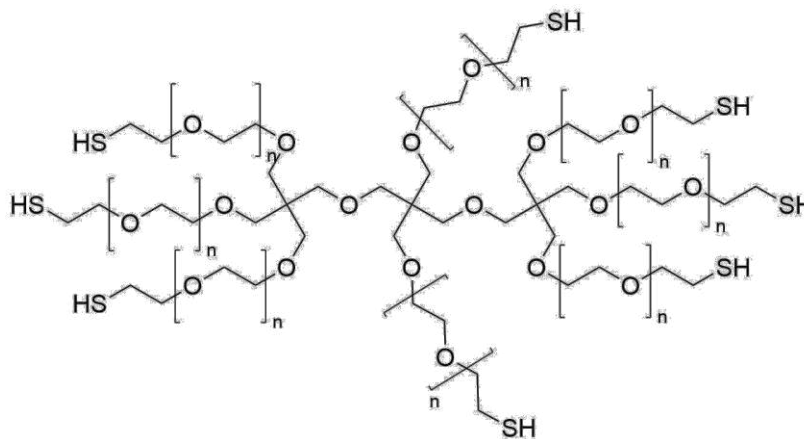


Figure 66: Molecular structure of 8arm-PEG20k-SH with a trientaerythritol core

6.3.2.1 Optimization of the photoinitiator concentration

At first, the lowest required concentration of highly water-soluble photoinitiator LiTPO^[136] was established, as an excess of photoinitiator is known to induce degradation of disulfide cross-linked hydrogels and can even lead to reverse gelation.^[25d] Moreover, a minimal concentration of photoinitiator should be used to reduce the impact on encapsulated cells.

Stock solutions of 8armPEG20k-SH, linker **Nor-D,L-HCys** (190 mM) and LiTPO (18 mM) were prepared in PBS. The stock solutions were combined to give sample solutions with final

⁴ Preliminary tests revealed, that using a tool diameter of 25 mm and a low gap size (50 μm , 100 μm) leads to artefacts (delamination). Besides a high amount of sample is required. Moreover, only hydrogel films are created, which inappropriate for swelling tests.

concentrations of 10 wt% 8armPEG20k-SH, 22 mM **Nor-D,L-HCys** (SH:ene = 1:1) and a variable LiTPO concentration (0.2 mM, 0.4 mM, 0.6 mM, 15 mM). After 1 min of equilibration time, the prepolymer formulations were exposed to 385 nm light ($\sim 6 \text{ mW cm}^{-2}$) for 5 min. Figure 67 displays the averaged storage moduli G' of hydrogels created with different concentrations of LiTPO. At low photoinitiator concentrations (0.2 mM, 0.4 mM, 0.6 mM), the delay of polymerization is decreasing with increasing amounts of photoinitiator, while the final storage modulus is increasing from $17.6 \pm 1.7 \text{ kPa}$ for 0.2 mM, over $20.2 \pm 2.2 \text{ kPa}$ for 0.4 mM to $22.9 \pm 3.9 \text{ kPa}$ for 0.6 mM LiTPO. Here, G' is unaffected by further irradiation after a plateau is reached. This behavior indicates that the crosslinking reaction occurs quicker than the degradation of disulfide bonds and photoinitiator concentrations of 0.6 mM and below are sufficient for crosslinking without provoking degradation of the network.

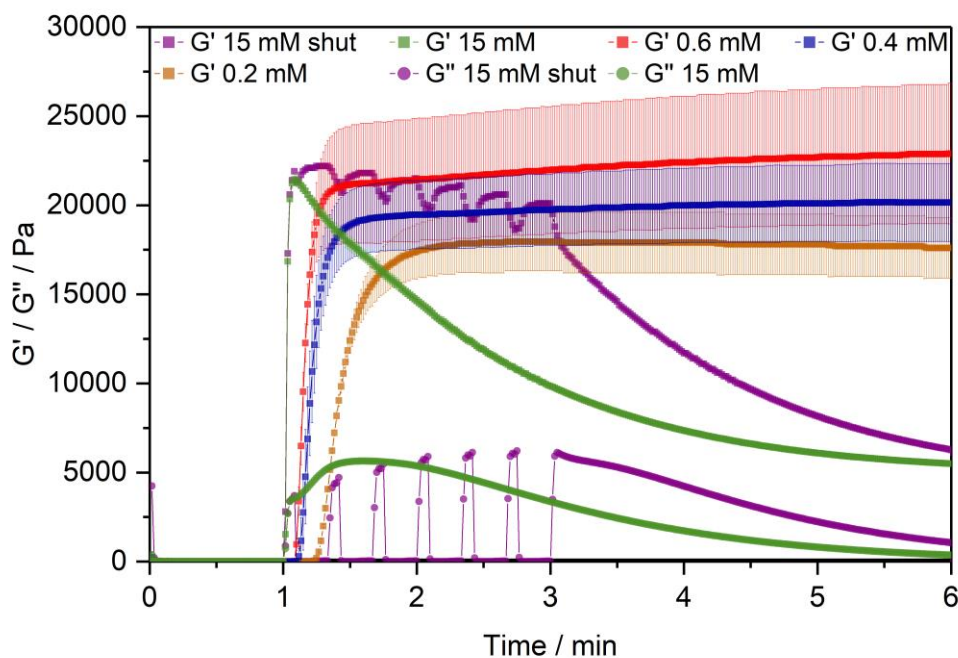


Figure 67: *In situ* oscillatory photorheology of hydrogel formulations containing 10 wt% 8armPEG20k-SH, Nor-D,L-HCys (22.2 mM, SH:ene = 1:1) and variable concentrations of Li-TPO. The prepolymer solutions were exposed to 385 nm light ($\sim 6 \text{ mW cm}^{-2}$) for 5 min after a normalization phase of 1 min. Alternatively, light was shuttered with 5 s on-time and 15 s off-time. Measurements were performed at least in triplicates, except for the shuttered measurement which was only performed once.

On the contrary, when a high amount of photoinitiator (15 mM) is used, G' rises very rapidly within 5 s to a maximal value of $21.5 \pm 0.3 \text{ kPa}$, before it decreasing again. This result indicates initial very rapid polymerization followed by cleavage of disulfide crosslinks by excess photoinitiator, demonstrating that the thiol-norbornen addition is preferred over radical-mediated disulfide-cleavage. Additionally, also the loss modulus G'' is significantly increasing during irradiation in

this case. Such a large increase in G'' upon irradiation indicates a significant shift in the viscoelastic properties of the network from an almost purely elastic to a more fluid behavior,^[90] which is typically observed for networks crosslinked by dynamic linkages.^[137] Nevertheless, 15 mM LiTPO is not sufficient for complete reverse gelation of the hydrogel based on 22 mM **Nor-D,L-HCys** linker. Hence, after 5 min of irradiation G' reaches a plateau indicating the presence of intact disulfide-crosslinks.

Besides, when the light is dynamically shuttered (5 s on-time, 15 s off-time, 15 mM, Figure 67) the partial reversibility of the disulfide cleavage induced by radical photoinitiator fragments becomes apparent.^[87] While during periods of irradiation G' decreases and G'' increases, the inverse behavior is observed when irradiation is interrupted, indicating reformation of disulfide bonds by thiyl-radical recombination. Nevertheless, with every irradiation cycle G' is gradually reduced, as thiyl-radicals are consumed by photoinitiator fragments, impeding full restoration of the initial crosslinking density and G'_{\max} .^[25d]

As the final storage moduli G' for hydrogels produced with 0.4 mM (20.2 ± 2.2 kPa) and 0.6 mM LiTPO (22.9 ± 3.9 kPa) were in the same range and it was decided to conduct all further experiments with the lower photoinitiator concentration of 0.4 mM to reduce the later impact on encapsulated cells to a minimum. Hence, most of the following characterization experiments were performed with a hydrogel created from 10 wt% 8armPEG20k-SH, **Nor-D,L-HCys** (SH:ene = 1:1) and 0.4 mM Li-TPO, which will be referred to as **8arm-D,L-HCys (1:1)** hydrogel in the following chapters.

6.3.2.2 Thermostability of disulfide-crosslinked PEG hydrogel

Since for cell-culture applications prolonged incubation of the hydrogels at cell-culture conditions (37°C, 5% CO₂) is an essential requirement, the thermal stability of the disulfide-based hydrogel was investigated. Therefore, a sample of **8arm-D,L-HCys (1:1)** hydrogel was *in situ* photopolymerized at 20 °C as described above, before the temperature was continuously increased up to 90 °C at a heating rate of 1 °C/min. To prevent evaporation of water, the hydrogel sample was sealed with a ring of paraffin. Only at temperatures above 60 °C a significant decrease of G' could be observed, demonstrating thermal stability of the hydrogel at cell-culture conditions.

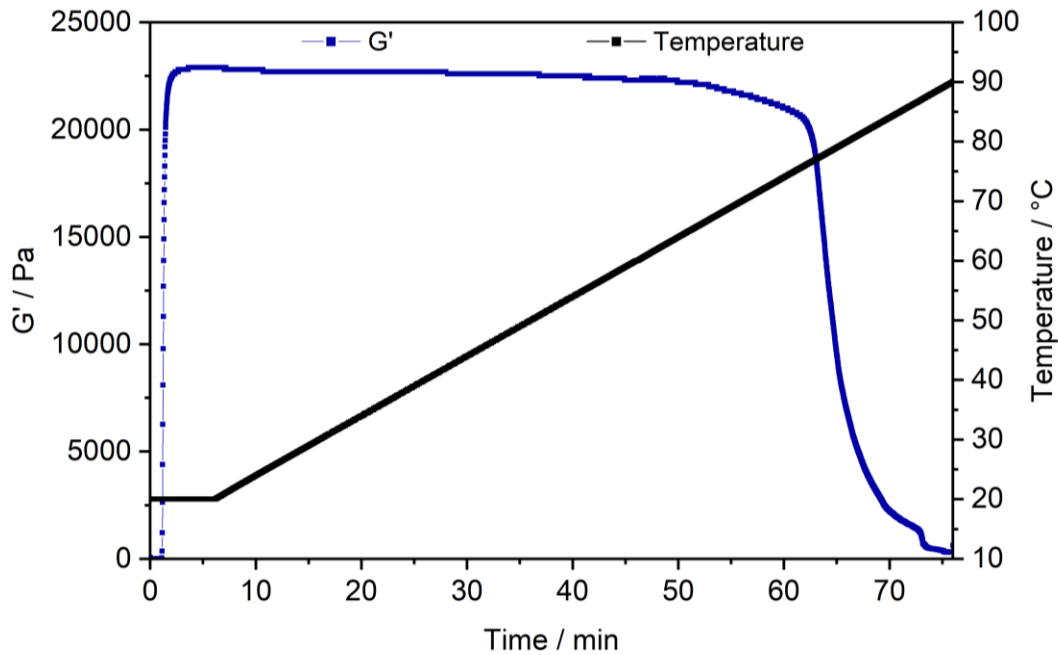
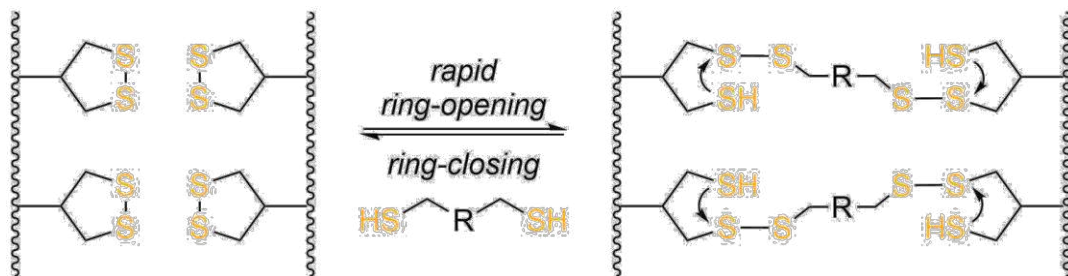


Figure 68: The temperature sensitivity of **8arm-D,L-HCys (1:1) hydrogel** was investigated by oscillatory photorheology. After *in situ* photopolymerization at 20 °C the temperature was increased up to 90 °C at a heating rate of 1° C / min. Only at temperatures above 60 °C G' significantly changes revealing stability of the hydrogel at cell-culture conditions.

6.3.2.3 Mechanostability of disulfide-crosslinked PEG hydrogel

Disulfide bonds can undergo thiol-disulfide metathesis reaction. In 1,2-dithiolane-containing polymer networks crosslinked by dithiols, this even leads to dynamic shear-thinning behavior (Scheme 41).^[138] In this special case, a free thiol in very close proximity to a crosslinking disulfide bond is present, leading to reversible gelation by ring closure to 1,2-dithiolane.



Scheme 41: Pendant thiol groups in close proximity to crosslinking disulfide linkages lead to structurally dynamic hydrogels exhibiting shear thinning behavior.^[138] If a high amount of unreacted thiols were present in the investigated photo-crosslinked disulfide-based hydrogels as well, reversible shear-thinning behavior would be observable.

However, such high concentration of unreacted thiols in close proximity to disulfide-linkages is unlikely in the photocrosslinked disulfide-based hydrogels under investigation. Nevertheless, the shear-thinning behavior of 8arm-D,L-HCys (1:1) hydrogel was investigated, to exclude instability due to reversible bond formation. For this reason, first an amplitude sweep was performed. After *in situ* photo-polymerization, the amplitude of the applied strain was logarithmically increased from 0.1% to 1000% at a constant frequency of 1 Hz. Up until a strain of 100% the hydrogel behaves like an elastic solid (linear viscoelastic regime) with the value of the storage modulus G' being two magnitudes above that of the loss modulus G'' (Figure 69). Starting at a strain of $\sim 300\%$, the loss modulus G'' surpasses the storage modulus G' , indicating that the gel behaves like a liquid suggesting reverse gelation. However, inspection of the sample revealed rupture of the hydrogel.

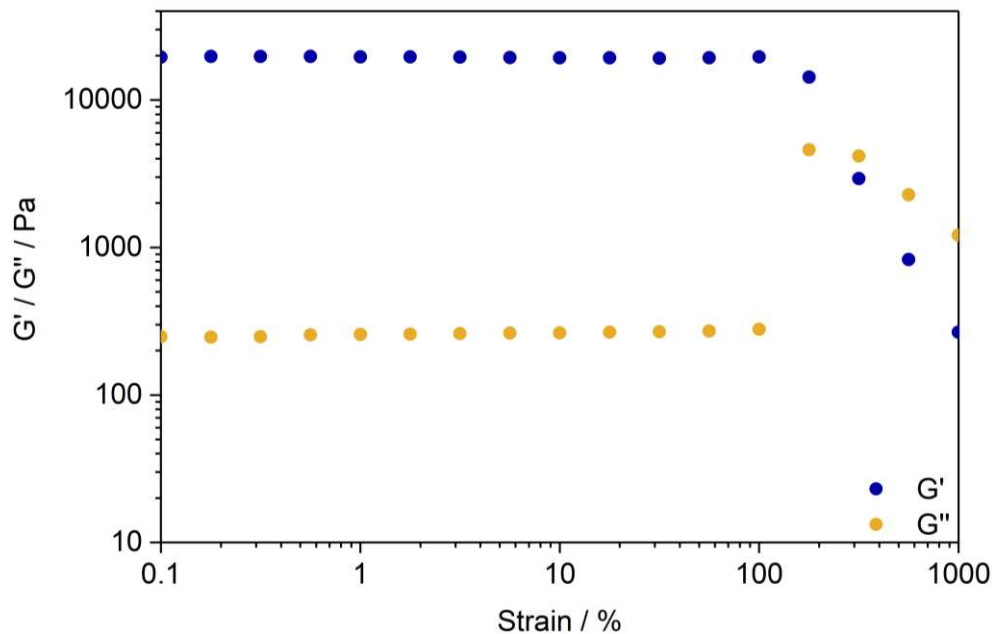


Figure 69: Frequency sweep of 8arm-D,L-HCys (1:1) hydrogel. The amplitude was logarithmically increased from 0.1% to 1000% at a constant frequency of 1 Hz. Below strains of 100% the hydrogels is within its linear viscoelastic region.

Nevertheless, since G'' surpasses G' at strains above 100% a dynamic strain amplitude cycling experiment was performed to test shear-thinning behavior. Hence, after *in situ* polymerization of 8arm-D,L-HCys (1:1) hydrogel, a series of four strain cycles was applied varying strains between 350% and 1% in 60 s periods (Figure 70). In phases of high strain G' was lower than G'' , while when strain was released G' increased again. Nevertheless, no full recovery of G' but gradual reduction was observed with every cycle, after an initial peak when the strain was released.

Hence, it can be deduced that 8arm-D,L-HCys (1:1) hydrogel is not reversibly shear-thinning but damaged at high strains.

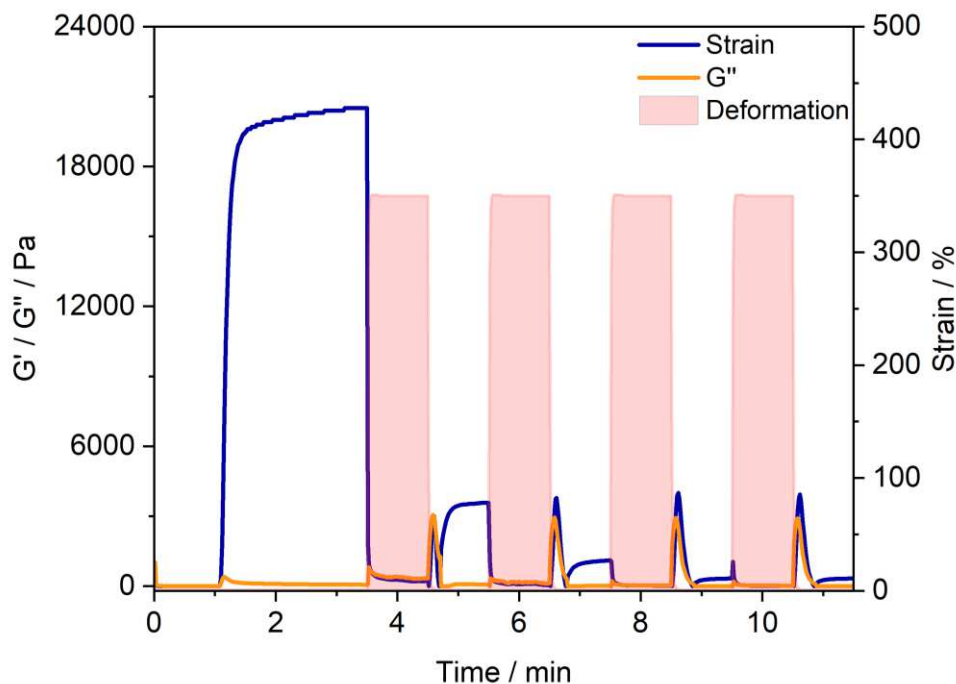


Figure 70: Dynamic strain amplitude cycling, displaying storage- and loss-modulus (G' , G'') over time of 8arm D,L-HCys (1:1) hydrogel at alternating strains of 1% and 350%. After every high strain phase G' is gradually reduced, excluding reversible shear-thinning behavior.

6.3.3 Stabilization of 8arm-D,L-HCys (1:1) hydrogel

When immersed in PBS at room temperature, **8arm-D,L-HCys (1:1)** hydrogel started swelling heavily leading to first deformation and finally dissolution within a few days, with the first of the three samples already dissolving within 24 Figure 71. In an alternative experiment triplicates of **8arm-D,L-HCys (1:1)** hydrogel were immersed in **10x PBS** for the first 20 h. Due to the increased ion concentration in the swelling medium, the samples were losing mass due to osmosis in this initial period. After the swelling medium was changed to normal PBS, samples began swelling and gained in mass, but interestingly remained their shape and did not dissolve. These samples were monitored for more than a month, but were stable much longer. Most probably, this behavior can be explained by formation of additional crosslinks by reaction between unreacted thiols upon condensing of the hydrogel due to initial negative swelling. Nevertheless, the ion concentration in 10x PBS is many times higher than the physiological concentration and hence this approach is impractical for stabilization of **8arm-D,L-HCys (1:1)** hydrogel.

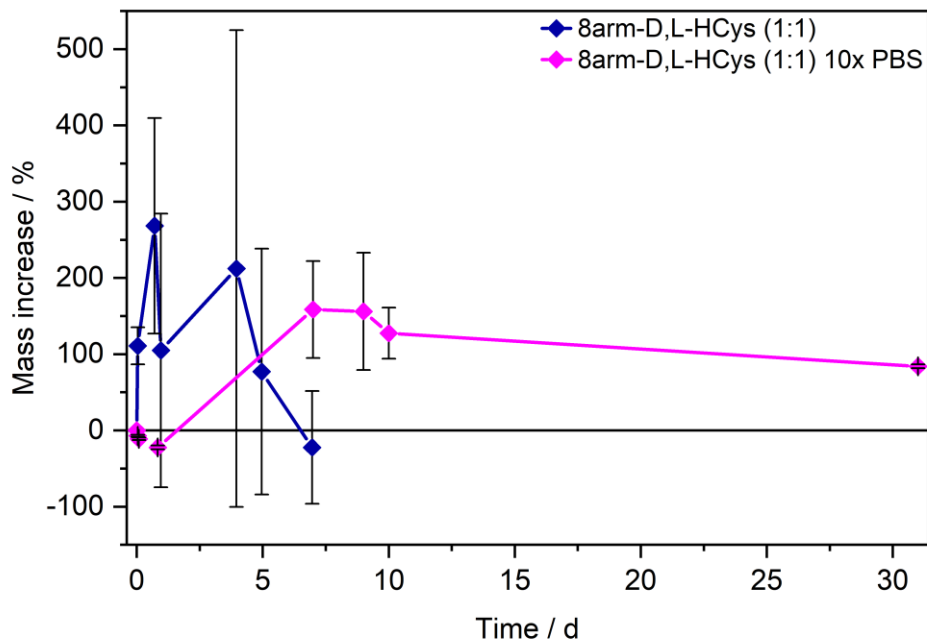


Figure 71: When immersed in PBS, **8arm-D,L-HCys (1:1) hydrogel** was deforming and swelling heavily leading finally to disintegration within a few days. On the contrary, when **8arm-D,L-HCys (1:1) hydrogel** was immersed in **10x PBS** in the initial 20 h, samples were first losing mass due to osmosis. After changing to normal PBS, samples were swelling as well, but remained their shape and did not dissolve anymore. These samples were monitored for more than a month but were stable much longer.

In the course of macroscopical deformation of **8arm-D,L-HCys (1:1) hydrogel** by swelling, the sample loses its cylindrical shape by turning into a spherical cap (Figure 72).

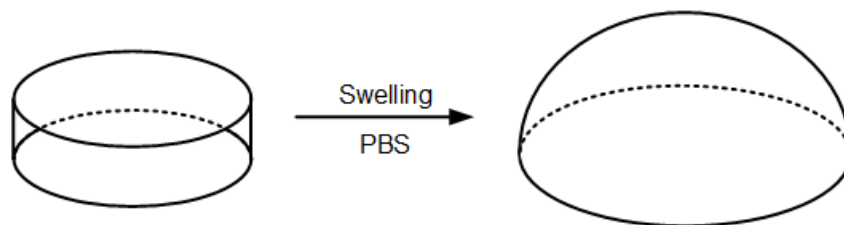
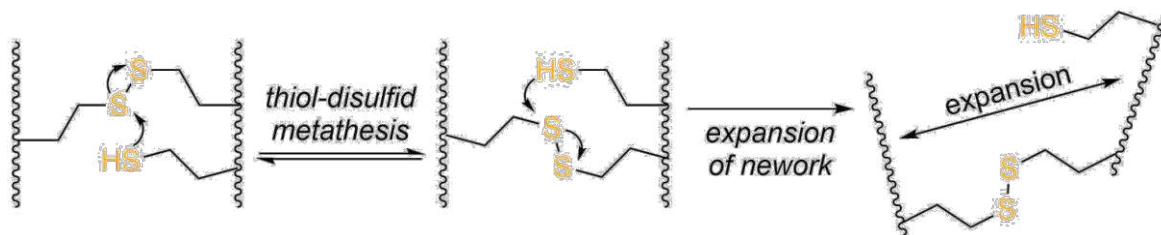


Figure 72: In the course of swelling in PBS at room temperature **8arm-D,L-HCys (1:1) hydrogel** samples lose their cylindrical shape by turning into a spherical caps.

This behavior indicates relaxation of surface tension, most likely occurring via thiol-disulfide metathesis involving unreacted thiol groups (Scheme 42). This is expectable, as the $^1\text{H-NMR}$ reactivity estimation revealed incomplete ene-conversion of **Nor-D,L-HCys** (Figure 64). Moreover, this behavior is in accordance with the observation that partly degraded disulfide networks adapted to an applied strain to minimize the free energy of the system (self-healing behavior) as described by Fairbanks *et al.*^[25d] Upon swelling and relaxation by thiol-disulfide

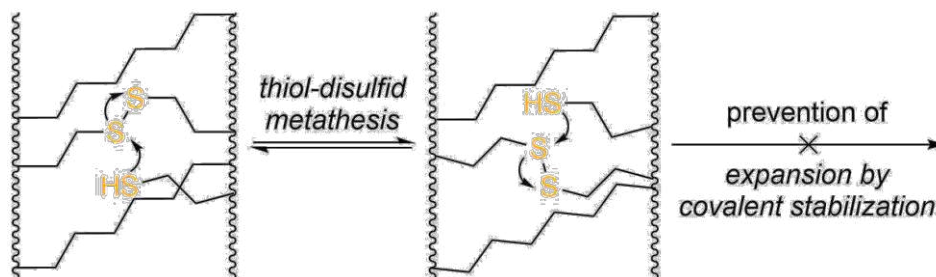
metathesis, the hydrogel expands. Since the linkers contain carboxylate anions to facilitate solubility, further swelling of water into the hydrogel volume is provoked due to the increased ion concentration, finally leading to dissolution of the hydrogel. To proof this hypothesis a series of experiments was conducted, which will be discussed in the following sub-chapters.



Scheme 42: Unreacted thiols can undergo thiol-disulfide metathesis with crosslinks leading to relaxation of internal stress and resulting in expansion of the network. Because of the increased ion concentration within the hydrogel due to the carboxylate groups of the linkers, further diffusion of water into the hydrogel is promoted as well.

6.3.3.1 Stabilization by a non-cleavable background network

The first stabilization strategy involves the introduction of non-cleavable aliphatic crosslinks to prevent shape-relaxation by addition of the reference linker **Nor-O-CC** (Scheme 43). Whereas this background network prevents complete degradation of the hydrogel network, the hydrogel can still be softened by cleavage of disulfide bonds. In order to stabilize the network consisting of 8armPEG20k-SH, at least two arms of the macromere must be connected by the non-cleavable linker to meet the percolation threshold. Hence, 25% of difunctional **Nor-D,L-HCys** must be substituted by **Nor-O-CC** to form a continuous non-cleavable network, in which every macromere is theoretically connected to two molecules of **Nor-O-CC**. If the ratio of **Nor-O-CC** to **Nor-D,L-HCys** is lower, the percolation threshold is not met, which is expected to not stabilize the network.



Scheme 43: The introduction of a non-cleavable background network should inhibit detrimental swelling. Thus, thiol-disulfide metathesis can still occur, whereas excessive swelling of the hydrogel is prevented.

In order to proof this hypothesis, hydrogel formulations consisting of 10 wt% 8armPEG20k-SH, 22.2 mM linkers (SH:ene = 1:1) and LiTPO (0.4 mM) were *in situ* polymerized on the photo-rheometer (Figure 73). The linker compositions were varied from 100% **Nor-O-CC (8arm-CC)** to a combination including 75% **Nor-D,L-HCys** and 25% **Nor-O-CC (8arm-SS-CC (3:1))** as well as a mixture of 87.5% **Nor-D,L-HCys** and 12.5% **Nor-O-CC (8arm-SS-CC (7:1))**. Whereas **8arm-CC** (23.8 ± 0.7 kPa) exhibits a higher storage modulus than exclusively disulfide-linked **8arm-D,L-HCys (1:1)** hydrogel (20.2 ± 2.2 kPa), interestingly combinations of both linker types result in lower storage moduli. Here, **8arm-SS-CC (3:1)** (19.2 ± 4.3 kPa) containing a larger fraction of **Nor-O-CC** exhibits a higher G' than **8arm-SS-CC (7:1)** (17.4 ± 1.5 kPa).

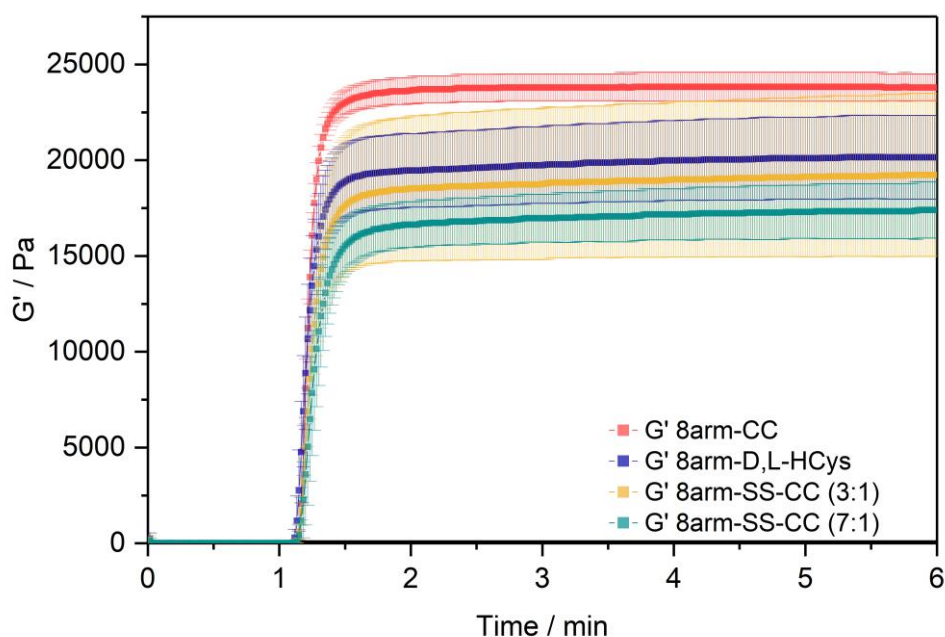


Figure 73: Photopolymerization of hydrogel formulations based on 10 wt% 8armPEG20k-SH, variable combinations of Nor-D,L-HCys and Nor-O-CC at equimolar thiol-ene ratio (22.2 mM) and 0.4 mM Li-TPO was monitored by oscillatory photorheology. The hydrogel solely crosslinked by non-cleavable Nor-O-CC (**8arm-CC**) exhibits a higher storage modulus G' than the hydrogel connected by disulfide-linkages only (**8arm-D,L-HCys**). Interestingly, combinations of both linker types result in lower storage moduli (**8arm-SS-CC (3:1)** and **8arm-SS-CC (7:1)**).

Nevertheless, hydrogels consisting of a non-cleavable background network cannot be fully degraded, but softened. The latter fact was demonstrated by forming **8arm-SS-CC (3:1)** hydrogel in presence of a high LiTPO concentration of 15 mM (Figure 74). When **8arm-SS-CC (3:1) 15 mM** hydrogel was continuously irradiated G' decreased until a plateau was reached demonstrating cleavage of disulfide bonds. However, as in the case of **8arm-D,L-HCys (1:1)** hydrogel polymerized in presence of 15 mM LiTPO (Figure 67), the photoinitiator concentration applied

was not sufficient for complete cleavage of all disulfide bonds (16.5 mM). When the light was dynamically shuttered (5 s on-time, 15 s off-time, **SS-CC (3:1) 15 mM shut**), gradual reformation of disulfide bonds during off-times could be indirectly observed by the limited recovery of G' .

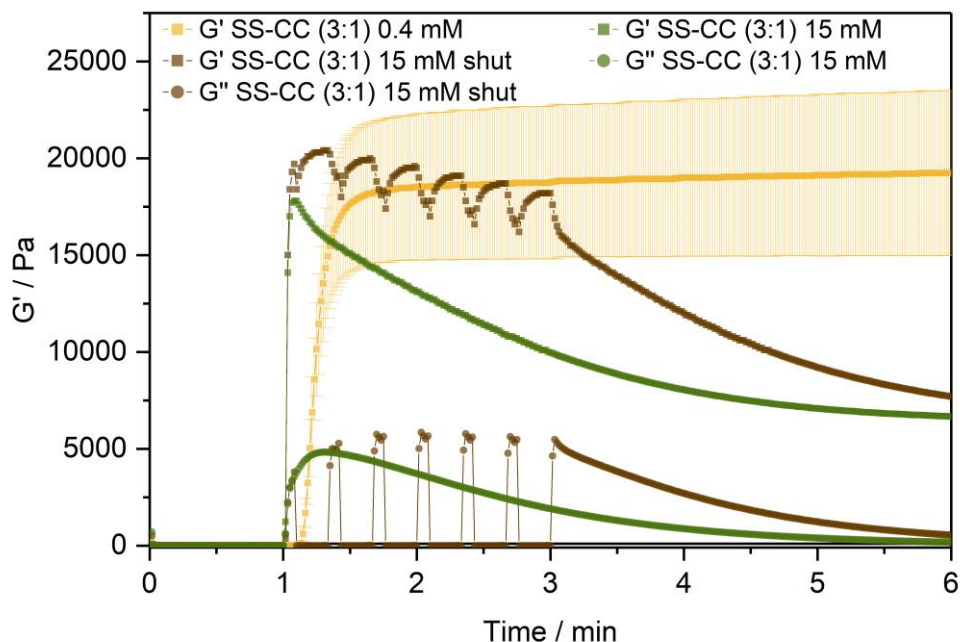


Figure 74: Hydrogels consisting of disulfide bonds and a non-cleavable background network (8arm-SS-CC (3:1)**) can be softened by irradiation in presence of a high concentration of photoinitiator (15 mM LiTPO). This leads to softening of the hydrogel, whereas no complete reverse gelation is expected.**

The swelling behavior of the hydrogel samples confirmed the hypothesis of stabilization by formation of a non-cleavable background network (Figure 75). Both the non-stabilized **8arm-D,L-HCys** hydrogel as well as the hydrogel containing 12.5% **Nor-O-CC (8arm-SS-CC (7:1))** dissolved within a few days. In contrast, with 25% of **Nor-D,L-HCys** being substituted by **Nor-O-SS (8arm-SS-CC (3:1) 0.4 mM)** the percolation threshold was met and the hydrogel was stabilized. Hence, the respective samples were monitored for more than 3 months. Samples partially degraded by irradiation in presence of 15 mM LiTPO (**8arm-SS-CC (3:1) 15 mM**) were also stable for this period.⁵ Nevertheless, due to the decreased crosslinking density, these samples were swelling much more (~factor 2). The hydrogel crosslinked by the non-cleavable aliphatic linker (**8arm-CC**) showed the lowest mass increase of below 100%. Samples of this

⁵ One sample dissolved within 9 days.

hydrogel were monitored for more than 90 days. After 70 days mass increase occurred, which might be due to incipient ester hydrolysis.

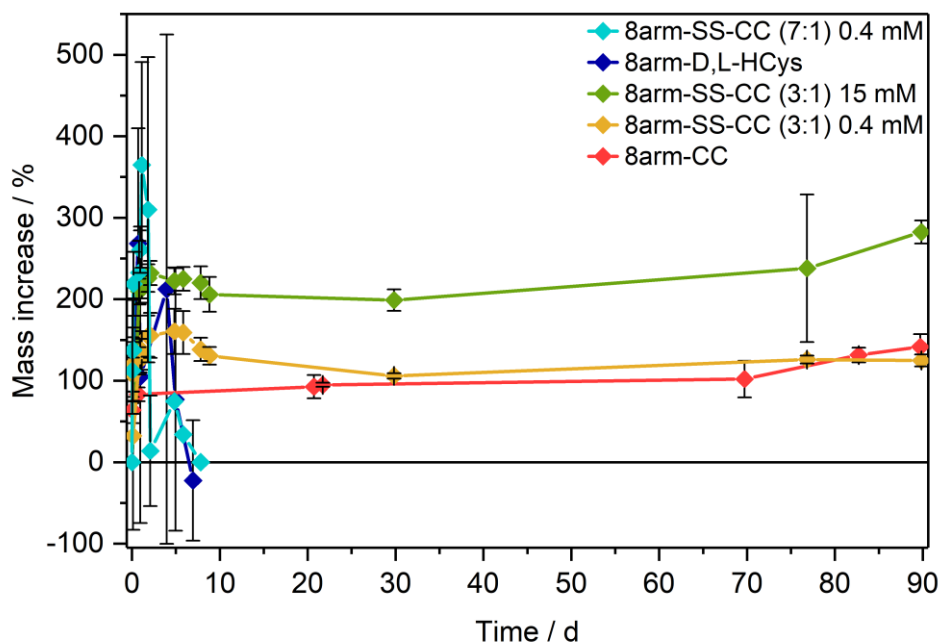
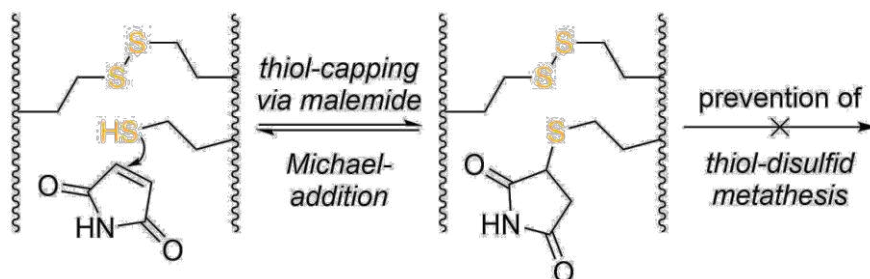


Figure 75: Swelling behavior of hydrogels containing different ratios of Nor-D,L-HCys and Nor-O-SS. Both non-stabilized 8arm-D,L-HCys and 8arm-SS-CC (7:1) are disintegrating within a few days. With 25% of Nor-D,L-HCys being substituted by Nor-O-SS the percolation threshold is met and the hydrogel is stabilized.

Hence it could be demonstrated, that unrestricted expansion of the hydrogel is the cause for final dissolution of the network. The most probable cause for this unrestricted expansion is the dynamic reformation of linkages, which is expected to occur via thiol-disulfide metathesis. Besides impeding the hydrogel from expanding by forcing it into its shape, an alternative solution is preventing the presence of free thiols.

6.3.3.2 Capping of free thiols by maleimide

In order to proof the hypothesis, that relaxation and unrestricted swelling of the hydrogel network is based on thiol-disulfide metathesis, the occurrence of pendant thiols needs to be verified. This can be achieved indirectly by capping free thiols and hence disabling their participation in thiol-disulfide metathesis. Since free thiols readily react with Michael-acceptors in a thiol-Michael addition reaction,^[53a] preformed hydrogel samples can be simply immersed in a solution of a non-crosslinking small molecule Michael-acceptor in order to consume unreacted thiols (Scheme 44), as recently demonstrated by Waymouth and co-workers.^[138]



Scheme 44: Small molecule Michael-acceptors as maleimide can be used to irreversibly bind free thiols and thus prevent thiol-disulfide metathesis.

Hence, after polymerization samples of **8arm-D,L-HCys (1:1)** hydrogel were immersed in a solution of maleimide (4 mM) in PBS for 1 h. Thereafter the maleimide-treated samples were swollen in PBS and their mass increase was observed (Figure 76). Indeed this treatment stabilized the hydrogel and samples were monitored for a period of more than 2 months, except for one of the samples, which only existed for 21 d.

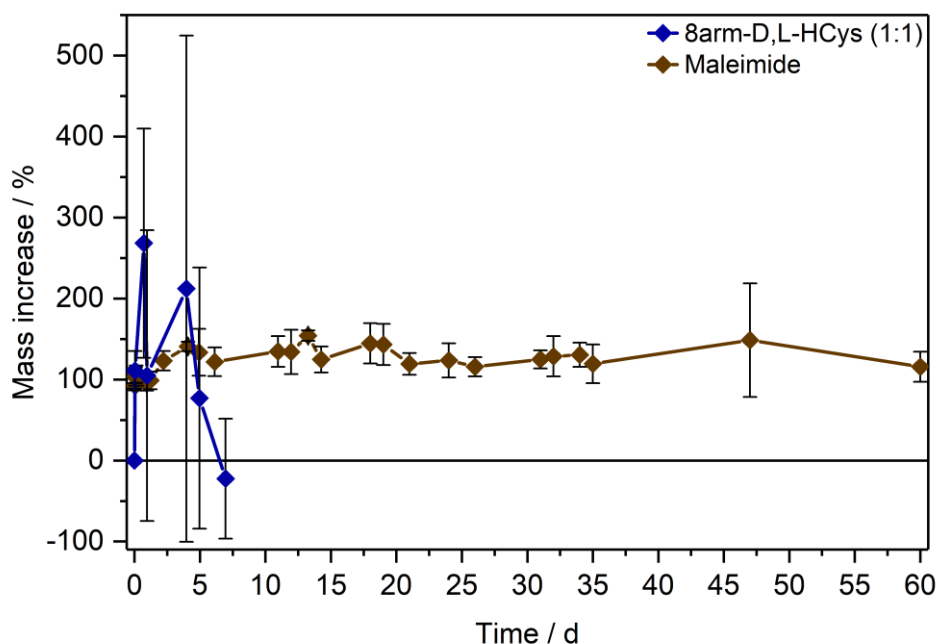


Figure 76: Unstable 8arm-D,L-HCys (1:1) hydrogel can be stabilized via treatment with maleimide (4 mM) by soaking the sample for 1 h prior to swelling in PBS. Hence, free thiols are consumed and cannot interact with disulfide crosslinks.

This crucial experiment illustrates both (i) the presence of unreacted thiols as well as (ii) their involvement in the instability of the hydrogel. Furthermore, it demonstrates the possibility of post-gelation modification of this hydrogel type. Nevertheless, maleimide is toxic and hence this strategy is not practicable for biological applications and was hence not further explored.

6.3.3.3 Consumption of free thiols by an excess of linker

Another simple yet convenient method to prevent the presence of free thiols is crosslinking with an excess of linker. However, the ene-excess has to be optimized precisely, since using an excess of crosslinker also reduces the overall connectivity of the network, leading to pending norbornenes. Hence, three formulations based on 10 wt% 8armPEG20k-SH with increasing ene-excess including **15 mol%**, **20 mol%** and **23.5 mol%** were tested by photorheology (Figure 77). While an ene-excess of **15 mol%** (20.4 ± 0.4 kPa) doesn't significantly alter G' when compared to **8arm-D,L-HCys (1:1)** hydrogel (20.2 ± 2.2 kPa) with equimolar thiol:ene ratio, higher ene-concentrations lead to increases in G' (**20 mol%**: 27.4 ± 1.3 kPa, **23.5 mol%**: 26.7 ± 2.5 kPa). This result is of particular interest, since it demonstrates again, that **Nor-D,L-HCys** does not fully react when applied at an 1:1 thiol-ene ration. Consequently, an excess of ene is required to both consume all thiols and consequently even maximize the crosslinking density.

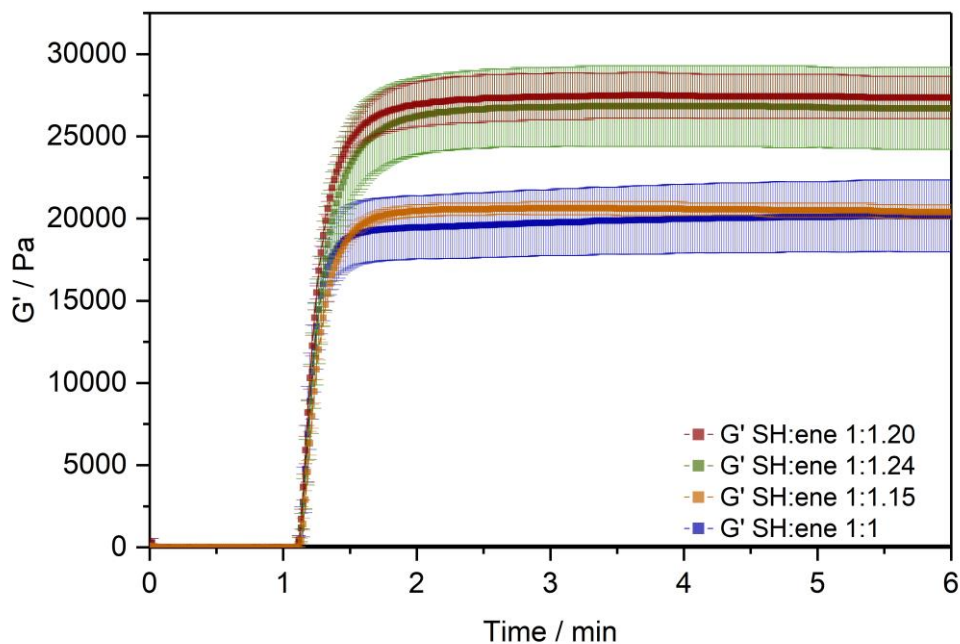


Figure 77: Photopolymerization of hydrogels based on 10 wt% 8armPEG20k-SH and an excess of Nor-D,L-HCys was monitored by photorheology. Whereas G' of 8arm-D,L-HCys (1:1.15) hydrogel prepared with a low ene-excess of 15% was in the same range as that of the equimolar 8arm-D,L-HCys (1:1) hydrogel, an increased excess of ene (1:1.20, 1:1.24) lead to higher stiffness.

Monitoring the swelling behavior confirmed successful stabilization of the hydrogel by using an ene-excess of 20% (**8arm-D,L-HCys (1:1.20)**). The resulting hydrogel samples were examined for a period of 2 months (Figure 78).⁶ While an ene-excess of 15% appeared not to be sufficient

⁶ One sample was lost 18 days, as the petri dish broke.

to stabilize the hydrogel (**8arm-D,L-HCys (1:1.15)**), interestingly when an excess of 23.5% was used (**8arm-D,L-HCys (1:1.24)**) the hydrogel dissolved as well. Hence, an ene-excess of 20% seems to be the optimum for this formulation.

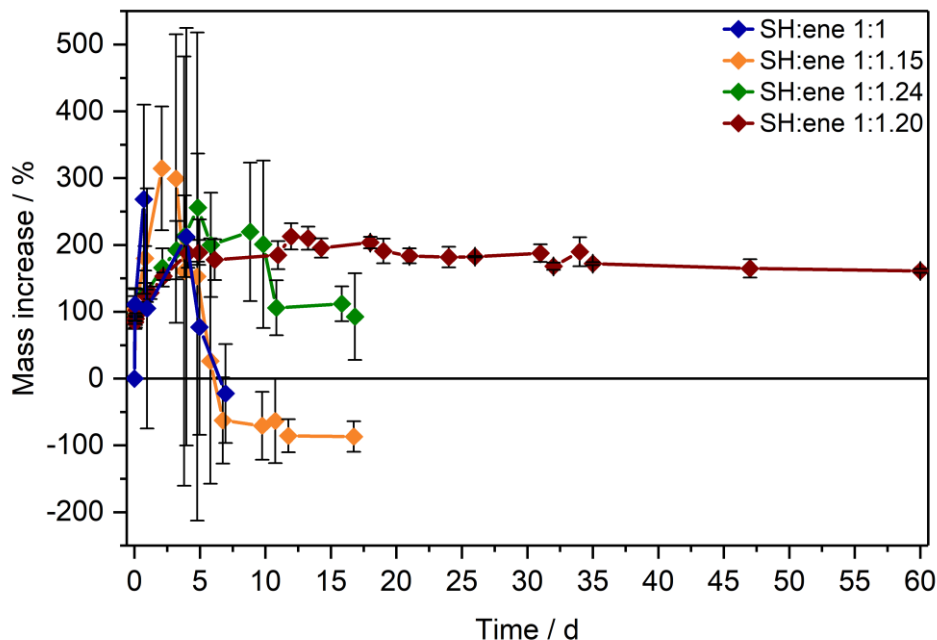


Figure 78: Swelling behavior of hydrogels based on 10 wt% 8armPEG20k-SH and an excess of Nor-D,L-HCys. Whereas formulations with an ene-excess of 15 mol% and 24 mol% were not stabilized, using 20 mol% excess of ene seems to be the optimum for prolonged stabilization.

These experiments could well demonstrate, that (i) with **Nor-D,L-HCys** ene-conversion is incomplete when reacted at an 1:1 ratio of functional groups. Moreover, (ii) the crosslinking density and stiffness can even be increased by using an excess of ene, whereby an optimum excess of ene could be established at 20 mol%.

Although it might seem reasonable at first glance, to use the introduced pending norbornenes for further postgelation modification by first swelling and then binding thiol-containing bioactive molecules into the network. However, such modifications can lead to partial degradation of the network by thiol-disulfide metathesis as well, as again the concentration of free thiols within the network is difficult to control.

Nevertheless, for cell culture applications bioinert PEG-based hydrogels need to be modified with peptide sequences such as RGD to allow for cellular attachment.^[12b] RGDC containing cysteine is commercial available and can be readily copolymerized in a thiol-ene reaction. To investigate this copolymerization, two formulations based on 10 wt% 8armPEG20k-SH, 1 mM RGDC and different amounts of **Nor-D,L-HCys** were analyzed by photorheology (Figure 79). The addition of

1 mM RGDC results in an increase in thiols of 2.3 mol% when copolymerized with 10 wt% 8armPEG20k-SH. Hence, in one formulation this additional amount of thiol (**22.3 mol% ene-excess**) was compensated, while the second formulation contained **20 mol% excess of ene** besides 1 mM RGDC. Interestingly, the latter formulation based on **20 mol% excess of ene plus RGDC** (29.5 ± 1.7 kPa) exhibited a higher storage modulus than both the reference formulation with **20 mol% excess of ene** but no RGDC (27.4 ± 1.3 kPa) and the formulation based on an increased excess of **22.3 mol% ene plus RGDC** (23.5 ± 1.3 kPa). Noteworthy, in the formulation containing **20 mol% excess of ene plus RGDC** the peptide was first combined with the linker before PEG was added, while in the formulation based on **22.3 mol% ene plus RGDC** it was added last.

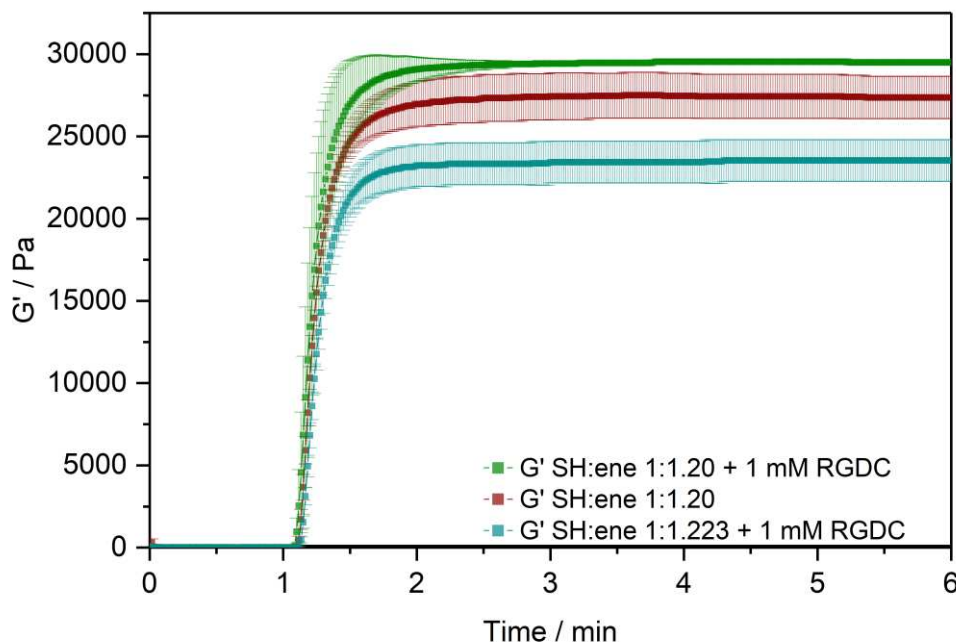


Figure 79: Formation of hydrogels based on 10 wt% 8armPEG20k-SH and an excess of Nor-D,L-HCys in presence of 1mM RGDC was monitored by photorheology. Interestingly, a 20 mol% excess of ene resulted in higher G' values than an ene-excess of 22.3 mol%, compensating for the excess thiols introduced by RGDC. G' of the latter was even below that of the reference formulation with a 20 mol% excess of ene but no RGDC.

The swelling behavior of the investigated hydrogels corresponds to the rheological observations. Samples with an **ene-excess of 20 mol% plus RGDC**, which exhibited the highest G', showed lower swelling (~factor 2) than the reference samples without RGDC added (**8arm-D,L-HCys (1:1.20)**) and were monitored for a period of more than 2 months. In contrast, the samples based on an increased excess of **22.3 mol% ene plus RGDC** were not stabilized and disintegrated within a few days. It is not clear, if this is a consequence of the applied thiol-ene ratio or the fact that RGDC was not premixed with the linker but added last to this formulation.

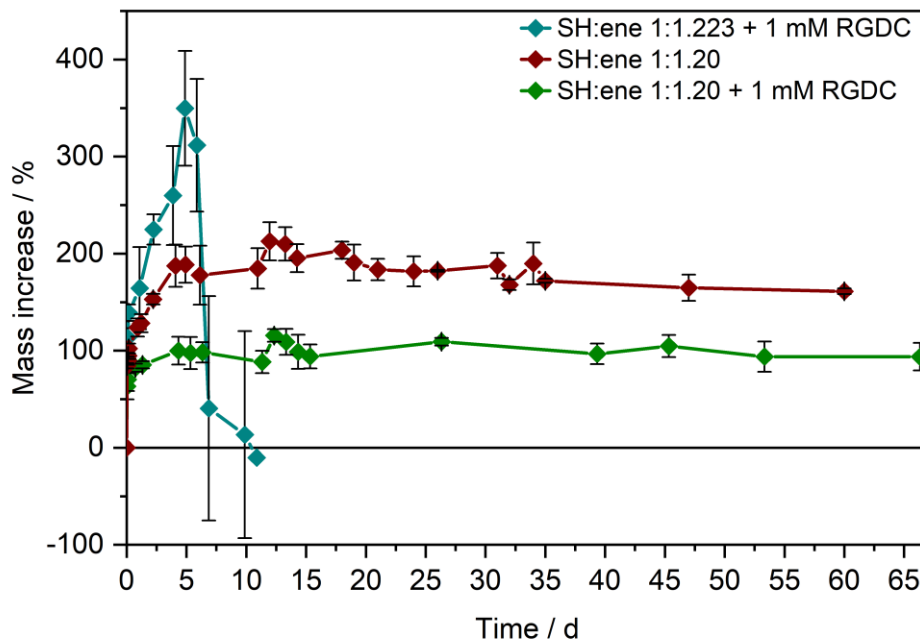


Figure 80: Swelling behavior of hydrogels based on 10 wt% 8armPEG20k-SH and an excess of Nor-D,L-HCys, which were copolymerized with 1mM RGDC.

Nevertheless, successful copolymerization of stable hydrogels with RGDC could be demonstrated, allowing for cell encapsulation and culturing in this hydrogel type.

6.3.4 Stabilization of 8armPEG-based hydrogels by the use of Nor-L-HCys

Opposed to **Nor-D,L-HCys**, the isomeric linker **Nor-L-HCys** based on an enantiopure L-homocysteine core showed the highest reactivity of the linker series and quantitative conversion of ene in the model reaction study with 2-mercaptoethanol (Figure 64). The effect of complete ene-conversion leads to remarkable behavior in corresponding rheological and swelling experiments, when comparing hydrogel formulations based on 10 wt% 8armPEG20k-SH and either **Nor-L-HCys** or **Nor-D,L-HCys**. While formulations with **Nor-L-HCys** react slightly slower, they reach higher G' values than their **Nor-D,L-HCys** based counterparts (Figure 81). More importantly, whereas in the case of **Nor-D,L-HCys** a 20 mol% excess of ene leads to a maximum storage modulus (**8arm-D,L-HCys 1:1.2**, 27.4 ± 1.3 kPa), with **Nor-L-HCys** the equimolar formulation exhibits the highest G' of the series (**8arm-L-HCys 1:1**, 32.4 ± 0.3 kPa). On the other hand, the stiffness of **8arm-L-HCys (1:1.2)** hydrogel (21.3 ± 1.7 kPa) is within the range of **8arm-D,L-HCys (1:1)** hydrogel (20.2 ± 2.2 kPa).

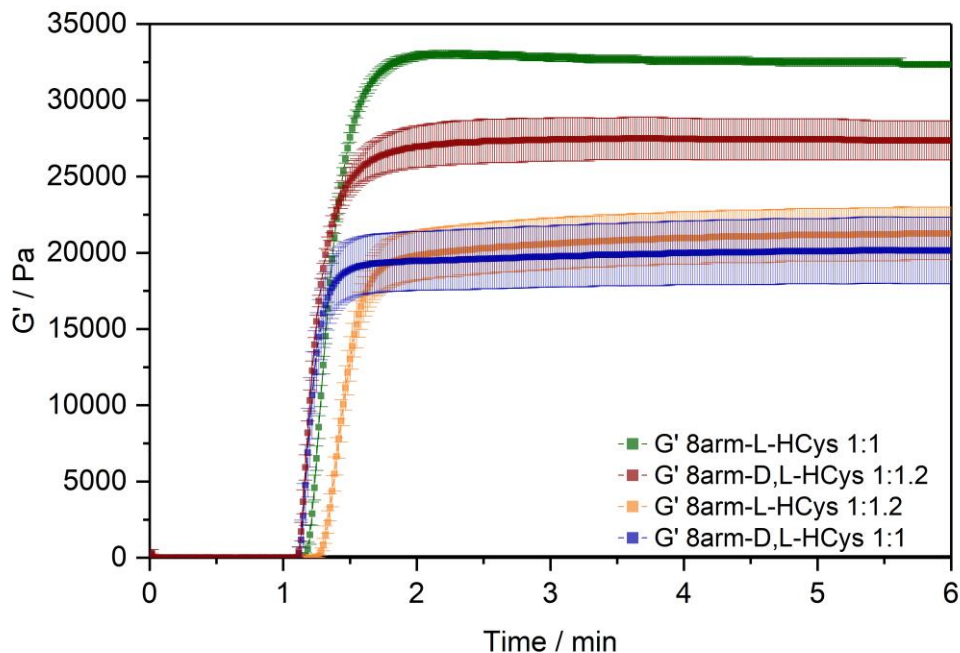


Figure 81: Effect of changing the homocysteine-based linkers. Comparison of the photopolymerization of hydrogel formulations based on 10 wt% 8armPEG20k-SH, 0.4 mM LiTPO and either Nor-L-HCys or Nor-D,L-HCys. While Nor-L-HCys based formulations react slightly slower, they reach higher G' values than their Nor-D,L-HCys based counterparts. While in the case of Nor-D,L-HCys a 20 mol% excess of ene (8arm-D,L-HCys 1:1.2**) leads to a higher storage modulus, with Nor-L-HCys the equimolar formulation (**8arm-L-HCys 1:1**) exhibits the highest G' of the series.**

These results evidence very high to quantitative ene-conversion. Apparently, the equimolar formulation of **Nor-L-HCys** reaches an increased crosslinking density, since here the storage modulus was higher than when a 20 mol% excess of ene was used. Conversely, by applying an excess of ene the network connectivity is decreased with **Nor-L-HCys**. Furthermore, the swelling behavior also confirms very high to quantitative thiol-consumption when **Nor-L-HCys** is used, since hydrogels of both formulations remain stable (Figure 82). Interestingly, the equimolar formulation with **Nor-L-HCys** even exhibits the lowest swelling of the whole series.

While with **Nor-D,L-HCys** ene-conversion is incomplete when reacted at an equimolar thiol-ene ratio and hence an excess of ene is required to increase stiffness, the opposite behavior was observed for **Nor-L-HCys**. Here the equimolar formulation reaches higher G' values than when an excess is used. Moreover, since with an equimolar thiol-ene ratio the network connectivity is maximized, **Nor-L-HCys** based formulations surpass those based on **Nor-D,L-HCys** in maximal achievable stiffness.

Furthermore, the swelling behavior also evidences very high to quantitative thiol-consumption when **Nor-L-HCys** is used, since hydrogels of both formulations remain stable (Figure 82).

Interestingly, in this case the equimolar formulation not only exhibits lower swelling than the excess-formulation, but the lowest swelling of the whole series.

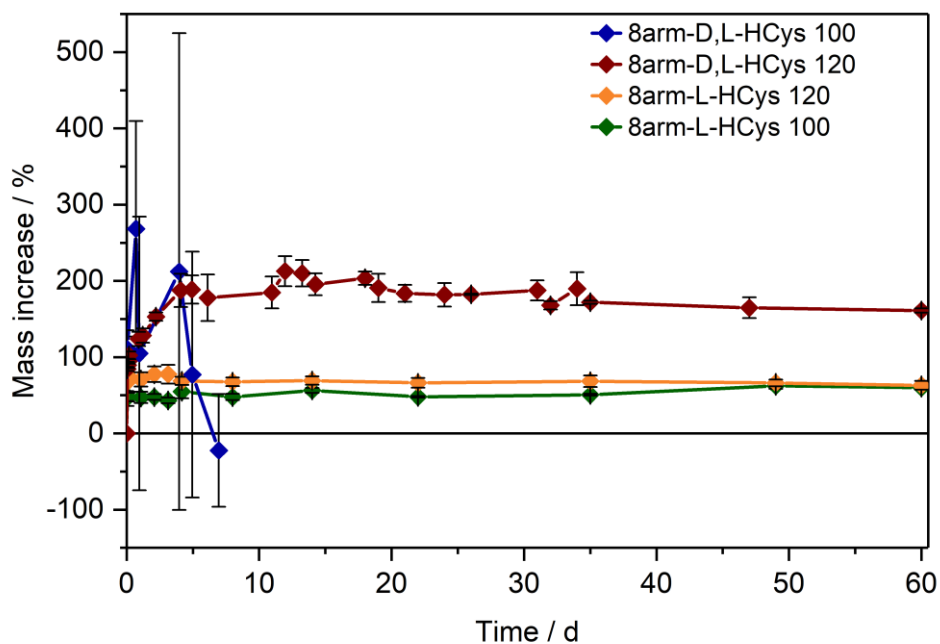


Figure 82: Swelling behavior of hydrogels made from 10 wt% 8armPEG20k-SH and linkers based on a homocysteine core

These results particularly confirm the findings of the $^1\text{H-NMR}$ reactivity estimation, which revealed that **Nor-L-HCys** reaches full ene-conversion. They further highlight the importance of complete ene-conversion with regard to hydrogel stability and demonstrate that complete conversion is less a matter of decreasing functional group mobility in the course of proceeding gelation, but rather based on linker reactivity.

6.3.5 Crosslinking 4armPEG-based hydrogels

In principle, thiol-terminated 8-armed PEG (8armPEG20k-SH, $M_w \sim 20$ kDa) is the dimer of the corresponding 4-armed PEG (4armPEG10k-SH, $M_w \sim 10$ kDa, Figure 83). Hence, 10 wt% solutions of both compounds should contain the same amount of thiols and react analogue. However, due to the additional connection in 8armPEG20k-SH the crosslinking density and the network geometry as well as the network stability differ.

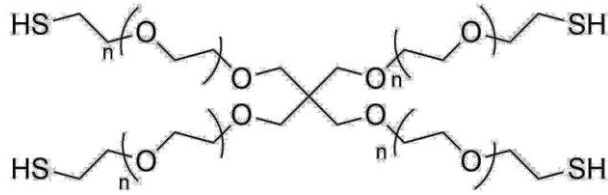


Figure 83: Molecular structure of 4arm-PEG10k-SH with a pentaerythritol core.

This becomes obvious when examining the rheological behavior of hydrogels made from 4armPEG10k-SH and homocysteine-based linkers (Figure 84). Due to the lower crosslinking density and different network geometry, the observed storage moduli are lower than when 8armPEG20k-SH was used (Figure 81), albeit the order of stiffness with respect to the formulations does not change.

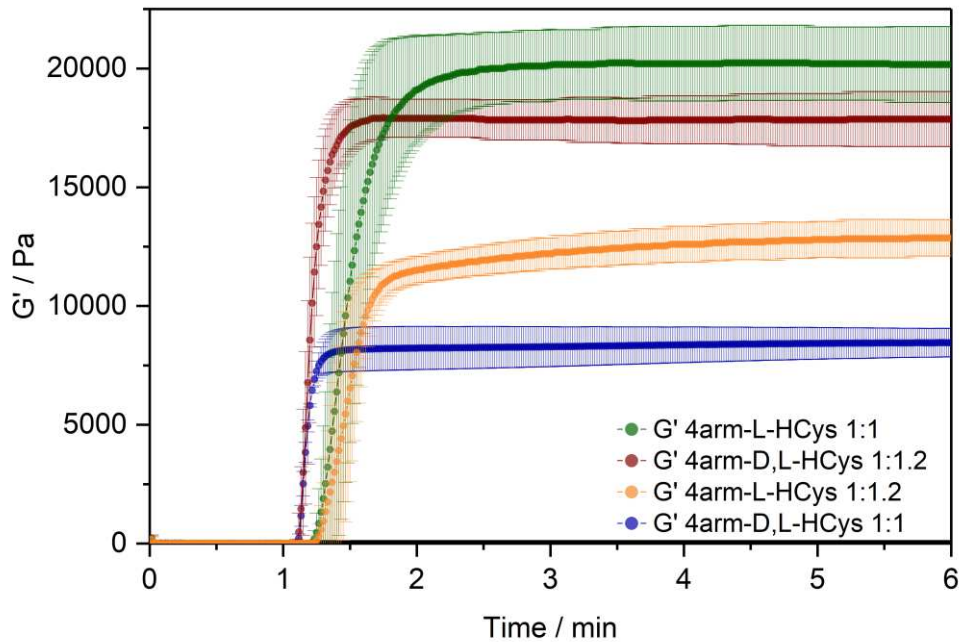


Figure 84: Crosslinking of 4armPEG10k-SH with homocysteine-based linkers. Photopolymerization of hydrogel formulations based on 10 wt% 4armPEG10k-SH, 0.4 mM LiTPO and either Nor-L-HCys or Nor-D,L-HCys was monitored by photorheology. Again Nor-L-HCys based formulations react slower but reach higher G' values than their Nor-D,L-HCys based counterparts. Opposed to the case of Nor-D,L-HCys, with Nor-L-HCys the equimolar formulation exhibits a higher G' than when an excess of ene is used.

Again, **Nor-L-HCys** based formulations achieve higher storage moduli than those based on **Nor-D,L-HCys** and with **Nor-L-HCys** the equimolar formulation exhibits better mechanical properties, whereas for **Nor-D,L-HCys** an excess of ene is required for this purpose. Nevertheless, 4armPEG-hydrogels crosslinked by **Nor-D,L-HCys** were swelling heavily and dissolved after a few days, even when an excess of ene was used. In contrast, **Nor-L-HCys**-based 4armPEG-

hydrogels reached equilibrium swelling within a day and remained stable. As in the case of 8armPEG20k-SH, with **Nor-L-HCys** the equimolar formulation was swelling less, indicating higher crosslinking density.

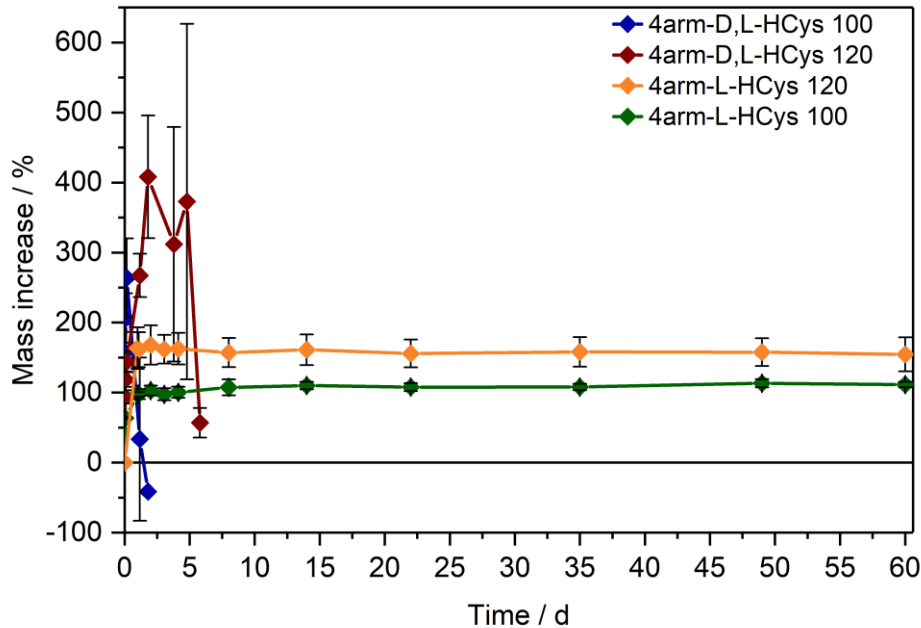


Figure 85: Swelling behavior of hydrogels made from 10 wt% 4armPEG10k-SH and linkers based on a homocysteine core. While Nor-D,L-HCys does not give stable hydrogels, Nor-L-HCys does.

Hydrogels from 4armPEG10k-SH are interesting for cell encapsulation, due to their lower stiffness compared to 8armPEG-based hydrogels. However, 4armPEG-based hydrogels can only be formed with **Nor-L-HCys**.

6.4 Two-photon micropatterning of disulfide-crosslinked hydrogels in presence of DAS

As demonstrated before, disulfide crosslinked networks can be cleaved by irradiation with light in presence of a photoinitiator.^[25d] This concept also works under two-photon irradiation regime. The application of water-soluble two-photon chromophore P2CK bears the disadvantages of limited cytocompatibility at concentrations above 0.1 mM, interference with LIVE/DEAD viability assay in fluorescence microscopy and potential crosslinking of thiol terminated PEG due to the presence of two double bonds.^[112, 116] On the contrary, water-soluble diazosulfonate-based two-photon initiator DAS is the better option, as it is cleavable and hence produces less cytotoxic radical oxygen species (ROS) and does not interfere with stainings and due to its single double bond it cannot act as a crosslinker for thiols.^[49a, 139]

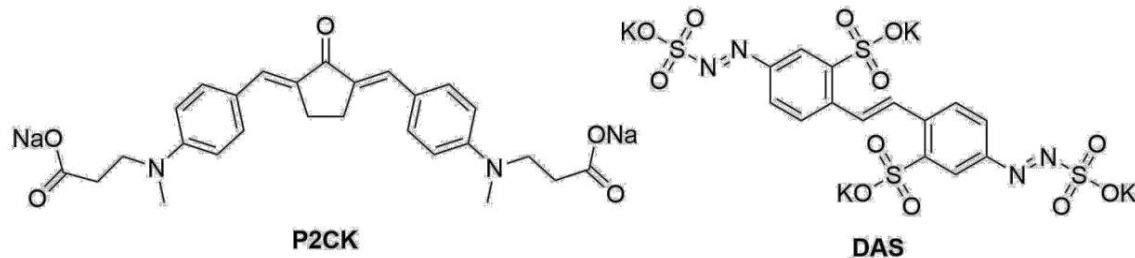


Figure 86: Molecular structures of two-photon active chromophores P2CK and DAS.

The two-photon micropatterning in presence of DAS was tested on samples of **8arm-D,L-HCys (1:1.2)** hydrogel and **8arm-L-HCys (1:1)** hydrogel, since these hydrogels exhibited the highest G' values of the investigated series and hence had the highest network connectivity. Hydrogel samples were formed in molds ($\varnothing = 6$ mm, $d = 0.8$ mm) on methacrylated ibidi μ -dishes by irradiating in a Boekel-UV-oven (365 nm, 2 J). The hydrogels were first swollen for 3 d in PBS to reach equilibrium swelling. Subsequently, the hydrogels were submersed in solutions of DAS in PBS at different concentrations (0.5 mM, 1.0 mM, 2.0 mM) for at least 5 h to allow diffusion of the chromophore into the network (Figure 87). Thereafter, the hydrogel samples were cut with a scalpel and then two-photon micropatterned using a fs-pulsed NIR-laser at 720 nm focused through a water immersion objective (32x, 0.85 NA) and a constant writing speed of 200 mm s⁻¹. Parallel channels with quadratic cross sections (300 μ m x 20 μ m x 20 μ m) were eroded from the edge into the bulk of the hydrogel at different laser powers ranging from 10–120 mW and scanning along the x-axis. Individual x,y-planes were either scanned once or twice. For examination of the photoeroded channels by LSM, the samples were swollen in a solution of fluorescein modified dextran (1 mg mL⁻¹) with an average molecular weight of ~2,000 kDa (FITC2000) for at least 4 h. Due to its size FITC2000 only infiltrates open micro-channels but not the bulk hydrogel.

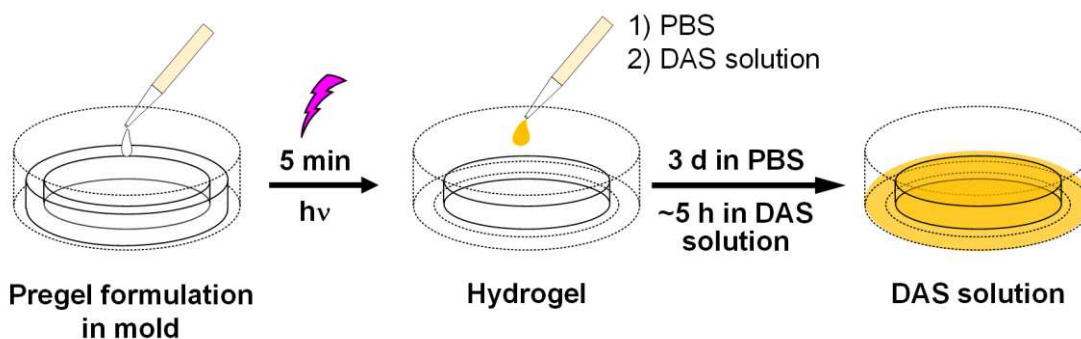


Figure 87: Workflow of hydrogel formation and treatment with DAS prior to two-photon micropatterning. Disulfide-crosslinked PEG hydrogels were formed by photoinduced thiol-ene addition upon irradiation with UV-light. Thereafter, hydrogels were swollen in PBS before they were soaked in solutions of DAS for approx. 5 hours.

When **8arm-D,L-HCys (1:1.2)** hydrogel was micropatterned in presence of 2.0 mM DAS, open microchannels formed after a single scan at laser powers starting from 20 mW (Figure 88). At lower concentrations it was necessary to scan each x,y-plane twice to produce open microchannels with **8arm-D,L-HCys (1:1.2)** hydrogel. At a concentration of 1 mM DAS bright fluorescence was as well visible at 30 mW, while at 0.5 mM DAS at least 40 mW were necessary to give a bright fluorescence signal (Figure 88 and Figure 89). However, when no DAS was present, no fluorescence could be observed at all.

The scanning parameters for complete hydrogel degradation can be optimized in many ways. In the present experiment, a hatch distance of 0.1 μm and a z-layer distance of 0.5 μm was used. At DAS concentrations below 2mM x,y-planes had to be scanned twice. In contrast, to ensure complete photodegradation of an oNB-based hydrogel 5-7 frame repeat scans using 1.9 W laser power with a pixel dwell time of 2 μs were reported to be required in recent literature.^[29b]

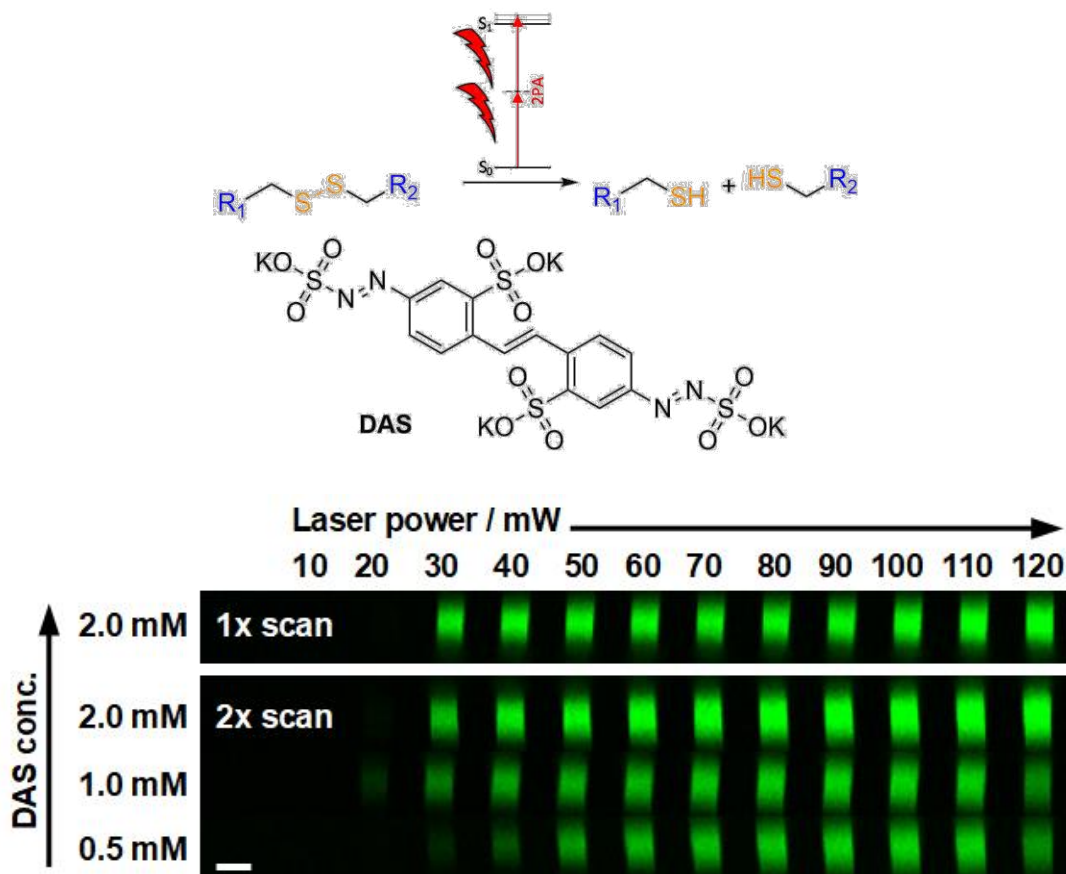


Figure 88: Micro-channel were fabricated by two-photon degradation of **8arm-D,L-HCys (1:1.2)** hydrogel in presence of two-photon initiator DAS (0.5–2.0 mM). Individual x,y-planes were either scanned once or twice along the x-axis. Thereafter, the hydrogels were soaked in a solution FITC2000 and analyzed by confocal microscopy. Images display orthogonal cross sections (y,z-plane) of micro-channels. Scale bar 20 μm .

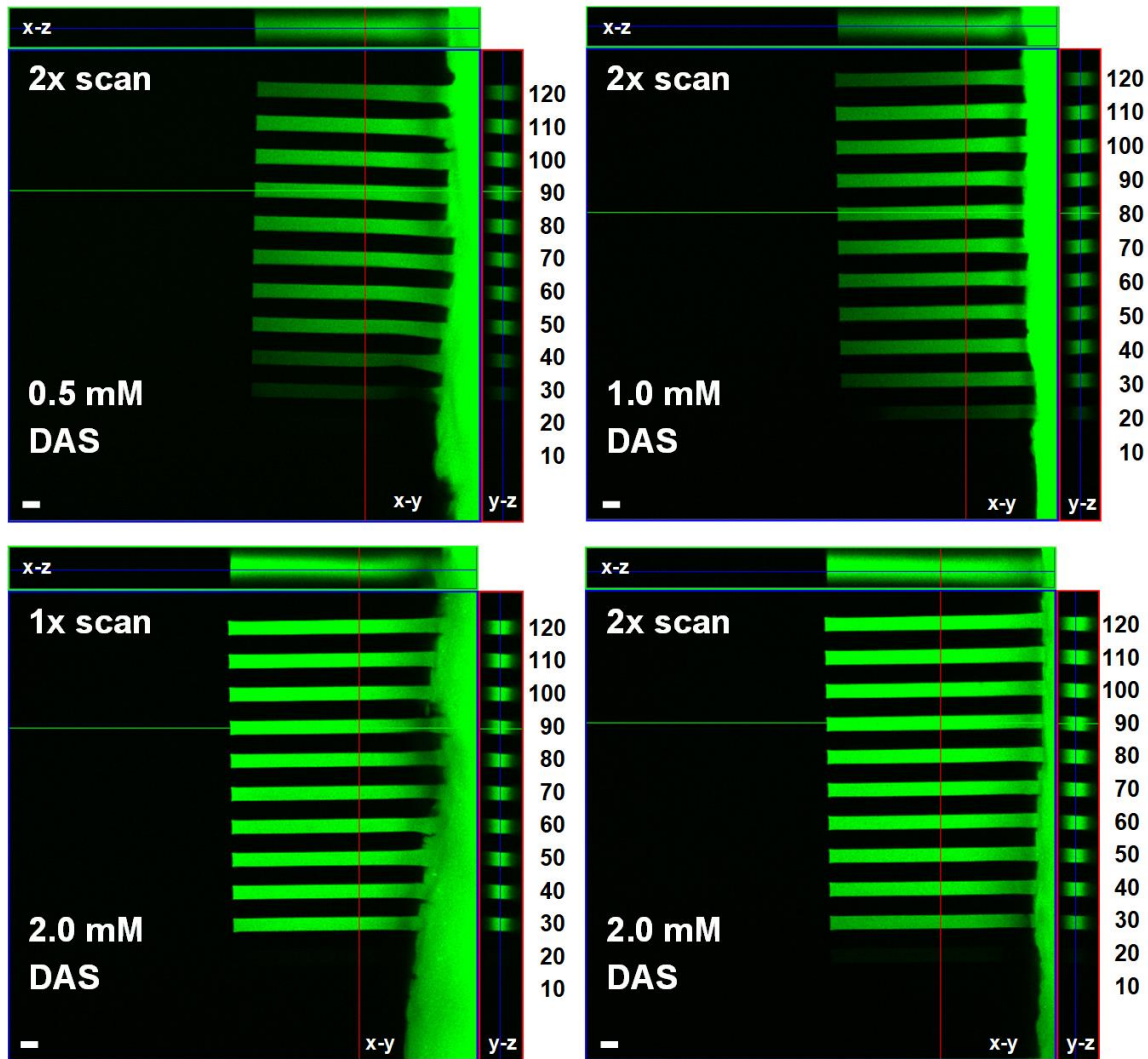


Figure 89: Top-down views of confocal z-stacks with corresponding orthogonal projections of channels ($300 \times 20 \times 20 \mu\text{m}^3$) fabricated at increasing laser powers (10–120 mW) in **8arm-D,L-HCys (1:1.2)** in presence of different concentrations of DAS ranging from 0.5-2.0 mM. Micro-channels were visualized by soaking in a solution of FITC2000. Scale bars = 20 μm .

Compared to **8arm-D,L-HCys (1:1.2)** hydrogel ($27.4 \pm 1.3 \text{ kPa}$) **8arm-L-HCys (1:1)** hydrogel ($32.4 \pm 0.3 \text{ kPa}$) is much stiffer indicating a higher crosslinking density. Consequently, when using the same scanning parameters, double scanning in presence of 2.0 mM DAS was required to produce open micro-channels at laser powers of 40 mW and above, which could be penetrated by FITC2000 (Figure 90). With lower molecular weight fluorescent dextran ($M_w \sim 500 \text{ kDa}$, FITC500) channels fabricated at 30 mW were visible as well (Figure 91). In contrast, micro-channels produced in presence of 1.0 mM DAS by double scanning at laser powers of 50 mW and above in **8arm-L-HCys (1:1)** hydrogel required swelling in FITC500 for visualization, indicating incomplete degradation at the scanning parameters used.

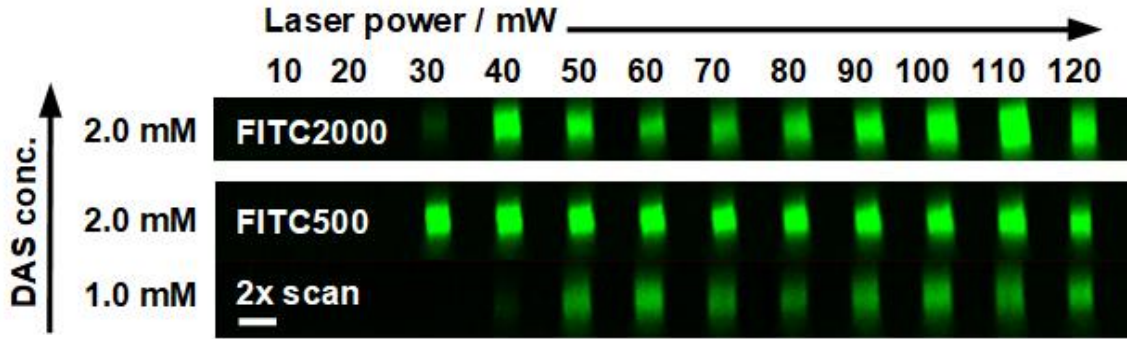


Figure 90: Two-photon induced micro-channel fabrication in 8arm-L-HCys (1:1) hydrogel required double scanning in presence of 2.0 mM DAS for complete erosion. Thus, microchannels could be visualized with FITC2000 by confocal microscopy. When 1 mM DAS was used channels could only be visualized using lower molecular weight fluorescent dextran (Mw ~500 kDa, FITC500). Images display orthogonal cross sections (y,z-plane) of micro-channels. Scale bar 20 μm .

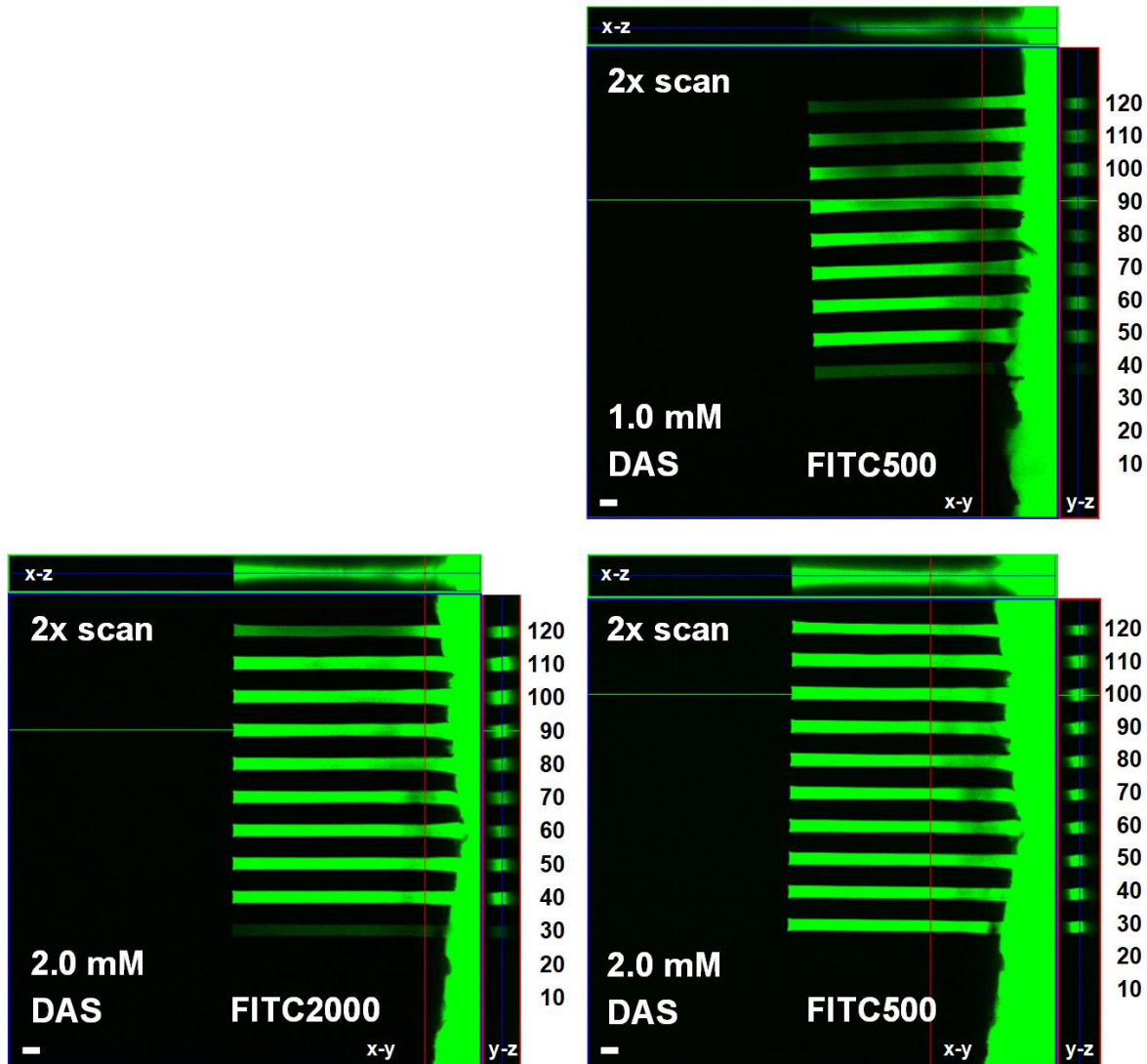


Figure 91: Top-down views of confocal z-stacks with corresponding orthogonal projections of channels ($300 \times 20 \times 20 \mu\text{m}^3$) fabricated at increasing laser powers (10–120 mW) in 8arm-L-HCys (1:1) in presence of of 1.0 or 2.0 mM DAS. Micro-channels were visualized by soaking in solutions of either FITC2000 (2 mM DAS) or FITC500 (1.0 mM DAS). Scale bars = $20 \mu\text{m}$.

Nevertheless, two-photon degradation of disulfide-crosslinked PEG-based hydrogels in presence of DAS was successfully demonstrated by this experiment series. However, optimization of scanning parameters and scanning modes is required for each individual hydrogel formulation in order to achieve either complete degradation or localized softening of the material.

6.5 Cell encapsulation and micro-channel formation

To test the compatibility of the developed hydrogel platform as well as the two-photon induced cleavage process for cell culture applications cell encapsulation experiments were performed. These experiments were conducted together with Dr. Marica Markovic who performed cell culture and encapsulation experiments as well as LIVE/DEAD viability assays at the Institute of Materials Science and Technology (E308).

Spheroids ($\varnothing \sim 200 \mu\text{m}$) of mCherry-labeled human umbilical vein endothelial cell (HUVECs) together with single human adipose-derived stromal cells (ASCs) were encapsulated into **8arm-D,L-HCys (1:1.2)** hydrogel, **8arm-L-HCys (1:1)** hydrogel and **4arm-L-HCys (1:1)** hydrogel in presence of 1 mM RGDC. Hence, cells were carefully suspended in the respective prepolymer solutions by pipetting before the formulations were molded and crosslinked by irradiation in a Boekel-UV-oven (365 nm, 1 J). Thereafter, molds were carefully removed and hydrogels were submerged in adequate cell culture medium and maintained in cell culture conditions (5% CO_2 , 37 °C). 4 d after encapsulation laser scanning microscopy revealed that spheroids had not been properly transferred into the hydrogels. Instead, smaller cell clusters of approx. 100 μm diameter were present in **8arm-L-HCys (1:1)** hydrogel and **4arm-L-HCys (1:1)** hydrogel (Figure 92). In contrast, in **8arm-D,L-HCys (1:1.2)** hydrogel not sufficient cell clusters for further experiments were present. Nevertheless, cell encapsulation protocols require some optimization.

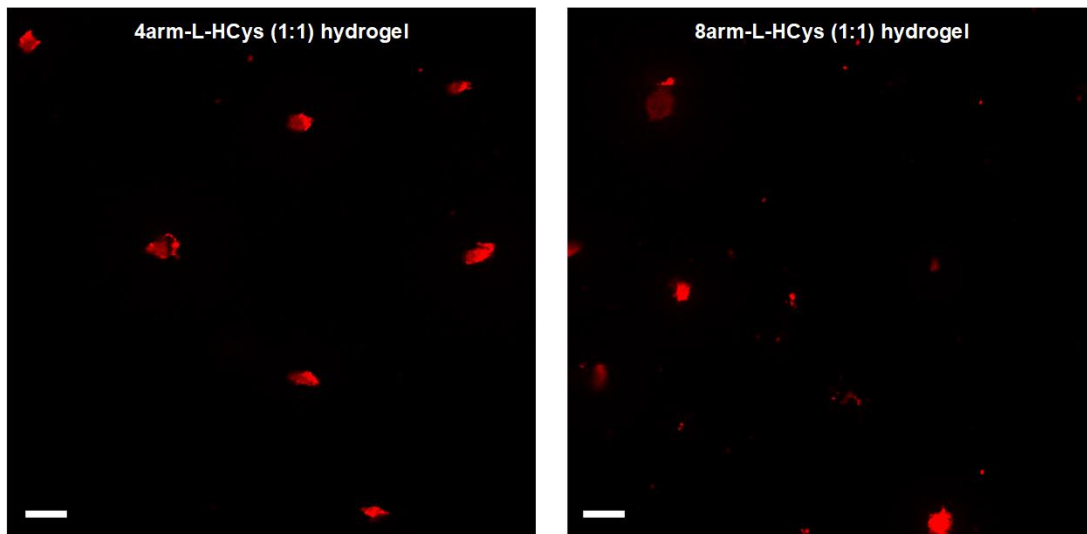


Figure 92: Clusters of encapsulated HUVECs (mCherry) 4 d after encapsulation in 4arm-L-HCys hydrogel (left) and 8arm-L-HCys hydrogel (right). Scale bar 100 μm .

Anyhow, to test the disulfide cleavage reaction in presence of encapsulated cells, the **4arm-L-HCys** hydrogel sample was swollen in a 1 mM solution of DAS in ECM-2 cell culture medium for at least 4 h. Then round micro-channels with a diameter of 20 μm were formed between cell

clusters by two-photon irradiation at 720 nm at a constant laser power of 60 mW. All other parameters were equal to those applied in previous micropatterning experiments and channels were only scanned once. During the scanning process, free movement of small particles could be observed in irradiated areas by LIVE-microscopy, demonstrating complete hydrogel degradation. Thereafter, the DAS solution was exchanged for media and cells were cultured for 2 d. Light microscopy revealed that cells started starching into channels (Figure 93).

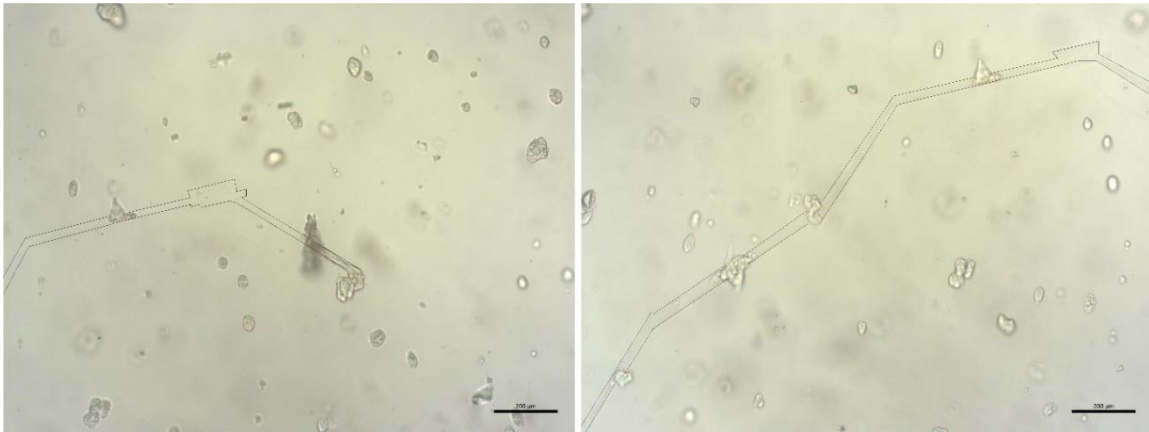


Figure 93: Light microscopy image of cells and micro-channels in 4arm-L-HCys hydrogel 2 d after two-photon micropatterning. Channels were marked for better contrast. Scale bar 200 µm.

5 days after micropatterning cells had filled up the entire micro-channel (Figure 94). Interestingly not HUVECS but ASCs seemed to spread in the channels, since cells in the channels could not be visualized by scanning for mCherry. However, HUVECS were still present.

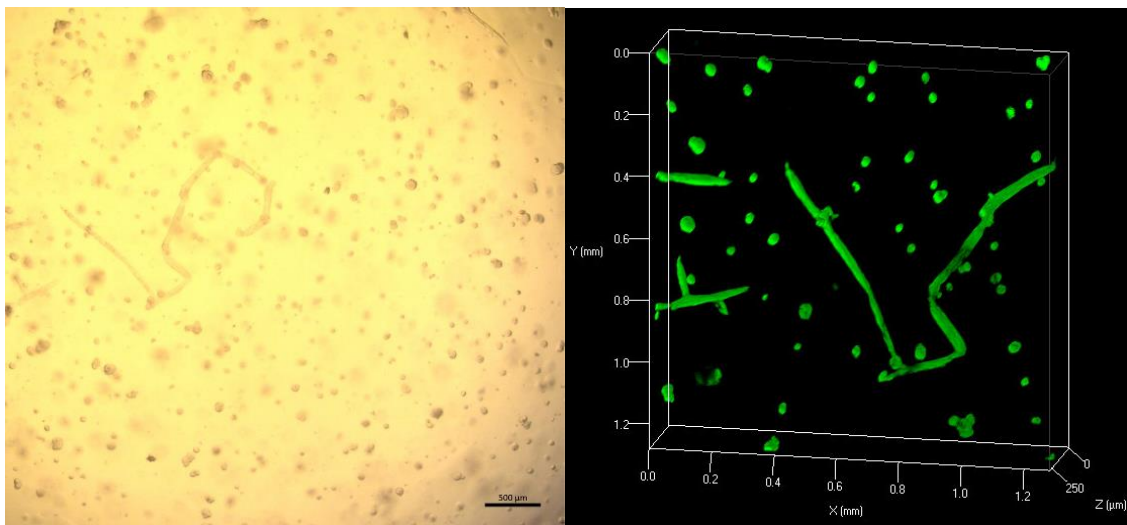


Figure 94: left: Light microscopy image of cells and micro-channels in 4arm-L-HCys hydrogel 5 d after two-photon micropatterning. Cells had almost filled up the entire microchannel. Scale bar 500 µm. right: 3D rendering of confocal z-stack of ASCs after applying LIVE/DEAD viability assay. Green: calcein; red: propidium iodide.

Hence, LIVE/DEAD viability assay was applied to visualize ASCs revealing ASCs spreading along the several mm long microchannel. Herewith the cytocompatibility of both the hydrogel as well as the encapsulation process and the two-photon micropatterning technique could be demonstrated. However, for further cell culture studies the encapsulation protocol has to be optimized to maximize the number of encapsulated spheroids.

6.6 Conclusion

A water-soluble disulfide-containing crosslinker for the photochemical formation of cleavable hydrogels by thiol-ene chemistry in presence of disulfide-bonds was developed. Hence, the molecular design was thoroughly optimized to maximize the double bond conversion. Interestingly, linkers based on homocysteine were highly reactive, whereas those based on cystine exhibited relatively hindered thiol-norbornene addition. With the optimized linker configuration, thiol-terminated macromers were crosslinked to form hydrogels, which were stable for several weeks in PBS. Two-photon induced cleavage of disulfide-based hydrogels in presence of DAS was demonstrated by microchannel fabrication. This approach could as well be applied in the presence of encapsulated stem cells, revealing the great potential of this hydrogel platform and cleavage methodology for both cell culture studies mimicking dynamic cell environment as well as fabrication of microfluidic devices.

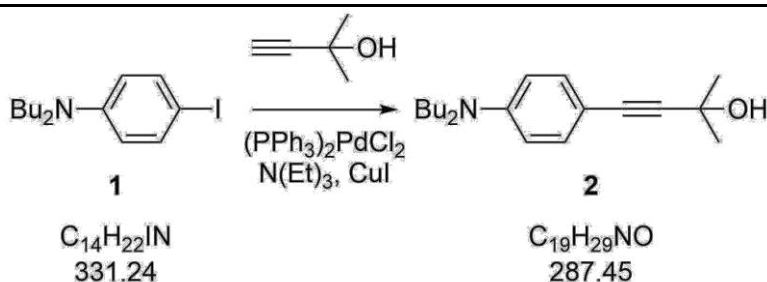
Experimental Part

1. SYNTHESIS AND EVALUATION OF YNE-MODIFIED TRIAZINES AS TWO-PHOTON ACTIVE CHROMOPHORES

1.2 Synthesis of 1,3,5-triazine-based chromophores

1.2.1 Synthesis of the alkyne-substituent 4-(ethynyl)-*N,N*-dibutylbenzeneamine, **3**

The alkyne-precursor *N,N*-dibutyl-4-ethynyl-benzenamine **3** was synthesized starting from *N,N*-dibutyl-4-iodo-aniline **1** via 4-[4-(*N,N*-dibutylamino)phenyl]-2-methyl-3-butyn-2-ol **2** in two steps according to literature.^[48]



N,N-Dibutyl-4-iodo-aniline **1** (4.636 g, 14.0 mmol, 1.0 eq) was dissolved in abs. trimethylamine (135 mL) and degassed using argon. 2-Methyl-3-butyne-2-ol (1.648 g, 19.6 mmol, 1.4 eq), bis(triphenylphosphine)palladium (II) dichloride (0.197 g, 0.3 mmol, 2 mol%) and copper(I)iodide (0.053 g, 0.3 mmol, 2 mol%) were added sequentially under a counter flow of argon. The reaction mixture was stirred at 40°C overnight. The progress of the reaction was monitored by TLC. After full conversion, the reaction mixture was filtered over a pad of silica to remove catalyst remains. The solid residue was washed with DCM (300 mL). The combined organic layers were washed with water (3x 100 mL) and brine (100 mL), dried over sodium sulfate and the volatile compounds were removed under reduced pressure. The product was purified by column chromatography (silica, PE:EE = 0-10%) twice yielding 3.292 g (11.5 mmol, 82%) of **2** as an orange liquid.

¹H-NMR (400 MHz, CDCl₃): δ = 7.24 (d, J = 9.0 Hz, 2H, Ar-H), 6.52 (d, J = 9.0 Hz, 2H, Ar-H), 3.25 (t, J = 7.7 Hz, 4H, -N-CH₂-), 2.02 (s, 1H, -OH), 1.60 (s, 6H, -C-CH₃), 1.55 (m, 4H, -N-CH₂-CH₂-), 1.34 (m, 4H, -CH₂-CH₃), 0.95 (t, J = 7.3 Hz, 6H, -CH₂-CH₃) ppm.

Chloro-[2-[4-(*N,N*-dibutylamino)phenyl]ethynyl]zinc

4-Ethynyl-*N,N*-dimethyl-aniline (413 mg, 1.80 mmol, 1.0 eq) was dissolved in 10 mL of dry THF in a Schlenk tube under argon atmosphere and cooled down to -78°C in an acetone-dry ice bath. Subsequently, *n*-BuLi (0.76 mL, 1.89 mmol, 1.05 eq) was added to the reaction mixture, followed by a solution of anhydrous ZnCl₂ (294 mg, 2.16 mmol, 1.2 eq) in dry THF (8 mL). The solid ZnCl₂ was pre-dried by melting in high vacuum using a heat gun. The mixture was allowed to react for 1 hour under constant stirring. The obtained product was directly used for the next step assuming 100% yield (1.0 eq).

Tris-4-[2-(4,6-dichloro-1,3,5-triazin-2-yl)ethynyl]-*N,N*-dibutyl-aniline, **3armTri**

2,4,6-Trichloro-1,3,5-triazine (66 mg, 0.36 mmol, 0.2 eq) was dissolved in 1 mL of dry THF in a three-neck-flask in argon atmosphere. Tetrakis(triphenylphosphine)palladium(0) (21 mg, 0.02 mmol, 1 mol%) was subsequently added in a counter flow of argon. To the reaction mixture the solution obtained in the previous step was added at room temperature and under argon atmosphere, which resulted in an instantaneous color change to red. The reaction was refluxed until full conversion was shown by TLC (PE:DEE = 15%).

After the reaction mixture was cooled to room temperature 0.1 M HCl (10 mL) was added and it was extracted with diethyl ether (3 x 20 mL). The organic phase was washed with brine (40 mL) and dried over sodium sulfate. The solvent was evaporated and the raw product was purified by column chromatography (silica, PE:DEE = 0-50%) and subsequent extraction of residual impurities by stirring in boiling *n*-hexane yielding 129 mg (0.2 mmol, 47%) of **3arm-Tri** as an orange solid.

¹H-NMR (600 MHz, CDCl₃): δ = 7.53 (d, J = 9.0 Hz, 6H, Ar-H), 6.57 (d, J = 9.0 Hz, 6H, Ar-H), 3.30 (t, J = 7.8 Hz, 12H, -N-CH₂-), 1.60 (m, 12H, -N-CH₂-CH₂-), 1.36 (m, 12H, -CH₂-CH₃), 0.97 (t, J = 7.4 Hz, 18H, -CH₂-CH₃) ppm.

¹³C-NMR (150 MHz, CDCl₃): δ = 160.5 (s, triazine), 149.7 (s, C-N), 135.3 (d, -C-C-C≡C), 111.2 (d, C-C-N), 105.5 (s, C-C≡C-triazine), 97.2 (s, -C≡C-triazine), 87.3 (d, -C≡C-triazine), 50.9 (t, -N-CH₂-), 29.4 (t, -N-CH₂-CH₂-), 20.4 (t, -CH₂-CH₃), 14.1 (q, -CH₂-CH₃) ppm.

HRMS (ESI): [M + H]⁺ m/z calcd. for C₅₁H₆₇N₆⁺ 763.5422; found 763.5412.

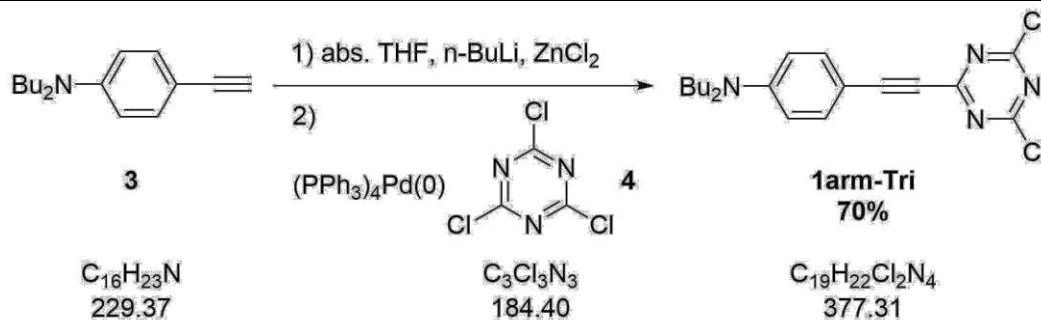
HRMS (ESI): [M + 2H]²⁺ m/z calcd. for C₅₁H₆₈N₆²⁺ 382.2747; found 382.2743.

R_f (PE:DEE = 40%) = 0.64

T_m = 141 °C

1.2.3 Synthesis of 4-[2-(4,6-Dichloro-1,3,5-triazin-2-yl)ethynyl]-*N,N*-dibutyl-aniline, **1arm-Tri**

Dipolar triazine **1armTri** was synthesized in two consecutive steps according to a protocol described in literature.^[57, 140]



Chloro-[2-[4-(*N,N*-dibutylamino)phenyl]ethynyl]zinc

N,N-Dibutyl-4-ethynyl-benzenamine **3** (275 mg, 1.20 mmol, 1.0 eq) was dissolved in 6 mL of abs. THF in a Schlenk tube under argon atmosphere and cooled to -78°C in an acetone-dry ice bath. Subsequently, *n*-BuLi (0.50 mL, 1.26 mmol, 1.05 eq) was added to the reaction mixture, followed by a solution of anhydrous ZnCl₂ (196 mg, 1.44 mmol, 1.2 eq) in dry THF (4 mL). The solid ZnCl₂ was pre-dried by melting in high vacuum using a heat gun. The mixture was allowed to react for 1 hour under constant stirring. The obtained product was directly used for the next step.

4-[2-(4,6-Dichloro-1,3,5-triazin-2-yl)ethynyl]-*N,N*-dibutyl-aniline, **1armTri**

To the reaction mixture obtained in the previous step and stirred at room temperature and under argon atmosphere, 2,4,6-trichloro-1,3,5-triazine **4** (221 mg, 1.2 mmol, 1 eq assuming 100% yield on the step 1) was added. Tetrakis(triphenylphosphine)palladium(0) (69 mg, 0.06 mmol, 5 mol%) was subsequently added to the reaction mixture resulting in an instantaneous color change to red. The reaction was allowed to proceed for 1 hour at room temperature under constant stirring, until TLC showed full consumption of starting materials. The reaction mixture was flashed over a pad of silica using PE and DEE as eluent. The raw product was purified by column chromatography (silica, PE:DEE = 0-10%) giving 316 mg (0.8 mmol, 70%) of **1arm-Tri** as a dark red solid after drying in high vacuum.

$^1\text{H-NMR}$ (600 MHz, CD_2Cl_2): δ = 7.52 (d, J = 9.1 Hz, 2H, Ar-H), 6.63 (d, J = 9.1 Hz, 2H, Ar-H), 3.34 (t, J = 7.8 Hz, 4H, -N-CH₂-), 1.59 (m, 4H, -N-CH₂-CH₂-), 1.37 (m, 4H, -CH₂-CH₃), 0.97 (t, J = 7.4 Hz, 6H, -CH₂-CH₃) ppm.

$^{13}\text{C-NMR}$ (150 MHz, CD_2Cl_2): δ = 171.5 (s, triazine), 162.3 (s, triazine), 151.1 (s, C-N), 136.2 (d, -C-C-C≡C), 111.8 (d, C-C-N), 104.0 (s, C-C≡C-triazine), 103.6 (s, -C≡C-triazine), 87.8 (d, -C≡C-triazine), 51.1 (t, -N-CH₂-), 29.6 (t, -N-CH₂-CH₂-), 20.6 (t, -CH₂-CH₃), 14.1 (q, -CH₂-CH₃) ppm.

HRMS (ESI): $[\text{M} + \text{H}]^+$ m/z calcd. for $\text{C}_{19}\text{H}_{23}\text{Cl}_2\text{N}_4^+$ 377.1294; found 377.1291.

R_f (PE:DEE = 40%) = 0.84

T_m = 81 °C

1.3 Testing of 1,3,5-triazine-based dyes as two-photon initiators

Sample solutions of the two-photon dyes in a 1:1 (w/w) mixture of acrylate monomers trimethylolpropane triacrylate (TTA, Sartomer) and ethoxylated-(20/3)-trimethylolpropane triacrylate (ETA, Sartomer SR415) at a concentration of $1 \mu\text{mol g}^{-1}$ were prepared. Acetone was used as co-solvent and the dyes were dissolved via ultrasonication (30 min). Thereafter, acetone was evaporated using high vacuum. Sample solutions were drop casted onto a methacrylate functionalized (3-(trimethoxysilyl)propyl methacrylate, Sigma-Aldrich) glass-bottom μ -dishes (35 mm, Ibidi GmbH, Germany) and two-photon polymerized. Details of the experimental two-photon lithography setup have been reported previously.^[112, 141] The setup is based on a tunable femtosecond laser (MaiTai DeepSee, Spectra Physics) with a pulse length of 70 fs after the objective (UPlanSApo 10x / 0.40 NA, Olympus). Arrays of μ -cubes ($100 \times 100 \times 100 \mu\text{m}^3$) at different writing speeds and laser powers were fabricated at 720 nm and 780 nm. The laser power was increased from 10-100 mW (Δ 10 mW), while the writing speed was varied from 100-900 mm s^{-1} (Δ 200 mm s^{-1}). The hatch and dz were maintained constant at 0.4 μm and 0.5 μm respectively. After two-photon polymerization the arrays were examined by light microscopy first, and via laser scanning microscopy (LSM 700, ZEISS) after development with 2-propanol overnight. In the latter case, the fluorescence emission signal of the two-photon chromophores embedded in the polymer network was exploited (488 nm excitation).

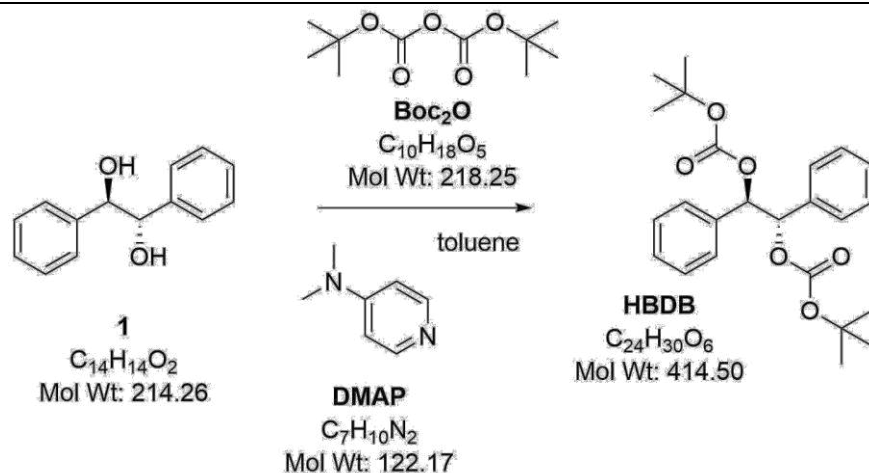
2. RADICAL FRAGMENTATION INDUCED BY HYDROGEN ATOM ABSTRACTION

2.2 Molecular Design and Synthesis – Symmetric Approach

2.2.1 Synthesis of meso-O,O'-diBoc-hydrobenzoin, HBDB

HBDB was synthesized following two protocols by Basel and Hassner.^[66]

Variant A:



In a flat bottom flask **1** (429 mg, 2.0 mmol, 1.0 eq), Boc_2O (1091 mg, 5.0 mmol, 2.5 eq) and DMAP (24 mg, 0.2 mmol, 0.1 eq.) were dissolved in 20 mL of dry toluene and stirred at room temperature. A white suspension formed during the reaction. After 15 min GCMS indicated total consumption of starting material (2 peaks + broad peak) and after 60 min slight conversion from one peak to the other. As there was no significant further conversion after 18 h, 30 mL of dry toluene were added to dissolve the solid. Finally after altogether 9 days the reaction mixture was diluted with CHCl_3 (60 mL) and then washed with 5% aqueous HCl (55 mL) before it was dried over Na_2SO_4 , filtered and the solvent was evaporated *in vacuo* yielding 792 mg (96%) of **HBDB** as white solid.

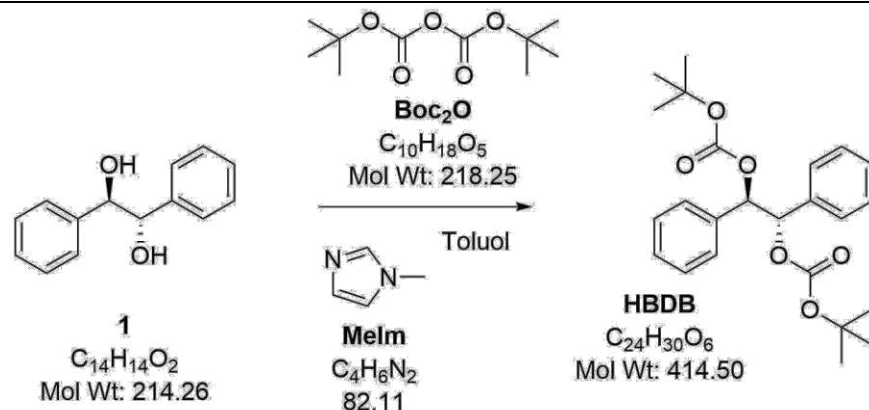
$^1\text{H-NMR}$ (200 MHz, CDCl_3 , FID LUM016/20): $\delta = 7.28$ (m, 10H, Ar-H), 5.89 (s, 2H, -O-CH-), 1.36 (s, 18H, -C(CH₃)₃) ppm.

$^{13}\text{C-NMR}$ (50 MHz, CDCl_3 , FID LUM016/23): $\delta = 152.6$ (s, -O-C=O-O-), 135.9 (s, Ar-C¹), 128.5 (d, Ar-C), 128.2 (d, Ar-C), 127.9 (d, Ar-C), 82.5 (s, -C(CH₃)₃), 79.2 (d, -O-CH-), 27.8 (q, -C(CH₃)₃) ppm.

HRMS (ESI): $[\text{M} + \text{NH}_4]^+$ m/z calcd. for $\text{C}_{24}\text{H}_{34}\text{NO}_6^+$ 432.2381; found 432.2403.

$T_m = 187\text{-}191$ °C (decomposition)

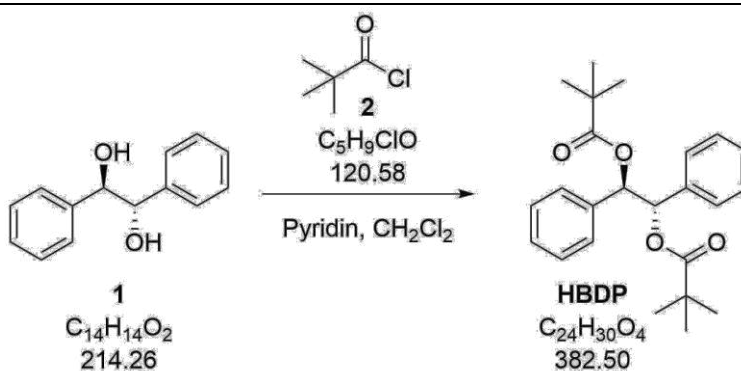
Variant B:



In a flat bottom flask **1** (214 mg, 1.0 mmol, 1.0 eq) and Boc_2O (641 mg, 2.9 mmol, 2.9 eq) were almost dissolved in 20 mL of dry toluene at room temperature before Melm (0.08 mL, 1.0 mmol, 1.0 eq) was added and the mixture was stirred at room temperature. After altogether 9 days the reaction mixture was diluted with $CHCl_3$ (30 mL) and then washed with 5% aqueous HCl (25 mL) before it was dried over Na_2SO_4 , filtered and the solvent was evaporated *in vacuo* yielding 402 mg (97%) of **HBDB** as white solid.

1H -NMR (200 MHz, $CDCl_3$, FID LUM017/10): δ = 7.28 (m, 10H, Ar-H), 5.89 (s, 2H, -O-CH-), 1.36 (s, 18H, -C(CH₃)₃) ppm.

2.2.2 Synthesis of meso-hydrobenzoin dipivalinate, HBDP



To a solution of **1** (536 mg, 2.5 mmol, 1.0 eq) in 14 mL of dry DCM in a round bottom flask (25 mL) was added a solution of pyridine (0.8 mL, 10.0 mmol, 4.0 eq.) and pivaloyl chloride **2** (0.8 mL, 6.3 mmol, 2.5 eq.) in 2.5 mL of dry DCM at room temperature. 2.5 mL of dry DCM were

additionally used to purge the flask. The reaction was stirred at room temperature overnight. Formation of both monoester and diester was monitored via GCMS. As the conversion to the diester did not proceed quickly, the reaction mixture was heated to reflux in argon atmosphere on the following day. Since refluxing of the reaction mixture for 6 h did not boost the conversion, more pivaloyl chloride (0.3 mL, 2.5 mmol, 1.0 eq) was added and stirring was continued at room temperature overnight. Finally, after overall 6 days a white precipitate had formed and GCMS showed full conversion. The reaction mixture was poured into water. After phase separation the aqueous phase was extracted twice with DCM. The combined organic layers were washed with sat. NaHCO₃ solution before being dried over Na₂CO₃, filtered and dried in vacuum giving 0.989 g (103%) of a white solid. The raw product was recrystallized from EtOH and washed with PE yielding 485.7 mg (51%) of **HBDP** as white fluffy solid.

¹H-NMR (200 MHz, CDCl₃, FID LUM013/30): δ = 7.28 – 7.25 (m, 6H, Ar-H), 7.22 – 7.18 (m, 4H, Ar-H), 6.02 (s, 2H, -O-CH-) 1.09 (s, 18H, -C(CH₃)₃) ppm.

¹³C-NMR (50 MHz, CDCl₃, FID LUM013/33): δ = 176.9 (s, -O-C=O-), 136.8 (s, Ar-C¹), 128.4 (d, Ar-C), 128.2 (d, Ar-C), 127.6 (d, Ar-C), 76.6 (d, -O-CH-), 38.9 (s, -C(CH₃)₃), 27.1 (q, -C(CH₃)₃) ppm.

HRMS (ESI): [M + Na]⁺ m/z calcd. for C₂₄H₃₀O₄Na⁺ 405.2036; found 405.2036.

T_m = 157-160 °C

2.2.3 Reactivity testing of target compounds via ¹H-NMR-experiments

Formulations of target compounds and reactants in benzene-d₆ solution were prepared in GCMS vials, degassed with argon and then irradiated for 10 min using either an Ivoclar Vivadent irradiation apparatus with program P2 (Ivocerin®) or a Lumen Dynamics OmniCure® S2000 UV-curing system at an intensity of 1 W cm⁻² (320-500 nm, benzophenone). Samples were then transferred into an NMR-tube and ¹H-NMR was measured using a Bruker Avance DRX-400 spectrometer (400 MHz).

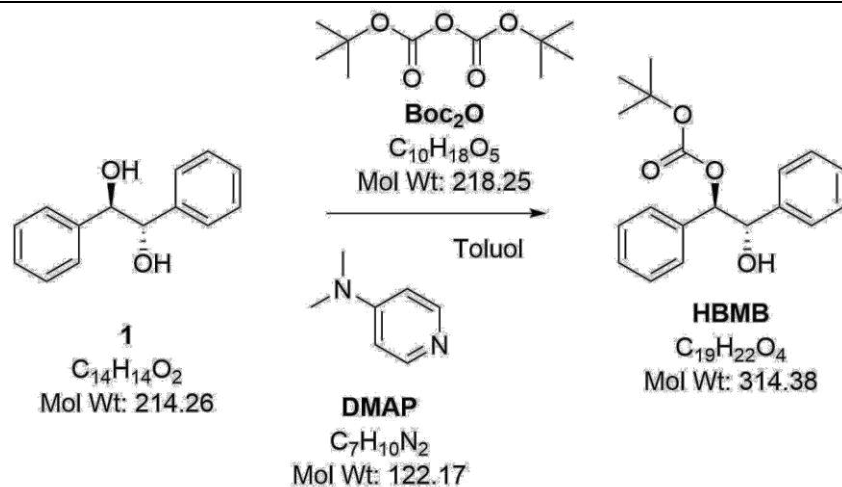
2.2.4 ¹H-NMR-experiments of symmetric test molecules HBDB and HBDP

Test formulations either consisted of symmetric test molecules (30 mM), monomer (120 mM) and Ivocerin® (1 mM) or symmetric test molecules (12.5 mM) and benzophenone (12.5 mM) in benzene-d₆. Thiols were used at a concentration of 120 mM. Experiments were conducted as described in section 2.2.3.

2.3 Molecular design and synthesis – asymmetric approach

2.3.1 Synthesis of *meso*-O-mono-Boc-hydrobenzoin, HBMB

HBMB was synthesised following a procedure from Basel and Hassner.^[66]



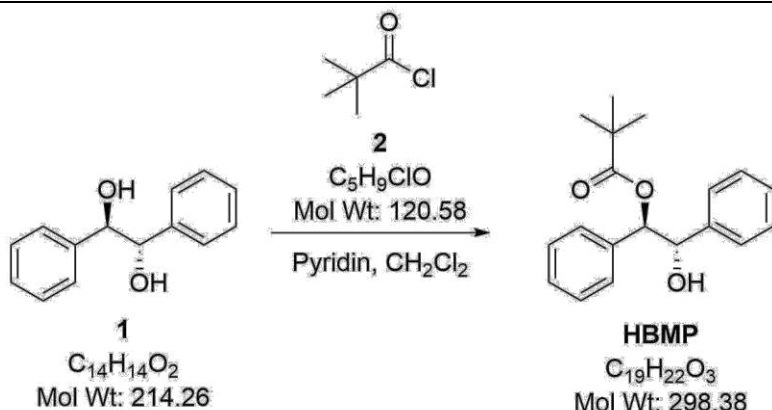
In a flat bottom flask *meso*-hydrobenzoin **1** (321 mg, 1.5 mmol, 1.0 eq), Boc₂O (330 mg, 1.5 mmol, 1.01 eq) and DMAP (25 mg, 0.2 mmol, 0.13 eq) were dissolved in 20 mL of dry toluene and stirred at room temperature. After 2 h TLC (PE/EE) indicated full consumption of starting material. The reaction mixture was diluted with CHCl₃ (25 mL) and then washed with 5% aqueous HCl (20 mL) before it was dried over Na₂SO₄, filtered and the solvent was evaporated *in vacuo* yielding 554 mg (118%) of a white solid. Crude NMR revealed that the solid consisted of starting material **1** (16%), desired product **HBMB** (66%) and difunctionalized product **HBDB** (16%, 1:4:1). Separation was performed by column chromatography (42 g silica, PE/EE = 15 %, liquid application in DCM) yielding 262 mg (56%) of **HBMB** as white solid.

¹H-NMR (200 MHz, CDCl₃, FID LUM019/30): δ = 7.36–7.31 (m, 10H, Ar-H), 5.72 (d, J = 5.8 Hz, 1H, BOC-O-C-H), 5.06 (d, J = 5.8 Hz, 1H, HO-C-H), 2.23 (s, 1H, -OH) 1.39 (s, 9H, -C(CH₃)₃) ppm.

NMR-Reference: **1f**^[142]

T_m = 127-129 °C

2.3.2 Synthesis of meso-hydrobenzoin monopivalinate, HBMP



To a stirred solution of **1** (536 mg, 2.5 mmol, 1.0 eq) in 19 mL of dry DCM in a round bottom flask (25 mL) was added pyridine (0.8 mL, 10.0 mmol, 4.0 eq) and pivaloyl chloride **2** (0.6 mL, 5.0 mmol, 2.0 eq) at room temperature. Reaction control was performed by GCMS (1.5 h, 3 h, 5 h, 7 h, 24 h). Formation of both mono- and diester was confirmed after 24 h. The reaction mixture was poured into 5% HCl (10 mL). After phase separation the aqueous phase was extracted twice with DCM (2x 15 mL). The combined organic layers were washed with sat. $NaHCO_3$ solution (15 mL) before it was dried over Na_2CO_3 , filtered and dried in vacuum giving 791 mg (106%) of a white solid. The raw product was purified by column chromatography (42 g silica, PE/EE = 5-10%, solid application, 3 g silica) yielding 456 mg (61%) of **HBMP** as white solid.

R_f : 0.56 (15% EE), 0.22 (5% EE), UV-Signal is rather weak, use Cerium Ammonium Molybdate (CAM)-Stain

1H -NMR (400 MHz, $CDCl_3$, FID LUM035/2): δ = 7.37–7.27 (m, 10H, Ar-H), 5.87 (d, J = 6.8 Hz, 1H, CO-O-C-H), 4.93 (d, J = 6.8 Hz, 1H, HO-C-H), 2.17 (s, 1H, -OH) 1.07 (s, 9H, -C(CH₃)₃) ppm.

^{13}C -NMR (100 MHz, $CDCl_3$, FID LUM035/3): δ = 177.2 (s, -O-C=O-), 139.9 (s, Ar-C¹), 137.4 (s, Ar-C¹), 128.5 (d, Ar-C), 128.2 (d, Ar-C), 128.2 (d, Ar-C), 127.5 (d, Ar-C), 127.3 (d, Ar-C), 78.6 (d, -O-CH-), 77.0 (d, -O-CH-), 38.8 (s, -C(CH₃)₃), 27.6 (q, -C(CH₃)₃) ppm.

HRMS (ESI): $[M + Na]^+$ m/z calcd. for $C_{19}H_{22}O_3Na^+$ 321.1461; found 321.1424.

T_m = 112-114 °C

2.3.3 ¹H-NMR test-experiments of asymmetric test molecule HBMB

Test formulations either consisted of **HBMB** (30 mM), monomer (120 mM) and Ivocerin® (1 mM) or **HBMB** (12.5 mM) and hydrogen abstractors (12.5 mM) in benzene-d₆. Experiments were performed as described in section 2.2.3.

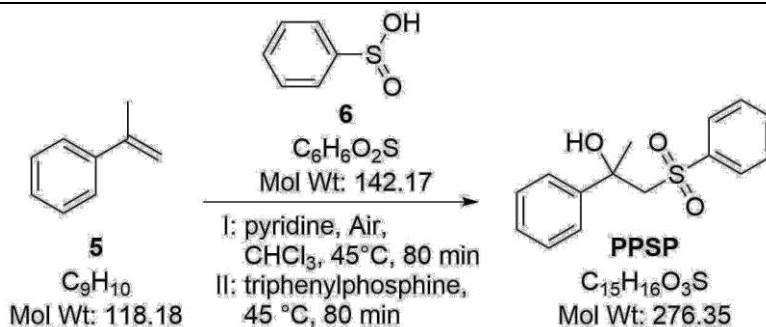
2.3.4 ¹H-NMR-experiments of *meso*-hydrobenzoin monopivalinate HBMP

Test formulations consisted of **HBMP** (12.5 mM) and hydrogen abstractors (12.5 mM) in benzene-d₆. Experiments were conducted as described in section 2.2.3.

2.4 EWG-conjugation Approach

2.4.1 Synthesis of 2-Phenyl-1-(phenylsulfonyl)propan-2-ol, PPSP

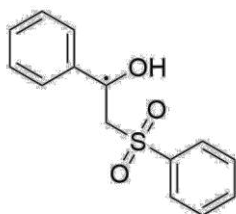
Compound **PPSP** was synthesized according to Lu *et al.*^[73]



Benzensulfinic acid was derived by neutralization of an almost saturated aqueous solution of the Na salt of benzenesulfinic acid with 6N HCl (pH = 1), filtration of the white precipitate and drying in a vacuum desiccator over $CaCl_2$.

To an oven-dried Schlenk tube equipped with a stir bar was added chloroform (30 mL) and it was heated to an oil bath temperature of 45 °C, before benzene sulfinic acid **6** (995 mg, 7.0 mmol, 2.0 eq) was added. A balloon filled with dry air was attached to the Schlenk tube through the side arm. Then, $CHCl_3$ (40.0 mL) was added, before pyridine (0.25 mL, 3.2 mmol, 0.9 eq) and α -methylstyrene **5** (0.45 mL, 3.5 mmol, 1.0 eq) were sequentially injected into the reaction tube. The reaction mixture was allowed to stir at 45 °C (oil bath temperature) for approx. 3.5 h, then the oil bath temperature was risen to 50 °C and it was stirred overnight. GCMS confirmed that almost no conversion of α -methylstyrene took place. Therefore, the reaction mixture was heated for

another night. A decrease of α -methylstyrene and an increase of a peak with a mass signal of 261.11 m/z was monitored by GCMS. This mass signal was assigned to demethylated product.



Chemical Formula: $C_{14}H_{13}O_3S^+$

Exact Mass: 261.06

Finally, after a reaction time of 2 days triphenyl phosphine (918 mg, 3.5 mmol, 1.0 eq) was added and it was stirred for 75 min. Subsequently the reaction mixture was dried *in vacuo* (raw yield: 2.880 g). The raw product was dissolved again and evaporated onto silica (5 g). Purification was performed on a silica gel column with gradient elution using petrol ether and ethyl acetate (2-5%) giving 606 mg (63%) of **PPSP** as white solid.

R_f: 0.35 (PE/EE=20%)

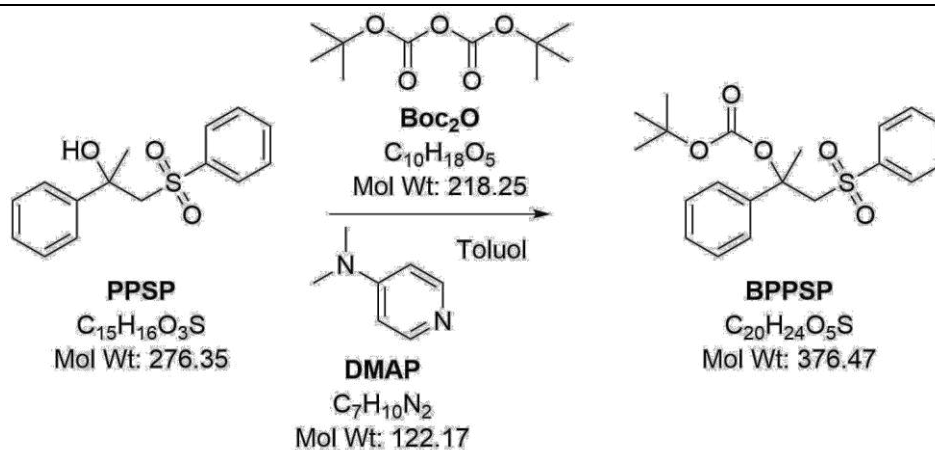
$^1\text{H-NMR}$ (200 MHz, CDCl_3 , FID LUM040/4): δ = 7.62–7.16 (m, 10H, Ar-H), 4.62 (s, 1H, O-H), 3.74 (d, J = 7.8 Hz, 1H, C-HH), 3.62 (d, J = 7.8 Hz, 1H, C-HH), 1.71 (s, 3H, CH₃) ppm.

NMR-Reference: 3aa^[73]

T_m = 107-109 °C

2.4.2 Synthesis of O-Boc-2-Phenyl-1-(phenylsulfonyl)propan-2-ol, BPPSP

Compound **BPPSP** was synthesised according to an adopted protocol from Basel and Hassner.^[66]



In a round bottom flask sulfone **PPSP** (276 mg, 1.0 mmol, 1.0 eq), **Boc₂O** (273 mg, 1.25 mmol, 1.25 eq) and **DMAP** (12 mg, 0.1 mmol, 0.1 eq) were dissolved and stirred in 10 mL of dry toluene at room temperature overnight until full conversion of starting material was confirmed by GCMS and TLC (silica, PE/EE = 20%). The reaction mixture was diluted with CHCl₃ (60 mL) and then washed with 5% aqueous HCl (40 mL) before it was dried over Na₂SO₄, filtered and the solvent was evaporated *in vacuo*. Following this procedure, 365 mg (97%) of **BPPSP** as off-white solid could be obtained.

R_f: 0.54 (PE/EE=20%)

¹H-NMR (400 MHz, CDCl₃, FID LUM041/1): δ = 7.82-7.79 (m, 2H, Ar-H), 7.61-7.56 (m, 1H, Ar-H), 7.49-7.45 (m, 2H, Ar-H), 7.30-7.21 (m, 5H, Ar-H), 4.19 (d, 1H, -CHH-), 3.86 (d, 1H, -CHH-), 2.11 (s, 3H, -CH₃), 1.38 (s, 9H, -C(CH₃)₃) ppm.

¹³C-NMR (50 MHz, CDCl₃, FID LUM016/23): δ = 151.2 (s, -O-C=O-O-), 142.9 (s, Ar-C-C), 141.0 (s, Ar-C-S), 133.5 (d, Ar-C), 129.1 (d, Ar-C), 128.7 (d, Ar-C), 128.1 (d, Ar-C), 128.0 (d, Ar-C), 124.3 (d, Ar-C), 82.5 (s, -C(CH₃)₃), 81.0 (s, -O-C-CH₃), 64.0 (t, -CH₂-), 27.8 (q, -C(CH₃)₃), 26.6 (q, -CH₃) ppm.

HRMS (ESI): [M + Na]⁺ m/z calcd. for C₂₀H₂₄O₅SNa⁺ 399.1237; found 399.1237.

T_m = 134-135 °C (decomposition)

2.4.3 ¹H-NMR-test-experiments of BPPSP

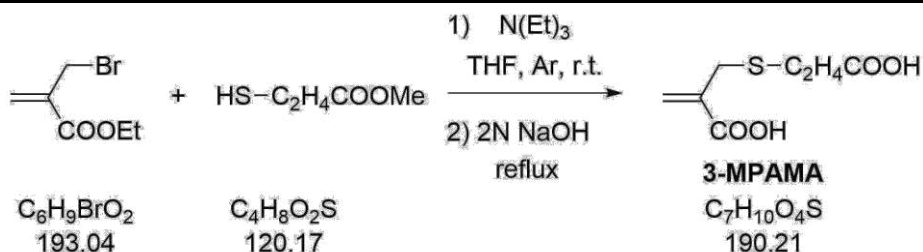
Test formulations either consisted of **BPPSP** (30 mM), monomer (120 mM) and Ivocerin® (1 mM) or **BPPSP** (12.5 mM) and hydrogen abstractors (12.5 mM) in benzene-d₆. Experiments were conducted as described in section 2.2.3.

3. WATER-SOLUBLE AFCT REAGENTS FOR CLEAVAGE OF DISULFIDE NETWORKS

3.3 Preliminary reactivity testing

Ethyl 2-((n-dodecylthio)methyl)acrylate **ADTE**^[88] (0.17 M), 2,2'-dihydroxyethyl disulfide (0.17 M) and Darocur 1173 (3 mol%) were dissolved in acetone-d₆ (1.2 mL). Half of the formulation was transferred to a brown NMR tube, whereas the rest of the solution was irradiated in an UV-oven (Intelli-Ray 600) for 5 min at 50% power. The samples were then analyzed by ¹H-NMR using a Bruker Avance DRX-400 spectrometer (400 MHz).

3.4 Synthesis of water-soluble AFCT reagent [(2-carboxyethyl)thiomethyl]acrylic acid, 3-MPAMA



In a three neck flask (250 mL), methyl 3-mercaptopropanoate (4.45 g, 37.0 mmol, 1.0 eq) and triethylamine (5.24 g, 51.8 mmol, 1.4 eq) were dissolved in degassed dry THF (90 mL). Ethyl 2-(bromomethyl)acrylate (6.95 g, 36.0 mmol, 1.0 eq) was added dropwise to the stirred reaction mixture in argon atmosphere. During the addition of the acrylate instantaneously a fine white precipitation formed. TLC (and GCMS) after 30 min confirmed full conversion (PE:EE = 12:1). 2 N aqueous NaOH (100 mL) were added to the reaction mixture and it was refluxed for 2.25 h. TLC (EE + 2 drops of AcOH) showed full conversion, but a slight spot above the product spot was present (both UV and I₂). The pH of the reaction mixture was adjusted to 1 using 6 N HCl and it was then extracted with EE (4x). The combined organic layers were washed with brine, dried with Na₂SO₄, filtered and dried in vacuum giving 6.92 g (quant.) of an off-white solid. The raw product

(6.73 g) was recrystallized from water giving 5.03 g (74%) of a white solid. However, a marginal impurity remained after recrystallization.

$^1\text{H-NMR}$ (400 MHz, $(\text{CD}_3)_2\text{CO}$, FID LUM008/50): δ = 10.67 (bs, 2H, $-\text{COOH}$), 6.18 (d, J = 1.56 Hz, 1H, H-C=C), 5.79 – 5.78 (m, 1H, H-C=C), 3.43 (m, 2H, $=\text{C-CH}_2\text{-S-}$), 2.74 – 2.70 (m, 2H, $-\text{S-CH}_2\text{-CH}_2\text{-}$), 2.63 – 2.59 (m, 2H, $-\text{S-CH}_2\text{-CH}_2\text{-}$) ppm.

$^{13}\text{C-NMR}$ (100 MHz, $(\text{CD}_3)_2\text{CO}$, FID LUM008/53): δ = 173.3 (s, $-\text{COOH}$), 167.5 (s, $-\text{COOH}$), 138.6 (s, $=\text{C-COOH}$), 126.1 (t, $\text{H}_2\text{C=C}$), 34.8 (t, $-\text{CH}_2\text{-S-}$), 32.9 (t, $-\text{S-CH}_2\text{-CH}_2\text{-}$), 26.9 (t, $-\text{S-CH}_2\text{-CH}_2\text{-}$) ppm.

NMR-Reference: $3^{[143]}$

T_m = 146-150 °C

3.5 Reactivity testing of water-soluble AFCT reagent 3-MPAMA

3-MPAMA (125 mM), 2,2'-dihydroxyethyl disulfide (125 mM) and Darocur 1173 (5 mol%) were dissolved in acetone- d_6 (1.0 mL). For the aqueous formulation, **3-MPAMA** (125 mM), 2,2'-dihydroxyethyl disulfide (125 mM) and LiTPO (5 mol%) was suspended in D_2O (1.0 mL) before 40% NaOD in D_2O (12.8 mg) was added. Half of each formulation was transferred to a brown NMR tube, whereas the rest was irradiated in an UV-oven (Intelli-Ray 600) for 5 min at 50% power. To the aqueous formulation more LiTPO (1.8 mg) was added and it was irradiated again for 5 min at 90% power. The samples were analyzed by $^1\text{H-NMR}$ using a Bruker Avance DRX-400 spectrometer (400 MHz).

4. A MODULAR APPROACH TO SENSITIZED TWO-PHOTON PATTERNING OF PHOTODEGRADABLE HYDROGELS

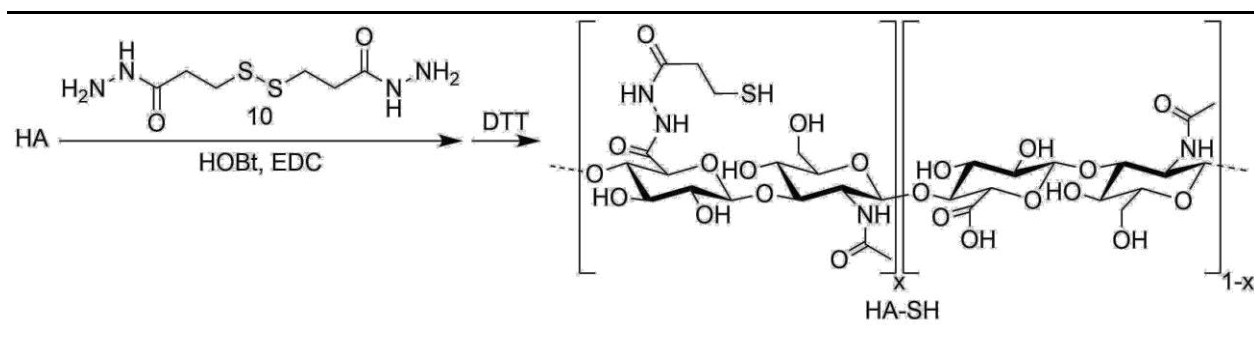
4.2 Design and synthesis of the photocleavable hydrogel platform

4.2.1 Synthesis

Thiol-modified hyaluronic acid (HA-SH) was synthesized following a previously described procedure.^[109] The photocleavable linker **PEG-(oNB-A)₂** was synthesized according to a modified protocol.^[98] The water soluble two-photon dye P2CK was synthesized as described previously.^[49b]

4.2.1.1 Synthesis of thiol-modified hyaluronic acid, HA-SH

The synthesis of HA-SH was conducted by Dr. Liyang Shi at Uppsala University.^[116]

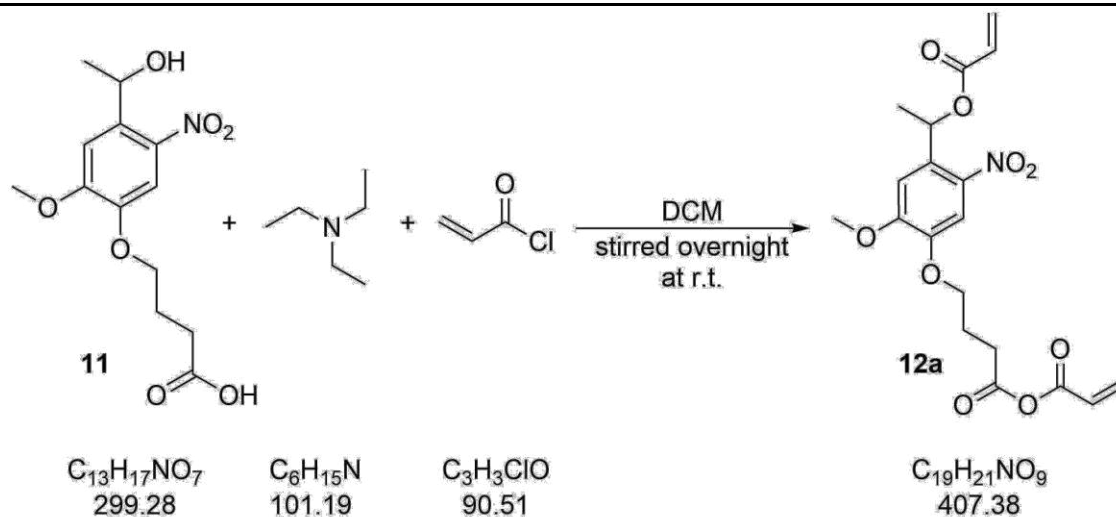


Hyaluronic acid (200 mg, M_w 150 kDa, Lifecore Biomedical, HA) was dissolved in deionized water at a concentration of 8 mg mL^{-1} . Dihydrazide linker **10** was added to the HA solution at a reagent to HA disaccharide molar ratio of 0.3:1. *N*-hydroxybenzotriazole (HOBt) was separately dissolved in a 1:1 (v/v) mixture of acetonitrile-water at a concentration of 0.2 M and added to the solution of HA at a molar ratio of HOBt to HA disaccharide of 1:1. The pH of the resultant solution was adjusted to 4.7 after which the coupling reaction was initiated by addition of 1-ethyl-3-(3-dimethylaminopropyl) carbodiimide (EDC, 0.5 molar equivalents per HA disaccharide units) to the reaction mixture. The mixture was stirred overnight and then basified to pH 8.5 using 1 M NaOH. *DL*-Dithiothreitol (DTT) was added to the solution in a 5-fold molar excess relative to the estimated amount of disulfide linkages in the HA derivative to ensure the cleavage of disulfide bonds by the reagent. The mixture was stirred overnight. Thereafter the solution was transferred to a dialysis tube (M_w cutoff = 3500 Da) and dialyzed against dilute HCl (pH 3.5) containing 0.1 M NaCl, followed by two dialysis steps against dilute HCl (pH 3.5). After lyophilization of the dialyzed solution thiol-modified HA (181 mg, 80% yield) was obtained as a white solid. HA-SH was estimated to have ~50% of its repetition units functionalized with thiol groups using $^1\text{H-NMR}$ analysis (D_2O) by comparing the integrals of the $-\text{CH}_2\text{CH}_2\text{SH}$ side chain methylene peaks at 2.58 and 2.73 ppm with the *N*-acetyl moiety of HA at 1.97 ppm (Figure 28).

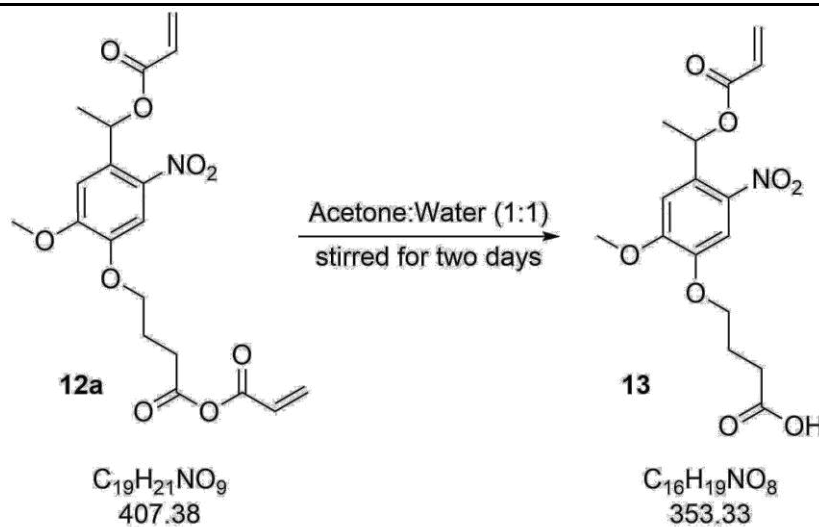
4.2.1.2 Synthesis of 3,3'-Dithiobis(propionic hydrazide), 10

3,3'-Dithiobis(propionic hydrazide) **10** was synthesized as previously described.^[109]

4.2.1.3 Synthesis of 4-(4-(1-(acryloyloxy)ethyl)-2-methoxy-5-nitrophenoxy)butanoic acid, 13



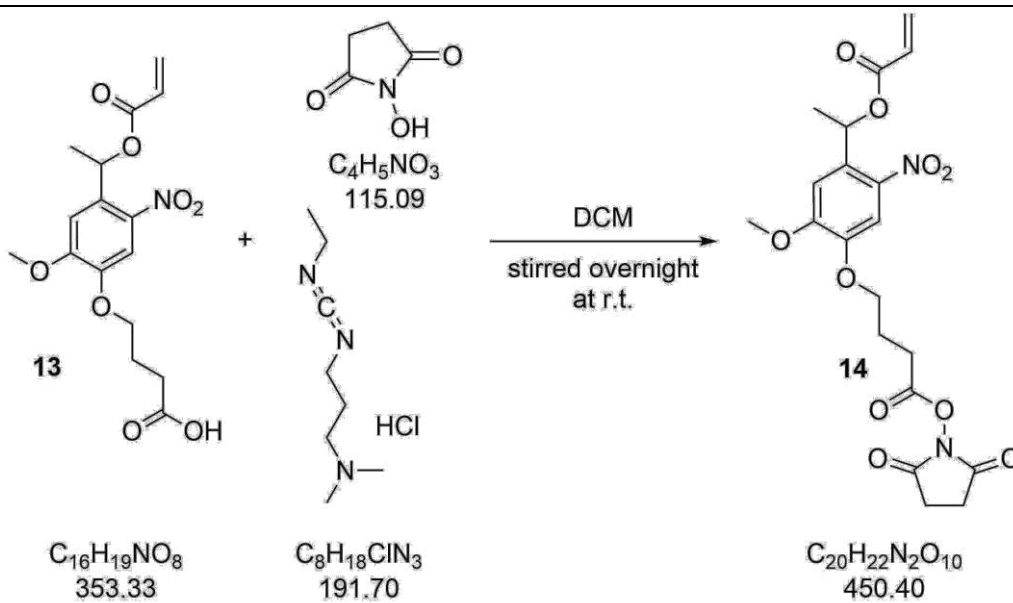
4-(4-(1-Hydroxyethyl)-2-methoxy-5-nitrophenoxy)butanoic acid **11** (488 mg, 1.63 mmol, 1 eq, CAS: 175281-76-2) and anhydrous DCM (3 mL) were added to a 25 mL round-bottom flask. Triethylamine (661 mg, 6.53 mmol, 4.0 eq) was added to the round-bottom flask under an argon atmosphere. To the ice cooled solution of starting materials a solution of acryloyl chloride (470 μ L, 5.77 mmol, 3.5 eq) in anhydrous dichloromethane (DCM, 1 mL) was added drop-wise and the combined mixture was stirred overnight. On the next day the reaction had turned yellow/brown containing white triethylamine•HCl crystals. The reaction mixture was filtered and the organic phase was washed with sodium bicarbonate, 0.1 M aqueous HCl, and concentrated brine. After washing, the solvent was removed by rotary evaporation giving the mixed anhydride **12a**.



An acetone-water mixture (50 mL, 1:1 v/v) was added to the residue **12a** and the resulting mixture was stirred overnight. The next day, acetone was removed by rotary evaporation and the remaining water layer was washed four times with DCM. The organic phase was thereafter washed with 0.1 M HCL and brine. DCM was finally evaporated and the product was dried under vacuum overnight, yielding 75% of product **13** (430 mg, 1.22 mmol) as a waxy solid.

$^1\text{H-NMR}$ (400 MHz, CD_3Cl , δ): 7.59 (s, 1H, aromatic-H), 7.00 (s, 1H, aromatic-H), 6.54 (q, $J = 6.4$ Hz, 1H, -CH(CH₃)O-), 6.44 (dd, $J_{\text{vic}} = 17.3$ Hz, $J_{\text{gem}} = 1.3$ Hz, 1H, -CH=C $\underline{\text{H}}\text{H}$), 6.17 (dd, $J_{\text{vic}} = 17.3$, 10.4 Hz, 1H, -C $\underline{\text{H}}\text{=CHH}$), 5.87 (dd, $J_{\text{vic}} = 10.4$ Hz, $J_{\text{gem}} = 1.3$ Hz, 1H, -CH=C $\underline{\text{H}}\text{H}$), 4.12 (t, $J = 6.1$ Hz, 2H, 4-CH₂ of butanoate), 3.92 (s, 3H, CH₃O-), 2.61 (t, $J = 7.1$ Hz, 2H, 2-CH₂ of butanoate), 2.19 (quint, $J = 6.6$ Hz, 2H, 3-CH₂ of butanoate), 1.66 (d, $J = 6.4$ Hz, 3H, -CH(CH₃)O-).

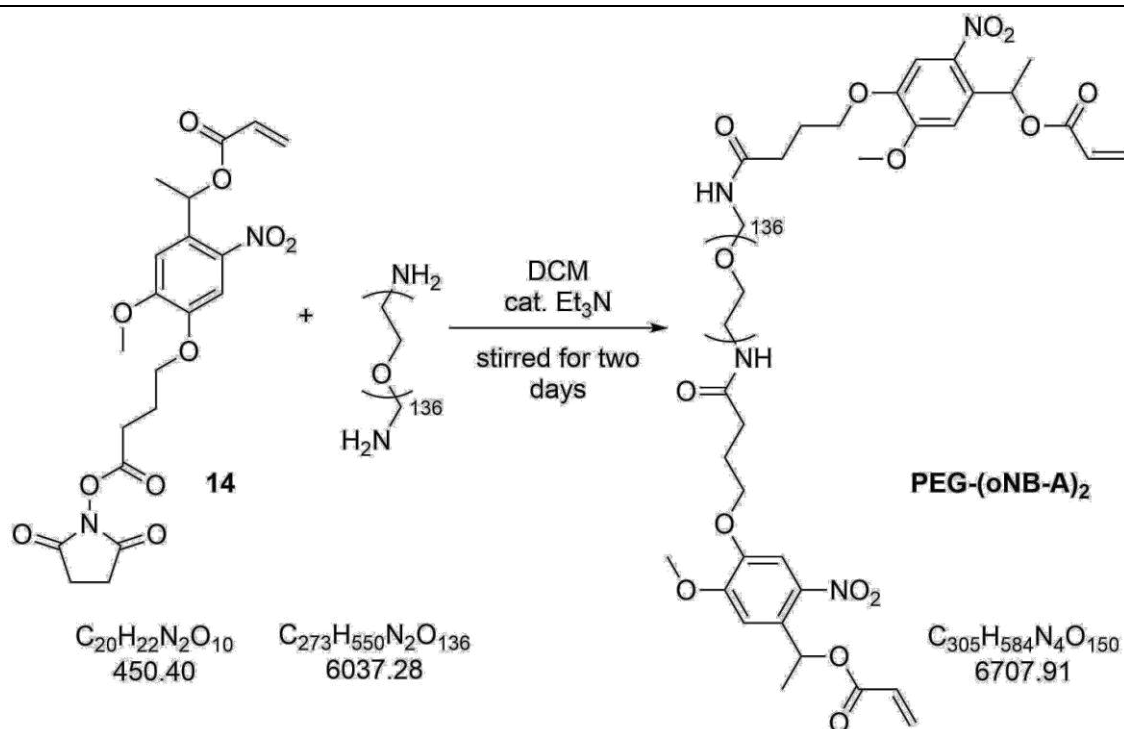
4.2.1.4 Synthesis of 4-(4-(1-(acryloyloxy)ethyl)-2-methoxy-5-nitrophenoxy)butanoic acid *N*-hydroxysuccinimide ester, **14**



4-(4-(1-(Acryloyloxy)ethyl)-2-methoxy-5-nitrophenoxy)butanoic acid **13** (79.6 mg, 0.225 mmol, 1.0 eq), *N*-hydroxysuccinimide (29.4 mg, 0.27 mmol, 1.2 eq) and 1-(3-dimethylaminopropyl)-3-ethylcarbodiimide hydrochloride (EDCI, 43.4 mg, 0.28 mmol, 1.2 eq) were added to a 25 mL round bottom flask and it was purged with argon. Anhydrous DCM (4 mL) was then added and the reaction mixture was stirred overnight at room temperature. It was then washed three times with concentrated brine and dried with magnesium sulfate. The solvent was evaporated and the obtained residue was dried under vacuum overnight, yielding 68% of product **14** (69 mg, 0.153 mmol) as highly viscous liquid.

$^1\text{H-NMR}$ (400 MHz, CD_3Cl , δ): 7.60 (s, 1H, aromatic-H), 7.01 (s, 1H, aromatic-H), 6.54 (q, $J = 6.2$ Hz, 1H, $-\text{CH}(\text{CH}_3)\text{O}-$), 6.43 (dd, $J_{\text{vic}} = 17.3$ Hz, $J_{\text{gem}} = 1.3$ Hz, 1H, $-\text{CH}=\text{CHH}$), 6.17 (dd, $J_{\text{vic}} = 17.3, 10.5$ Hz, 1H, $-\text{CH}=\text{CHH}$), 5.87 (dd, $J_{\text{vic}} = 10.5$ Hz, $J_{\text{gem}} = 1.3$ Hz, 1H, $-\text{CH}=\text{CHH}$), 4.16 (t, $J = 6.0$ Hz, 2H, 4- CH_2 of butanoate), 3.93 (s, 3H, $\text{CH}_3\text{O}-$), 2.90-2.82 (m, 6H, NHS and 2- CH_2 of butanoate), 2.28 (quint, $J = 6.7$ Hz, 2H, 3- CH_2 of butanoate), 1.66 (d, $J = 6.4$ Hz, 3H, $-\text{CH}(\text{CH}_3)\text{O}-$).

4.2.1.5 Coupling of 4-(4-(1-(acryloyloxy)ethyl)-2-methoxy-5-nitrophenoxy)butanoic acid *N*-hydroxysuccinimide to PEG diamine, PEG-(*o*NB-A)₂



4-(4-(1-(Acryloyloxy)ethyl)-2-methoxy-5-nitrophenoxy)butanoic acid *N*-hydroxysuccinimide ester **14** (117 mg, 0.26 mmol, 2.6 eq) and PEG diamine (600 mg, 0.10 mmol, $M_n \sim 6,000$ Da, 1 eq, ABCR GmbH) were added to a 50 mL round bottom flask. The flask was purged with argon and 13 mL of anhydrous DCM was added to the flask. Triethylamine (2 μL , 0.02 mmol, 2 mol%) was added to the reaction mixture and it was stirred overnight. After 24 h it was precipitated in cold diethyl ether. The precipitate was centrifuged (1400 rcf, 4 $^\circ\text{C}$, 20 min), washed again and then dried in vacuum finally yielding 93% (624 mg, 0.93 mmol) of **PEG-(*o*NB-A)₂** as a white powder.

$^1\text{H-NMR}$ (400 MHz, CD_3Cl , δ): 7.58 (s, 2H, aromatic-H), 7.00 (s, 2H, aromatic-H), 6.52 (q, $J = 6.4$ Hz, 2H, $-\text{CH}(\text{CH}_3)\text{O}-$), 6.42 (dd, $J_{\text{vic}} = 17.3$ Hz, $J_{\text{gem}} = 1.2$ Hz, 2H, $-\text{CH}=\text{CHH}$), 6.25 (bs, 2H, NH), 6.16 (dd, $J_{\text{vic}} = 17.3, 10.5$ Hz, 2H, $-\text{CH}=\text{CHH}$), 5.86 (dd, $J_{\text{vic}} = 10.5$ Hz, $J_{\text{gem}} = 1.2$ Hz, 2H, $-\text{CH}=\text{CHH}$), 4.10 (t, $J = 6.2$ Hz, 4H, 4- CH_2 of butanamide), 3.93 (s, 6H, $\text{CH}_3\text{O}-$), 3.82-3.44 (m,

~616H, PEG diamine), 2.40 (t, $J = 7.3$ Hz, 4H, 2-CH₂ of butanamide), 2.19 (quint, $J = 6.6$ Hz, 4H, 3-CH₂ of butanamide), 1.65 (d, $J = 6.4$ Hz, 6H, -CH(CH₃)O-).

4.2.2 Gel formation of PEG-HA-SH hydrogel via Michael thiol-ene reaction

HA-SH was dissolved in Dulbecco's modified Eagle's medium (DMEM) or endothelial cell growth medium (EGM-2, Lonza) and neutralized with aqueous NaOH (0.1 M) to form an 18 mg mL⁻¹ solution. **PEG-(oNB-A)₂** was dissolved in PBS giving a solution of 150 mg mL⁻¹. The solutions were combined with 1:1 stoichiometry of functional groups at 6.7 wt% total macromer concentration and used immediately. Hydrogels based on HA-SH with different DS were prepared analog but resulting in a different total macromer concentration (HA-SH DS = 40%: 5.5 wt%).

4.2.3 Gel formation of 4armPEG-SH hydrogel via Michael thiol-ene reaction

A photodegradable hydrogel based on **PEG-(oNB-A)₂** and thiol-terminated four-armed poly(ethylene glycol) (4armPEG-SH) was fabricated as previously reported by Tibbitt *et al.*^[52] 4armPEG-SH ($M_w \sim 5,000$ kDa, Sigma-Aldrich) and **PEG-(oNB-A)₂** were separately dissolved in deionized water to form 20 wt% stock solutions. The solutions were combined with 1:1 stoichiometry of functional groups at 12.5 wt% total macromer concentration. In a typical example, 7.8 μ L of 4armPEG-SH solution, 20.9 μ L of **PEG-(oNB-A)₂** solution and 10.3 μ L of PBS were combined. To accelerated hydrogel formation, 1 μ L of NaOH (0.1 mM) was added and the hydrogel precursor solution was immediately used.

4.2.4 Photo-rheology measurement of photodegradable hydrogels

The time required for network formation was estimated by measuring the shear storage modulus G' using a MCR-302 WESP rheometer with a P-PTD 200/GL peltier glass plate and a PP25 measuring system (Anton-Paar). Hydrogel samples were prepared as described in the above sections. For control experiments involving P2CK the linker **PEG-(oNB-A)₂** was dissolved in an adequate amount of P2CK solution (1.0 mM) and PBS so that the resulting hydrogel formulation contained 0.1 mM P2CK. Immediately after mixing of the components 55 μ L of the solution were placed at the center of the glass plate. The measurements were conducted at 20 °C using a plate-plate measuring system ($\varnothing = 25$ mm, gap size = 50 μ m). The formulations were sheered with a strain of 1% and a frequency of 1 Hz. Gelation was assumed to be complete when G' reached a plateau. Photo-degradation of hydrogel samples was induced by UV-irradiation projected *via* a waveguide (35 min, 320–500 nm, ~ 20 mW cm⁻² at the measuring platform) from the underside of the glass plate using an OmniCure® S2000 Spot UV Light Curing System (Excelitas Technologies).^[144]

4.3 Sensitized two-photon micropatterning of photocleavable hydrogels

4.3.1 Preparation of P2CK solutions

Solutions of P2CK at concentrations ranging from 1.00 to 0.01 mM were freshly prepared before each experiment by dilution of a stock solution in PBS (10 mM) with either adequate cell culture medium or PBS.

4.3.2 Two-photon micropatterning of channels in photocleavable hydrogels

Aliquots (40 μ l) of the mixed PEG-HA-SH hydrogel precursor solutions were drop casted onto methacrylized (see Materials, Methods and Instrumentation) glass-bottom μ -dishes (35 mm, Ibidi GmbH, Germany) and allowed to gel at room temperature for 90 min in accordance to the gelation duration observed by rheological measurements. The solidified hydrogel droplets were immersed in either DMEM or solutions of P2CK and swollen for \sim 5 h at room temperature before one half of each sample was cut away using a scalpel to generate a sharp edge. Aliquots (27 μ l) of the mixed 4armPEG-SH hydrogel precursor solutions were formed in cylindrical silicon molds ($d = 6$ mm, $h = 0.7$ mm) between glass-bottom μ -dishes and hydrophobized cover glass. After 40 min the molds were carefully removed and the 4armPEG-SH hydrogels were swollen in PBS overnight before they were treated with P2CK as described above.

Microfabrication was performed by means of two-photon degradation. Details of the experimental setup have been reported previously.^[112] Briefly, the setup is based on a femtosecond laser (MaiTai DeepSee, Spectra Physics) operating at 800 nm, with a pulse length of 70 fs after the objective (C-Achroplan 32x/0.85 W, ZEISS). Parallel channels with rectangular cross sections ($l = 300$ μ m, $A = 20$ μ m x 50 μ m) were fabricated starting from the edge into the bulk of the hydrogel at a height of \sim 60 μ m (\sim 200 μ m in case of 4armPEG-SH hydrogels) above the glass plate with varied mean laser power per channel (10–100 mW, 10 mW steps) and a constant scanning speed of 200 mm/s (hatch distance: 0.1 μ m, z-layer distance: 0.5 μ m). The samples were washed with PBS twice and then soaked in a solution of FITC–dextran (1 mg mL⁻¹, $M_w \sim$ 2,000 kDa, TdB Consultancy AB, Sweden) in PBS at room temperature overnight. Channels were visualized by laser scanning microscopy (LSM 700, ZEISS).

4.4 Micro-mechanical analysis of micropatterned regions by AFM

Atomic force microscopy (AFM) indentation testing of two-photon micropatterned cuboids in PEG-HA-SH hydrogel

A droplet (10 μ L) of PEG-HA-SH hydrogel was prepared in a cylindrical mold ($d = 6$ mm, $h = 0.2$ mm) on methacrylized glass bottom μ -dishes. To ensure a smooth surface no lid was used

for molding. After 90 min the mold was removed and the hydrogel sample was swollen in PBS for 2.5 h. Cuboids ($A = 100 \times 100 \mu\text{m}^2$) with an approximate depth of 100–150 μm were two-photon micropatterned from the upper surface into the hydrogel starting above the surface. The mean laser power was varied per cuboid (10–100 mW, 10 mW steps) and a constant scanning speed of 200 mm/s (hatch distance: 0.1 μm , z-layer distance: 0.5 μm) was used. Subsequently, PBS was exchanged for a 0.1 mM solution of P2CK in PBS and the sample was maintained at room temperature for 1 h. Again, cuboids were micropatterned into the hydrogel at the same parameters as before. Thereafter, the hydrogel was swollen in PBS overnight. A NanoWizard® ULTRA SpeedA AFM system (JPK Instruments AG, Germany) equipped with an inverted optical microscope (Axio Observer.D1, ZEISS) was used for AFM experiments. The micromechanical assessment was performed via AFM cantilever-based microindentation experiments using a silicon nitride rectangular cantilever (0.0196 N m^{-1} measured spring constant; MSNL, Bruker) equipped with a colloidal probe of 4.75 μm in radius. The thermal noise method^[145] was used to calibrate the cantilever spring constant. The deflection sensitivity was obtained by performing 16 force measurements on the glass surface next to the sample.^[113] After calibration, the cantilever was fabricated with the colloidal probe^[146] and its diameter was measured as previously described.^[113] In total, 50-60 force curves were recorded at 1 nN maximum load and 2 $\mu\text{m s}^{-1}$ of z-displacement speed per irradiated section. The Oliver-Pharr method was used to analyze the force curves and estimate the indentation modulus, as previously described, in a custom MATLAB script (v R2015b, MathWorks, USA).^[113] For the analysis, the Poisson's ratio of the hydrogel was taken as 0.5. The relative height measurement results are presented as mean \pm standard deviation. The indentation modulus results are presented as mean \pm standard error of the mean.

4.5 Biocompatibility & Cell Culture Application

4.5.1 Cell culture and encapsulation spheroids

hTERT immortalized human adipose-derived mesenchymal stem cell line ASC/TERT1 (Evercyte GmbH, Austria) was retrovirally transfected with green fluorescent protein (GFP) to obtain stably transfected green labeled cells following a previously established protocol.^[114] ASC/TERT1 were cultured in EGM-2 media supplemented with 10% fetal bovine serum (Lonza). MG-63 cells (Sigma-Aldrich) were cultured in DMEM supplemented with 10% fetal bovine serum and 1% penicillin/streptomycin (Lonza).

Cells were maintained in an incubator (5% CO_2 , 37 °C) and the medium was exchanged every second day. Cell spheroids were formed in 2% agarose molds (MicroTissues® 3D Petri Dish®,

Sigma-Aldrich) according to the manufacturer's instructions. In order to generate spheroids with a diameter of 200 μm 81,000 cells were seeded per micromold corresponding to 1000 cells per spheroid. Cells were incubated for 24 to 48 h. For ASC/TERT1 encapsulation 0.90 mM tetrapeptide Arg-Gly-Asp-Cys (RGDC, Bachem AG, Switzerland) was added to the PEG-(oNB-A)₂ stock solution and reacted for 10 min. Spheroids of two molds were combined and collected before they were resuspended in 100 μl of premixed PEG-HA-SH hydrogel precursor solution (ASC/TERT1: with RGDC (0.29 mM); MG-63s: HA-SH with DS = 40%) by cautious pipetting ($\sim 5\times$). Aliquots of the suspension (30 μl) were drop casted onto methacrylized glass bottom μ -dishes. After short reaction time (~ 10 min) the samples were maintained in the incubator for 90 min to allow hydrogel formation to complete before cell culture media was added (2.5 mL).

4.5.2 Evaluation of P2CK cytocompatibility

The cytocompatibility of two-photon sensitizer P2CK was evaluated using PrestoBlue® cell viability reagent (Thermo Fisher Scientific). Two 96-well plates were seeded with 5,000 cells per well and maintained in the incubator overnight to allow cells to attach. Next day, cells were incubated with 100 μL of different dilutions of P2CK (1.00, 0.50, 0.10, 0.05 and 0.01 mM) for 3 h and 24 h respectively. Both plates contained wells with non-treated cells as control samples. After the respective incubation period, the cell culture medium was exchanged twice to remove residues of P2CK and cell viability was evaluated. Resazurin-based reagent PrestoBlue® was diluted 1:10 with medium and 100 μL were applied per well and incubated for 60 min. Because of the reducing environment of viable cells, this reagent is transformed and turns red, becoming highly fluorescent. The fluorescence was measured with a plate reader (Synergy BioTek, excitation 560 nm, emission 590 nm). After correction for background fluorescence, the signals of the cells exposed to different concentrations of P2CK were compared to each other and to the controls (non-stimulated cells) by one-way ANOVA and Dunnett's multiple comparisons test. The metabolic activity of the 3 h control was assumed to be 100%. Statistical data evaluation was performed using the software package GraphPad Prism 5 (GraphPad Software, USA) and Excel 2016 (MS Office, Microsoft).

4.5.3 Two-photon micropatterning, cell viability and spreading

PEG-HA-SH hydrogel with encapsulated spheroids was soaked in a solution of P2CK (0.1 mM in adequate medium) for 5.5 h (MG-63s: 1 h). Thereafter, channels were eroded with varying laser intensities around spheroids in a star-shaped manner into the bulk hydrogel at constant writing speed of 200 mm s^{-1} (hatch distance: 0.1 μm , z-layer distance: 0.5 μm). The laser power was increased clockwise (30–100 mW, 10 mW steps). All other parameters were kept identical as

described above. The samples were washed with medium twice and then incubated (5% CO₂, 37 °C) in cell culture medium overnight. LIVE/DEAD viability assay (Life Technology) was used to monitor MG-63 viability and spreading. Samples were stained for 20 min at 37 °C with a solution of calcein AM (0.2 μM) and propidium iodide (0.6 μM, PI) in PBS and thereafter imaged by the use of LSM. For better evaluation of ASC/TERT1 viability additional PI staining was applied on day 7 and 14.

4.6 Mechanistic considerations

For absorption and emission measurements solutions of oNB **11** (190 μM) and P2CK (11 μM) in PBS were prepared. Rheological experiments were conducted as described in section 4.2.4. Alternatively, an OmniCure® LX400 LED UV Spot Curing System with a 460 nm LED head (Excelitas Technologies) was used for irradiation with a specific power of ~17 mW cm⁻² at the measuring platform. PEG-HA-SH hydrogel formulations were prepared containing 0.1 mM P2CK.

5. SIMPLIFYING THE SYSTEM – TWO-PHOTON CLEAVAGE OF DISULFIDE BONDS

5.2 Two-photon degradation of 4arm-PEG5k-SH hydrogel in presence of two-photon sensitizers

The disulfide-crosslinked 4arm-PEG5k-SH hydrogel was prepared from thiol-terminated four-armed polyethylene glycol with a molecular weight of 5 kDa (4armPEG5k-SH) according to literature.^[25d]

In a typical experiment, 4armPEG5k-SH (24.13 mg) was dissolved in deionized water (188.2 μL). Subsequently, 21.7 μL of a 10 mM NaI solution in deionized water and 7.2 μL of 30% hydrogen peroxide were added. The final PEG concentration was 10 wt%. After vortexing aliquots of the hydrogel precursor solution (27 μL) were placed in two molds on three methacrylated ibidi dishes each and a cover glass was placed atop. Gelling occurred almost too quickly and the solution was hardly pipettable in the end. Nevertheless, the samples were pressed into the molds and fused together. After one hour, the mold was removed and the samples were swollen in deionized water at room temperature for an hour. Then the water was exchanged and the samples were maintained in the fridge for one to two days.

Thereafter, the hydrogel samples were swollen in solutions of either P2CK (0.1 mM) or DAS (1 mM) in PBS for more than 90 min and then cut using a scalpel. Microchannels (300 μm x 20 μm x 50 μm) were structured (10-100 mW, 200 mm s^{-1} , 0.1 μm hatch, 0.5 μm dz) either at 800 nm (pure gel or P2CK) or 720 nm (DAS) using the setup described in section 4.3.3. Visualization was performed by light microscopy and LSM (Zeiss, LSM 700) after swelling in FITC2000 (2000 kDa, 1 mg/mL) overnight.

5.3 One-photon irradiation of 4armPEG5k-SH hydrogel in presence of P2CK

A 10% 4arm-PEG5k-SH hydrogel was prepared as described above and swollen in 0.5 mM P2CK solution at room temperature overnight and irradiated for 15 min (5 cm distance, 6 mW cm^{-2}) in presence of 0.5 mM P2CK using an OmniCure® LX400 LED UV Spot Curing System with a 460 nm LED head (Excelitas Technologies).

5.4 Two-photon microchannel fabrication in organogels

Organogels were prepared by the following procedure. 4armPEG5k-SH (11.0 mg) was dissolved in MeCN (85.8 μL), which took long (45 min). 9.9 μL of a 10 mM NaI solution in deionized water was added. Thereafter, 30% hydrogen peroxide (3.3 μL) was added and the solution was vortexed. After vortexing the hydrogel precursor solution (27 μL) were placed in 3 silicon molds on three methacrylated ibidi μ -dishes and a cover glass was placed atop. The samples were allowed to gel for 90 min and then submersed in 2-Propanol overnight. This was necessary, as MeCN would have affected the ibidi μ -dishes. Large silicon molds (1 cm^2) were stuck to high

precision glass slides (ibidi) using silicon dentist glue. The hydrogels were transferred to these reservoirs and submersed in MeCN for 1 h, causing swelling. Thereafter, organogels submersed in MeCN solutions of either M2CMK or R8 in MeCN (both 0.5 mM) for at least 3 h and then cut with a scalpel. Microchannels were fabricated at 800 nm using laser powers from 10-100 mW at a scanning speed of 200 mm s⁻¹ (0.1 μm hatch, 0.5 μm dz). Additionally, also a sample swollen in only MeCN was tested. The samples were analyzed by light microscopy.

5.5 Two-photon induced cleavage of a disulfide-based hyaluron network

HA-SH 8% (25.9 mg) was dissolved in DMEM (807.4 μL) and neutralized with 1M NaOH (30 μL). The pink solution was drop-casted onto methacrylate-functionalized ibidi μ-dishes. To induce network formation, a droplet of 3% hydrogen peroxide (10 μL) was pipetted onto the HA-SH drop and it was maintained at room temperature for 30 min. Solid gel formation was verified by tilting. The hydrogel was then cut and swollen for 45 min in a 0.1 mM solution of P2CK. Microchannels (300 μm x 20 μm x 20 μm) were produced and analyzed as described in section 5.2.

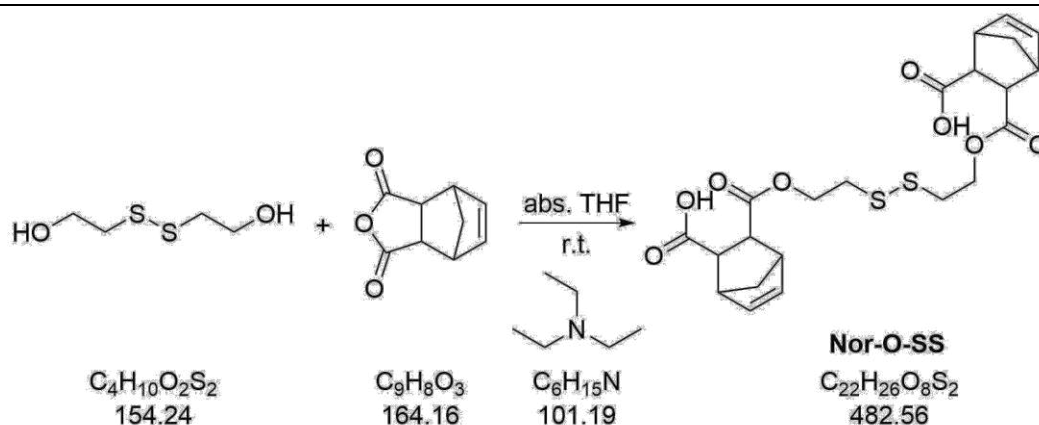
6. INTRODUCING DISULFIDE LINKAGES BY THE USE OF LIGHT

6.2 Development of disulfide-based crosslinkers

6.2.1 A Nor-SS-Nor crosslinker from cheap starting materials

6.2.1.1 Synthesis of 3,3'-(((disulfanediybis(ethane-2,1-diyl))bis(oxy))bis(carbonyl))-bis(bicyclo[2.2.1]hept-5-ene-2-carboxylic acid), Nor-O-SS

The synthesis of **Nor-O-SS** was conducted according to a modified procedure.^[147]



2-Hydroxyethyl disulfide (573 mg, 3.7 mmol, 1 eq) was dissolved in dry THF (5 mL) in Ar atmosphere. A solution of carbic anhydride (1220 mg, 7.4 mmol, 2 eq) in dry THF (15 mL) was added to the stirred solution. Thereafter, trimethylamine (1.55 mL, 11.1 mmol, 3 eq) was added slowly and the reaction was stirred at room temperature overnight. After 14 h ¹H-NMR showed 80% consumption of starting materials. Hence, the reaction mixture was refluxed for 3 h to increase the conversion. Then the reaction mixture was dried in vacuum before it was dissolved in sat. aq. NaHCO₃ solution (50 mL) to give a “clear” solution. The product was precipitated using conc. HCl giving a sticky white solid. Ethyl acetate (100 mL) was added to dissolve the product. After phase separation the aqueous layer was extracted with more ethyl acetate (3x 50 mL) and the combined organic layers were washed with brine, dried over Na₂SO₄ and the solvent was removed in vacuum yielding a whitish oil (1.907 g, 106%). The raw product contained traces of solvent and both starting materials. Hence, the raw product was purified by column chromatography (110 g silica) using PE:EE (1% glacial acetic acid) = 20%-55% as eluent. After drying in high vacuum while heating to 50 °C a colourless liquid was received still containing starting material due to the decomposition of **Nor-O-SS** (1.678 g, 94%).

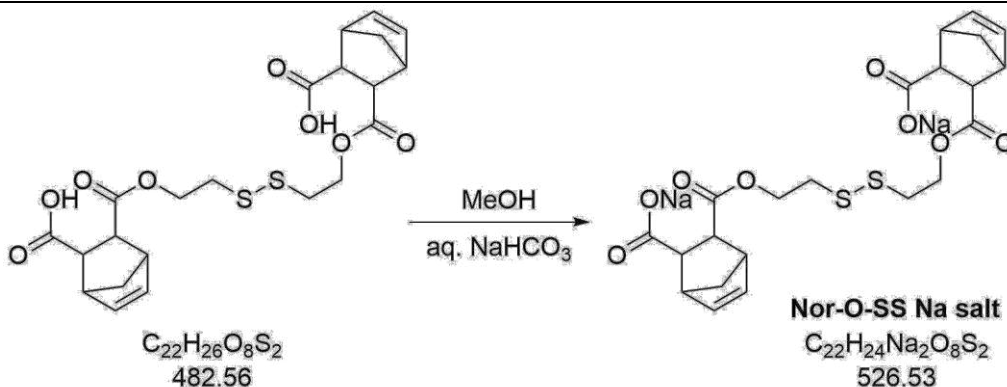
A further attempt of purification included dissolution of the product in diethyl ether (10 mL) and addition of light petrol (80 mL) to precipitate the product as white sticky solid. After centrifugation at 5000 rpm (6 °C, 20 min), the supernatant was decanted off and the white precipitate was dissolved in DCM and transferred to a round bottom flask. After drying in vacuum 1.274 g (71%) of a viscous white liquid were received, still containing carbic anhydride and 2-hydroxyethyl disulfide.

¹H-NMR (400 MHz, DMSO-d₆, FID LUM071/10): δ = 11.94 (s, 2H, -COOH), 6.19-6.17 (dd, J = 3.0 Hz, 2.9 Hz, 2H, CH=CH), 6.07-6.05 (dd, J = 3.0 Hz, 2.9 Hz, 2H, CH=CH), 4.21-4.06 (m, 4H, CH₂-CH₂S), 3.32-3.23 (m, 4H, aliphatic), 3.05-3.02 (m, 4H, aliphatic), 2.91-2.88 (m, 4H, S-CH₂), 1.36-1.26 (m, 4H, CH-CH₂-CH) ppm.

¹³C-NMR (100 MHz, DMSO-d₆, FID LUM071/11): δ = 173.1 (s, COOH), 171.9 (s, COOCH₂), 135.2 (d, CH=CH), 134.3 (d, CH=CH), 61.5 (t, COOCH₂), 48.0 (t, CH-CH₂-CH), 47.9 (d, CHCOOCH₂), 47.1 (d, CHCOOH), 46.0 (d, CHCH-ester), 45.5 (d, CHCH-acid), 36.3 (t, S-CH₂) ppm.

HRMS (ESI): [M + H]⁺ m/z calcd. for C₂₂H₂₇O₈S₂⁺ 483.1142; found 481.1145.

6.2.1.2 Synthesis of sodium 3,3'-(((disulfanediy)bis(ethane-2,1-diyl))bis(oxy))-bis(carbonyl))bis(bicyclo[2.2.1]hept-5-ene-2-carboxylate), Nor-O-SS Na salt

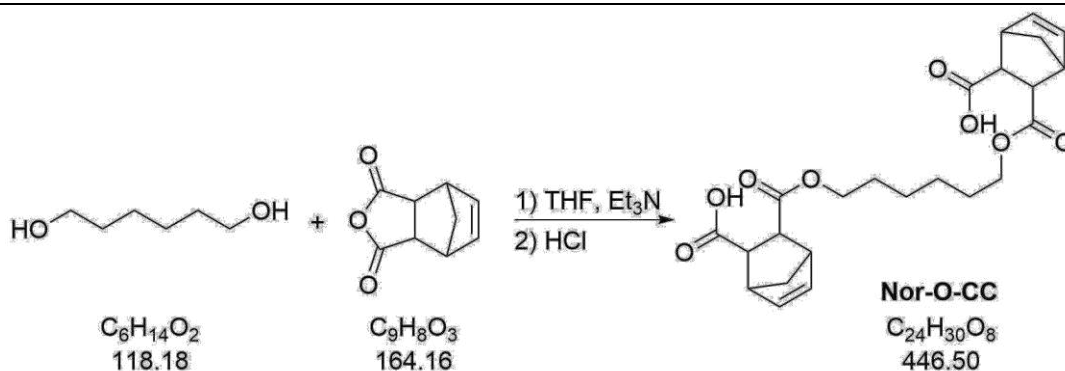


Nor-O-SS (117 mg, 0.24 mmol, 1 eq) was dissolved in dry MeOH (1 mL) and added dropwise to a stirred aqueous solution of NaHCO₃ (0.1 M, 4.86 mL, 0.49 mmol, 2 eq). Formation of gas and a solid film which rapidly dissolved again was observed. After complete addition, MeOH (1 mL) was used to transfer remaining **Nor-O-SS** to the aqueous solution. The solution was stirred for 15 min and then dried in high vacuum yielding a transparent glass with crystalline sites (127 mg, quant.). The product still contained decomposition products.

$^1\text{H-NMR}$ (400 MHz, D_2O , FID LUM075/1): δ = 6.31-6.29 (dd, J = 2.9 Hz, 2.7 Hz, 2H, $\text{CH}=\text{CH}$), 6.20-6.18 (dd, J = 2.9 Hz, 2.7 Hz, 2H, $\text{CH}=\text{CH}$), 4.41-4.35 (m, 2H, O-CHH-CH_2), 4.25-4.19 (m, 2H, O-CHH-CH_2), 3.36-3.25 (m, 4H, aliphatic), 3.11 (m, 4H, aliphatic), 3.05-2.98 (m, 4H, S-CH_2), 1.43-1.36 (m, 4H, $\text{CH-CH}_2\text{-CH}$) ppm.

6.2.1.3 Synthesis of 2,2'-(1,6-hexanediyl)bicyclo[2.2.1]hept-5-ene-2,3-dicarboxylic acid ester, Nor-O-CC

The synthesis of bicyclo[2.2.1]hept-5-ene-2,3-dicarboxylic acid, 2,2'-(1,6-hexanediyl) ester **Nor-O-CC** was conducted according to a modified procedure.^[147]



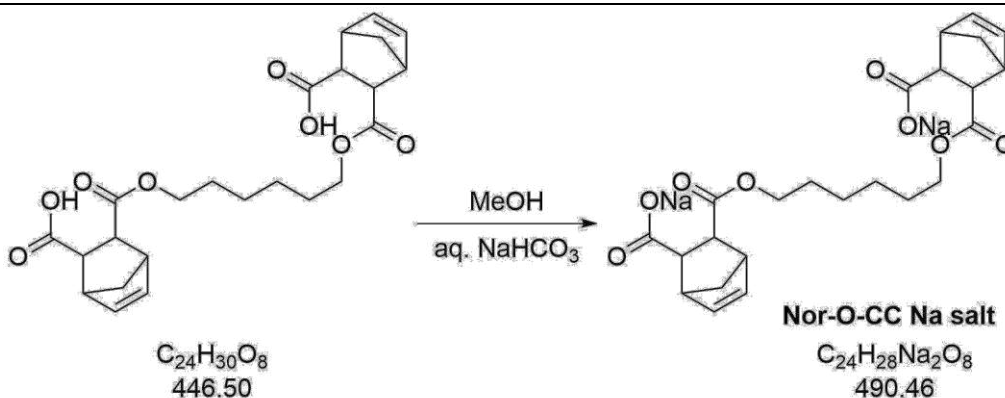
1,6-Hexanediol (1.43 g, 12 mmol, 1 eq) was dissolved in dry THF (20 mL) in Ar atmosphere. A solution of carbic anhydride (3.97 g, 24 mmol, 2 eq) in dry THF (25 mL) was added to the stirred solution. Thereafter, trimethylamine (6.25 mL, 48 mmol, 4 eq) was added slowly and the reaction was stirred at room temperature. After 14 h of stirring, $^1\text{H-NMR}$ showed 80% consumption of starting materials. Hence, the reaction mixture was refluxed for 3 h to increase the conversion. The solvent was removed in vacuum and the white residue was dissolved in sat. aq. NaHCO_3 solution (50 mL) to give a “clear” solution. The product was precipitated using conc. HCl giving a sticky white solid. The aqueous phase was extracted with diethyl ether (3 x 200 mL) and the combined organic layers were washed with brine. The organic phase was dried over Na_2SO_4 and the solvent was removed in vacuum yielding a whitish oil. The raw product was purified by column chromatography (110 g silica) using DE:EE = 50% as eluent. To remove residual monosubstituted derivative, it was recrystallized from toluene twice yielding a white solid (4.23 g, 79%).

$^1\text{H-NMR}$ (400 MHz, DMSO-d_6 , FID SIL03/12): δ = 11.89 (s, 2H, $-\text{COOH}$), 6.15-6.13 (dd, J = 2.9 Hz, 2.9 Hz, 2H, $\text{CH}=\text{CH}$), 6.10-6.06 (dd, J = 2.9 Hz, 2.9 Hz, 2H, $\text{CH}=\text{CH}$), 3.94-3.79 (m, 4H, $\text{O-CH}_2\text{-CH}_2$), 3.29-3.21 (m, 4H, aliphatic), 3.03-3.00 (m, 4H, aliphatic), 1.52-1.49 (m, 4H, aliphatic), 1.34-1.25 (m, 8H, aliphatic) ppm.

^{13}C -NMR (100 MHz, DMSO- d_6 , FID SIL03/13): δ = 173.2 (s, $\underline{\text{C}}\text{OOH}$), 172.0 (s, $\underline{\text{C}}\text{OOCH}_2$), 135.0 (d, $\underline{\text{C}}\text{H}=\underline{\text{C}}\text{H}$), 134.3 (d, $\text{C}\text{H}=\underline{\text{C}}\text{H}$), 63.5 (t, $\text{COO}\underline{\text{C}}\text{H}_2$), 47.8 (t, $\text{C}\text{H}-\underline{\text{C}}\text{H}_2-\text{C}\text{H}$), 47.3 (d, $\underline{\text{C}}\text{HCOOCH}_2$), 47.1 (d, $\underline{\text{C}}\text{HCOOH}$), 45.9 (d, $\underline{\text{C}}\text{HCH}$ -ester), 45.6 (d, $\underline{\text{C}}\text{HCH}$ -acid), 27.9 (t, aliphatic), 25.1 (t, aliphatic) ppm.

HRMS (ESI): $[\text{M} + \text{Na}]^+$ m/z calcd. for $\text{C}_{24}\text{H}_{30}\text{O}_8\text{Na}^+$ 469.1833; found 469.1844.

6.2.1.4 Synthesis of sodium 2,2'-(1,6-hexanediyl) bicyclo[2.2.1]hept-5-ene-2,3-dicarboxylic acid ester, Nor-O-CC Na salt



Nor-O-CC (4.1 g, 9.2 mmol, 1 eq) was dissolved in MeOH (20 mL) and an aqueous solution of NaHCO_3 (1 M, 18.4 mL, 18.4 mmol, 2 eq) was added dropwise to a stirred solution. Formation of gas was observed. The solution was stirred for 15 min, the solvent was evaporated and the solid residue was then dried in high vacuum for two days yielding a transparent glass (4.5 g, quant.).

^1H -NMR (400 MHz, D_2O , FID SIL03/9): δ = 6.29-6.27 (dd, J = 2.9 Hz, 2.6 Hz, 2H, $\underline{\text{C}}\text{H}=\underline{\text{C}}\text{H}$), 6.22-6.20 (dd, J = 2.9 Hz, 2.6 Hz, 2H, $\text{C}\text{H}=\underline{\text{C}}\text{H}$), 4.10-4.05 (m, 2H, $\text{O}-\underline{\text{C}}\text{H}\text{H}-\text{C}\text{H}_2$), 4.00-3.94 (m, 2H, $\text{O}-\underline{\text{C}}\text{H}\text{H}-\text{C}\text{H}_2$), 3.38-3.13 (m, 8H, aliphatic), 1.63-1.62 (m, 4H, aliphatic), 1.45-1.38 (m, 8H, aliphatic) ppm.

6.2.2 Formal translocation of the carboxylic acid

6.2.2.1 Synthesis of Nor-L-Cys Na salt

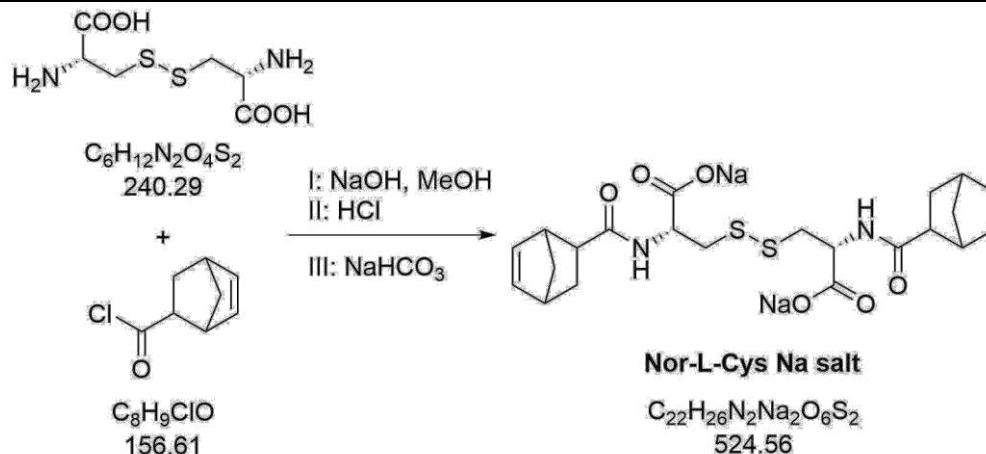
6.2.2.1.1 Synthesis of bicyclo[2.2.1]hept-5-ene-2-carbonyl chloride, NorCOCl

Variant A: Diels-Alder reaction of acryloyl chloride and cyclopentadiene to NorCOCl

The synthesis was conducted according to a modified protocol from Mukhina *et al.*^[131]

6.2.2.1.2 Synthesis of disodium *N,N'*-bis(bicyclo[2.2.1]hept-5-ene-2-ylcarbonyl)-L-cystine, Nor-L-Cys Na salt

The synthesis of **Nor-L-Cys** is roughly based on a modified protocol described previously.^[124a]



Powdered NaOH (640 mg, 16.0 mmol, 2.5 eq) was first dissolved in dry MeOH (200 mL) before L-cystine (1538 mg, 6.4 mmol, 1 eq) was added in argon atmosphere. To the cooled solution (ice bath) NorCOCl (2506 mg, 16.0 mmol, 2.5 eq) was added dropwise. After 20 h of reaction time, the solvent was removed under reduced pressure. The yellow residue was first washed with diethyl ether (3 x 100 mL) to remove NorCOMe. Subsequently, it was dissolved in deionized water (100 mL) and acidified with 1 N HCl. The aqueous phase was extracted with diethyl ether (5 x 200 mL). The combined organic layers were washed with brine, dried over sodium sulfate and the solvent was removed in vacuum yielding **Nor-L-Cys** (2338 mg, 76%).

For conversion into the Na salt, **Nor-L-Cys** (1425 mg, 3.0 mmol, 1 eq) was dissolved in MeOH (20 mL) and aqueous NaHCO₃ solution (1 M, 6.0 mL, 6.0 mmol, 2 eq) was added. The mixture was stirred for 15 min and then dried in vacuum yielding 1555 mg (quant.) of a beige powder.

Nor-L-Cys:

¹H-NMR (400 MHz, DMSO-d₆, FID SIL10/10): δ = 12.79 (bs, 2H, COOH), 8.31-7.96 (m, 2H, NH), 6.13-5.81 (m, 4H, HC=CH), 4.48-4.37 (m, 2H, CH-NH), 3.21-3.08 (m, 4H, aliphatic), 2.98-2.80 (m, 6H, aliphatic), 1.81-1.25 (m, 8H, aliphatic) ppm.

HRMS (ESI): [M + H]⁺ m/z calcd. for C₂₂H₂₉N₂O₆S₂⁺ 481.1462; found 481.1472.

Nor-L-Cys Na salt:

$^1\text{H-NMR}$ (400 MHz, D_2O , FID SIL10/5): $\delta = 6.28\text{-}5.98$ (m, 4H, $\underline{\text{H}}\text{C}=\underline{\text{C}}\text{H}$), 4.55-4.42 (m, 2H, $\underline{\text{C}}\text{H-NH}$), 3.33-3.19 (m, 4H, aliphatic), 3.09-2.95 (m, 6H, aliphatic), 2.01-1.75 (m, 2H, aliphatic), 1.60-1.24 (m, 6H, aliphatic) ppm.

6.2.3 Reactivity estimation on the molecular level by $^1\text{H-NMR}$

NMR-experiments with Nor-linkers and 2-mercaptoethanol

For reactivity testing, the Nor-linkers were reacted with 2-mercaptoethanol at a functional group ratio of 1:1 in D_2O or DMSO-d_6 by irradiation at 400-500 nm (20 mW cm^{-2}) in presence of 0.6 mM LiTPO (D_2O) or TPO-L (DMSO-d_6). Stock solutions of the respective linker (150 mM), 2-mercaptoethanol (300 mM) and photoinitiator (6 mM) in the respective deuterated solvent were prepared. In a typical experiment, to 420 μL of solvent 60 μL of each stock solution were added to give final concentrations of 15 mM linker, 30 mM 2-mercaptoethanol and 0.6 mM photoinitiator (2 mol% of ene) in a total volume of 600 μL . The samples were prepared in GC-MS vials, vortexed and then irradiated on the measuring platform of a photorheometer for various irradiation periods. The photorheometer (MCR-302 WESP, Anton-Paar) was coupled to an OmniCure®S2000 Spot UV Light Curing System (Excelitas Technologies) from the underside of the glass plate via a waveguide. The total irradiation intensity was measured through the glass bottom of a GC-MS vial at the measuring platform using an Ocean Optics USB 2000+ spectrometer. After irradiation, the sample solutions were transferred to brown NMR-tubes and measured by $^1\text{H-NMR}$ (Bruker Avance DRX-400 spectrometer). For estimation of norbornene-consumption, the integral of the norbornene protons ($\underline{\text{H}}\text{C}=\underline{\text{C}}\text{H}$, 4H at $t = 0 \text{ s}$) was monitored. In experiments conducted in D_2O , the signal of the proton at the α -carbon ($\underline{\text{C}}\text{H-NH}$, 2H) served as internal reference for calibration, whereas in DMSO-d_6 the amide-proton ($\underline{\text{N}}\text{H}$, 2H) was used.

6.2.4 Optimization strategies of the linker on the molecular level

6.2.4.2 Synthesis of modified linkers

General procedure for the preparation of (homo)cystine-based linkers

The general procedure is roughly based on a modified method described previously.^[124a]

Cys or HCys (1 eq) and finely ground NaOH (4 eq) were added to a one-neck flask and purged with Ar. Dry MeOH was added while stirring until a clear solution was obtained. Thereafter, the

stirred reaction mixture was cooled with an ice bath and freshly distilled norbornene acid chloride (2 eq) was slowly added. After 1 h the ice bath was removed and stirring was continued at room temperature until complete conversion was observed by ¹H-NMR reaction monitoring. MeOH was removed under reduced pressure. The obtained solid typically smelled heavily of NorCOOMe. The solid was washed three times with DCM, DEE or EE to remove most of NorCOOMe. The product was dissolved in deionized H₂O and 1 M HCl was added until pH 1 was obtained. The protonated product precipitated as white to yellow solid and was obtained by dissolving the precipitate with DEE or EE and extraction of the remaining aqueous phase.

The combined organic layers were washed with brine, dried with sodium sulfate and filtered before the solvent was removed under reduced pressure. The obtained solid was washed with DCM twice to remove remaining NorCOOMe and then dried in HV. For removing of remaining solvent traces the product can be carefully heated with warm air while on HV.

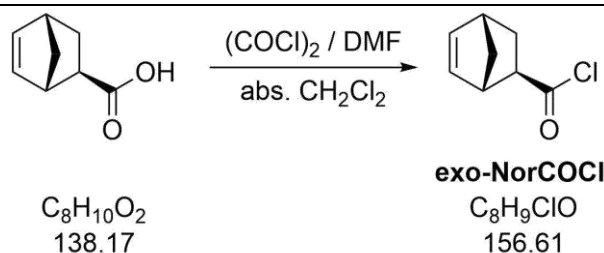
General procedure for the conversion of (homo)cystine-based linkers into the salt form

For the transformation into its water-soluble Na salt, the respective linker was dissolved in MeOH until a clear solution was obtained. A solution of NaHCO₃ in water (1 M, 2 eq.) was slowly added to the stirred linker solution causing bubble formation. After 15 min of stirring, solvents were removed under reduced pressure. The obtained solid was further dried under HV for several hours.

6.2.4.2.1 Synthesis of *exo*-Nor-L-Cys and its Na salt

6.2.4.2.1.1 Synthesis of *exo*-5-norbornenecarboxylic acid chloride, *exo*-NorCOCl

Exo-NorOCl was synthesized analog to **NorCOCl** by variant B.^[132]

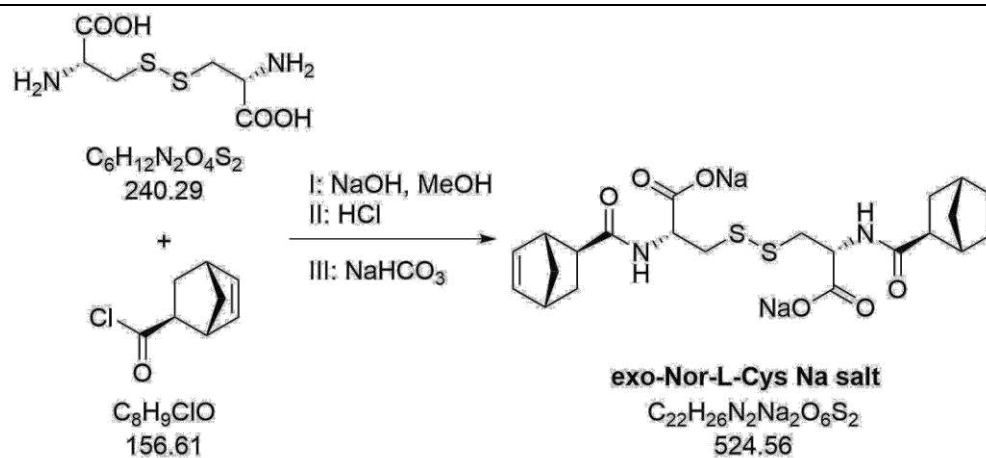


exo-NorCOOH (1.00 g, 7.2 mmol, 1 eq, CAS: 934-30-5) was reacted with oxalyl chloride (3.67 g, 29.0 mmol, 4 eq) in presence of a droplet of DMF in dry DCM (8.0 mL) in Ar atmosphere until full conversion was achieved. Remaining oxalyl chloride and DCM were removed under reduced

pressure. The obtained brown liquid was purified by distillation at 15 mbar, T = 70-75 °C). **exo-NorCOCl** was obtained as a clear translucent liquid (0.96 g, 85%).

¹H-NMR (400 MHz, CDCl₃, FID ST07/2): δ = 6.22-6.20 (m, 1H, CH=CH), 6.13-6.11 (m, 1H, CH=CH), 3.28 (m, 1H, =CH-CH-CH-COCl), 2.99 (m, 1H, =CH-CH), 2.75-2.72 (m, 1H, CH-COCl), 2.05-2.00 (m, 1H, aliphatic), 1.55-1.41 (m, 3H, aliphatic) ppm.

6.2.4.2.1.2 Synthesis of disodium *N,N'*-bis-(*exo*-bicyclo[2.2.1]hept-5-ene-2-ylcarbonyl)-L-cystine, *exo*-Nor-L-Cys Na salt



exo-Nor-L-Cys was prepared according to the general procedure from L-cystine (705 mg, 3 mmol, 1 eq), **exo-NorCOCl** (918 mg, 6 mmol, 2 eq), NaOH (465 mg, 12 mmol, 4 eq) and dry MeOH (43 mL). After 17 h of reaction time 1038 mg (72%) of crude **exo-Nor-L-Cys** were received as white to yellow powder. 227 mg (0.43 mmol) of crude **exo-Nor-L-Cys** were converted into the Na salt by dissolving in 25 mL MeOH and adding to NaHCO₃ solution (1 M, 945 μL) yielding 248 mg (quant.) of a beige powder after drying in high vacuum. The remaining **exo-Nor-L-Cys** was purified via reversed phase chromatography (Sepacore® C18 80 g) using MeOH:H₂O = 1:1 as eluent yielding a white to slightly beige powder (65% recovery).

exo-Nor-L-Cys:

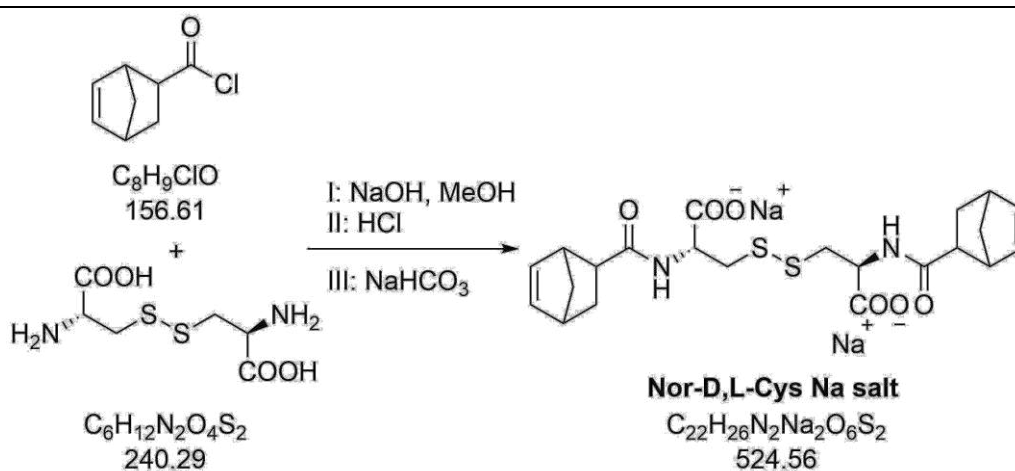
¹H-NMR (400 MHz, DMSO-d₆, FID ST08/11): δ = 12.90 (bs, 2H, COOH), 8.31-8.22 (m, 2H, NH), 6.13 (m, 4H, HC=CH), 4.56-4.44 (m, 2H, CH-NH), 3.20-3.12 (m, 2H, =CH-CH-CH-CON), 2.94-2.88 (m, 2H, =CH-CH), 2.83 (m, 4H, S-CH₂), 2.11-2.10 (m, 2H, CH-CON), 1.80-1.77 (m, 2H, aliphatic), 1.58-1.56 (m, 2H, aliphatic), 1.16-1.15 (m, 4H, aliphatic) ppm.

HRMS (ESI): [M + Na]⁺ m/z calcd. for C₂₂H₂₈N₂O₆S₂Na⁺ 503.1281; found 503.1287.

exo-Nor-L-Cys Na salt:

$^1\text{H-NMR}$ (400 MHz, D_2O , FID ST19/1): $\delta = 6.22$ (m, 4H, $\underline{\text{H}}\text{C}=\underline{\text{C}}\text{H}$), 4.57-4.50 (m, 2H, $\text{C}\underline{\text{H}}\text{-NH}$), 3.32-3.19 (m, 2H, $=\text{CH}\text{-C}\underline{\text{H}}\text{-CH}\text{-CO}$), 3.01-2.95 (m, 6H, aliphatic), 2.26 (m, 2H, aliphatic), 1.84-1.75 (m, 2H, aliphatic), 1.54-1.52 (m, 2H, aliphatic), 1.46-1.34 (m, 4H, aliphatic) ppm.

6.2.4.2.2 Synthesis of disodium *N,N'*-bis(bicyclo[2.2.1]hept-5-ene-2-ylcarbonyl)-D,L-cystine, Nor-D,L-Cys Na salt



Nor-D,L-Cys was synthesized according to the general procedure from D,L-cystine (1000 mg, 4.2 mmol, 1 eq, CAS: 923-32-0), NorCOCl (1304 mg, 8.3 mmol, 2 eq) and pulverized NaOH (666 mg, 16.6 mmol, 4 eq) in dry MeOH (52 mL). After a reaction time of 20 h, MeOH was evaporated and orange crystals were obtained. The solid was washed with DCM (3 x 20 mL) to remove unreacted NorCOOMe. Thereafter the solid was dissolved in deionized water (50 mL) and acidified using HCl (1 M) causing precipitation of a sticky orange solid. The solid was dissolved in EE and the aqueous phase was extracted with EE (4 x 50 mL). The combined organic layers were washed with brine (50 mL) and dried over Na_2SO_4 before the solvent was removed under reduced pressure. After drying in vacuum 1.093 g (55%) of **Nor-D,L-Cys** were received as a beige foam.

For conversion into the Na salt, **Nor-D,L-Cys** (240 mg, 0.50 mmol, 1 eq) was dissolved in MeOH (2 mL) and aqueous NaHCO_3 solution (1 M, 1.00 mL, 2 eq) was added. The mixture was stirred for 15 min and then dried in vacuum yielding 234 mg (89%) of a beige powder.

Nor-D,L-Cys:

$^1\text{H-NMR}$ (400 MHz, DMSO- d_6 , FID LUM92/7): δ = 12.78 (bs, 2H, COOH), 8.26-7.97 (m, 2H, NH), 6.13-5.82 (m, 4H, HC=CH), 4.48-4.39 (m, 2H, CH-NH), 3.19 (m, 2H, =CH-CH-CH-CON), 3.14-3.06 (m, 2H, =CH-CH), 2.99-2.90 (m, 2H, aliphatic), 2.84-2.81 (m, 4H, aliphatic), 2.14-1.57 (m, 3H, aliphatic), 1.33-1.22 (m, 5H, aliphatic) ppm.

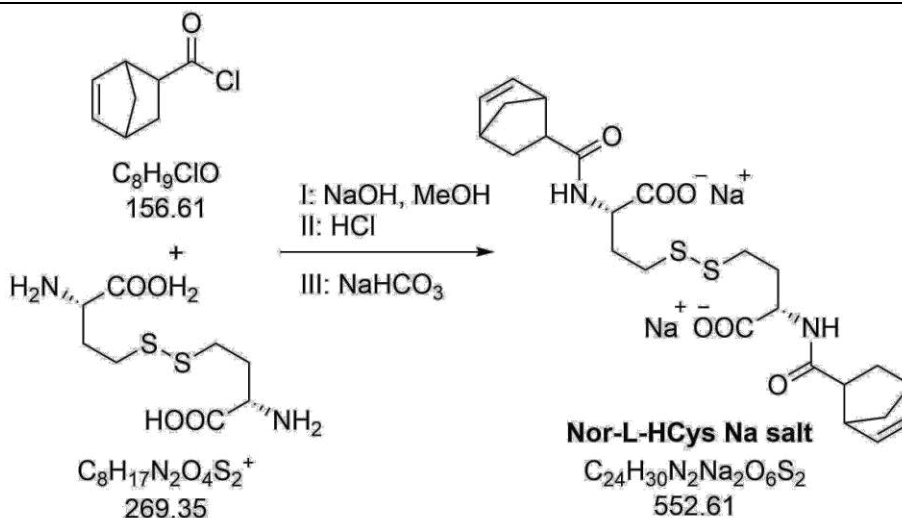
HRMS (ESI): $[M + H]^+$ m/z calcd. for $\text{C}_{22}\text{H}_{29}\text{N}_2\text{O}_6\text{S}_2^+$ 481.1462; found 481.1465.

Nor-L-Cys Na salt:

$^1\text{H-NMR}$ (400 MHz, D_2O , LUM92/10): δ = 6.27-6.00 (m, 4H, HC=CH), 4.51-4.43 (m, 2H, CH-NH), 3.30-2.95 (m, 9H, aliphatic), 2.40-1.25 (m, 9H, aliphatic) ppm.

6.2.4.2.3 Synthesis of Nor-L-HCys and Nor-D,L-HCys and the corresponding Na salts

6.2.4.2.3.1 Preparation of disodium *N,N'*-bis(bicyclo[2.2.1]hept-5-ene-2-ylcarbonyl)-L-homocysteine, Nor-L-HCys Na salt



Nor-L-HCys was prepared according to the general procedure from L-homocystine (197 mg, 0.7 mmol, 1 eq, CAS: 626-72-2), powdered NaOH (117 mg, 2.9 mmol, 4 eq) and NorCOCl (229 mg, 1.5 mmol, 2 eq) in dry MeOH (14 mL). During addition of NorCOCl a whitish turbid suspension formed. The ice bath was removed after 40 min. and the reaction mixture was stirred for 22 h at room temperature. MeOH was removed under reduced pressure. The obtained residue was dissolved in deion. H_2O (100 mL) and washed with DCM (2 x 50 mL). The aqueous layer was acidified with HCl (1 M, 7.5 mL) causing precipitation of a white solid. The aqueous phase was extracted with EE (4 x 50 mL). The organic phase was washed with brine (50 mL) and dried over

sodium sulfate. Solvents were removed in vacuum and the residue was dissolved in MeOH, filtered through a nylon syringe filter and transferred to a smaller flask. After drying in high vacuum, **Nor-L-HCys** (225 mg, 60%) was obtained as a white foam.

For conversion into the Na salt, **Nor-L-HCys** (222 mg) was dissolved in MeOH (3 mL) and aqueous NaHCO₃ solution (1 M, 873 μL, 2 eq) was added. It was stirred for 10 min before the solvents were removed in vacuum yielding a white foam (243 mg, quant.).

Nor-L-HCys:

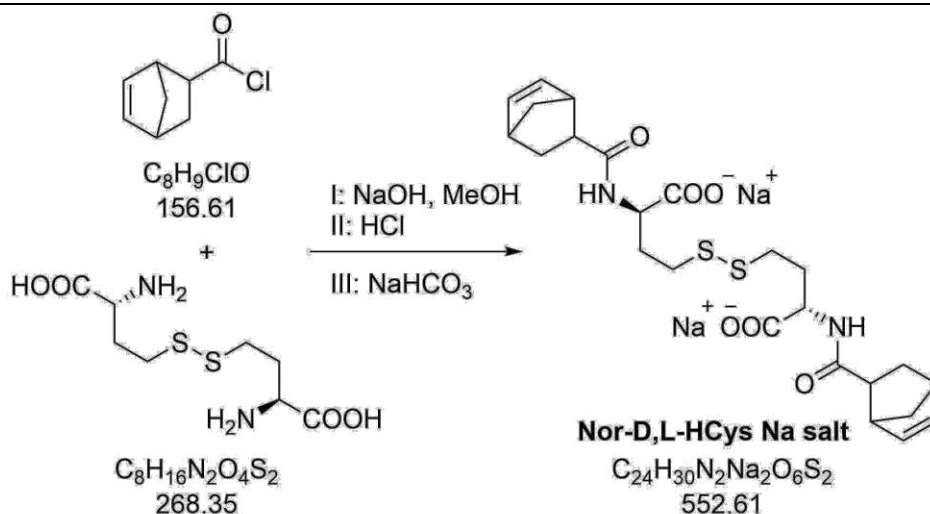
¹H-NMR (400 MHz, DMSO-d₆, FID ST05/18): δ = 12.56 (bs, 2H, COOH), 8.17-7.85 (m, 2H, NH), 6.14-5.76 (m, 4H, HC=CH), 4.29-4.23 (m, 2H, CH-NH), 3.19 (m, 2H, =CH-CH-CH-CO), 2.83-2.67 (m, 8H, aliphatic), 2.11-2.07 (m, 2H, aliphatic), 1.99-1.92 (m, 2H, aliphatic), 1.79-1.68 (m, 2H, aliphatic), 1.59-1.15 (m, 6H, aliphatic) ppm.

HRMS (ESI): [M + H]⁺ m/z calcd. for C₂₄H₃₃N₂O₆S₂⁺ 509.1775; found 509.1779.

Nor-L-HCys Na salt:

¹H-NMR (400 MHz, D₂O, FID LUM102/5): δ = 6.30-5.96 (m, 4H, HC=CH), 4.35-4.26 (m, 2H, CH-NH), 3.21 (m, 2H, =CH-CH-CH-CO), 3.08-2.94 (m, 4H, aliphatic), 2.84-2.68 (m, 4H, aliphatic), 2.29-2.15 (m, 2H, aliphatic), 2.12-1.71 (m, 4H, aliphatic), 1.55-1.23 (m, 6H, aliphatic).

6.2.4.2.3.2 Preparation of disodium *N,N'*-bis(bicyclo[2.2.1]hept-5-ene-2-ylcarbonyl)-D,L-homocystine, **Nor-D,L-HCys Na salt**



Nor-D,L-HCys was prepared according to the general procedure from D,L-homocystine (5.99 g, 22 mmol, 1 eq, CAS: 870-93-9), NaOH (3.58 g, 90 mmol, 4 eq) and NorCOCl (7.01 g, 45 mmol,

2 eq) in dry MeOH (460 mL). The reaction mixture was stirred for 17 h at room temperature. Due to the large scale synthesis, the work-up differs from the general procedure. First, MeOH was removed under reduced pressure. The obtained solid was then washed with DEE (3 x 50 mL), dissolved in H₂O and acidified with HCl (1 M) causing precipitation. The precipitate was dissolved in MeOH and filtered to remove NaCl. The aqueous phase was extracted with DEE. The organic phase was washed with brine and dried over sodium sulfate. After evaporation of solvents, the obtained white solids were united and, washed with DCM to remove remaining NorCOOMe. After drying in vacuum, 6.68 g (59%) of **Nor-D,L-HCys** were obtained as a white, highly viscous liquid. 3.00 g (5.9 mmol, 1 eq) of **Nor-D,L-HCys** were converted into the Na salt by dissolving in 400 mL MeOH at 40°C and adding to NaHCO₃ solution (1 M, 11.8 mL, 2 eq) yielding 3.27 g (quant.) of a white powder after drying in high vacuum.

Nor-D,L-HCys:

¹H-NMR (400 MHz, DMSO-d₆, FID ST14/6): δ = 12.56 (bs, 2H, COOH), 8.17-7.84 (m, 2H, NH), 6.12-5.75 (m, 4H, HC=CH), 4.23 (m, 2H, CH-NH), 3.20 (m, 2H, =CH-CH-CH-CO), 2.82-2.72 (m, 8H, aliphatic), 2.11-2.07 (m, 2H, aliphatic), 1.94-1.93 (m, 2H, aliphatic), 1.74-1.68 (m, 2H, aliphatic), 1.59-1.15 (m, 6H, aliphatic) ppm.

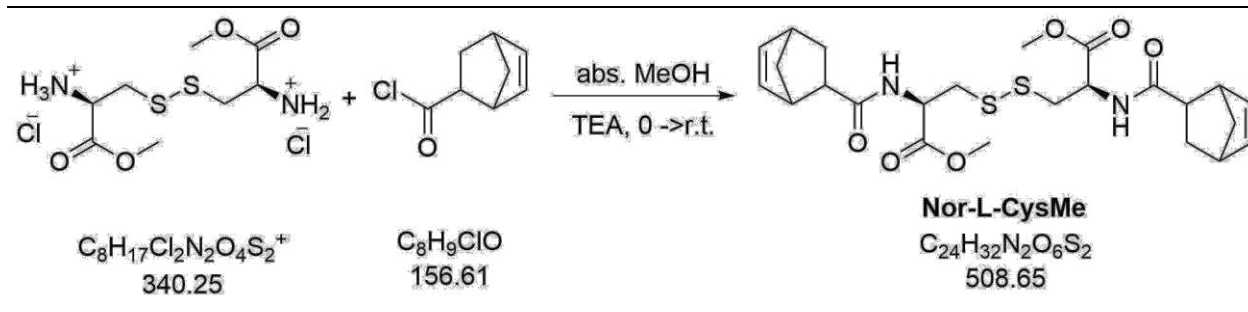
HRMS (ESI): [M + H]⁺ m/z calcd. for C₂₄H₃₃N₂O₆S₂⁺ 509.1775; found 509.1776.

Nor-D,L-HCys, Na salt:

¹H-NMR (400 MHz, D₂O, FID ST14/8): δ = 6.29-5.95 (m, 4H, HC=CH), 4.34-4.26 (m, 2H, CH-NH), 3.22 (m, 2H, =CH-CH-CH-CO), 3.08-2.96 (m, 4H, aliphatic), 2.77-2.66 (m, 4H, aliphatic), 2.25-2.15 (m, 2H, aliphatic), 2.12-1.71 (m, 4H, aliphatic), 1.58-1.21 (m, 6H, aliphatic).

6.2.4.2.4 Synthesis of disodium 1,1'-dimethyl-*N,N'*-bis(bicyclo[2.2.1]hept-5-ene-2-ylcarbonyl)-L-cystine ester, Nor-L-CysMe

The synthesis of **Nor-L-CysMe** was conducted according to a modified protocol.^[148]



L-Cystine dimethyl ester dihydrochloride (1195 mg, 3.5 mmol, 1.0 eq) and triethylamine (2.0 mL, 14.7 mmol, 4.2 eq) were suspended in dry DCM (30 mL) in a round bottom flask equipped with a septum. The mixture was cooled to 0 °C and norbornoyl chloride (1.1 mL, 7.7 mmol, 2.2 eq) was added dropwise using a syringe. After complete addition, the ice bath was removed and the reaction mixture was stirred at room temperature. The progress of the reaction was monitored by ¹H-NMR. After 5.5 h the reaction mixture was diluted with EE (100 mL) and extracted with saturated sodium bicarbonate solution (50 mL), water (50 mL) and brine (50 mL). The organic phase was dried over sodium sulfate and the solvent was removed in vacuum. The raw product (solid foam) was purified by column chromatography using PE:EE (50-60%) as eluent. Two fractions were received of which one contained both exo- and endo-norbornene based products (514 mg, 29%) and the other only the endo-norbornene product (1004 mg, 56%). The white liquids were dried at HV while being carefully heated with warm air.

endo-Nor-L-CysMe:

¹H-NMR (400 MHz, DMSO-d₆, FID LUM97/8): δ = 8.13 (t, J = 7.4 Hz, 2H, NH), 6.08 (m, 2H, HC=CH), 5.80 (m, 2H, HC=CH), 4.47 (m, 2H, CH-NH), 3.63 (m, 6H, OCH₃), 3.19 (m, 2H, =CH-CH₂-CH-CO), 3.14-3.07 (m, 2H, =CH-CH₂), 2.97-2.91 (m, 2H, aliphatic), 2.86-2.81 (m, 4H, aliphatic), 1.74-1.69 (m, 2H, aliphatic), 1.32-1.24 (m, 6H, aliphatic) ppm.

HRMS (ESI): [M + H]⁺ m/z calcd. for C₂₄H₃₃N₂O₆S₂⁺ 509.1775; found 509.1775.

6.3 Development of the Disulfide-based Hydrogel Platform

6.3.1 Extended reactivity estimation on the molecular level by $^1\text{H-NMR}$

Experiments were conducted as described in section 6.2.3. Reactivity estimation on the molecular level by $^1\text{H-NMR}$.

6.3.2 Hydrogel optimization

Photorheology

If not stated otherwise, the following parameters were used for photorheology experiments.

Light-induced hydrogel formation was investigated with selected linkers of the series by means of photorheology using a MCR-302 WESP rheometer equipped with a P-PTD 200/GL peltier glass plate, a H-PTD 200 peltier-temperature-controlled hood, and a D-CP/PP 7 measuring tool (Anton-Paar). Hydrogel samples were prepared by reacting linkers with 10 wt% of thiol-terminated eight-armed PEGs (4armPEG10k-SH, $M_w \sim 10$ kDa or 8armPEG20k-SH, $M_w \sim 20$ kDa) using LiTPO as photoinitiator. For mixing a vortex and a micro-centrifuge were used. Samples were prepared in 500 μL safe-lock tubes. The rheological analysis was performed with a plate-plate geometry (PP08 disposable, $\varnothing = 8$ mm, gap size = 0.8 mm) at 20 $^\circ\text{C}$. After mixing of the components, 45 μL of the sample solution were pipetted into the gap (1 mm) between measuring tool and glass plate utilizing capillary force, before the tool was lowered into the measuring position at a gap of 0.8 mm. The formulations were sheered with a strain of 1% and a frequency of 1 Hz. After 1 min of equilibration, photocuring of the hydrogel samples was induced by UV-irradiation projected *via* a waveguide from the underside of the glass plate using an OmniCure® LX400 LED UV Spot Curing System with a 385 nm LED head (Excelitas Technologies) with a specific power of ~ 6 mW cm^{-2} at the measuring platform.^[144] All measurements were performed at least in triplicates. The formed hydrogels disks were utilized for subsequent swelling tests in PBS.

6.3.2.1 Optimization of the photoinitiator concentration

Stock solutions of 8armPEG20k-SH, linker **Nor-D,L-HCys** (190 mM) and LiTPO (18 mM) were prepared in PBS. The stock solutions were combined to give sample solutions with final concentrations of 10 wt% 8armPEG20k-SH, 22 mM **Nor-D,L-HCys** (SH:ene = 1:1) and a variable LiTPO concentration (0.2 mM, 0.4 mM, 0.6 mM, 15 mM). For high LiTPO concentrations (15 mM), 8armPEG20k-SH was directly dissolved in the LiTPO stock solution. Aliquots of 45 μL of the sample solutions were measured on the photorheometer at the settings described in section 6.3.2.0. After 1 min of equilibration time, the prepolymer formulations were exposed to 385 nm

light ($\sim 6 \text{ mW cm}^{-2}$) for 5 min. The formulation containing 15 mM LiTPO was also polymerized with shuttered light (60 s off-time; 6 cycles of 5 s on-time and 15 s off-time, 3 min of constant irradiation).

6.3.2.2 Thermostability of disulfide-crosslinked PEG hydrogel

An aliquot (45 μL) of **8arm-D,L-HCys (1:1)** prepolymer solution (containing 0.4 mM LiTPO) was *in situ* photopolymerized at 20 °C on the photorheometer at the settings described in section 6.3.2.0, before the temperature was continuously increased up to 90°C at a heating rate of 1 °C/min. To prevent evaporation of water, the measuring system was sealed with a ring of paraffin.

6.3.2.3 Mechanostability of disulfide-crosslinked PEG hydrogel

For the amplitude sweep, after *in situ* photo-polymerization of 8arm-D,L-HCys (1:1) prepolymer solution, the amplitude of the applied strain was logarithmically increased from 0.1% to 1000% at a constant frequency of 1 Hz. For the dynamic strain amplitude cycling experiment, after *in situ* polymerization, a series of four strain cycles was applied varying strains between 350% and 1% in 60 s periods.

6.3.3 Stabilization of 8arm D,L-HCys (1:1) hydrogel

6.3.3 Swelling experiments

For swelling experiments the *in situ* polymerized hydrogel disks were carefully removed from the photorheometer measuring platform and placed in individual tared petri dishes. After initial weighing of the hydrogel disks, they were swollen in PBS ($\sim 2 \text{ mL}$). For weighing, the liquid was pipetted off, and the hydrogel disks were carefully patted dry with paper towel. Thereafter, the disks were submersed in fresh PBS again. All swelling experiments were performed in triplicates.

6.3.3.1 Stabilization by a non-cleavable background network

Several prepolymer solutions were prepared from stock solutions of 8armPEG20k-SH (11.4 wt%), **Nor-D,L-HCys** (190 mM), **Nor-O-SS** (190 mM) and LiTPO (18 mM) in PBS. Mixed linker stock solutions were prepared at a ratio of 1:3 (CC:SS) and 1:7 (CC:SS). The stock solutions were

combined to give sample solutions with final concentrations of 10 wt% 8armPEG20k-SH, 22 mM total linker (SH:ene = 1:1) and 0.4 mM LiTPO. For the preparation of **8arm-SS-CC (3:1) 15 mM** formulation, 8armPEG20k-SH was directly dissolved in the LiTPO stock solution and combined with the 1:3 (CC:SS) linker stock at a 1:1 ratio of SH:ene. The rheological experiments were conducted as described in sections 6.3.2.0 and 6.3.2.1.

6.3.3.2 Capping of free thiols by maleimide

After in situ polymerization of **8arm-D,L-HCys (1:1)** hydrogel, samples were weighted and then swollen in a solution of maleimide (4 mM) in PBS for 1 h. Thereafter, the samples were further swollen in PBS.

6.3.3.3 Consumption of free thiols by an excess of linker

Stock solutions of linker **Nor-D,L-HCys** (190 mM), LiTPO (18 mM) and RGDC (30 mM) were prepared in PBS. 8armPEG20k-SH was dissolved in PBS and combined with the stock solutions to give sample solutions with final concentrations of 10 wt% 8armPEG20k-SH, 0.4 mM LiTPO and a variable concentration of **Nor-D,L-HCys** depending on the SH:ene ratio (1:1 = 22.2 mM, 1:1.15 = 25.6 mM, 1:1.20 = 26.7 mM, 1:1.24 = 27.6 mM). Formulations containing 1 mM RGDC had SH:ene ratios of 1:1.20 (26.7 mM) and 1:1.223 (27.2 mM).

6.3.4 Stabilization of 8armPEG-based hydrogels by the use of Nor-L-HCys

Stock solutions of linker **Nor-L-HCys** (190 mM) and LiTPO (18 mM) were prepared in PBS. 8armPEG20k-SH was dissolved in PBS and combined with the stock solutions to give sample solutions with final concentrations of 10 wt% 8armPEG20k-SH, 0.4 mM LiTPO and a variable concentration of **Nor-L-HCys** depending on the SH:ene ratio (1:1 = 22.2 mM, 1:1.20 = 26.7 mM).

6.3.5 Crosslinking 4armPEG-based hydrogels

Stock solutions of linkers **Nor-L-HCys** (190 mM), **Nor-D,L-HCys** (190 mM) and LiTPO (18 mM) were prepared in PBS. 4armPEG10k-SH was dissolved in PBS and combined with the stock solutions to give sample solutions with final concentrations of 10 wt% 8armPEG20k-SH, 0.4 mM LiTPO and a variable concentration of individual linkers depending on the SH:ene ratio (1:1 = 22.2 mM, 1:1.20 = 26.7 mM).

6.4 Two-photon micropatterning of disulfide-crosslinked hydrogels in presence of DAS

Prepolymer formulations (25 μ l) of **8arm-D,L-HCys (1:1.2)** hydrogel and **8arm-L-HCys (1:1)** hydrogel were polymerized in cylindrical silicon molds ($\varnothing = 6$ mm, $d = 0.8$ mm) between methacrylate glass-bottom μ -dishes (35 mm, Ibbidi GmbH, Germany) and cover glass by irradiation in a Boekel-UV-oven (365 nm, 2 J). Subsequently, the molds were removed and the solidified hydrogel disks were swollen in PBS for 3 d to reach equilibrium swelling. Thereafter, the hydrogels were submersed in solutions of DAS in PBS at different concentrations (0.5 mM, 1.0 mM, 2.0 mM) for at least 5 h to allow diffusion of the chromophore into the network. Then samples were cut using a scalpel to generate a sharp edge. Micropatterning was performed by means of two-photon degradation. Details of the experimental setup have been reported previously.^[112] Briefly, the setup is based on a femtosecond laser (MaiTai DeepSee, Spectra Physics) operating at 720 nm, with a pulse length of 70 fs after the objective (C-Achroplan 32x/0.85 W, ZEISS). Parallel micro-channels with quadratic cross sections ($l = 300$ μ m, $A = 20$ μ m \times 20 μ m) were eroded from the edge into the bulk of the hydrogel at different laser powers ranging from 10–120 mW and scanning along the x-axis. The scanning speed was 200 mm/s (hatch distance: 0.1 μ m, z-layer distance: 0.5 μ m). Individual x,y-planes were either scanned once or twice. After micropatterning, the samples were washed with PBS twice and then soaked in a solution of high molecular weight FITC–dextran (FITC2000, 1 mg mL⁻¹, $M_w \sim 2,000$ kDa, TdB Consultancy AB, Sweden) in PBS at room temperature for more than 4 h. Channels were visualized by laser scanning microscopy (LSM 700, ZEISS). If no channels were visible, the hydrogels were also imaged after swelling in lower molecular weight FITC–dextran (FITC500, 1 mg mL⁻¹, $M_w \sim 500$ kDa, TdB Consultancy AB, Sweden) for at least 5 h.

6.5 Cell encapsulation and micro-channel formation

6.5.1 Cell culture and cell encapsulation

Human Umbilical Vein Endothelial Cells (HUVECs, PELOBiotech GmbH, Germany) were transfected with red fluorescent protein (RFP)-lentiviral particles to obtain stably transfected red labeled cells (RFP-HUVECs). HUVECs were cultured in Endothelial Cell Growth Medium 2 (EGM-2, Lonza) supplemented with 5% fetal bovine serum (FBS). hTERT immortalized human adipose-derived mesenchymal stem cell line ASC/TERT1 (Evercyte GmbH, Austria) were

cultured in EGM-2 supplemented with 10% fetal bovine serum. Cells were maintained in an incubator (5% CO₂, 37 °C, high humidity) and the medium was exchanged every second day.

RFP-HUVEC-spheroids were formed in 2% agarose molds (MicroTissues® 3D Petri Dish®, Sigma-Aldrich) according to the manufacturer's instructions. In order to generate spheroids with a diameter of ~200 µm, 81,000 cells were seeded per micromold corresponding to 1000 cells per spheroid. Cells were incubated for 24 to 48 h in presence of methylcellulose (20 v/v% of stock solution 12 g L⁻¹) in EGM-2.

RFP-HUVEC-spheroids together with single ASCs were encapsulated into **8arm-D,L-HCys (1:1.2)** hydrogel, **8arm-L-HCys (1:1)** hydrogel and **4arm-L-HCys (1:1)** hydrogel in presence of 1 mM RGDC (Bachem AG, Switzerland).

The **8arm-D,L-HCys (1:1.2)** prepolymer solution was prepared as follows: 8arm-PEG20k-SH (14.83 mg) was dissolved EGM-2 (86.1 µL). **Nor-D,L-HCys** (6.11 mg) was dissolved in 58.2 µL of EGM-2 to give a 190 mM stock solution. To 17.68 µL of the linker solution were added 4.2 µL of RGDC solution (30 mM) first, before 81.3 µL of the PEG solution and finally 2.8 µL of the LiTPO solution (6 mM) were added (resulted in 0.4 mM LiTPO). Between all addition steps the mixture was vortexed and centrifuged for homogenization. The prepolymer solution was mixed with 20 µL of a cell-spheroid suspension by cautious pipetting (~5x).

The **8arm-L-HCys (1:1)** prepolymer solution was prepared as follows: 8arm-PEG20k-SH (15.13 mg) was dissolved EGM-2 (86.2 µL). **Nor-L-HCys** (6.40 mg) was dissolved in 61.0 µL of EGM-2 to give a 190 mM stock solution. To 16.42 µL of the linker solution were added 3.9 µL of RGDC solution (30 mM) first, before 71.1 µL of the PEG solution and finally 2.6 µL of the LiTPO solution (6 mM) were added (resulted in 0.4 mM LiTPO). Between all addition steps the mixture was vortexed and centrifuged for homogenization. The prepolymer solution was mixed with 20 µL of a cell-spheroid suspension by cautious pipetting (~5x).

The **4arm-L-HCys (1:1)** prepolymer solution was prepared as follows: 4arm-PEG10k-SH (14.92 mg) was dissolved EGM-2 (88.0 µL). **Nor-L-HCys** (6.40 mg) were dissolved in 61.0 µL of EGM-2 to give a 190 mM stock solution. To 13.83 µL of the linker solution were added 3.9 µL of RGDC solution (30 mM) first, before 76.7 µL of the PEG solution and finally 2.6 µL of the LiTPO solution (6 mM) were added (results in 0.4 mM LiTPO). Between all addition steps the mixture was vortexed and centrifuged for homogenization. The prepolymer solution was mixed with 20 µL of a cell-spheroid suspension by cautious pipetting (~5x).

Aliquots of these cell suspensions (25 μL) were pipetted into four molds on two methacrylized ibidi μ -dishes each and then covered with a glass plate. Hydrogels irradiated in a Boekel-UV-Oven (365 nm) with 1 J. After photo-crosslinking the glass slides were carefully removed using a tweezer and EGM-2 (2 mL) was added to the samples and they were incubated (37 $^{\circ}\text{C}$, 5% CO_2).

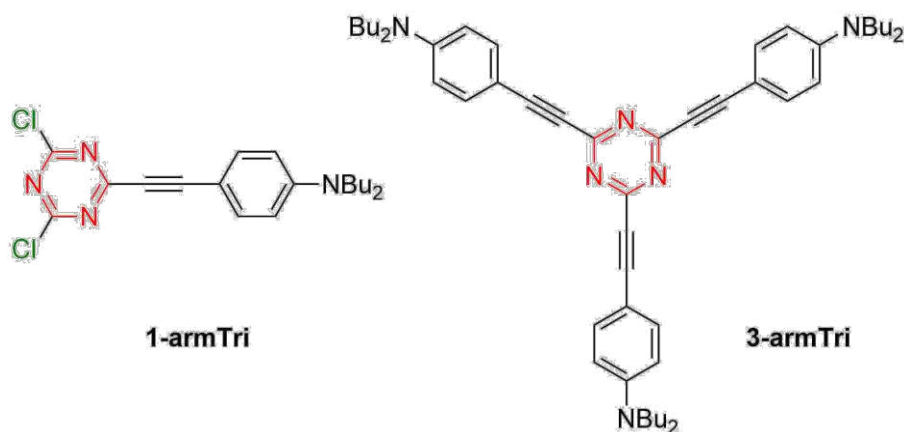
6.5.2 Microchannel fabrication, cell viability and spreading

4arm-L-HCys hydrogel with encapsulated cells was soaked in a solution of DAS (1 mM in ECM-2) for 4 h. Thereafter, round micro-channels with a diameter of 20 μm were formed between cell clusters by two-photon irradiation at 720 nm at a laser power of 60 mW and a writing speed of 200 mm s^{-1} . All other parameters were equal to those applied in previous micropatterning experiments. Channels were only scanned once. Thereafter, the DAS solution was exchanged for media and cells were incubated. Cells-spreading was examined by light microscopy. 5 days after micropatterning LIVE/DEAD viability assay (Life Technology) was used to monitor ASCs viability and spreading. Samples were stained for 20 min at 37 $^{\circ}\text{C}$ with a solution of calcein AM (0.2 μM) and propidium iodide (0.6 μM , PI) in PBS and thereafter imaged by the use of LSM. HUVECS were imaged via the mCherry channel of the Zeiss LSM700.

SUMMARY

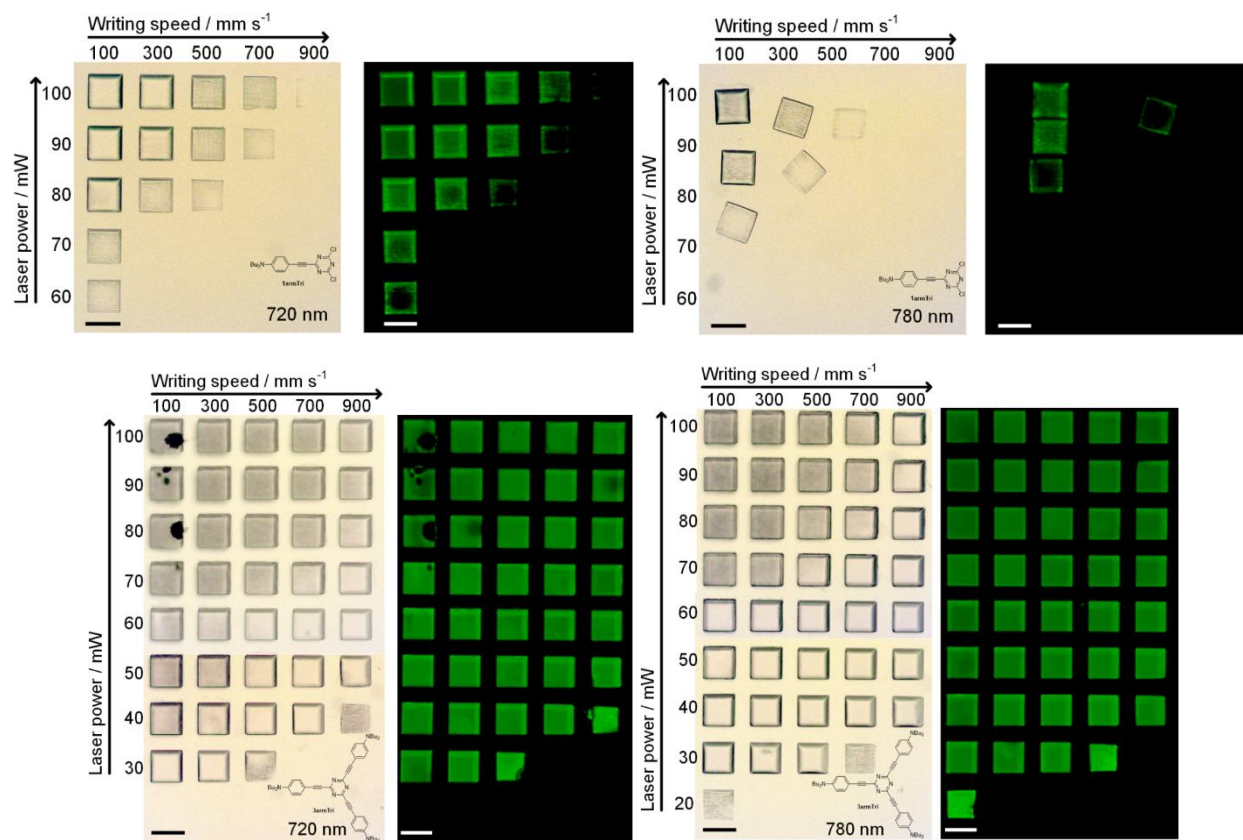
Two-photon lithography is a powerful emerging technology that permits the processing of light-sensitive materials in the (sub)micrometre range by the use of fs-pulsed NIR-laser light. Owing to its unique features, including free-form 3D-patterning and the non-invasiveness to areas outside the focal volume, this method is particularly suited for micropatterning of hydrogels in presence of cells. Besides two-photon (2P) polymerization, which allows fabrication of scaffolds-like constructs in a bottom-up approach from a macromer solution, 2P-degradation of pre-formed photoactive hydrogels allows for localized micro-channel formation or in-situ modification of cell surroundings.^[149] Nevertheless, due to the high resolution two-photon lithography offers and the resulting small feature sizes of created constructs, maximizing the achievable writing speed, with the aim to push the feasible spatial dimensions in the cubic cm regime, is a current key challenge.^[45] Besides engineering of advanced multi-photon printing devices, the development of highly efficient two-photon induced chemistries is a major optimization strategy for this purpose.

In a first approach, two yne-modified triazines were synthesised and evaluated as two-photon active initiators. Synthetic routes towards linear **1-armTri** and quatrupolar **3armTri** molecules were developed and substantially optimized starting from aryl alkyne **3** and cyanur chloride **4** and utilizing Pd-catalyzed Negishi cross-coupling reaction. As the cross-coupling reaction proceeds gradually, depending on the equivalents applied of alkyne **3** either target molecule **1-armTri** or **3-armTri** can be received as the final product.



The performance of the target molecules as two-photon initiators was evaluated at two different wavelengths (720 nm, 780 nm) by speed power-screenings. Hence, arrays of cubes were two-photon polymerized from ETA:TTA resin in presence of the low concentrations of the respective chromophore ($1 \mu\text{mol g}^{-1}$). Whereas both compounds can be used as initiators for two-photon polymerization, the octupolar **3armTri** exhibited much better performance than the dipolar

derivative, especially at high writing speeds. Moreover, it also proved to be more versatile, as good polymerization results could be achieved at both 720 nm and 780 nm. These findings are in accordance with observations discussed in literature demonstrating that the two-photon absorption and performance is increasing with the number of branches when comparing a dipolar to an octupolar molecule of the same basic structural motif.

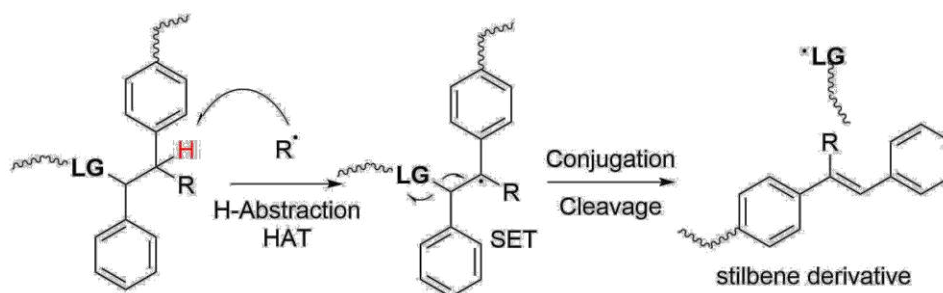


Photolabile hydrogels are dynamically tunable smart materials. By the integration of photocleavable functional groups the chemical and mechanical properties can be altered by the use of UV-VIS or pulsed NIR-laser light.

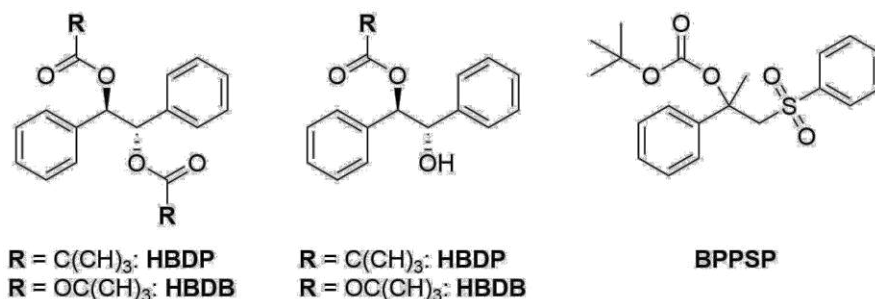
Nevertheless, the inherent light-sensitivity of photocleavable functionalities, can as well be considered a drawback, since it necessitates sample handling under light protection and can complicate light-based examination methods as microscopy.

Hence, first a potential photocleavable molecular system, in which light sensitivity is decoupled from the cleavable functionality, was investigated. The aim was to find a molecular core unit that can be integrated into a polymer backbone, and which upon hydrogen atom transfer (HAT) responds with an intramolecular single electron transfer (SET) cascade, finally leading to fragmentation and therefore disintegration of the backbone was designed. As further driving force

conjugation was anticipated. For activation, a photoinitiator should be modularly added to trigger HAT upon irradiation.



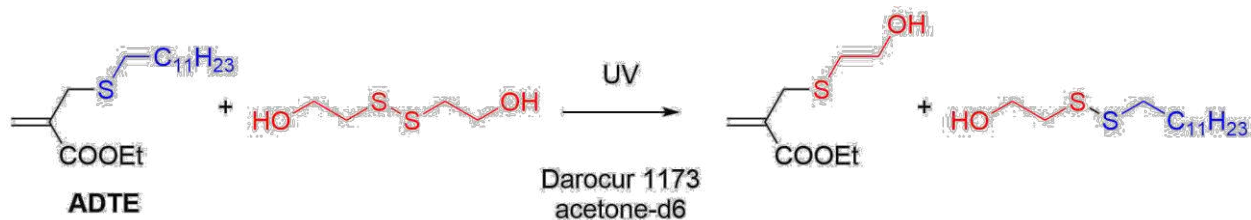
In total five test molecules were synthesized starting either from *meso*-hydrobenzoin or α -methylstyrene and phenylsulfonic acid, containing ester or carbonate functionalities to permit decarboxylation.



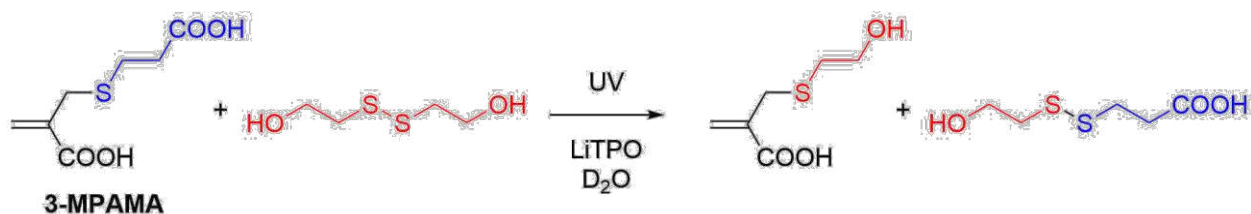
The test molecules were irradiated in presence of photoinitiator, monomers or hydrogen abstractors and analyzed by 1H -NMR. Nevertheless, in none of these simple experiments a desired fragmentation reaction in sufficient efficiency was observed. Reasons could be either due to sterical hindrance of H-abstraction or due to thermodynamic barriers. As the molecular systems did not easily cleave under the simple experimental conditions in solution, this approach was not further investigated.

Instead, disulfide cleavage by locally triggered thiol-disulfide metathesis was researched, since disulfide linkages are of particular interest as reversible linkages in biomaterials. Whereas high concentrations of photoinitiator can be used to permanently cleave disulfide-based networks, this approach would surpass the concentration acceptable for cells by far. Hence, again a modular system was examined, in which a simple small molecule thiol-releasing water-soluble addition-fragmentation chain transfer (AFCT) reagent is added to a disulfide-based network to promote degradation. Upon photoinitiation reversible AFCT is triggered and a thiyl radical is released, which can attack a disulfide linkage, again releasing a thiyl radical and resulting in an amplified

photodegradation cycle. This system was first investigated in a preliminary model reaction in acetone-d₆ involving 2-hydroxyethyl disulfide and readily available AFCT reagent ethyl 2-((n-dodecylthio)methyl)acrylate **ADTE**.



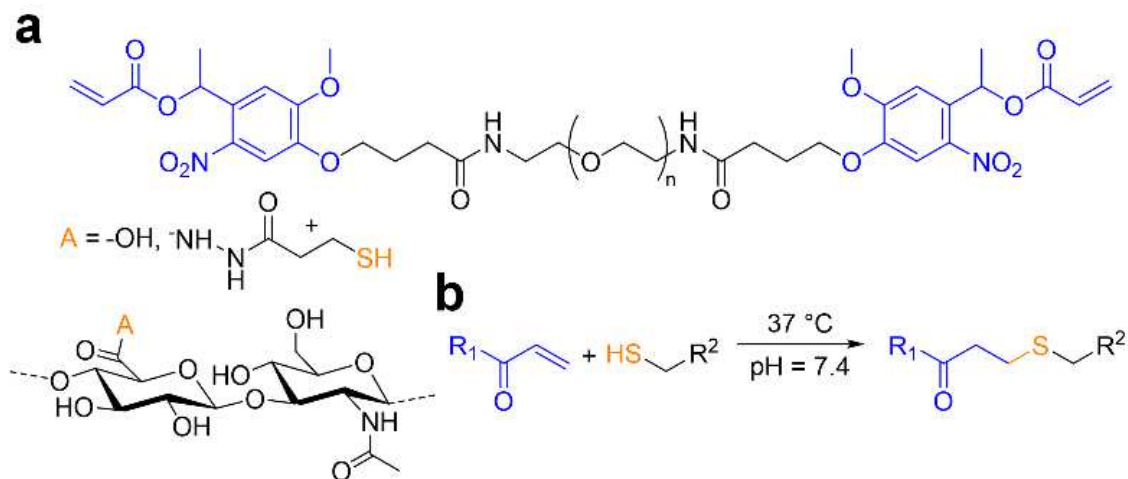
Proof of principle was observed by ¹H-NMR, showing conversion of the AFCT reagent in the range of 50% (equilibrium state) and confirming the proposed reaction mechanism. Subsequently, water-soluble AFCT reagent **3-MPAMA** was synthesized in a straightforward two-step one-pot reaction. While **3-MPAMA** showed adequate reactivity in acetone-d₆ in presence of Darocur 1173, hindered reactivity in aqueous environment in presence of LiTPO even after repeated addition of photoinitiator was observed.



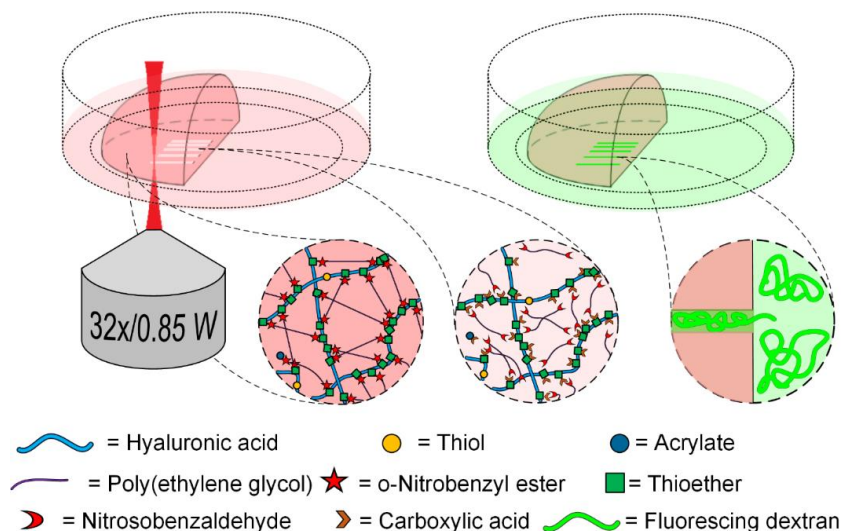
Anyhow, since in the course of this experimental investigation, a closely related approach was published by the Anseth group,^[90] revealing that the concept under investigation was already extensively researched and comprehensively demonstrated, this study was not further conducted at this point.

Furthermore, an approach for the improvement of the 2P-induced degradation of o-nitrobenzyl ester (oNB) containing hydrogels was developed. oNB derivatives are photocleavable groups commonly included in photosensitive materials for tissue engineering applications and mechanobiology studies.¹ However, as the 2P-absorption cross-sections of these functionalities are usually rather low, relatively high laser intensities and long irradiation times are required for their cleavage, which can harm living cells encapsulated in the material. To increase the reactivity towards pulsed laser light, a modular system was developed permitting the sensitization of the 2P induced oNB photocleavage. By adding the water-soluble small molecule 2P sensitizer P2CK,^[49b] the efficiency of the oNB photo-scission could be effectively promoted in a concentration dependent manner.

First, a photodegradable hydrogel (PEG-HA-SH hydrogel) was designed. It was formed via thiolene Michael-addition by combining stock solutions of thiol modified hyaluronic acid (HA-SH, DS = 50%, **a**)^[109] and a photodegradable poly(ethylene glycol) (PEG) based cross-linker containing acrylate terminals (**b**).^[98]

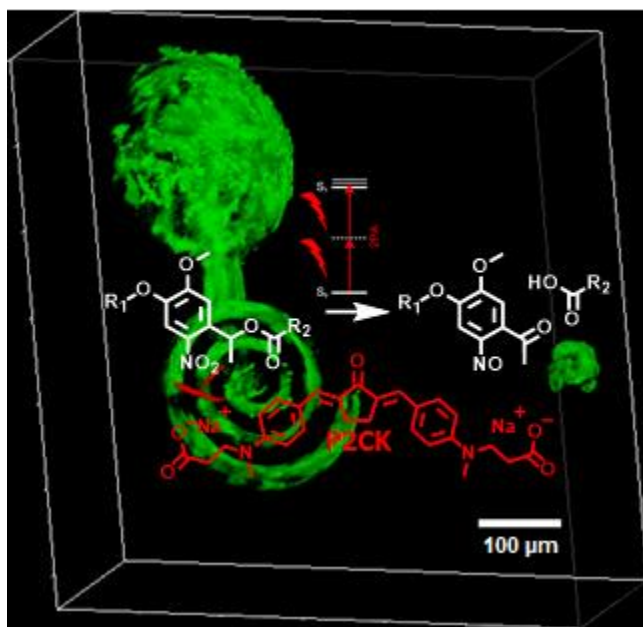


The hydrogel was then 2P-micropatterned at 800 nm in presence of cyclic benzylidene ketone P2CK.^[112] Depending on the concentration of P2CK, the threshold laser power for 2P-micropatterning of oNB-based hydrogels could be significantly decreased. By adjusting the laser power and the concentration of the sensitizer used, the material can be either fully eroded to form open microchannels or partially degraded to soften the material by reducing the local density of crosslinks. This effect was demonstrated by LSM after swelling microchannels with high molecular weight fluorescent dextran (FITC2000) and AFM.



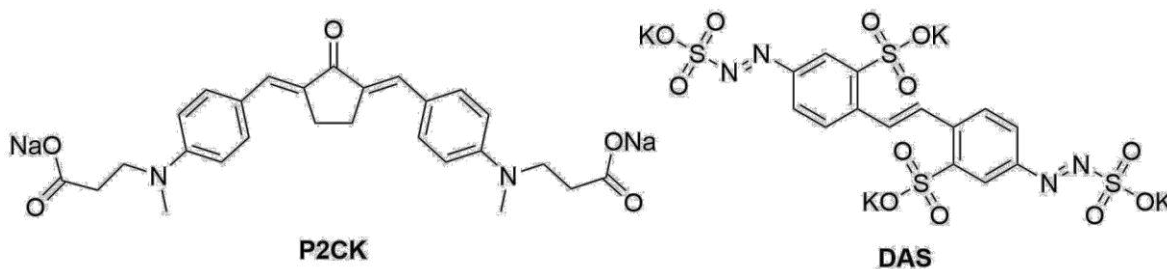
Moreover, generality of the two-photon sensitization approach was demonstrated by producing similar results with a 4armPEG-SH based hydrogel. Biocompatibility of both the promoted

micropatterning process and the PEG-HA-SH hydrogel platform was confirmed by cell culture studies using adipose derived stem cell spheroids (ASC/TERT1). To demonstrate the efficacy of the modular 2P-sensitization approach, various microchannels were fabricated around spheroids in presence of low concentrations of P2CK (0.1 mM) and evaluated by LSM at different time points.

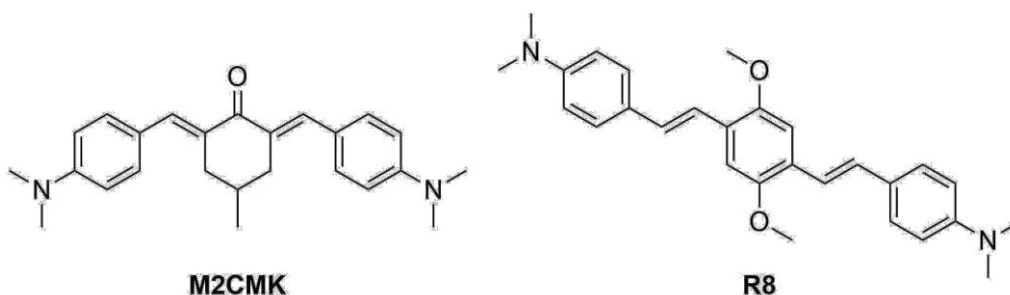


Due to its modularity, the developed hydrogel platform is a useful tool for studies of cell matrix interactions in 3D where spatio-temporal control over the cell surrounding matrix by 2P-micropatterning of photolabile hydrogels at moderate laser powers is required.

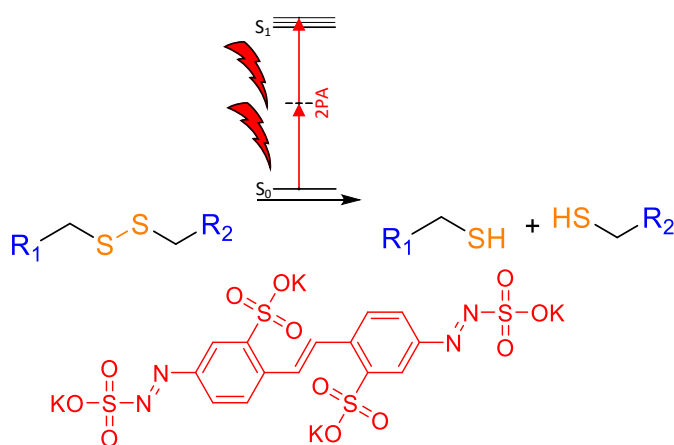
In addition, the same approach was also tested on disulfides, which are much simpler cleavable linkages as oNB, which requires multi-step synthesis. Surprisingly, the radical-mediated cleavage of disulfide has only been examined in one-photon excitation regime so far. Reasonably, the two-photon induced cleavage of disulfide-based networks in presence of two-photon active compounds P2CK^[49b] or DAS^[49a] was explored as missing link in the techniques for disulfide network degradation, especially allowing for localized cleavage.



A disulfide network based on 4armPEG-SH was used as platform to demonstrate the two-photon sensitized cleavage reaction. Preformed hydrogels were swollen in P2CK or DAS and the 2P-micropatterned. Microchannels were again visualized with LSM after swelling in FITC2000. To demonstrate the generality of the approach, the experiments were also performed on an organogel platform using M2CMK^[48a] and R8^[118] as two-photon sensitizer.

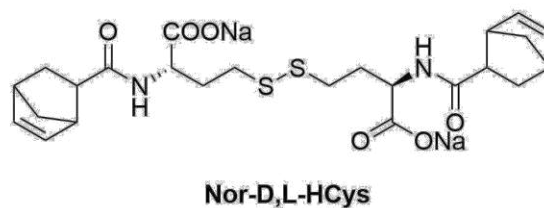
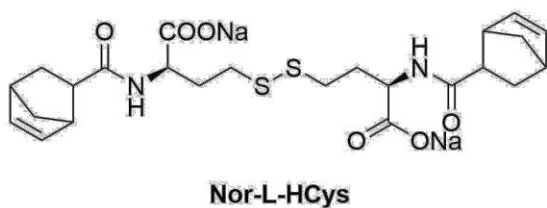
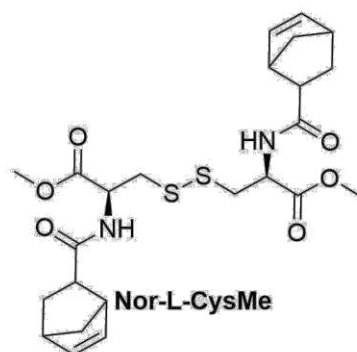
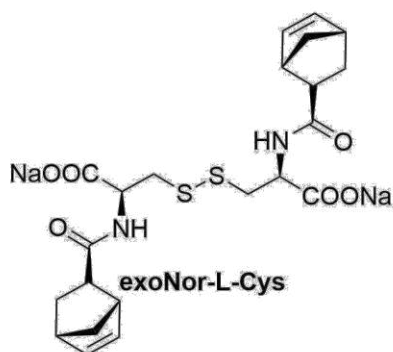
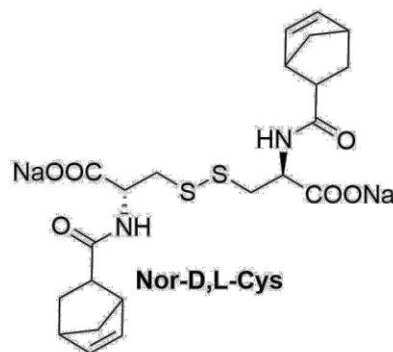
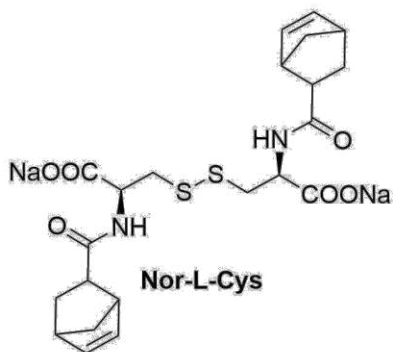
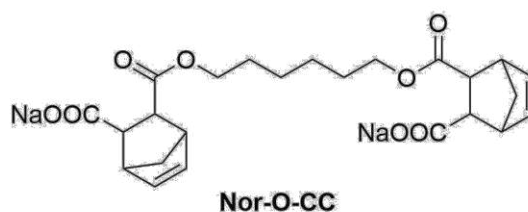
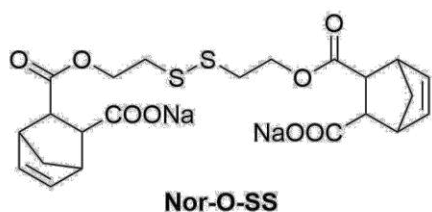


Moreover, in a further experiment a hydrogel was produced from thiol-modified hyaluronic acid with a DS of 8% (HA-SH 8%) by oxidative crosslinking as alternative substrate. After swelling in P2CK again microchannels were successfully fabricated by two-photon irradiation, while in contrary in the absence of P2CK no open channels formed.

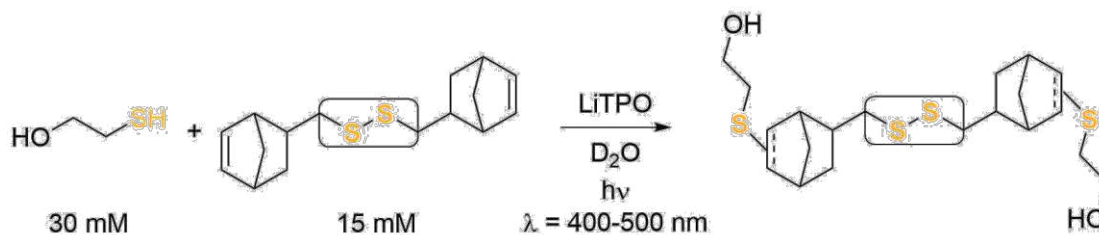


In this simple study, the feasibility of two-photon sensitized disulfide-cleavage could be successfully demonstrated. Moreover, it was shown that two-photon degradable hydrogels can be produced directly from thiol-containing precursors without the use of additional linkers containing photolabile chromophores as oNB, significantly simplifying precursor preparation. However, the formation of disulfide-crosslinked hydrogels by direct oxidation of thiols to disulfides proved to be unpractical since it is hard to control and mediated by harmful compounds as hydrogen peroxide.

Hence, to ease the formation of networks based on disulfide linkages, a simple disulfide containing linker was developed that can be reacted with thiol-terminated precursors using thiol-norbornene click chemistry. This approach significantly improves handling of precursor solutions and simplifies cell encapsulation experiments. To keep the approach simple and practical, this linker should have been synthesized from cheap and readily available starting materials. Nevertheless, due to unexpected instabilities or hindered thiol-norbornene reactivity, the molecular design of this linker had to be reconsidered and the molecular design was thoroughly optimized to maximize the double bond conversion. As a result, a series of eight different water-soluble linkers was synthesized in total.

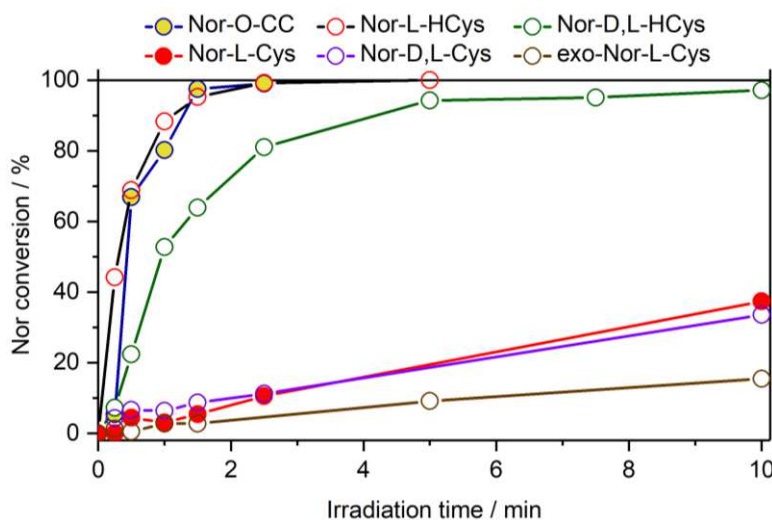


The reactivity of the linkers towards thiol-ene coupling was estimated in a $^1\text{H-NMR}$ study using 2-mercaptoethanol as molecular probe. The respective linker was combined with the thiol in an equimolar thiol-ene ratio and irradiated in presence of LiTPO in D_2O for different time periods.



Based on this study, the reactivity of the linkers regarding thiol-ene addition was graded in the following order:

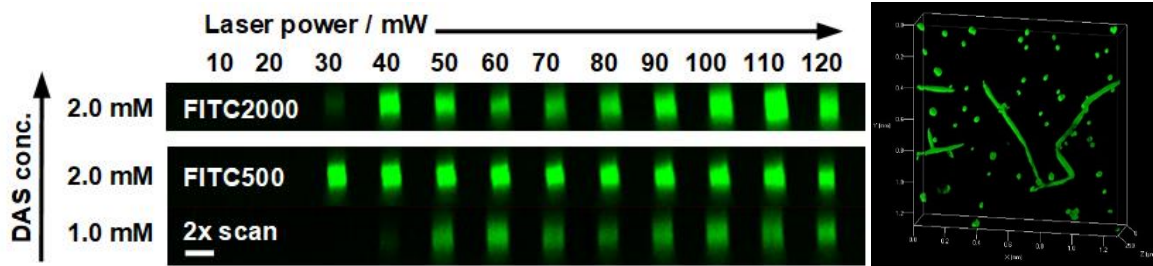
Nor-O-CC ~ Nor-L-HCys > Nor-D,L-HCys >> Nor-L-Cys ~ Nor-D,L-Cys > exo-Nor-L-Cys



Interestingly, linkers based on homocysteine were highly reactive, whereas those based on the shorter cystine spacer exhibited relatively low thiol-norbornene reactivity. Consequently, hydrogels made of cystine-linkers were unstable. Hydrogels based on the **Nor-D,L-HCys** linker could be stabilized after an extensive examination of the hydrogel platform using photorheology and swelling experiments. Incomplete thiol consumption was identified as cause for hydrogel disintegration. Free thiols can undergo thiol-disulfide metathesis with disulfide linkages inducing relaxation and finally dissolution of the network. Methods for stabilization of the hydrogel platform included (i) the introduction of a non-cleavable background network, (ii) capping of free thiols by maleimide and (iii) the consumption of free thiols by an excess of norbornene.

In contrast, using the **Nor-L-HCys** linker none of these optimization strategies were needed and stable hydrogels could be formed from both 4armPEG10k-SH and 8armPEG20k-SH. With the

optimized linker configuration, hydrogels were produced, which were stable for several weeks in PBS. Two-photon induced cleavage of disulfide-based hydrogels in presence of DAS was demonstrated by microchannel fabrication.



The approach could as well be applied in the presence of encapsulated stem cells. ASCs spread along two-photon fabricated microchannels, revealing the great potential of this hydrogel platform and cleavage methodology for both cell culture studies mimicking dynamic cell environment as well as fabrication of microfluidic devices.

MATERIALS, METHODS AND INSTRUMENTATION

Materials

All photosensitive steps were performed under light protection. Unless otherwise stated, chemicals used in the current work were purchased from either Sigma-Aldrich, TCI, Apollo or ABCR and used without further purification. The photoinitiators Darocur 1173 from Ciba-Geigy and Ivocerin® provided by Ivoclar Vivadent were used for photopolymerization experiments. LiTPO, P2CK and DAS were synthesized at TU Wien following literature procedures.^[49a, 49b, 150] TLC aluminum foils coated with silica gel 60 F254 from Merck were used. Column chromatography was performed on Merck silica gel 60 (0.040-0.063 mm).

Instrumentation

NMR spectra were recorded at 600 MHz for ¹H and 150 MHz for ¹³C on a Bruker Avance III HD spectrometer and at 400 MHz for ¹H and 100 MHz for ¹³C on a Bruker Avance DRX-400 spectrometer. Data for ¹H NMR are reported as follows: chemical shift in units of parts per million (ppm) from tetramethylsilane (TMS) using the residual non-deuterated solvent signal of CD₂Cl₂ ($\delta_{\text{H}} = 5.32$ ppm), CDCl₃ ($\delta_{\text{H}} = 7.26$ ppm), D₂O ($\delta_{\text{H}} = 4.79$ ppm) or DMSO-*d*₆ ($\delta_{\text{H}} = 2.50$ ppm) as internal reference. Multiplicities are reported by using the following abbreviations; bs: broad singlet; s: singlet; d: doublet; t: triplet; q: quartet; quint: quintet, m: multiplet; *J*: coupling constants in Hertz (Hz). ¹³C NMR data are reported in ppm from TMS using the central peak of the solvent as reference (CD₂Cl₂: $\delta_{\text{C}} = 53.84$ ppm, CDCl₃: $\delta_{\text{C}} = 77.16$ ppm, DMSO-*d*₆: $\delta_{\text{C}} = 39.52$ ppm); the multiplicity with respect to H (s = quaternary C, d = CH, t = CH₂, q = CH₃) is deduced from attached proton test (APT) experiments.

HRESIMS spectra (*m/z* 50-1900) were obtained on a maXis ESI-Qq-TOF mass spectrometer (Bruker Daltonics, Bremen, Germany) in the positive-ion mode by direct infusion. The sum formulas of the detected ions were determined using Bruker Compass DataAnalysis 4.0 based on the mass accuracy ($\Delta m/z \leq 5$ ppm) and isotopic pattern matching (SmartFormula algorithm).

Alternatively, HRESIMS analysis was carried out from methanol or acetonitrile solutions (concentration: 10 ppm) using an HTC PAL system autosampler (CTC Analytics AG, Zwingen, Switzerland), an Agilent 1100/1200 HPLC with binary pumps, degasser and column thermostat (Agilent Technologies, Waldbronn, Germany) and Agilent 6230 AJS ESI-TOF mass spectrometer (Agilent Technologies, Palo Alto, United States).

UV-VIS absorption spectra were recorded using a Lambda 35 UV-Vis spectrometer (PerkinElmer). Photoluminescence spectra were collected on a LS 50 fluorescence spectrometer (PerkinElmer).

Melting points were obtained using an Optimelt MPA100 automated melting point apparatus.

GC-MS measurements were conducted on a Thermo Scientific GC-MS DSQ II using a BGB 5 column (l = 30 m, d = 0.32 mm, 1.0 μ m film, achiral).

Column chromatography was performed with a Büchi MPLC-system equipped with the control unit C-620, fraction collector C-660, and UV-photometer C-635.

Functionalization of glass surfaces (methacrylization)

Glass bottom μ -dishes were pre-treated in a plasma cleaner (PDC-002, Harrick Plasma, USA) for 10 min. A methacrylization solution was prepared by combining deionated water (50% v/v), ethanol (48% v/v), glacial acetic acid (0.3% v/v) and 3-(trimethoxysilyl)propyl methacrylate (2% v/v). The solution was stirred for 15 min before aliquots (\sim 1 mL) were pipetted into the μ -dishes. After 30 min of surface treatment, μ -dishes were rinsed with deionated water twice and then dried in a drying chamber (50 $^{\circ}$ C) for \sim 1 h. Cover glass were hydrophobized in a similar manner using n-octadecyltrimethoxysilane (ABCR GmbH, Germany)

ABBREVIATIONS

1PA	one-photon absorption
2PA	two-photon absorption
Boc ₂ O	di- <i>t</i> -butyl dicarbonate
DCM	dichloromethane
DEE	diethyl ether
DMAP	4-dimethylaminopyridine
DMF	dimethylformamide
DS	degree of substitution
ECM	extracellular matrix
EE	ethyl acetate
FITC	fluorescein isothiocyanate modified dextran
G'	storage modulus
G''	loss modulus
GCMS	gas chromatography–mass spectrometry
GM	Goeppert-Mayer
HA	hyaluronic acid
HRMS	high resolution mass spectrometry
HV	high vacuum
LiTPO	lithium phenyl-2,4,6-trimethylbenzoylphosphinate
LSM	laser scanning microscopy
MeCN	acetonitrile
Melm	1-methyl-1 <i>H</i> -imidazole
<i>o</i> NB	<i>o</i> -nitrobenzyl
PE	light petrol
PEG	polyethylene glycol
PI	photoinitiator
quant.	quantitatively
R _f	retention factor (thin layer chromatography)
RGD	tripeptide Arg-Gly-Asp
TLC	thin layer chromatography
T _m	melting point
THF	tetrahydrofuran
UV-vis	ultraviolet–visible

BIBLIOGRAPHY

- [1] R. Langer, J. P. Vacanti, *Science* **1993**, *260*, 920.
- [2] A. Khademhosseini, R. Langer, J. Borenstein, J. P. Vacanti, *Proceedings of the National Academy of Sciences of the United States of America* **2006**, *103*, 2480.
- [3] L. G. Griffith, G. Naughton, *Science* **2002**, *295*, 1009-1014.
- [4] L. M. Caballero Aguilar, S. M. Silva, S. E. Moulton, *J. Controlled Release* **2019**, *306*, 40-58.
- [5] R. Subbiah, R. E. Guldborg, *Adv. Healthcare Mater.* **2019**, *8*, 1801000.
- [6] A. Khademhosseini, R. Langer, *Nat. Protoc.* **2016**, *11*, 1775.
- [7] a) M. W. Tibbitt, K. S. Anseth, *Biotechnol. Bioeng.* **2009**, *103*, 655-663; b) S. R. Caliari, J. A. Burdick, *Nat Meth* **2016**, *13*, 405-414.
- [8] G. Huang, F. Li, X. Zhao, Y. Ma, Y. Li, M. Lin, G. Jin, T. J. Lu, G. M. Genin, F. Xu, *Chem. Rev.* **2017**, *117*, 12764-12850.
- [9] N. A. Peppas, J. Z. Hilt, A. Khademhosseini, R. Langer, *Adv. Mater.* **2006**, *18*, 1345-1360.
- [10] J. M. Aamodt, D. W. Grainger, *Biomaterials* **2016**, *86*, 68-82.
- [11] M. Mehrli, A. Thakur, C. P. Pennisi, S. Talebian, A. Arpanaei, M. Nikkhah, A. Dolatshahi-Pirouz, *Adv. Mater.* **2017**, *29*, 1603612.
- [12] a) E. Ruoslahti, M. D. Pierschbacher, *Science* **1987**, *238*, 491; b) J. A. Burdick, K. S. Anseth, *Biomaterials* **2002**, *23*, 4315-4323.
- [13] C. A. DeForest, D. A. Tirrell, *Nat. Mater.* **2015**, *14*, 523-531.
- [14] P. M. Kharkar, K. L. Kiick, A. M. Kloxin, *Chem. Soc. Rev.* **2013**, *42*, 7335-7372.
- [15] H. Wang, S. C. Heilshorn, *Adv. Mater.* **2015**, *27*, 3717-3736.
- [16] A. M. Rosales, S. L. Vega, F. W. DelRio, J. A. Burdick, K. S. Anseth, *Angew. Chem. Int. Ed.* **2017**, *56*, 12132-12136.
- [17] a) M. W. Tibbitt, K. S. Anseth, *Science Translational Medicine* **2012**, *4*, 160ps124-160ps124; b) A. M. Hilderbrand, E. M. Ovidia, M. S. Rehmann, P. M. Kharkar, C. Guo, A. M. Kloxin, *Curr. Opin. Solid State Mater. Sci.* **2016**; c) T. E. Brown, K. S. Anseth, *Chem. Soc. Rev.* **2017**, *46*, 6532-6552.
- [18] C. M. Madl, S. C. Heilshorn, *Adv. Funct. Mater.* **2018**, *28*, 1706046.
- [19] a) L. Li, J. M. Scheiger, P. A. Levkin, *Adv. Mater.* **2019**, *0*, 1807333; b) E. R. Ruskowitz, C. A. DeForest, *Nature Reviews Materials* **2018**, *3*, 17087.
- [20] a) S. M. Jay, W. M. Saltzman, *Nat. Biotechnol.* **2009**, *27*, 543-544; b) M. P. Lutolf, *Nat. Mater.* **2009**, *8*, 451-453.
- [21] Y. Luo, M. S. Shoichet, *Nat. Mater.* **2004**, *3*, 249-253.
- [22] A. M. Kloxin, A. M. Kasko, C. N. Salinas, K. S. Anseth, *Science* **2009**, *324*, 59-63.
- [23] a) P. Klán, T. Šolomek, C. G. Bochet, A. Blanc, R. Givens, M. Rubina, V. Popik, A. Kostikov, J. Wirz, *Chem. Rev.* **2013**, *113*, 119-191; b) D. R. Griffin, A. M. Kasko, *J. Am. Chem. Soc.* **2012**, *134*, 13103-13107.
- [24] H. Zhao, E. S. Sterner, E. B. Coughlin, P. Theato, *Macromolecules* **2012**, *45*, 1723-1736.
- [25] a) M. A. Azagarsamy, D. D. McKinnon, D. L. Alge, K. S. Anseth, *ACS Macro Lett.* **2014**, *3*, 515-519; b) M. S. Lee, J.-C. Kim, *J. Appl. Polym. Sci.* **2012**, *124*, 4339-4345; c) D. Y. Wong, D. R. Griffin, J. Reed, A. M. Kasko, *Macromolecules* **2010**, *43*, 2824-2831; d) B. D. Fairbanks, S. P. Singh, C. N. Bowman, K. S. Anseth, *Macromolecules* **2011**, *44*, 2444-2450; e) Y. Zheng, A. Farrukh, A. del Campo, *Langmuir* **2018**, *34*, 14459-14471; f) A. Farrukh, J. I. Paez, A. del Campo, *Adv. Funct. Mater.* **2019**, *29*, 1807734; g) S. Theis, A. Iturmendi, C. Gorsche, M. Orthofer, M. Lunzer, S. Baudis, A. Ovsianikov, R. Liska, U. Monkowius, I. Teasdale, *Angew. Chem. Int. Ed.* **2017**, *56*, 15857-15860; h) T. Rapp, C. Highley, B. Manor, J. Burdick, I. J. Dmochowski, *Chem. Eur. J.* **2018**, *24*, 2328-2333.

- [26] C. G. Bochet, *J. Chem. Soc., Perkin Trans. 1* **2002**, 125-142.
- [27] D. Geißler, Y. N. Antonenko, R. Schmidt, S. Keller, O. O. Krylova, B. Wiesner, J. Bendig, P. Pohl, V. Hagen, *Angew. Chem. Int. Ed.* **2005**, *44*, 1195-1198.
- [28] a) C. A. DeForest, K. S. Anseth, *Nat. Chem.* **2011**, *3*, 925-931; b) M. W. Tibbitt, A. M. Kloxin, K. U. Dyamenahalli, K. S. Anseth, *Soft Matter* **2010**, *6*, 5100-5108.
- [29] a) C. A. DeForest, K. S. Anseth, *Angew. Chem. Int. Ed.* **2012**, *51*, 1816-1819; b) C. K. Arakawa, B. A. Badeau, Y. Zheng, C. A. DeForest, *Adv. Mater.* **2017**, *29*, 1703156.
- [30] *Multiphoton Lithography: Techniques, Materials and Applications*, Wiley-VCH Verlag GmbH & Co. KGaA Weinheim, **2017**.
- [31] G. M. Maria, *Annalen der Physik* **1931**, *401*, 273-294.
- [32] W. Kaiser, C. G. B. Garrett, *Phys. Rev. Lett.* **1961**, *7*, 229-231.
- [33] W. Denk, J. Strickler, W. Webb, *Science* **1990**, *248*, 73-76.
- [34] W. R. Zipfel, R. M. Williams, W. W. Webb, *Nat. Biotechnol.* **2003**, *21*, 1369-1377.
- [35] a) E.-S. Wu, J. H. Strickler, W. R. Harrell, W. W. Webb, *Two-photon lithography for microelectronic application, Vol. 1674*, SPIE, **1992**; b) S. Maruo, O. Nakamura, S. Kawata, *Opt. Lett.* **1997**, *22*, 132-134.
- [36] J. Fischer, M. Thiel, M. Wegener, *IEEE Spectrum* **2014**, *51*, 34-58.
- [37] M. Rumi, J. W. Perry, *Advances in Optics and Photonics* **2010**, *2*, 451-518.
- [38] T. Yu, C. K. Ober, S. M. Kuebler, W. Zhou, S. R. Marder, J. W. Perry, *Adv. Mater.* **2003**, *15*, 517-521.
- [39] C. N. LaFratta, J. T. Fourkas, T. Baldacchini, R. A. Farrer, *Angew. Chem. Int. Ed.* **2007**, *46*, 6238-6258.
- [40] W. Zhou, S. M. Kuebler, K. L. Braun, T. Yu, J. K. Cammack, C. K. Ober, J. W. Perry, S. R. Marder, *Science* **2002**, *296*, 1106-1109.
- [41] S.-H. Lee, J. J. Moon, J. L. West, *Biomaterials* **2008**, *29*, 2962-2968.
- [42] N. Corrigan, J. Yeow, P. Judzewitsch, J. Xu, C. A. J. M. Boyer, *Angew. Chem.* **2019**, *58*, 5170-5189.
- [43] M. Albota, *Science* **1998**, *281*, 1653-1656.
- [44] M. Pawlicki, H. A. Collins, R. G. Denning, H. L. Anderson, *Angew. Chem. Int. Ed.* **2009**, *48*, 3244-3266.
- [45] C. Barner-Kowollik, M. Bastmeyer, E. Blasco, G. Delaittre, P. Müller, B. Richter, M. Wegener, *Angew. Chem. Int. Ed.* **2017**, *56*, 15828-15845.
- [46] G. S. He, L.-S. Tan, Q. Zheng, P. N. Prasad, *Chem. Rev.* **2008**, *108*, 1245-1330.
- [47] K. J. Schafer, J. M. Hales, M. Balu, K. D. Belfield, E. W. Van Stryland, D. J. Hagan, *J. Photochem. Photobiol. A: Chem.* **2004**, *162*, 497-502.
- [48] a) Z. Li, M. Siklos, N. Pucher, K. Cicha, A. Ajami, W. Husinsky, A. Rosspeintner, E. Vauthey, G. Gescheidt, J. Stampfl, R. Liska, *J. Polym. Sci., Part A: Polym. Chem.* **2011**, *49*, 3688-3699; b) N. Pucher, A. Rosspeintner, V. Satzinger, V. Schmidt, G. Gescheidt, J. Stampfl, R. Liska, *Macromolecules* **2009**, *42*, 6519-6528.
- [49] a) M. Tromayer, A. Dobos, P. Gruber, A. Ajami, R. Dedic, A. Ovsianikov, R. Liska, *Polym. Chem.* **2018**, *9*, 3108-3117; b) Z. Li, J. Torgersen, A. Ajami, S. Mühleder, X. Qin, W. Husinsky, W. Holnthoner, A. Ovsianikov, J. Stampfl, R. Liska, *RSC Adv.* **2013**, *3*, 15939-15946; c) A. K. Nguyen, R. J. Narayan, *Mater. Today* **2017**, *20*, 314-322.
- [50] W. A. Green, *Industrial Photoinitiators: A Technical Guide*, Boca Raton, Fla.: CRC Press: Taylor & Francis, London, **2010**.
- [51] G. Moad, D. H. Solomon, *The Chemistry of Free Radical Polymerization*, 1. ed., Pergamon, Oxford, **1995**.
- [52] M. W. Tibbitt, A. M. Kloxin, L. A. Sawicki, K. S. Anseth, *Macromolecules* **2013**, *46*, 2785-2792.
- [53] a) C. E. Hoyle, C. N. Bowman, *Angew. Chem. Int. Ed.* **2010**, *49*, 1540-1573; b) H. C. Kolb, M. G. Finn, K. B. Sharpless, *Angew. Chem. Int. Ed.* **2001**, *40*, 2004-2021.

- [54] N. B. Cramer, S. K. Reddy, A. K. O'Brien, C. N. Bowman, *Macromolecules* **2003**, *36*, 7964-7969.
- [55] E. R. Ruskowitz, C. A. DeForest, *ACS Biomaterials Science & Engineering* **2019**, *5*, 2111-2116.
- [56] S. R. Marder, *Chem. Commun.* **2006**, 131-134.
- [57] B. Dereka, D. Svechkarev, A. Rosspointner, M. Tromayer, R. Liska, A. M. Mohs, E. Vauthey, *J. Am. Chem. Soc.* **2017**, *139*, 16885-16893.
- [58] M. Tromayer, P. Gruber, A. Rosspointner, A. Ajami, W. Husinsky, F. Plasser, L. González, E. Vauthey, A. Ovsianikov, R. Liska, *Sci. Rep.* **2018**, *8*, 17273.
- [59] W. Liu, H. Wang, C.-J. Li, *Org. Lett.* **2016**, *18*, 2184-2187.
- [60] K. S. Sindhu, G. Anilkumar, *RSC Adv.* **2014**, *4*, 27867-27887.
- [61] M. Sonoda, A. Inaba, K. Itahashi, Y. Tobe, *Org. Lett.* **2001**, *3*, 2419-2421.
- [62] B. N. E., S. Linus, L. B. V., S. Wolfgang, *Chem. Eur. J.* **2015**, *21*, 7866-7873.
- [63] S. L. Raut, J. D. Kimball, R. Fudala, I. Bora, R. Chib, H. Jaafari, M. K. Castillo, N. W. Smith, I. Gryczynski, S. V. Dzyuba, Z. Gryczynski, *Phys. Chem. Chem. Phys.* **2016**, *18*, 4535-4540.
- [64] D. G. Hendry, T. Mill, L. Piszkiwicz, J. A. Howard, H. K. Eigenmann, *J. Phys. Chem. Ref. Data* **1974**, *3*, 937.
- [65] M. P. Plesniak, H.-M. Huang, D. J. Procter, *Nature Reviews Chemistry* **2017**, *1*, 0077.
- [66] Y. Basel, A. Hassner, *J. Org. Chem.* **2000**, *65*, 6368-6380.
- [67] C. B. Rao, B. Chinnababu, Y. Venkateswarlu, *The Journal of Organic Chemistry* **2009**, *74*, 8856-8858.
- [68] J. A. Marshall, S. Xie, *The Journal of Organic Chemistry* **1995**, *60*, 7230-7237.
- [69] H. G. O. Becker, *Organikum: organisch-chemisches Grundpraktikum*, Wiley-VCH, Weinheim, **2001**.
- [70] G. R. Fulmer, A. J. M. Miller, N. H. Sherden, H. E. Gottlieb, A. Nudelman, B. M. Stoltz, J. E. Bercaw, K. I. Goldberg, *Organometallics* **2010**, *29*, 2176-2179.
- [71] Q. Dong, N. Li, R. Qiu, J. Wang, C. Guo, X. Xu, *Journal of Organometallic Chemistry* **2015**, *799-800*, 122-127.
- [72] P. S. Engel, L. Pan, K. H. Whitmire, I. Guzman-Jimenez, M. R. Willcott, W. B. Smith, *J. Org. Chem.* **2000**, *65*, 1016-1021.
- [73] Q. Lu, J. Zhang, F. Wei, Y. Qi, H. Wang, Z. Liu, A. Lei, *Angew. Chem. Int. Ed.* **2013**, *52*, 7156-7159.
- [74] S. P. Black, J. K. M. Sanders, A. R. Stefankiewicz, *Chem. Soc. Rev.* **2014**, *43*, 1861-1872.
- [75] a) J. A. Yoon, J. Kamada, K. Koynov, J. Mohin, R. Nicolaÿ, Y. Zhang, A. C. Balazs, T. Kowalewski, K. Matyjaszewski, *Macromolecules* **2012**, *45*, 142-149; b) J. Canadell, H. Goossens, B. Klumperman, *Macromolecules* **2011**, *44*, 2536-2541.
- [76] J. Zhang, A. Skardal, G. D. Prestwich, *Biomaterials* **2008**, *29*, 4521-4531.
- [77] N. V. Tsarevsky, K. Matyjaszewski, *Macromolecules* **2002**, *35*, 9009-9014.
- [78] R. Singh, G. V. Lamoureux, W. J. Lees, G. M. Whitesides, *Methods Enzymol.* **1995**, *251*, 167-173.
- [79] Y. Chujo, K. Sada, A. Naka, R. Nomura, T. Saegusa, *Macromolecules* **1993**, *26*, 883-887.
- [80] H. Otsuka, S. Nagano, Y. Kobashi, T. Maeda, A. Takahara, *Chem. Commun.* **2010**, *46*, 1150-1152.
- [81] Y. Amamoto, H. Otsuka, A. Takahara, K. Matyjaszewski, *Adv. Mater.* **2012**, *24*, 3975-3980.
- [82] U. F. Fritze, M. von Delius, *Chem. Commun.* **2016**, *52*, 6363-6366.
- [83] R. Caraballo, M. Rahm, P. Vongvilai, T. Brinck, O. Ramström, *Chem. Commun.* **2008**, 6603-6605.
- [84] C. Wei, M. Chen, D. Liu, W. Zhou, M. Khan, X. Wu, N. Huang, L. Li, *Polym. Chem.* **2015**, *6*, 4067-4070.

- [85] a) A. M. Belenguer, T. Friščić, G. M. Day, J. K. M. Sanders, *Chemical Science* **2011**, *2*, 696-700; b) A. M. Belenguer, G. I. Lampronti, D. J. Wales, J. K. M. Sanders, *J. Am. Chem. Soc.* **2014**, *136*, 16156-16166.
- [86] H. Xiang, J. Yin, G. Lin, X. Liu, M. Rong, M. Zhang, *Chem. Eng. J.* **2019**, *358*, 878-890.
- [87] B. D. Fairbanks, M. P. Schwartz, C. N. Bowman, K. S. Anseth, *Biomaterials* **2009**, *30*, 6702-6707.
- [88] S. C. Ligon, K. Seidler, C. Gorsche, M. Griesser, N. Moszner, R. Liska, *J. Polym. Sci., Part A: Polym. Chem.* **2016**, *54*, 394-406.
- [89] N. Moszner, K. Rist, I. Lamparth, P. Burtscher, C. Gorsche, R. Liska, Ivoclar Vivadent AG, Technische Universität Wien, **2016**.
- [90] T. E. Brown, I. A. Marozas, K. S. Anseth, *Adv. Mater.* **2017**, *29*, 1605001.
- [91] a) N. R. Gandavarapu, M. A. Azagarsamy, K. S. Anseth, *Adv. Mater.* **2014**, *26*, 2521-2526; b) J. C. Grim, T. E. Brown, B. A. Aguado, D. A. Chapnick, A. L. Viert, X. Liu, K. S. Anseth, *ACS Central Science* **2018**, *4*, 909-916.
- [92] K. Uto, J. H. Tsui, C. A. DeForest, D.-H. Kim, *Prog. Polym. Sci.* **2017**, *65*, 53-82.
- [93] a) I. Aujard, C. Benbrahim, M. Gouget, O. Ruel, J.-B. Baudin, P. Neveu, L. Jullien, *Chem. Eur. J.* **2006**, *12*, 6865-6879; b) C. Brieke, F. Rohrbach, A. Gottschalk, G. Mayer, A. Heckel, *Angew. Chem. Int. Ed.* **2012**, *51*, 8446-8476; c) G. Bort, T. Gallavardin, D. Ogden, P. I. Dalko, *Angew. Chem. Int. Ed.* **2013**, *52*, 4526-4537.
- [94] K. König, in *Handbook Of Biological Confocal Microscopy* (Ed.: J. B. Pawley), Springer US, Boston, MA, **2006**, pp. 680-689.
- [95] C. P. Holmes, *J. Org. Chem.* **1997**, *62*, 2370-2380.
- [96] S. Gug, F. Bolze, A. Specht, C. Bourgogne, M. Goeldner, J.-F. Nicoud, *Angew. Chem. Int. Ed.* **2008**, *47*, 9525-9529.
- [97] a) H. Zhao, B. Hou, Y. Tang, W. Hu, C. Yin, Y. Ji, X. Lu, Q. Fan, W. Huang, *Polym. Chem.* **2016**, *7*, 3117-3125; b) E. Cueto Diaz, S. Picard, M. Klausen, V. Hugues, P. Pagano, E. Genin, M. Blanchard-Desce, *Chem. Eur. J.* **2016**, *22*, 10848-10859; c) S. Picard, E. J. Cueto-Diaz, E. Genin, G. Clermont, F. Acher, D. Ogden, M. Blanchard-Desce, *Chem. Commun.* **2013**, *49*, 10805-10807.
- [98] A. M. Kloxin, M. W. Tibbitt, K. S. Anseth, *Nat. Protoc.* **2010**, *5*, 1867-1887.
- [99] C. A. DeForest, B. D. Polizzotti, K. S. Anseth, *Nat. Mater.* **2009**, *8*, 659-664.
- [100] a) F. Yanagawa, S. Sugiura, T. Takagi, K. Sumaru, G. Camci-Unal, A. Patel, A. Khademhosseini, T. Kanamori, *Adv. Healthcare Mater.* **2015**, *4*, 246-254; b) M. Tamura, F. Yanagawa, S. Sugiura, T. Takagi, K. Sumaru, T. Kanamori, *Sci. Rep.* **2015**, *5*, 15060; c) V. X. Truong, K. M. Tsang, G. P. Simon, R. L. Boyd, R. A. Evans, H. Thissen, J. S. Forsythe, *Biomacromolecules* **2015**, *16*, 2246-2253.
- [101] a) K. Peng, I. Tomatsu, B. van den Broek, C. Cui, A. V. Korobko, J. van Noort, A. H. Meijer, H. P. Spaink, A. Kros, *Soft Matter* **2011**, *7*, 4881-4887; b) J. You, A. Haque, D.-S. Shin, K. J. Son, C. Siltanen, A. Revzin, *Adv. Funct. Mater.* **2015**, *25*, 4650-4656.
- [102] C. B. Highley, G. D. Prestwich, J. A. Burdick, *Curr. Opin. Biotechnol.* **2016**, *40*, 35-40.
- [103] a) M. Guvendiren, J. A. Burdick, *Nat. Commun.* **2012**, *3*, 792; b) S. Khetan, M. Guvendiren, W. R. Legant, D. M. Cohen, C. S. Chen, J. A. Burdick, *Nat. Mater.* **2013**, *12*, 458-465.
- [104] a) S. C. Owen, S. A. Fisher, R. Y. Tam, C. M. Nimmo, M. S. Shoichet, *Langmuir* **2013**, *29*, 7393-7400; b) F. Yu, X. Cao, Y. Li, X. Chen, *ACS Macro Lett.* **2015**, *4*, 289-292.
- [105] a) W. M. Gramlich, I. L. Kim, J. A. Burdick, *Biomaterials* **2013**, *34*, 9803-9811; b) R. J. Wade, E. J. Bassin, W. M. Gramlich, J. A. Burdick, *Adv. Mater.* **2015**, *27*, 1356-1362.
- [106] P. M. Kharkar, K. L. Kiick, A. M. Kloxin, *Polym. Chem.* **2015**, *6*, 5565-5574.
- [107] M. Viola, D. Vigetti, E. Karousou, M. L. D'Angelo, I. Caon, P. Moretto, G. De Luca, A. Passi, *Glycoconjugate J.* **2015**, *32*, 93-103.
- [108] A. B. Lowe, *Polym. Chem.* **2010**, *1*, 17-36.

- [109] X. Z. Shu, Y. Liu, Y. Luo, M. C. Roberts, G. D. Prestwich, *Biomacromolecules* **2002**, *3*, 1304-1311.
- [110] S. McMahon, R. Kennedy, P. Duffy, J. M. Vasquez, J. G. Wall, H. Tai, W. Wang, *ACS Applied Materials & Interfaces* **2016**, *8*, 26648-26656.
- [111] M. W. Tibbitt, J. A. Shadish, C. A. DeForest, in *Multiphoton Lithography* (Eds.: J. Stampfl, R. Liska, A. Ovsianikov), Wiley-VCH Verlag GmbH & Co. KGaA, **2016**, pp. 183-220.
- [112] A. Ovsianikov, S. Mühleder, J. Torgersen, Z. Li, X.-H. Qin, S. Van Vlierberghe, P. Dubruel, W. Holnthoner, H. Redl, R. Liska, J. Stampfl, *Langmuir* **2014**, *30*, 3787-3794.
- [113] L. Kain, O. G. Andriotis, P. Gruber, M. Frank, M. Markovic, D. Grech, V. Nedelkovski, M. Stolz, A. Ovsianikov, P. J. Thurner, *Journal of the Mechanical Behavior of Biomedical Materials* **2018**, *85*, 225-236.
- [114] L. Knezevic, M. Schaupper, S. Mühleder, K. Schimek, T. Hasenberg, U. Marx, E. Priglinger, H. Redl, W. Holnthoner, *Front. Bioeng. Biotechnol.* **2017**, *5*.
- [115] C. Heller, N. Pucher, B. Seidl, K. Kalinyaprak-Icten, G. Ullrich, L. Kuna, V. Satzinger, V. Schmidt, H. C. Lichtenegger, J. Stampfl, R. Liska, *J. Polym. Sci., Part A: Polym. Chem.* **2007**, *45*, 3280-3291.
- [116] M. Lunzer, L. Shi, O. G. Andriotis, P. Gruber, M. Markovic, P. J. Thurner, D. Ossipov, R. Liska, A. Ovsianikov, *Angew. Chem. Int. Ed.* **2018**, *57*, 15122-15127.
- [117] M. M. Zieger, P. Mueller, A. S. Quick, M. Wegener, C. Barner-Kowollik, *Angew. Chem. Int. Ed.* **2017**, *56*, 5625-5629.
- [118] B. H. Cumpston, S. P. Ananthavel, S. Barlow, D. L. Dyer, J. E. Ehrlich, L. L. Erskine, A. A. Heikal, S. M. Kuebler, I. Y. S. Lee, D. McCord-Maughon, J. Qin, H. Röckel, M. Rumi, X.-L. Wu, S. R. Marder, J. W. Perry, *Nature* **1999**, *398*, 51.
- [119] Z. Li, N. Pucher, K. Cicha, J. Torgersen, S. C. Ligon, A. Ajami, W. Husinsky, A. Rosspeintner, E. Vauthey, S. Naumov, T. Scherzer, J. Stampfl, R. Liska, *Macromolecules* **2013**, *46*, 352-361.
- [120] D. Ret, in *Chemical and Physical Characterization of Native and Modified Hyaluronan*, TU Wien, Wien, **2017**.
- [121] D. D. McKinnon, T. E. Brown, K. A. Kyburz, E. Kiyotake, K. S. Anseth, *Biomacromolecules* **2014**, *15*, 2808-2816.
- [122] X. Z. Shu, Y. Liu, F. Palumbo, G. D. Prestwich, *Biomaterials* **2003**, *24*, 3825-3834.
- [123] S. Singh, F. Topuz, K. Hahn, K. Albrecht, J. Groll, *Angew. Chem. Int. Ed.* **2013**, *52*, 3000-3003.
- [124] a) M. Mackiewicz, K. Kaniewska, J. Romanski, E. Augustin, Z. Stojek, M. Karbarz, *Journal of Materials Chemistry B* **2015**, *3*, 7262-7270; b) K. Raghupathi, V. Kumar, U. Sridhar, A. E. Ribbe, H. He, S. Thayumanavan, *Langmuir* **2019**, *35*, 7929-7936.
- [125] W. Xu, J. Qian, Y. Zhang, A. Suo, N. Cui, J. Wang, Y. Yao, H. Wang, *Journal of Materials Chemistry B* **2016**, *4*, 3339-3350.
- [126] B. Husár, R. Liska, *Chem. Soc. Rev.* **2012**, *41*, 2395-2405.
- [127] a) B. D. Fairbanks, M. P. Schwartz, A. E. Halevi, C. R. Nuttelman, C. N. Bowman, K. S. Anseth, *Adv. Mater.* **2009**, *21*, 5005-5010; b) C. E. Hoyle, T. Y. Lee, T. Roper, *J. Polym. Sci., Part A: Polym. Chem.* **2004**, *42*, 5301-5338; c) S. R. Caliri, S. L. Vega, M. Kwon, E. M. Soulas, J. A. Burdick, *Biomaterials* **2016**, *103*, 314-323.
- [128] W. Lwowski, *Angew. Chem.* **1958**, *70*, 483-495.
- [129] K.-D. Gundermann, *Angew. Chem.* **1963**, *75*, 1194-1203.
- [130] L. J. Alcock, K. D. Farrell, M. T. Akol, G. H. Jones, M. M. Tierney, H. B. Kramer, T. L. Pukala, G. J. L. Bernardes, M. V. Perkins, J. M. Chalker, *Tetrahedron* **2018**, *74*, 1220-1228.
- [131] O. A. Mukhina, N. N. Bhuvan Kumar, T. M. Arisco, R. A. Valiulin, G. A. Metzger, A. G. Kutateladze, *Angew. Chem. Int. Ed.* **2011**, *50*, 9423-9428.

- [132] C.-G. Chae, Y.-G. Yu, H.-B. Seo, M.-J. Kim, R. H. Grubbs, J.-S. Lee, *Macromolecules* **2018**, *51*, 3458-3466.
- [133] a) B. Colak, J. C. S. Da Silva, T. A. Soares, J. E. Gautrot, *Bioconj. Chem.* **2016**, *27*, 2111-2123; b) D. M. Love, K. Kim, J. T. Goodrich, B. D. Fairbanks, B. T. Worrell, M. P. Stoykovich, C. B. Musgrave, C. N. Bowman, *J. Org. Chem.* **2018**, *83*, 2912-2919.
- [134] B. H. Northrop, R. N. Coffey, *J. Am. Chem. Soc.* **2012**, *134*, 13804-13817.
- [135] R. J. Boyd, J. S. Perkyins, R. Ramani, *Can. J. Chem.* **1983**, *61*, 1082-1085.
- [136] S. Benedikt, J. Wang, M. Markovic, N. Moszner, K. Dietliker, A. Ovsianikov, H. Grützmacher, R. Liska, *J. Polym. Sci., Part A: Polym. Chem.* **2015**, 473-479.
- [137] A. M. Rosales, K. S. Anseth, *Nature Reviews Materials* **2016**, *1*, 15012.
- [138] G. A. Barcan, X. Zhang, R. M. Waymouth, *J. Am. Chem. Soc.* **2015**, *137*, 5650-5653.
- [139] W. Steiger, P. Gruber, D. Theiner, A. Dobos, M. Lunzer, J. Van Hoorick, S. Van Vlierberghe, R. Liska, A. Ovsianikov, *Optical Materials Express* **2019**, *9*, 3567-3581.
- [140] L. Zhang, L. Zou, J. Xiao, P. Zhou, C. Zhong, X. Chen, J. Qin, I. F. A. Mariz, E. Macoas, *J. Mater. Chem.* **2012**, *22*, 16781-16790.
- [141] P. Gruber, *Development of a Novel Wavelength-tunable High-Speed 2-Photon Lithography Setup*, TU Wien, Wien, **2018**.
- [142] P. A. Clarke, N. E. Kayaleh, M. A. Smith, J. R. Baker, S. J. Bird, C. Chan, *The Journal of Organic Chemistry* **2002**, *67*, 5226-5231.
- [143] J. M. J. Paulusse, R. J. Amir, R. A. Evans, C. J. Hawker, *J. Am. Chem. Soc.* **2009**, *131*, 9805-9812.
- [144] C. Gorsche, R. Harikrishna, S. Baudis, P. Knaack, B. Husar, J. Laeuger, H. Hoffmann, R. Liska, *Anal. Chem.* **2017**, *89*, 4958-4968.
- [145] J. L. Hutter, J. Bechhoefer, *Rev. Sci. Instrum.* **1993**, *64*, 1868-1873.
- [146] C. Neto, V. S. J. Craig, *Langmuir* **2001**, *17*, 2097-2099.
- [147] S. Muthusamy, B. Gnanaprakasam, E. Suresh, *Org. Lett.* **2006**, *8*, 1913-1916.
- [148] F. N. Behrendt, H. Schlaad, *Macromol. Rapid Commun.* **2018**, *39*, 1700735.
- [149] J. Torgersen, X. H. Qin, Z. Li, A. Ovsianikov, R. Liska, J. Stampfl, *Adv. Funct. Mater.* **2013**, *23*, 4542-4554.
- [150] T. Majima, W. Schnabel, W. Weber, *Die Makromolekulare Chemie* **1991**, *192*, 2307-2315.

CURRICULUM VITAE

Dipl.-Ing. Markus Lunzer, BSc

Date of Birth 29th December 1988
Citizenship Austria
Address Haidgasse 12/14, 1020 Vienna, Austria
ORCID ID 0000-0002-8052-6517

EDUCATION

- 10/2014 – 01/2020 **TU Wien, Vienna, Austria**
Institute of Applied Synthetic Chemistry
Doctoral programme in engineering sciences – Technical Chemistry
PhD thesis: *New Concepts for Two-Photon Micropatterning of Biocompatible Hydrogels*
Supervisors: Prof. Robert Liska, Prof. Aleksandr Ovsianikov
- 03/2012 – 09/2014 **TU Wien, Vienna, Austria**
Institute of Applied Synthetic Chemistry
Master programme Technical Chemistry – Synthesis
Graduation with distinction
Master thesis: *Synthesis and Characterization of Triarylamine Based Materials as Two-Photon Absorption Photoinitiators*
Supervisor: Prof. Johannes Fröhlich
- 10/2008 – 03/2012 **TU Wien, Vienna, Austria**
Bachelor programme Technical Chemistry
- 10/2007 – 06/2008 **University of Vienna, Vienna, Austria**
Bachelor programme Chemistry

WORK EXPERIENCE

- 10/2019 – present **Materials Chemist**
UpNano GmbH, Vienna, Austria
Development of two-photon resins, materials testing
- 07/2016 – 09/2019 **University Assistant**
Institute of Materials Science and Technology, TU Wien
Research, student supervision
- 07/2015 – 07/2016 **Project Assistant**
Institute of Applied Synthetic Chemistry, TU Wien
Project: ERC Starting Grant LeBMEC (307701)
Research, student supervision

10/2012 – 06/2013

Freelancer

PORR Umwelttechnik GmbH, Vienna, Austria
Environmental analysis, sample preparation

08/2012 – 09/2012

Internship

PORR Umwelttechnik GmbH, Vienna, Austria
Environmental analysis, sample preparation

RESEARCH INTERNSHIP

11/2014

University of Geneva, Switzerland

Department of Physical Chemistry
Research group of Prof. Dr. Eric Vauthey
Measurements of two-photon excitation spectra

TEACHING EXPERIENCE

07/2016 – present

Co-Supervision of 2 bachelor theses and 4 master student internships, TU Wien

09/2014

Tutor in the laboratory course “Organic Synthesis”, TU Wien

SS 2014

Tutor in the “Synthesis Laboratory Course”, TU Wien

WS 2013/14

Tutor in the laboratory course “General Chemistry”, TU Wien

AWARDS AND HONORS

11/2018

682. WE-Heraeus-Seminar on Micro- and Nanostructured Biointerfaces – Best Poster Prize

11/2018

Belgian Symposium on Tissue Engineering – Poster Presentation Award

10/2018

International Society for Biofabrication – Travel Award

10/2014 – 03/2015

Research Scholarship of TU Wien

2013/14

Merit Grant of TU Wien

2012/13

Foundation Grant of TU Wien

2011/12

Merit Grant of TU Wien

LANGUAGE SKILLS

German

Native language

English

Business fluent

Italian

Basic

FURTHER QUALIFICATIONS

Certified Project Management Associate – IPMA Level D

Blasting permit

Driving licence B

PUBLICATIONS

PATENTS

Verwendung von Zweiphotonen-Photosensibilisatoren

Markus Lunzer, Stefan Baudis, Aleksandr Ovsianikov, Robert Liska, (Austria, **A 384/2018**, 20.12.2018)

SCIENTIFIC PAPERS

Fully automated z-scan setup based on a tunable fs-oscillator

Wolfgang Steiger, Peter Gruber, Dominik Theiner, Agnes Dobos, Markus Lunzer, Jasper Van Hoorick, Sandra Van Vlierberghe, Robert Liska, Aleksandr Ovsianikov, *Opt. Mater. Express*, **2019**, **9**, 3567–3581. DOI: 10.1364/OME.9.003567

Screening of two-photon activated photodynamic therapy sensitizers using a 3D osteosarcoma model

Agnes Dobos, Wolfgang Steiger, Dominik Theiner, Peter Gruber, Markus Lunzer, Jasper Van Hoorick, Sandra Van Vlierberghe, Aleksandr Ovsianikov, *Analyst*, **2019**, **144**, 3056–3063. DOI: 10.1039/C9AN00068B

Towards efficient initiators for two-photon induced polymerization: fine tuning of the donor/acceptor properties

Brigitte Holzer, Markus Lunzer, Arnulf Rosspeintner, Giuseppe Licari, Maximilian Tromayer, Sergej Naumov, Daniel Lumpi, Ernst Horkel, Christian Hametner, Aleksandr Ovsianikov, Robert Liska, Eric Vauthey, Johannes Fröhlich, *Mol. Syst. Des. Eng.*, **2019**, **4**, 437–448. DOI: 10.1039/C8ME00101D

A Modular Approach to Sensitized Two-Photon Patterning of Photodegradable Hydrogels

Markus Lunzer, Liyang Shi, Orestis G. Andriotis, Peter Gruber, Marica Markovic, Philipp J. Thurner, Dmitri Ossipov, Robert Liska, and Aleksandr Ovsianikov, *Angew. Chem. Int. Ed.*, **2018**, **57**, 15122–15127; *Angew. Chem.* **2018**, **130**, 15342–15347.

DOI: 10.1002/anie.201808908; 10.1002/ange.201808908

Metallo-Supramolecular Photocleavable Gels Sensitive to Visible and Near Infrared Irradiation

Sabrina Theis, Aitziber Iturmendi, Christian Gorsche, Marco Orthofer, Markus Lunzer, Stefan Baudis, Aleksandr Ovsianikov, Robert Liska, Uwe Monkowius, Ian Teasdale, *Angew. Chem. Int. Ed.*, **2017**, **56**, 15857–15860; *Angew. Chem.* **2017**, **129**, 16071–16075.

DOI: 10.1002/anie.201707321; 10.1002/ange.201707321

Specific Monitoring of Excited-State Symmetry Breaking by Femtosecond Broadband Fluorescence Upconversion Spectroscopy

Joseph S. Beckwith, Arnulf Rosspeintner, Giuseppe Licari, Markus Lunzer, Brigitte Holzer, Johannes Fröhlich, Eric Vauthey, *J. Phys. Chem. Lett.*, **2017**, **8**, 5878–5883. DOI: 10.1021/acs.jpcclett.7b02754

Dynamic Coordination Chemistry Enables Free Directional Printing of Biopolymer Hydrogel

Liyang Shi, Hauke Carstensen, Katja Hölzl, Markus Lunzer, Hao Li, Jöns Hilborn, Aleksandr Ovsianikov, Dmitri A. Ossipov, *Chem. Mater.*, **2017**, *29*, 5816–5823.

DOI: 10.1021/acs.chemmater.7b00128

A Versatile One-Pot Access to Cyanoarenes from *ortho*- and *para*-Quinones: Paving the Way for Cyanated Functional Materials

Florian Glöcklhofer, Markus Lunzer, Berthold Stöger, Johannes Fröhlich, *Chem. Eur. J.*, **2016**, *22*, 5173–5180. DOI: 10.1002/chem.201600004

Facile Synthesis of Cyanoarenes from Quinones by Reductive-Aromatization of Cyanohydrin Intermediates

Florian Glöcklhofer, Markus Lunzer, Johannes Fröhlich, *Synlett*, **2015**, *26*, 950–952.

DOI: 10.1055/s-0034-1380150

CONFERENCE CONTRIBUTIONS

A Modular Approach to Sensitized Two-Photon Micropatterning of Photolabile Hydrogels

M. Lunzer, L. Shi, P. Gruber, M. Markovic, D. Ossipov, R. Liska, A. Ovsianikov

Poster: 682. WE-Heraeus-Seminar, "Micro- and Nanostructured Biointerfaces", 25.-28.11.2018, Bad Honnef, Germany.

Two-Photon Micropatterning of a Photolabile Hydrogel Using a Two-Photon Sensitizer

M. Lunzer, L. Shi, O.G. Andriotis, P. Gruber, M. Markovic, P.J. Thurner, D. Ossipov, R. Liska, A. Ovsianikov

Poster: 6th Belgian Symposium on Tissue Engineering 2018, 21.-23.11.2018, Ghent, Belgium.

Sensitized Two-Photon Micropatterning in Presence of Cells

M. Lunzer, L. Shi, P. Gruber, M. Markovic, D. Ossipov, A. Ovsianikov, R. Liska

Poster: International Conference on Biofabrication 2018, 28.-31.10.2018, Würzburg, Germany.

Promoted Two-Photon Micropatterning of Biocompatible Materials

M. Lunzer, L. Shi, P. Gruber, M. Markovic, D. Ossipov, A. Ovsianikov, R. Liska

Poster: 5th European Symposium of Photopolymer Science 2018, 03.-06.09.2018, Mulhouse, France.

Advances in Two-Photon Initiation Based 3D Printing for Biological Applications

M. Lunzer, P. Gruber, K. Hölzl, M. Tromayer, M. Markovic, D. Ossipov, A. Ovsianikov, R. Liska

Talk: RadTech Europe Conference 2017, 17.-19.10.2017, Prague, Czech Republic.

Micropatterning of Hydrogels by Sensitized Two-Photon Cleavage of *o*-Nitrobenzyl Crosslinkages

M. Lunzer, D. Ossipov, P. Gruber, K. Hölzl, M. Markovic, A. Ovsianikov, R. Liska

Talk: Danube Vltava Sava Polymer Meeting 2017, 05.-08.09.2017, Vienna, Austria.

Promoted Two-Photon Induced Cleavage of *o*-Nitrobenzyl Linkages in a Hyaluronic Acid Based Hydrogel by a Two-Photon Initiator

M. Lunzer, D. Ossipov, J. Hilborn, P. Gruber, K. Hölzl, M. Markovic, M. Tromayer, J. Stampfl, R. Liska, A. Ovsianikov

Talk: TERMIS-EU 2016 conference, 28.06.-01.07.2016, Uppsala, Sweden.

Two-Photon Degradation of a Hyaluronic Acid Based Hydrogel Using a Two-Photon Initiator as Photosensitizer

M. Lunzer, D. Ossipov, J. Hilborn, P. Gruber, K. Hölzl, M. Markovic, J. Stampfl, R. Liska, and A. Ovsianikov
Talk: 10th World Biomaterials Congress 2016, 17.-22.05.2016, Montréal, Canada.

Poly(vinyl alcohol) Based Hydrogels for 3D Biomaterial Constructs

S. Baudis, D. Bomze, M. Lunzer, J. Stampfl, A. Ovsianikov, and R. Liska
Poster: 10th World Biomaterials Congress 2016, 17.-22.05.2016, Montréal, Canada.

Triarylamine Based Materials as Two-Photon Absorption Photoinitiators – Adjustment of Molecular Properties

M. Lunzer, A. Rosspeintner, B. Holzer, D. Lumpi, M. Tromayer, P. Gruber, E. Horkel, A. Ovsianikov, E. Vauthey, R. Liska, and J. Fröhlich
Poster: RadTech Europe Conference 2015, 13.-15.10.2015, Prague, Czech Republic.

Synthesis and Characterization of Novel Cap-Linker-Cap Type Structures as Two-Photon Absorption Photoinitiators

M. Lunzer, B. Holzer, M. Tromayer, D. Lumpi, E. Horkel, R. Liska, and J. Fröhlich
Poster: 3rd European Symposium of Photopolymer Science, 09.-12.09.2014, Vienna, Austria.

Synthesis of Novel Cap-Linker-Cap Structures as Potential Initiators for Two-Photon-Induced Polymerization

M. Lunzer, B. Holzer, D. Lumpi, E. Horkel, R. Liska, and J. Fröhlich
Poster: 15th Blue Danube Symposium on Heterocyclic Chemistry, 01.-05.09.2013, Olomouc, Czech Republic.